



NEUTRONS
FOR SOCIETY

INSTITUT LAUE-LANGEVIN

THE EUROPEAN NEUTRON SOURCE



Annual Report 20**19**

Annual Report 2019

INSTITUT LAUE-LANGEVIN



© D. Morel

Contents

	FOREWORD	4
	WHAT IS THE ILL	
	About the ILL	6
	Why neutron scattering is useful	7
	THE ILL IN THE PRESS	8
	SCIENTIFIC HIGHLIGHTS	12
	College introductions	14
	Magnetism	16
	Materials science	28
	Chemistry and crystallography	38
	Soft condensed matter	44
	Biology and health	56
	Nuclear and particle physics	62
	Theory	68
	MODERNISATION PROGRAMME AND TECHNICAL DEVELOPMENTS	72
	Modernisation programme and instrument upgrade	74
	Technical developments	84
	INDUSTRIAL ACTIVITIES	90
	EXPERIMENTAL AND USER PROGRAMME	
	User programme	93
	User and beamtime statistics	94
	Instrument list	98
	REACTOR OPERATION	100
	MORE THAN SIMPLY NEUTRONS	104
	Scientific support laboratories	106
	Training and outreach	108
	European programmes	110
	WORKSHOPS AND EVENTS	112
	Chronicle	113
	Scientific events	114
	FACTS AND FIGURES	118
	Facts and figures	119
	Publications	121
	Organisation chart	122
Publishing information		
Editors:		
Giovanna Cicognani and Mark Johnson		
Production team:		
Giovanna Cicognani, Virginie Guerard		
Scientific advisors:		
Sandra Cabeza, Nicolas Coquelle,		
Oscar Ramon Fabelo Rosa,		
Michael Marek Koza, Lucile Mangin-Thro,		
Caterina Michelagnoli, Sylvain Prevost,		
Alberto Rodriguez Velamazán, Tobias Weber		
Design:		
Morton Ward Limited		
Photography:		
Serge Claisse – ILL (unless otherwise specified)		
Further copies can be obtained from:		
Institut Laue-Langevin		
Communication Unit		
CS 20156, F-38042 Grenoble Cedex 9		
communication@ill.eu		
www.ill.eu		

FOREWORD



THE year 2019 was not without its difficulties for the ILL community (but how boring would life be without them?), but there was also cause for satisfaction and a significant number of very positive outcomes.

Probably the most important of the latter was the lifting of the formal 'mise en demeure' notice issued by the French nuclear safety authority ASN. This was achieved thanks to the enormous effort invested by the ILL's management and personnel in new management and documentation procedures. I would therefore like to take this opportunity to thank most warmly all the ILL staff. In particular, I would like to thank the Reactor Division and its director Hervé Guyon, who, with support from Jérôme Estrade and the ILL's Director and Science director—Helmut Schober and Mark Johnson, respectively—responded so successfully to the difficult but necessary requirements prescribed by the ASN.

There has also been significant progress on the preparation of a sixth ten-year Protocol amending the ILL's Intergovernmental Convention. This will extend the life of the Institute for a further ten years, with effect from the beginning of January 2024. The ILL's Associates have provided very positive input to the process. In the second half of 2019, UK ministry representatives joined them for preparatory discussions within the informal working group recently established by the Associates. Work on the Protocol is now sufficiently advanced for the discussions to include the ILL's management and representatives from the Associates' legal departments. We are optimistic about completing this on time and, hopefully, in the not-so-distant future.

Progress has also been achieved on the unfortunately necessary (given these difficult times) reinforcement of security on the ILL site. In the design of the measures being introduced, efforts have been made to minimise the impact on users' activities and to preserve as a whole the unity of the EPN campus, which remains one of the world's leading multidisciplinary venues for research. The ILL Associates have a very strong desire, understandably, to maintain the synergy and productive relations between all the institutes contributing to life on this unique campus (the ILL, ESRF, IBS, EMBL and several other partners, including the INCM).

Renewal of the Scientific Membership contracts is now almost complete, with a few final signatures pending. The high level of Scientific Member participation—now representing a quarter of the ILL's budget—is testimony to the appeal of the high-flux reactor. This offsets the significant disappointment felt at the recent drop in Italy's contributions. Italian scientists are scientifically very active; although they submitted a high number of proposals in response to the last call, the drop in Italy's contributions has resulted in a severe reduction in their access to the ILL's facilities.

As regards co-ordination at European and international level, the ILL has been asked to chair the European League of advanced Neutron Sources, LENS. Like LEAPS, its sister organisation for synchrotron science, LENS is expected to emerge strongly in the new Horizon Europe framework programme, playing a role in the co-ordination and exchange of knowledge and activities within the superadvanced neutron community.

Finally, I would like to reaffirm the German, UK and French Associates' commitment to ensuring that the ILL remains the world's leading neutron source for as long a period as possible. It is, of course, clear that at some point in this decade the ESS will be bringing on line a rising number of instruments with outstanding intensity and timing capacities. The Associates are already working on potential postILL scenarios such as a network of compact neutron sources, some of them hopefully based in Grenoble, to preserve the unique capabilities of a renewed EPN Campus beyond 2030.

Gabriel Chardin

CNRS, ILL Steering Committee Chair

FIND US ON:   **DIRECTOR'S FOREWORD**

ON 11 December 2019 the new Commissioner of the European Union, Ursula von der Leyen, presented Europe's Green Deal to the European Parliament. It is an ambitious plan, to build a society that is not only prosperous and fair but equally resource-neutral and environmentally friendly. This is a goal that can only be welcomed. The scientific community, who in the past laid the foundation for the technological progress that has made today's prosperity possible, enthusiastically supports Europe's Green Deal.

Given the urgency of the matter, it is evident that immediate and bold action is required. Despite this urgency, the transition to a resource-neutral and environmentally friendly economy will not happen overnight. It will require sustained effort for decades to come. This is true in particular for our research endeavours, which must be further intensified. It was the scientific community who first rang the alarm bells and who immediately set to working on the problem of sustainable development. The technical solutions that sprang up from this research are what make the Green Deal's immediate policy actions possible, whether in the form of high-efficiency solar or fuel cells, high-capacity batteries, low-consumption LEDs, the digital environment required for smart cities or innovative resource-efficient production processes.

The ILL is proud to have contributed to this success. Countless experiments performed over the decades on innovative materials and manufacturing processes have contributed to laying the materials research foundations of today's technologies. This report again contains a number of examples that highlight this contribution, from very fundamental work on magnetism looking towards the digital world of the future, to research on energy materials closely related to pressing health problems.

To be ready for the challenges of the future, the ILL is currently engaged in an important modernisation programme. This programme encompasses the renewal of a large number of instruments and guides; further upgrading of our auxiliary services, including laboratories, sample environment and digital infrastructure; and major maintenance work on our neutron source. While carrying out all this important work, we will make sure that we provide our users with the maximum possible number of beam days. Successfully completed, these projects will make the ILL fit for the coming decade. In parallel, the ILL's Associates are working towards the signing of the 6th protocol of the ILL's intergovernmental convention, which will provide the contractual framework for operation of the ILL to the horizon of 2030.

Working towards a prosperous and fair society that does not put strain on our natural environment is a great reason to get up in the morning. Success will require the mobilisation of all available talent. At the ILL, we are determined to make it happen.

Helmut Schober

ILL Director



© N. Bohère

WHAT IS THE ILL



© L. Thion/Ecliptique

About the ILL

The Institut Laue Langevin (ILL) is an international research centre providing world-leading facilities in neutron science and technology. Neutrons are used at the ILL to probe the microscopic structure and dynamics of a broad range of materials at molecular, atomic and nuclear level.

The ILL operates the most intense neutron source in the world: a 58.3 MW nuclear reactor designed for high brightness. The reactor normally functions round-the-clock for four 50-day cycles per year, supplying neutrons to a suite of 40 high-performance instruments constantly maintained at the highest state of the art.

The ILL is owned by its three founding countries—France, Germany and the United Kingdom. These three Associate countries contributed some 67 M€ to the Institute in 2019, a sum enhanced by significant contributions from the ILL's Scientific Member countries—Austria, Belgium, the Czech Republic, Denmark, Italy, Poland, Spain, Slovakia, Sweden and Switzerland. The ILL's overall budget in 2019 amounted to about 101 M€.

As a service institute, the ILL makes its facilities and expertise available to visiting scientists. It has a global user community of around 2 000 researchers from almost 40 countries who come to work at the ILL every year. The 850 experiments they perform annually are pre-selected by a scientific review committee. Between 550 and 600 scientific papers are published annually following the treatment and interpretation of data obtained using our facilities. Of these articles, 168 were published in high-impact journals in 2019.

NEUTRONS AND SOCIETY

The scope of the research carried out at the ILL is very broad, embracing condensed matter physics, chemistry, biology, materials and earth sciences, engineering, and nuclear and particle physics. Much of it impacts on many of the challenges facing society today, from sustainable sources of energy, better healthcare and a cleaner environment, to new materials for information and computer technology.

PREPARING FOR THE FUTURE

To maintain its status as a leader in neutron science, the Institute has constantly upgraded its instruments, infrastructure and scientific equipment over the last 50 years. The latest modernisation—the Endurance programme—will continue to develop the Institute's instrumentation and support services with a view to maintaining its world-leading position for another decade at least. Endurance phase I is currently running, with a second phase anticipated to run between 2020 and 2023.

Why neutron scattering is useful

When used to probe small samples of materials, neutron beams have the power to reveal what is invisible using other forms of radiation. Neutrons can appear to behave as particles, waves or microscopic magnetic dipoles; with these very specific properties they can provide information that is often impossible to obtain using other techniques. Below are a few of the special characteristics of neutrons.

WAVELENGTHS OF TENTHS OF NANOMETRES

Neutrons have wavelengths varying from 0.01 to 100 nanometres. This makes them ideal for probing atomic and molecular structures, whether composed of single atomic species or complex biopolymers.

ENERGIES OF MILLI-ELECTRONVOLTS

The milli-electronvolt energies associated with neutrons are of the same magnitude as the diffusive motions of atoms and molecules in solids and liquids, the coherent waves in single crystals (phonons and magnons) and the vibrational modes in molecules. Any energy exchange, therefore, of between 1 μ eV (or even 1 neV with neutron spin-echo techniques) and 1 eV between the incoming neutron and the sample is easy to detect.

MICROSCOPICALLY MAGNETIC

Neutrons possess a magnetic dipole moment that makes them sensitive to the magnetic fields generated by unpaired electrons in materials. They therefore play an important role in investigating the magnetic behaviour of materials at the atomic level. In addition, as the neutron scattering effect of the atomic nuclei in a sample depends on the orientation of the spin of both the neutron and the atomic nuclei, neutron scattering techniques are ideal for detecting nuclear spin order.

ELECTRICALLY NEUTRAL

As neutrons are electrically neutral they can penetrate far into matter without doing damage. They are therefore precious allies for research into biological samples or engineering components under extreme conditions of pressure, temperature or magnetic field, or within chemical-reaction vessels.

HIGH SENSITIVITY AND SELECTIVITY

The scattering from nucleus to nucleus in a sample varies in a quasi-random manner, even for different isotopes of the same atom. This means that light atoms remain visible in the presence of heavy atoms, and atoms close to each other in the periodic table can be clearly distinguished. This makes it possible to use isotopic substitution in order to vary the contrast in certain samples and thus highlight specific structural features.

Neutrons are also particularly sensitive to hydrogen atoms and are therefore essential for research into hydrogen storage materials, organic molecular materials, and biomolecular samples and polymers.

ILL IN THE PRESS

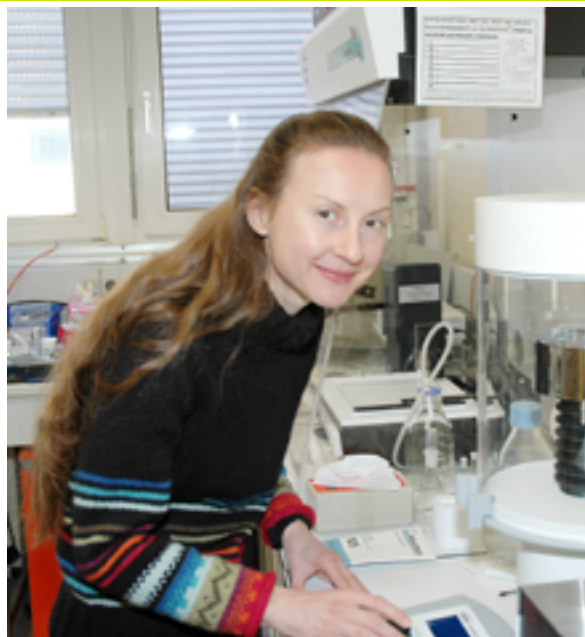
1. Isabelle Grillo
2. Published in *Nanowerk* on 27 September 2019
3. Published in *Laboratory News* on 19 August 2019

More articles at

<https://www.ill.eu/news-press-events/press-corner/ill-in-the-media/>

1. In memory of Isabelle Grillo

Isabelle passed away suddenly in her sleep at the beginning of August. She was a brilliant scientist, who joined the ILL at the tender age of just 25. In the space of two decades, she published some 225 articles, which have since been cited over 5 000 times. Her most recent article appeared in the prestigious journal *Nature Materials* the day before her funeral. She also performed a tremendous amount of experimental work, conducting around twenty experiments a year not just at the ILL but also at other institutes such as the LLB, ISIS and ESRF. As Mark Johnson pointed out, *'Isabelle, with her bright intellect, her smile and her openness, was truly committed to serving the ILL, our present and future users and the scientific community as a whole'*. We will cherish our memories of Isabelle.



2.

nano werk

Free Writing Tool
nano grammar, auto style and syntax
available for any writing

19 Aug 2019

Geometry goes viral: Researchers use maths to solve virus puzzle

Researchers have developed a new mathematical framework that changes the way we understand the structure of viruses such as Zika and Dengue.

The discovery by researchers at the University of York (UK) and San Diego State University (USA) opens the way for new insights into how viruses form, spread and what these forms and may eventually open up new avenues in anti-viral therapies.

Published in the journal *Nature Communications* (<https://doi.org/10.1038/s41467-019-10401-7>), the new theory accurately predicts the positions of atoms in the capsids of all known and yet-to-be-discovered for the first time. It simultaneously works for viruses that conform to ICH and for those that pose an unsolved problem to that theory.

The new mathematical framework changes the way we understand the structure of viruses such as Zika (Image: Prof Robert Terrence, University of York)

3.

laboratory news | Field | Sector | Dig

Home > Biology > Knowing a lot about very little

Knowing a lot about very little

19 Aug 2019

Share: [f](#) [t](#) [l](#) [e](#)

The potential of nanomedicine to tackle many diseases is immense, but we really don't know much about how they get into cells and what potential damage - as well as good - they could do. Here we learn why a combinatorial approach is set to change that...

The ability to manipulate and control a variety of nanoparticles has revolutionized science in the past three decades. From creating entirely new materials, to understanding the structures behind unusual scientific properties, the relatively new field of nanotechnology is being implemented into our daily lives and has massive potential for the future.

Nanoparticles are particles between 1 and 100 nanometres in size, and can be found naturally (for example as part of biological systems such as viruses or bone matrix) or can be artificially produced. They can range from carbon-based nanomaterials like fullerenes, to metal-based, such as silver and gold nanoparticles, nano-polymers, and composites of different nanomaterials. These are being used to engineer new materials and nanotechnologies across a variety of sectors.

4.

New Type of Electrolyte Could Enhance Supercapacitor Performance

From SciTechDaily: A new type of electrolyte could enhance supercapacitor performance, according to researchers at the University of California, San Diego. The researchers have developed a new type of electrolyte that could be used in supercapacitors to store energy. The new electrolyte is made of a porous material that allows ions to move through it more easily than traditional electrolytes. This could lead to supercapacitors that can store more energy and charge faster.

5.

Discovering new routes to cancer drug discovery with neutrons

From the world's flagship neutron science facility, Institut Laue-Langevin (ILL), Matthew Bakkelly shares insights into how they are harnessing the power of neutrons to aid their search for new cancer treatments.

By Matthew Bakkelly
July 2019

Understanding cancer – from anatomy to atomic

Cancer is the second most common cause of death worldwide, killing an estimated 9.6 million people in 2018. For understanding of cancer biology and treatment – both surgical and pharmaceutical – has progressed significantly over the last 100 years. Many theories have been proposed, but the scientific consensus is unclear.

6.

Ionisation energy of promethium fills one of the last holes in periodic table

From Chemistry World: The ionisation energy of promethium has been determined experimentally for the first time, solving an elusive 70-year-old mystery and filling in one of the final gaps in the periodic table. Promethium, element 61, only exists in trace quantities on Earth and can be synthesized through nuclear reactions. Scientists at the University of Mainz, Germany, used a laser to measure the ionisation energy of promethium, which is the minimum amount of energy required to remove an electron from a neutral atom. This is a significant achievement because promethium is highly radioactive and difficult to handle.

7.

Using diffraction to improve material understanding

From EngineerLive: Here José Antonio Alonso, Research Professor at the Instituto de Ciencia de Materiales de Madrid, C.S.I.C., outlines the benefits of neutron diffraction in understanding materials better. Progress towards developing sustainable energy solutions is becoming increasingly critical as concerns grow around the extent of carbon emissions released by burning fossil fuels – principally coal, oil and natural gas. The use of these fuels has led to an increase in greenhouse-gases, including carbon dioxide, which is contributing to human-induced climate change. The gradual increase in global temperatures is predicted to have major consequences – such as wreaking havoc on weather patterns and increasing the risk of floods and droughts, posing a major threat to agriculture. In the hunt for more efficient and sustainable energy solutions in future, researchers are turning to neutrons, neutral subatomic particles, to help unlock our understanding of how greenhouse-gases, fuels, and renewable sources interact with materials to develop more sustainable alternatives to our current energy cycle.

Revealing the inner workings of fuel cells and batteries

Hydrogen fuel cells have gained much attention in recent years as energy-conversion devices. Hydrogen is considered a more environmentally friendly alternative to fossil fuels. It can be produced in a more sustainable way – for example, by “splitting” water using the sun’s energy – whereas natural gas and oil extraction conversely can be highly damaging to the natural environment. Within a fuel cell, hydrogen can be used as a fuel, taking advantage of the energy released when it is electrochemically combined with oxygen.

4. Published in *SciTechDaily* on 14 August 2019
5. Published in *Drug Target Review* on 8 July 2019
6. Published in *Chemistry World* on 2 July 2019
7. Published in *EngineerLive* on 10 June 2019

ILL IN THE PRESS

8.

laboratory news | Field | Sector

Home > Biology > A sub-atomic solution

A sub-atomic solution

7 Jun 2019

Share: [Twitter](#) [Facebook](#) [LinkedIn](#) [Email](#)

Neurodegenerative diseases are becoming a major focus for an ageing population. Here we learn how neutrons are helping us understand the misfolded proteins thought to underlie many of these conditions.

The primary underlying cause of many of these degenerative conditions is the accumulation of misfolded proteins called amyloids.

The proteins themselves typically have a normal functional role but may be susceptible to abnormal denaturation that can lead to uncontrolled assembly of fibrils that aggregate in the body as plaques.

It has long been known that amyloid build-up in tissues throughout the body can cause major health problems, and may seriously compromise organ function in a wide range of diseases. However, the molecular mechanisms involved remain poorly understood. The toxicity effects at the root of amyloidosis are the focus of a great deal of research – ranging from studies of the precursor molecules of the plaques, to the amyloid assembly process itself, and the disruption caused to the correct function of membranes and the physical damage to the architecture of cells and tissues.

9.

nature physics

News & Views | Published: 29 April 2019

CONDENSED-MATTER PHYSICS

Antiferromagnetism with a twist

Elizabeth Blackburn

Nature Physics **15**, 625–626 (2019) | [Cite this article](#)

1941 Accesses | [15](#) Altmetric | [Metrics](#)

A variety of magnetic structures based around ferromagnetic spin spirals have been the topic of intense study over the past decade. The discovery of spin spirals that arise from antiferromagnetic order has just broadened the horizons for magnetic possibilities even further.

For any student delving deep into the physics of magnetism, it quickly becomes apparent that the standard textbook classification of magnetic materials as being either ferro- or antiferromagnetic rather undersells the sheer variety of magnetic structures that can exist in nature. A particularly relevant example concerns magnetic spiral structures: although

10.

PHYS.ORG

Home > Nanotechnology > Nanomaterials

Scientists explore the unknown behaviour of gold nanoparticles with neutrons

23 Apr 2019

Credit: ICI/Pablo Gomez

Nanoparticles of less than 100 nanometres in size are used to engineer new materials and nanotechnologies across a variety of sectors. Their small size means these particles have a very high surface area to volume ratio and their properties depend strongly on their size, shape and bound molecules. This offers engineers greater flexibility when designing materials that can be used in our everyday lives. Nanoparticles are found in sunblock creams and cosmetics as well as inside our bodies, as drug delivery vehicles and as contrast agents for pharmaceuticals. Gold nanoparticles are proving to be a next-generation tool in nanotechnology as an effective catalyst at such small dimensions. However, nanomaterials also pose a potential risk, as their interactions with living matter and the environment are not fully understood – meaning that they might not perform as expected, for instance in the human body.

11.

nature

NEWS | 15 APRIL 2019

How long do neutrons live? Physicists close in on decades puzzle

Researchers are narrowing down their measurements of subatomic particle survival on its own.

Researchers are narrowing down their measurements of subatomic particle survival on its own.

Researchers are narrowing down their measurements of subatomic particle survival on its own.

Physicists are drawing closer to solving long-standing mystery of the lifetime free-flying neutron lives.

Neutrons are electrically neutral particles that usually combine with protons to make up atomic nuclei. Some neutrons are not bound up in atoms: those free-floating neutrons decay radioactively into other particles in a matter of minutes.

But physicists can't agree on precisely how long a free neutron lives. Using one laboratory approach, they measure the average neutron lifetime as 880 seconds. Using a different approach, they get a smaller figure. The discrepancy has troubled researchers for nearly 50 years.

8. Published in *Laboratory News* on 7 June 2019

9. Published in *Nature Physics* on 29 April 2019

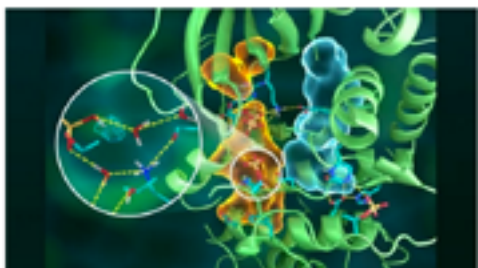
10. Published in *Phys.org* on 23 April 2019

11. Published in *Nature* on 15 April 2019

12.

Neutrons Paint Atomic Portrait of Protein Kinase A

news | 12 Mar 2019 | Original story from Oak Ridge National Laboratory



Read Time: 7 min

Direct observations of the structure and catalytic mechanism of a prototypical kinase enzyme – protein kinase A or PKA – will provide researchers and drug developers with significantly enhanced abilities to understand and treat fatal diseases and neurological disorders such as cancer, diabetes, and cystic fibrosis.

The discovery was made by an international team of researchers using macromolecular neutron crystallography at the Department of Energy Oak Ridge National Laboratory (ORNL) and the Institut Leva-Langevin (ILL) in Grenoble, France. Building on a decade-long investigation, the combined efforts revealed previously unknown characteristics of the archetypal protein kinase, including a complete map of the atomic structure and the underpinnings of the enzyme's chemistry used in cellular signaling. The details are published in the journal *Science Advances*.

13.



Cancer Research

Neutrons are Aiding the Fight Against Cancer

12/03/2018 | Author / Editor: Matthew Bakley* / Max Flatbush

Fig. 1. Examples of genetic mutations (source: medical news Europe)

The penetrative power of neutron beams, combined with their non-destructive nature, provides an ideal tool for analyzing chemical and biological material. Our knowledge of biological systems has evolved thanks to the increasing power of imaging techniques, which could have the potential to revolutionize drug target identification.

Cancer is the second leading cause of death globally, accounting for approximately one in six deaths: an estimated 9.6 million people in 2018. Our understanding of the types, treatments, and biology of cancer has exponentially grown over the last century, though the disease has been found in human remains dating back to 1500 BC. Many theories have been recorded over the past few centuries for why cancer might develop, including ideas of parasites, trauma, or chronic irritation leading to tumor development. In the 20th century, the elucidation of DNA structure and subsequently the discovery of oncogenes and tumor suppressor genes opened our eyes to the endless potential causes of cancer, with scientific and technological advances in imaging enabling this

14.

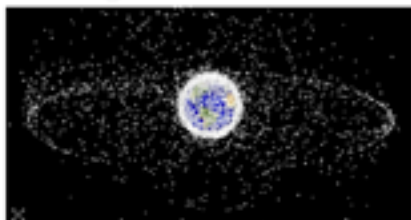
physicsworld

everyday science

EVERYDAY SCIENCE | NEWS

Satellites barely evade collision, stars are born in Van Gogh's work, and scientists experiment with limoncello

15 Feb 2018 Kim Taylor



Orionid space debris striking Earth, January 2018

A couple of weeks ago the actual satellite company *Esprit* was alerted that another craft was on a high-speed collision course with their payload. Great. Mission-critical items were urgently sent to the satellite and the crisis was averted, although the two objects will pass each other very close.

Space may be great and cool but it's getting crowded closer to Earth. According to the *Turkish Aerospace Industries* (TAI), more than 25,000 large pieces of debris are orbiting our planet – and many more smaller bits besides. And as satellite numbers, such as the one that this past month, often don't have propulsion systems to help them avoid impact, the risk of these numbers growing is increasing.

You can find out more about orbital debris on the *ESA* website.

15.

welt

WISSEN

FORSCHUNG

Forscher lüften das Geheimnis des Limoncello

Veröffentlicht am 01.01.2019 | Lesedauer: 2 Minuten

Von Robert Lohse



Limoncello schmeckt nicht nur gut, sondern auch milde. Warum liegt das? Ein Berliner Forscher hat es untersucht – und festgestellt, dass die physikalischen Eigenschaften sogar Einfluss auf den Geschmack haben.

Der italienische Likör Limoncello ist knallgelb, aber auch milde. Warum liegt das? Ein Berliner Forscher hat es untersucht – und festgestellt, dass die physikalischen Eigenschaften sogar Einfluss auf den Geschmack haben.

12. Published in *Phys.org*
on 20 March 2019

13. Published in *Lab Worldwide*
on 12 March 2019

14. Published in *Physics World*
on 15 February 2019

15. Published in *Welt*
on 1 January 2019

More articles at

<https://www.ill.eu/news-press-events/press-corner/ill-in-the-media/>

SCIENTIFIC HIGHLIGHTS

The scientific highlights presented in this annual report demonstrate how research with neutrons continues to push back the frontiers of science.

- 14** COLLEGE INTRODUCTIONS
- 16** MAGNETISM
- 28** MATERIALS SCIENCE
- 38** CHEMISTRY AND CRYSTALLOGRAPHY
- 44** SOFT CONDENSED MATTER
- 56** BIOLOGY AND HEALTH
- 62** NUCLEAR AND PARTICLE PHYSICS
- 68** THEORY

549 

ILL PUBLICATIONS RECORDED IN 2019
OF WHICH **168** PUBLISHED IN HIGH-IMPACT JOURNALS



19 PRESS RELEASES
WERE PRODUCED IN
2019, LEADING TO
34 ARTICLES IN
THE GENERAL PRESS



KEEP **UP-TO-DATE:**

 facebook.com/ILLGrenoble

 twitter.com/ILLGrenoble

 linkedin.com/company/institut-laue-langevin

THE USER community was at the heart of the project to build the ILL more than 50 years ago. While the success of the ILL still depends on the user community today, in many cases this is a vibrant partnership of co-creation, as illustrated by the scientific highlights in this section of the AR.

Scientific output is the main deliverable of our activity. However, there are striking examples of the partnership up-stream in the scientific process.

Neutron imaging is a new activity at the ILL, developed in collaboration with the Université Grenoble-Alpes (UGA). A state-of-the-art instrument providing *in situ* X-ray imaging has been developed and has already attracted a new user community to the ILL. In view of this success, in 2020 the instrument will transition to a public ILL instrument and the partnership with UGA will be extended to include Helmholtz-Zentrum Berlin (HZB) and their considerable expertise.

In situ X-ray techniques are also being developed on the D22 SANS instrument in collaboration with the University of Erlangen. Lab X-ray sources are comparable in flux to the neutron beams at the ILL, allowing a unique SAXS/SANS combination for probing sensitive systems and processes such as the cycling of electrochemical cells (batteries).

The same university was a key partner in developments on the backscattering spectrometer IN16B and in particular, the BATS time-of-flight option, which extends the energy range of the spectrometer by about one order of magnitude. This option involves novel, variable-focusing guide sections, which have been funded through the University of Tübingen, and will fully optimise the performance of the BATS mode.

At the ILL, we are also investing in ancillary equipment to make the most efficient use of beamtime and support new science. The single-crystal, X-ray diffractometer is now operational and will be used in conjunction with neutron diffraction experiments. An electrochemical lab for battery research has been installed in level C of the reactor and features, for example, a dedicated glove box and a battery-cycling device funded by the University of Amiens.

Battery research, as mentioned in the Director's forward, is of growing importance. The ILL, along with the ESRF, has joined a large consortium of academic and industry partners to submit a European project within the scope of the Battery 2030+ initiative. When funded, this project will give neutrons a clear and important role in battery research.



An already funded European project, InnovaXN (www.innovaxn.eu), involving the ILL and the ESRF, is also industry-oriented and, in a number of cases, battery-oriented. InnovaXN is an MSCA COFUND programme supporting 40 PhD positions on projects that must have an industry partner, offering at least three months of training for each PhD project. Twenty projects have been selected from 60 expressions of interest and the recruitment of students is now underway. There will be a second call for projects in 2020.

An important event in 2019 was the 'Artificial Intelligence workshop' in Grenoble, organised with the ESRF and the STFC. The rapid development in these data techniques led us to bring together experts in the field and instrument scientists to explore how the techniques could be used both to optimise instrument configuration and use and to guide less experienced users towards the most appropriate solutions in data analysis. This is timely, given that about 60 % of ILL users over any five-year period are new users.

The user community needs a continuous supply of new users. To this end, a number of outreach events have been organised in the context of the FILL2030 project (www.fill2030.eu – see p.110) e.g. in Ireland, Romania and Portugal in 2019. In 2020, we are looking forward to events in Israel, with ESS, and in Norway.

Finally, the ESS–ILL user meeting in Grenoble in 2018 with its 500+ participants was a clear measure of our vibrant community and partnership. In September 2020, the event will be repeated in Lund, led by the ESS—everyone is welcome!

Mark R. Johnson

Associate Director,
Head of Science Division

COLLEGE INTRODUCTIONS

COLLEGE 1 – APPLIED MATERIALS SCIENCE, INSTRUMENTATION AND TECHNIQUES

S. Cabeza (College 1 secretary)

College 1 deals with applied physics and new instrumentation techniques in neutron scattering. The main areas covered are metallurgy, applied neutron scattering, cultural heritage, new neutron-scattering techniques, instrumentation and scientific computing. This college hosts proposals from a diverse user community ranging from polymer scientists to metallurgists and nuclear physicists.

Neutron strain characterisation on SALSA accounted for around half of all the proposals submitted in 2019, and neutron-imaging studies will continue in 2020 with NeXT.

Batteries and metal additive manufacturing remain hot topics for neutron investigations, with both *in situ* and *in operando* experiments in these areas being popular. The ILL is committed to supporting this kind of work and has provided new set-ups and methodological improvements in the last year. Important contributions to the nuclear physics community have also been achieved recently, with studies on the double-differential neutron cross section of compounds for new, very-cold-neutron moderators, for example. In addition, spatial resolution and near-surface characterisation at SALSA is gaining attention, while the first stroboscopic measurements studying plasticity in high-cycle fatigue tests have also been successful.

The ILL's efforts over recent years to reach out to the materials science and engineering community have resulted in increasing interest in our techniques and the arrival of new users. Many of College 1's proposals include industry-related topics and collaboration with industry.

COLLEGE 2 – THEORY

N. Garcia (College 2 secretary)

College 2 covers three areas of science: soft matter, electronic structure and magnetism. The Theory Group delivers independent and highly advanced research on these topics while continuously benefitting from collaborations with experimentalists inside and outside the ILL. The College has a strong tradition of hosting visiting scientists working on topics such as geometrically frustrated and strongly correlated magnetism, the impact of human mobility on the spread of disease, coarse-graining of bovine serum albumin and polymer nanocomposites.

This year, some members of the group have been involved in neutron experiments at the ILL and at external labs in Europe and beyond. Others have provided theoretical input for local experiments, illustrating our desire to ensure a strong theoretical background to the interpretation of experimental data.

It has, therefore, been an exciting year for ideas and interaction. Our three postdocs are reaching the end of their time with the Theory Group and others will soon be arriving. Thus, we look forward to 2020, to the start of new projects and to the pursuit of those currently showing good promise.

COLLEGE 3 – NUCLEAR AND PARTICLE PHYSICS

C. Michelagnoli (College 3 secretary)

College 3 is dedicated to nuclear and particle physics research. In 2019, STEREO moved on to data-taking phase 3; this follows refinement of the analysis of data from phase 2 and submission of a detailed paper on oscillation analysis in relation to improving constraints on a hypothetical sterile neutrino. In addition, PERKEO was installed at PF1B, with considerable support from several of the ILL's technical services, while measurements of the Fierz interference term from the beta spectrum of unpolarised neutrons began and data is now being collected.

LOHENGRIN saw another successful fast-timing campaign, with several experiments measuring the lifetimes of excited nuclear states down to below 10 ps. Various types of diamond were also studied as fission fragment detectors; this is particularly important for the FIPPS fission campaigns. Furthermore, a number of experiments were performed on FIPPS using additional HPGe clovers from IFIN-HH, including a ^{233}U fission run with active target and the first experiment using a 2 GBq radioactive ^{63}Ni target (to shed more light on shape isomerism in light nuclei).

COLLEGE 4 – MAGNETIC EXCITATIONS

L. Mangin-Thro (College 4 secretary)

College 4 is dedicated to inelastic neutron scattering studies in magnetic compounds. A healthy number of proposals were received in 2019, with a significant increase in the second round. The proposals were well distributed over all the spectrometers designed for magnetic excitations, with the usual heavy demands on magnetic frustration, quantum magnetism and superconductors being observed. The actual trend, however, is towards ever more sophisticated set-ups. For the first time in several years a measurement requiring high pressure to study a quantum phase transition was proposed. It should be noted that there were also new proposals on molecular magnets—a very strong topic for College 4 in the past.

The thermal time-of-flight spectrometer PANTHER is now available, and the first commissioning experiments will study powder samples. In subsequent rounds, proposals with single crystals and various sample environments, including dilution fridges and magnets, will be investigated.

COLLEGE 5A – CRYSTALLOGRAPHY

O. Fabelo (College 5A secretary)

College 5A focuses primarily on fundamental science, including crystallographic studies using crystalline materials. The College uses both powder and single-crystal materials. The main objective of the experiments carried out in 2019 was to investigate the correlation between crystal structures and physical properties. Neutron techniques provide unique opportunities for determining the structural features underlying the physical properties of crystalline materials and property–material relations.

Over the last year, College 5A studied hydrogen storage materials, ionic conductors (cationic and anionic), superconductors, catalysts, shape-memory materials, high-voltage battery materials, crystal structure determination in inorganic materials, pharmaceutical compounds, hybrid materials and co-ordination polymers. More recent calls for proposals reveal a noticeable interest in materials for energy applications, including batteries and photovoltaic materials.

Our user community includes chemists as well as solid-state and condensed-matter physics researchers, originating for the most part from the ILL member countries. We should, however, stress the international character of our research teams, reflecting a well-established neutron network across international laboratories. As for ILL instruments, College 5A uses a broad range, most of them diffraction-related and showing a trend towards non-conventional conditions.

COLLEGE 5B – MAGNETIC STRUCTURES

A. Velamazán (College 5B secretary) and T. Saerbeck (focus group secretary)

College 5B is dedicated to the investigation of magnetic structures by means of powder or single-crystal diffraction, small-angle neutron scattering (SANS) and reflectometry. These include polarised neutron techniques that regularly produce results, as can be seen yet again in this year's Highlights. Frustrated magnets (including pyrochlores), triangular lattices and quantum-spin liquids continue to attract strong interest, while studies on low-dimensional magnetism have been gaining momentum recently. Multiferroic materials also remain among the most popular subjects. Other frequently investigated topics include superconductors, topological materials (Weyl semi-metals), intermetallics, spin-orbit coupled materials, multipolar orders and molecular magnets.

Both SANS and reflectometry feature strongly in the above-mentioned materials investigations. The main interest of the SANS community continues to be the study of skyrmion-hosting materials, although other topics include superconductivity and magnetic nanoparticles. Reflectometry studies investigate the magnetic properties of materials in the form of thin films and heterostructures, with a significant number of proposals looking at proximity effects at multiferroic oxide interfaces.

COLLEGE 6 – STRUCTURE AND DYNAMICS OF DISORDERED SYSTEMS

M.M. Koza (College 6 secretary)

In recent years, the request for beamtime in College 6 has resembled a rollercoaster ride. Subcommittee meeting after subcommittee meeting, low demand has alternated with all-time highs. The year 2019 was no exception to this persistent cycle. Of no exception either, was the very high quality of the proposed studies. A steadily increasing number of proposals demanding high pressures, polarisation capabilities, magnetic fields, multiple instruments and protocols with the simultaneous application of complementary techniques serves to underscore this point.

In addition, the scientific focus has shifted further, onto complex matter and materials. Interest in the structure and dynamics of molecular liquids, liquid alloys, molten salts, and confined and porous systems outranked attention directed at monatomic samples and glassy and amorphous compounds.

The growing technical and scientific complexity of the studies being proposed is nicely represented by the highlight of the autumn proposal round: a study seeking to understand the effect of high magnetic fields on the dynamic properties of magnetic ionic liquids—made possible by the recent implementation of a high-field magnet at IN5.

COLLEGE 7 – SPECTROSCOPY IN SOLID STATE PHYSICS AND CHEMISTRY

T. Weber (College 7 secretary)

College 7 deals with non-magnetic spectroscopy in solid-state systems, covering a broad range of topics that includes the determination of phonon dispersion relations and densities of states, phonon-softening effects due to anharmonic interactions, and structural and orbital-ordering phase transitions. Further topics include ionic relaxation and diffusion, as well as the dynamics of molecular and physio-/chemisorbed systems.

While College 7 has a wide variety of cold- and thermal-neutron spectrometers and diffractometers at its disposal, in the recent proposal

round most days of beamtime were awarded for experiments at the high-flux, thermal-neutron, three-axis spectrometer IN8, the time-of-flight spectrometers IN6-SHARP and IN5, the high-resolution spin-echo instrument IN11 and the IN1-LAGRANGE spectrometer. The complexity of both the investigated systems and the instrumental resolution functions typically require sophisticated theoretical models and data analysis tools. Assistance in these fields can be provided by the ILL's Theory and Scientific Computing groups.

COLLEGE 8 – STRUCTURE AND DYNAMICS OF BIOLOGICAL SYSTEMS

N. Coquelle (College 8 secretary)

College 8 focuses on biological molecules, using a large palette of techniques and instruments to unravel molecular structures and link these to their functions and/or dynamics. Neutron crystallography (D19, LADI and soon DALI) provides a technique for visualising hydrogen/deuterium protein atoms and understanding their catalytic mechanism or their mode of recognising small molecules. Studies in solutions are performed using our unique set of SANS machines (D11, D22 and D33). Signals from a molecular type (DNA vs protein or lipids vs protein for example) can be masked out using deuteration.

Reflectometers (Figaro, D17) and the diffractometer D16 are excellent instruments for studying the properties of bio-mimicking surfaces (model lipidic bilayers) and the mode of interaction or the type of modification triggered by specific macromolecules on these lipidic surfaces. Finally, the neutron spectrometers IN15, IN13 and IN11 are used to gain insight into the dynamics of these biological systems over a large range of time and q .

There are several laboratories available on the EPN campus to facilitate sample preparation, including the D-lab for the perdeuteration of biological molecules and the EMBL biology laboratories for specific operations. The PSB platform and the PSCM offer a large variety of complementary techniques to further characterise samples.

COLLEGE 9 – SOFT CONDENSED MATTER

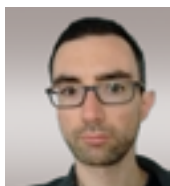
S. Prevost (College 9 secretary) and A. Maestro (focus group secretary)

College 9 covers the vast field of soft condensed matter, studying the architecture of complex fluids at the nano- to micrometre scales, its evolution with time-resolved experiments under various stresses, and the related dynamics. Over the last few proposal rounds we have observed growing demand for interfacial studies.

Our users benefit from the support of the PSCM for complementary measurements. Additionally, the SMSS offers an increasing number of techniques and sample environments that can be used both *ex situ* and *in situ*, such as the DLS currently commissioned for SANS, the automatic suite for adsorption and Langmuir troughs which increase performance and turnover in reflectometry, and the combined humidity, pH and pressure cell for both SANS and NR.

Many LSS instruments will benefit from the on-going Endurance Phase 2 programme, which will bring about the renewal of H15 including a full upgrade of D11 and new detectors for D11 and D22; as well as the D50/NeXt overhaul, which will bring imaging capabilities to the ILL, boosting the opportunities for College 9's users. The TOF instruments are more and more in demand from College 9 proposers, reflecting the importance of dynamics in relation to structure in colloids.

More information on the support facilities cited can be found on p.106.



Tom Fennell. British

Laboratory for Neutron Scattering,
Paul Scherrer Institute, Switzerland

'I study frustrated magnets, especially pyrochlores, using diffuse and inelastic neutron scattering. I am interested in the description of such systems by emergent field

theories and the exploration of new material properties, such as unconventional correlations and dynamics that are highlighted by this approach.'

Multiple Coulomb phase in the fluoride pyrochlore CsNiCrF_6

Three-axis spectrometer ThALES

In this study we investigated CsNiCrF_6 , a pyrochlore in which both structural and magnetic correlations can be identified as Coulomb phases: a charge ice and an antiferromagnetic Coulomb phase respectively. As far as we can determine, neither has been observed independently before. However, the combination is particularly interesting as it affords the possibility of studying not only structural or magnetic frustration but also their interplay.

AUTHORS

T. Fennell (Paul Scherrer Institute, PSI, Switzerland)
M. Boehm and P. Steffens (ILL)

ARTICLE FROM

Nat. Phys. (2019)—doi: <https://doi.org/10.1038/s41567-018-0309-3>

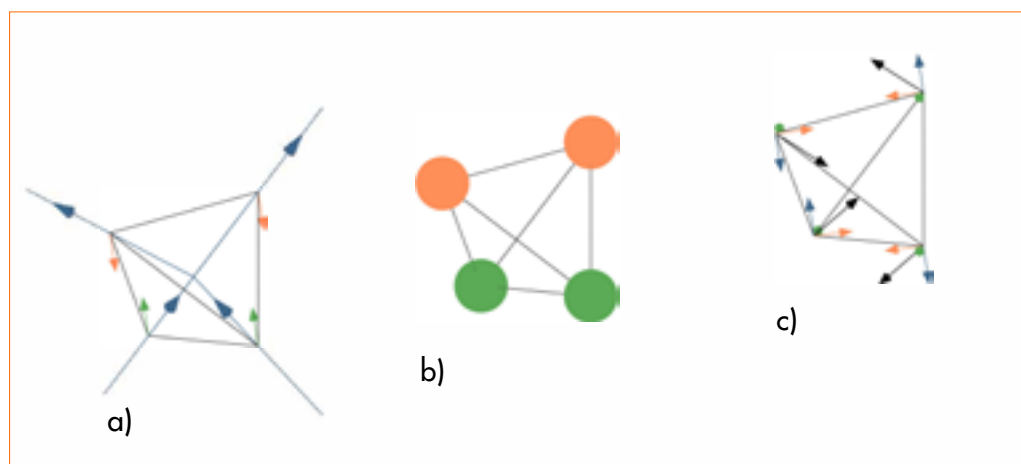
REFERENCES

- [1] C.L. Henley, Ann. Rev. Cond. Mat. Phys. 1 (2010) 179
- [2] S.T. Banks and S.T. Bramwell, EPL 97 (2012) 27005
- [3] P.H. Conlon and J.T. Chalker, Phys. Rev. Lett. 102 (2009) 237206
- [4] T. Fennell *et al.*, Nat. Phys. 15 (2019) 60

A Coulomb phase [1] is a state of matter in which the correlations of local degrees of freedom can be described by a non-divergent field (**figure 1**). Many systems can support Coulomb phases, including dimer models, ice models, correlated structural disorder and spin systems. Rather than long-range order, characterised by an order parameter and broken symmetry, or exponentially decaying short-range order, a Coulomb phase is critical with correlations that decay as a power-law ($1/r^3$ for three-dimensional examples). Coulomb phases are therefore of interest in the study of emergent, many-body physics and unconventional phase transitions: the former aspect derives from identification of the low energy states of the Coulomb phase with a free field in a vacuum, whose cooperative fluctuations are one type of dynamics of the system and in which fractional quasiparticle excitations that are the charges of the relevant field may be created/annihilated (and also give rise to dynamics); the latter aspect stems from the form of the correlations, which means that phase transitions out of a Coulomb phase will often fall outside the Landau–Ginzburg–Wilson paradigm.

Some of the most studied examples are spin systems, including spin ice and the pyrochlore Heisenberg antiferromagnet. Spin ice can be associated with the question of distributing two types of cation (*i.e.* with different charges) on the pyrochlore lattice. To minimise the energy of the structure, the cations should obey the condition that there are two of each type on every tetrahedron of the pyrochlore lattice—an example of an ice rule. This structure, a so-called charge ice, is interesting in the sense that it is a crystalline solid that hosts a fascinating type of disorder. The cations are disordered but not random—a form of correlated disorder whose simple underlying motif gives rise to non-trivial correlations.

CsNiCrF_6 is a candidate charge ice, since Ni^{2+} and Cr^{3+} jointly form the pyrochlore lattice. However, it has a further interesting feature in that both cations are magnetic and no magnetic order is observed, even far below the Curie–Weiss temperature. Despite the destruction of the high symmetry of exchange interactions in the pyrochlore lattice by the correlated disorder, a frustrated spin system is still obtained. The average structure of CsNiCrF_6 is a pyrochlore with Ni^{2+} and Cr^{3+} jointly distributed on the pyrochlore lattice (Vivaldi, ILL and TRiCS (now Zebra), PSI). However, separation of structural and magnetic correlations using polarised diffuse neutron scattering (D7, ILL) shows that both structural and

**Figure 1**

Coulomb phases on the pyrochlore lattice.

a) The ice rule (2-in/2-out) obeying spins of a spin ice on the pyrochlore lattice (tetrahedron) and fluxes of a lattice vector field on the bonds of the diamond lattice (tetrahedron centres) are in direct correspondence and connect simply with an ice rule for an Ising antiferromagnet on the pyrochlore lattice (2-up/2-down).

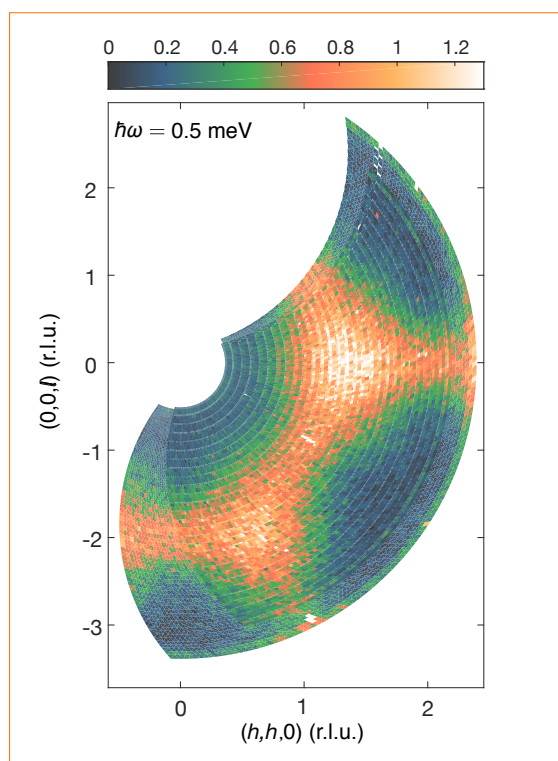
b) The cations of a charge ice map onto the spins of the Ising antiferromagnet.

c) In a pyrochlore Heisenberg antiferromagnet, any configuration in which the spins on a tetrahedron sum to zero is a ground state; all such states can be characterised by three families of Ising pseudo-spins, one for each component of the vector spins, simultaneously satisfying their ice rule. All these systems are Coulomb phases and all have the same underlying correlation functions encoded by the ice rules.

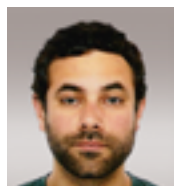
spin degrees of freedom have power-law correlations, as shown by the presence of pinch points in the diffuse scattering. Our numerical model of the structural diffuse scattering suggests that both a cation charge ice and anion displacement ice are present.

The presence of a magnetic Coulomb phase in the presence of such structural disorder is not completely unexpected—the simplest model of a magnetic charge ice has such a phase [2]. However, antiferromagnetic Coulomb phases on the pyrochlore lattice are few and far between. Thus, it is interesting to compare the magnetic dynamics with those of the pyrochlore Heisenberg antiferromagnet, which has been studied theoretically in considerable detail [3]. Inelastic neutron scattering measurements on the ILL spectrometer ThALES show that there is a connection. The pinch point structure factor of the diffuse scattering appears again at finite energy transfer, as expected, albeit with broadened pinch points (**figure 2**). Measurement of the wavevector dependence of the width and the energy of the inelastic response shows further elements of the theory of an ideal antiferromagnetic Coulomb phase: quasi-elastic scattering with identical width and linear temperature dependence appears at generic points on the structure factor, as expected for the relaxational dynamics of magnetic charge fluctuations (though due to the continuous spins, the monopoles of this system are not discrete quasiparticles as they are in spin ice); a weakly dispersive broad feature (a type of spin wave or fast dynamics of the correlated disordered structure) appears along nodal lines joining the pinch points, also as predicted.

In conclusion, diffuse and inelastic neutron scattering experiments provide considerable information about the structural and magnetic correlations and magnetic dynamics of CsNiCrF_6 . Despite the structural disorder, the magnetic dynamics show features of an ideal model frustrated antiferromagnetic Coulomb phase, suggesting a universality in the emergent dynamics of such systems. Further details can be found in [4].

**Figure 2**

Magnetic Coulomb phase dynamics in CsNiCrF_6 measured at ThALES (with FlatCone analyser) at 1.5 K.



Navid Qureshi. French

The ILL

'After finishing my PhD thesis at the ILL in 2008, I returned as an instrument scientist in 2014. My main research fields are frustrated magnetism, multiferroic materials and chiral structures, which I study using polarised neutrons and spherical neutron polarimetry in particular.'

Proof of the elusive high-temperature incommensurate phase in CuO by spherical neutron polarimetry

Spin-polarised diffractometer D3

CuO is a magnetic system that has been extensively investigated for more than 30 years [1, 2] as a building block of high-temperature superconductors. It is the only known binary multiferroic compound to date and has a high transition temperature (230 K [1]) into the multiferroic state. Compared with other prototype multiferroic materials it has close analogies with the sequence of magnetic phase transitions and the nature of the phases involved. However, the nature and even the existence of the high-temperature incommensurate—the so-called AF3—phase has been strongly debated, both experimentally and theoretically. Here, we present the first neutron scattering study in more than three decades able to overcome the difficulties of observing this phase, which includes a very small ordered magnetic moment ($\sim 0.06 \mu_B$) and a stability range of only 0.5 K below an elevated T_N .

Figure 1

Polarisation matrix elements as a function of temperature clearly revealing the magnetic phase transitions.

AUTHORS

N. Qureshi (ILL)
 E. Ressouche (Grenoble University UGA and CEA, Grenoble, France)
 A.A. Mukhin (Russian Academy of Science, Moscow, Russia)
 M. Gospodinov (Bulgarian Academy of Sciences, Sofia, Bulgaria)
 V. Skumryev (University of Barcelona and Institutó Catalana de Recerca, Barcelona, Spain)

ARTICLE FROM

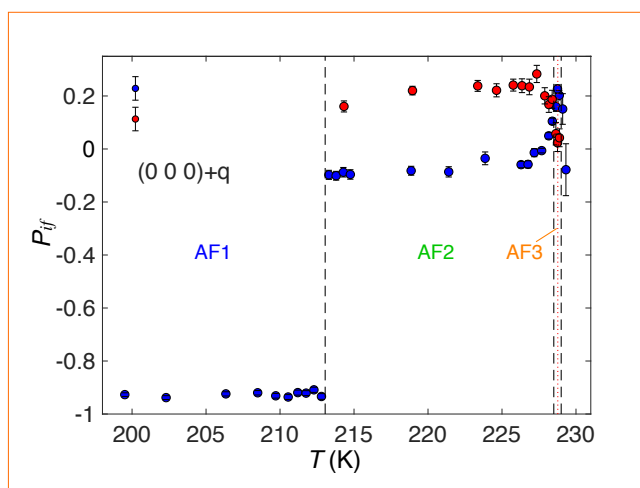
Submitted to Science Advances

REFERENCES

- [1] J.B. Forsyth, P.J. Brown and M.B. Wanklyn, *J. Phys. C. Solid State Phys.* 21 (1988) 2917
- [2] B.X. Yang *et al.*, *Phys. Rev. B* 39 (1989) 4343
- [3] N. Qureshi, *J. Appl. Cryst.* 52 (2019) 175

The key to our success was the use of spherical neutron polarimetry, which is extremely sensitive to the direction of magnetic moments and yields conclusive results with just a few magnetic Bragg peaks. By analysing the neutron spin after the scattering process with different initial polarisation directions one can deduce the three-dimensional rotation and eventual (de)polarisation of the neutron spin, which is summarised in the *polarisation matrix*.

Using this technique, we first confirmed the extensively studied magnetic structures in the AF1 and AF2 phases. Then, by following specific polarisation matrix elements—which are susceptible to change in the magnetic structure—as a function of temperature, we found unambiguous proof of the existence of the elusive AF3 phase in CuO, as shown in **figure 1**. In the chosen geometry with the sample's *b*-axis mounted vertically, the P_{yy} element is -1 if the magnetic moment is aligned along *b* and +1 if it is in the *ac* plane. The abrupt change in P_{yy} at 213 K is indicative of the first-order magnetic phase transition from the commensurate collinear AF1 structure to the incommensurate helical structure AF2 (see **figures 2a** and **2b**, respectively). Note that the non-zero P_{xy} term in the AF2 phase states that there is an imbalance between



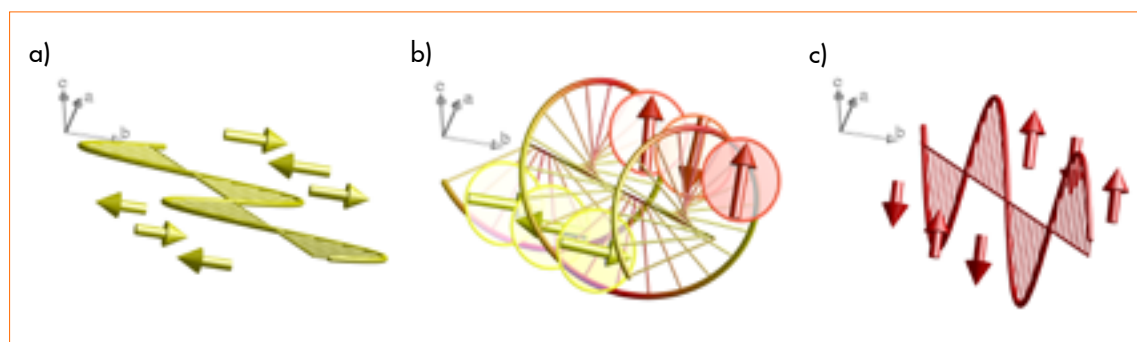


Figure 2

Magnetic structures in CuO: **a)** the AF1 phase, **b)** the AF2 phase and **c)** one of the spin-density wave structures which, together with a), represents the AF3 phase.

the two chiral domains, *i.e.* between a left-handed and a right-handed rotation of the helix. At approximately 227 K the P_{yy} term starts to rise and saturates at a plateau of ~ 0.2 at 228.8 K before it drops to zero at 229.3 K, which is already above the Néel temperature. Both the change in P_{yy} and the stability range are clear proofs of the existence of the AF3 phase in CuO. The disappearance of the P_{xy} term suggests a non-chiral magnetic structure.

We derived the magnetic structure of the AF3 phase by analysing polarisation matrices taken on different magnetic Bragg reflections using the *Mag2Pol* programme [3], based on representation analysis and on the correct description of up to four magnetic domains resulting from the successive breaking of symmetry elements via the group-subgroup relation. Surprisingly, and in contrast with other prototypical multiferroics, our data suggest the coexistence of two spin-density wave structures (shown in **figures 2a** and **2c**), each modulated by a different irreducible representation. The moment directions coincide with the main axes defining the helical structure at lower

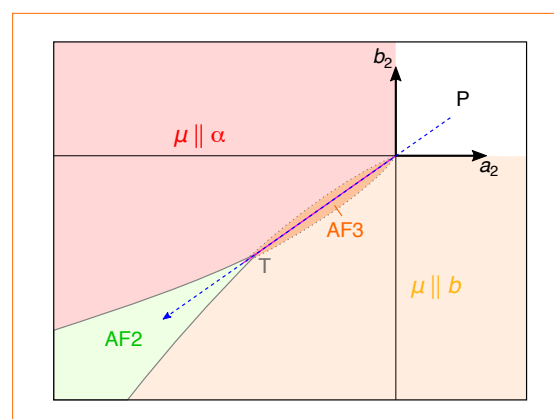
temperatures (**figure 2b**). The accidental degeneracy of two order parameters implies a delicate energy balance in the spin Hamiltonian.

We analysed the possible magnetic states and the phase transitions between them on the basis of Landau theory by minimising the thermodynamic potential, which was expanded up to the eighth degree with respect to the order parameter. For a particular set of temperature-dependent coefficients we derived a magnetic phase diagram defined in the parameter space of the two temperature-dependent coefficients a_2 and b_2 (related to quadratic terms of the order parameters), corroborating our experimental finding that the Néel point can be regarded as a multicritical point (see **figure 3**).

This study contributes unique information at an atomic level concerning the AF3 phase and the magnetic anisotropy in CuO, which was a missing piece of the puzzle of the complex behaviour of magnetic phases in this extensively studied multiferroic compound.

Figure 3

Theoretical phase diagram in the parameter space of temperature-dependent coefficients a_2 and b_2 . A multicritical Néel point with a degeneracy of two phases is indeed possible.





S.W. Lovesey. British
ISIS & Diamond Light Source Ltd,
Harwell Campus, UK

'I completed one of two apprenticeships. At 17 years I downed tools and took off my work overalls. Seven years later I was permanent staff in John Hubbard's group (the eponymous

Hamiltonian was published) equipped with an Oxford D.Phil. Shortly thereafter, I co-authored a monograph on neutron scattering. Aside from work on venture capital projects, and studies at the Harvard Business School, I have worked as a theoretical physicist at various universities and institutes.

Direct observation of anapoles by neutron diffraction

Spin-polarised diffractometer D3

Understanding magnetism at an atomic level of detail remains a great intellectual challenge, alongside parity violation and the homochirality of life, for example [1]. Knowledge about magnetic materials is vital for their use in machines and devices ('*You were not made to live like brute beasts, but to pursue virtue and knowledge*' — Dante's *Inferno*, Canto XXVI). Magnetic neutron scattering is a puissant tool for the experimentalist, and more so with our demonstration that neutrons are scattered by anapoles. They are dipoles in a church of Dirac multipoles; the elementary Dirac monopole—yet to be observed—possesses identical discrete symmetries to those of the electronic multipoles in question, namely, magnetic and polar ones.

AUTHORS

S.W. Lovesey, D.D. Khalyavin and G. van der Laan (ISIS & Diamond Light Source Ltd, Harwell Campus, UK)

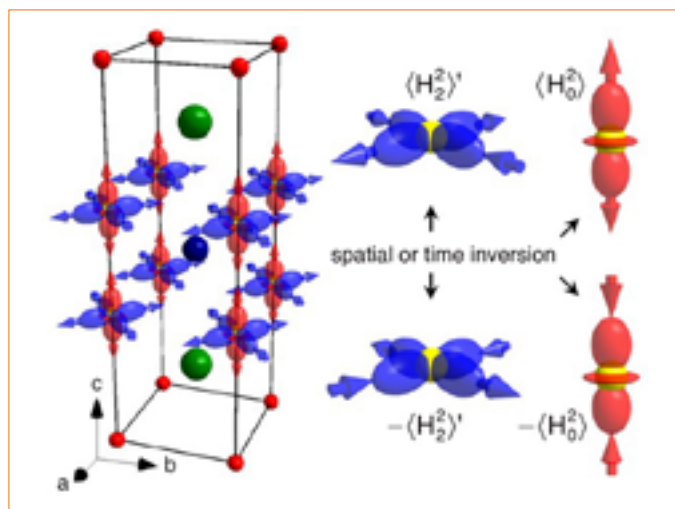
ARTICLE FROM

Phys. Rev. Lett. (2019)—doi: <https://doi.org/10.1103/PhysRevLett.122.047203>

REFERENCES

- [1] A. Doría-Urra and P. Bargeño, *Symmetry* 11 (2019) 661
- [2] P. Bourges *et al.*, *Phys. Rev. B* 98 (2018) 016501
- [3] S.W. Lovesey and D.D. Khalyavin, *J. Phys. Condens. Matter* 29 (2017) 215603
- [4] M. Fechner *et al.*, *Phys. Rev. B* 93 (2016) 174419

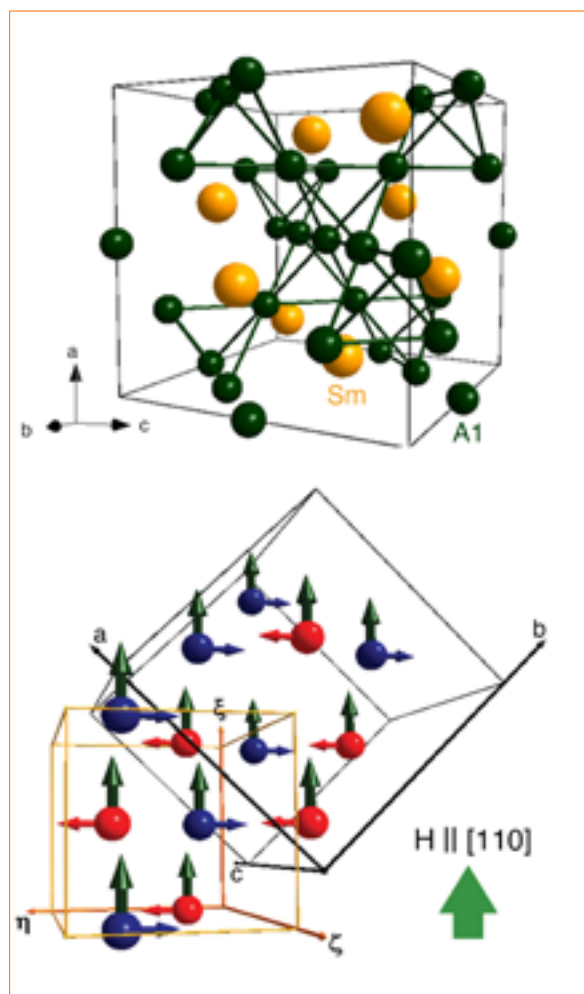
An anapole was studied by Zel'dovich in the course of investigating parity-violating interactions in electromagnetic theory. Parity violation in atomic and molecular systems with the observation of electronic anapoles can be traced back to 1974 [1]. Our direct observation by neutron diffraction makes a profound statement about the electronic properties of high- T_c superconductors, on which there is no consensus of opinion. The pseudo-gap phase of these materials probably holds the key to understanding the superconducting state. Does the pseudo-gap phase possess magnetic structure? Many neutron diffraction experiments provide evidence of long-range magnetic order in a variety of ceramic superconductors [2]. However, it is not conventional magnetic order, for this eludes detection by standard laboratory techniques; nor is it the antiferromagnetism predicted by Laughlin. Added to this, the detection of magnetic order by neutron diffraction in one ceramic compound, YBCO, has recently been challenged [2]. Set against this challenge, Dirac multipoles provide a comprehensive interpretation of the entire diffraction pattern obtained for the ceramic superconductor Hg1201, which is simpler than YBCO in having one Cu-O plane rather than two [3]. This result, that magnetic order in Hg1201 is a motif of Dirac quadrupoles (quantities $\langle H^k_Q \rangle$ in **figure 1**), occurs in a simulation of the electronic structure and Dirac quadrupoles [4].

**Figure 1**

Ferro-motif of Dirac quadrupoles in the Cu–O plane for Hg1201 in the pseudo-gap phase [3]. Arrows indicate spin (S) directions in Dirac quadrupoles $\langle H_0^z \rangle' \propto \langle 3S_z n_z - \mathbf{S} \cdot \mathbf{n} \rangle$ and $\langle H_2^z \rangle' \propto \langle S_x n_x - S_y n_y \rangle$, together with their response to space (\mathbf{n}) or time inversion. The basis is $\{(1, -1, 0), (1, 1, 0), (0, 0, 1)\}$ with respect to the tetragonal parent $P4/mmm$ labelled (x, y, z) , and lobes of $\langle H_2^z \rangle'$ are orientated at 45° with respect to cell edges.

Basis-forbidden Bragg spots in diamond-type structures have been painstakingly investigated for almost a century because they offer valuable information about the valence–electron distribution (the $(2, 2, 2)$ reflection was studied by W.H. Bragg, 1921). Participating electrons possess opposing parities because sites in the primitive cell are related by point inversion. Equivalent magnetic Bragg spots yield *unique* information on Dirac multipoles; the same type of information cannot be derived from NMR, NQR or muon spin-rotation experiments, for example.

Some Bragg spots in the diffraction pattern of SmAl_2 are fundamentally the same as those observed in diffraction by Hg1201 [3]. Specifically, spots indexed by Miller indices obeying $H + K + L = 4n + 2$, with n as an integer, are due to Al nuclei alone. Consequently, below the magnetic phase transition a magnetic contribution to a Bragg spot indexed by this condition must use unpaired electrons with opposite parities, e.g. Dirac multipoles created with Sm 4f and 5d electrons. The magnetic contribution in question was identified using polarisation analysis on the instrument D3. The motif of magnetic dipoles inferred from our diffraction patterns is displayed in **figure 2**.

**Figure 2**

Magnetic dipoles for magnetisation parallel to $[1, 1, 0]$ in SmAl_2 using a magnetic space-group $\text{Imm}'a'$ (#74.559). Cubic parent cell outlined in black, and orthorhombic magnetic cell (ξ, η, ζ) with $\xi = (1/2, 1/2, 0)$, $\eta = (1/2, -1/2, 0)$, $\zeta = (0, 0, -1)$ parallel to the ξ axis, while blue and red arrows that lie along the η axis denote anapoles related by point inversion.



Elsa Lhotel. French

Institut Néel, CNRS, Univ. Grenoble Alpes, France

'I am a senior scientist working on frustrated magnetic materials using very low temperature magnetometry and neutron scattering.'

Spin decoupling under a staggered field in the $Gd_2Ir_2O_7$ pyrochlore

High-intensity powder diffractometer D1B, disordered materials diffractometer D4, diffuse scattering diffractometer D7 and time-of-flight spectrometer IN6-SHARP Powder diffractometer G41 (LLB)

The complexity rooted in condensed matter nurtures the discovery of new states of matter, enriched by ingredients such as frustration. This is exemplified in pyrochlore compounds of the formula $R_2M_2O_7$, with R^{3+} a rare-earth ion and M^{4+} a metal ion, both occupying a lattice made of corner-sharing tetrahedra. Depending on the rare-earth ion, different anisotropies of the magnetic moments and different types of magnetic interactions between them can be present, giving rise to a considerable variety of magnetic behaviours. The presence of a magnetic metal ion such as Ir further expands the possible phases compared with the case of non-magnetic M , which is what we have shown in $Gd_2Ir_2O_7$ [1].

AUTHORS

E. Lhotel and V. Simonet (Néel Institute, CNRS and Grenoble University UGA, France)

L. Mangin-Thro and H. Fischer (ILL)

ARTICLE FROM

Phys. Rev. B (2019)—doi: 10.1103/PhysRevB.99.060401

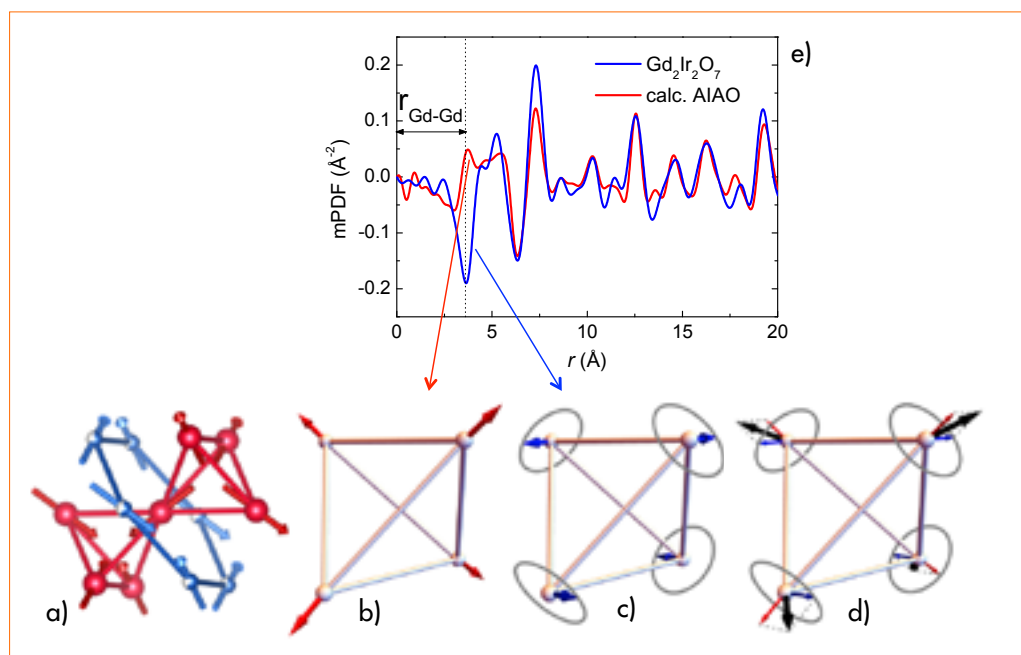
REFERENCES

- [1] E. Lefrançois, L. Mangin-Thro, E. Lhotel, J. Robert, S. Petit, V. Cathelin, H. E. Fischer, C.V. Colin, F. Damay, J. Ollivier, P. Lejay, L.C. Chapon, V. Simonet and R. Ballou, Phys. Rev. B Rapid Com. 99 (2019) 060401
- [2] E. Lefrançois, V. Cathelin, E. Lhotel, J. Robert, P. Lejay, C.V. Colin, B. Canals, F. Damay, J. Ollivier, B. Fak, L.C. Chapon, R. Ballou and V. Simonet, Nat. Commun. 8 (2017) 209

Indeed, the Ir sublattice orders magnetically at a temperature in the order of 100 K and then produces a local magnetic field, along which the rare-earth magnetic moments align in an exotic, non-collinear order all magnetic moments pointing inward or outward from each tetrahedron (all-in/all-out order) (**figure 1a**). New phenomena arise when, at a much lower temperature (in the order of 1 K), the rare-earth magnetic moments interact with each other in a manner that competes with the Ir local field. This has led, for Ising moments in Ho compounds, to the fragmentation of the magnetic moments (evidenced thanks to neutron scattering experiments at the ILL and LLB) into two equal components: one contributing to an ordered phase, the other to a fluctuating phase [2].

In the present case we focused on the rare-earth element Gd, which is the textbook example of an isotropic ion whose magnetic moment should orient indifferently in any spatial direction. Naively, one might therefore expect the $Gd_2Ir_2O_7$ compound to order in an all-in/all-out arrangement along the local field of the Ir and to remain in this state down to the lowest temperature, since it is compatible with the antiferromagnetic interactions between isotropic Gd magnetic moments. Surprisingly, by combining different neutron techniques we have shown that this is not the case.

Neutron diffraction measurements (on D1B and D4) also using polarised neutrons (on D7, at very low temperature using a dilution insert) showed that the Gd magnetic moment ordering occurs in two steps in two distinct temperature ranges (**figure 2**): the first corresponds to the ordering below 50 K of the all-in/all-out component of the magnetic moment along the local directions joining the centre to the corners of the tetrahedra (**figure 1b**);

**Figure 1**

a) Sketch of the all-in/all-out ordering produced on the rare-earth element (red) by the Ir all-in/all-out order (blue).

Scheme of different configurations of the Gd magnetic moment on a tetrahedron:

b) All-in/all-out order of the component of the magnetic moment along the local directions (diagonals) of the tetrahedron.

c) Palmer–Chalker non-collinear antiferromagnetic order of the complementary component in the planes perpendicular to the local directions.

d) Total magnetic moments (black) obtained from the superposition of the two components.

e) mPDF obtained by Fourier transforming the D4 magnetic diffractogram compared with that calculated from an all-in/all-out configuration only. The additional negative peak reveals local antiferromagnetic correlations in $Gd_2Ir_2O_7$ ascribed to the Palmer–Chalker component.

the second lower temperature range is related to the perpendicular component of the magnetic moment, which presents a tendency to order below 1 K in another antiferromagnetic pattern called ‘Palmer–Chalker’ (**figure 1c**). Note that the experiment on D4 allowed us to analyse the diffraction data using magnetic pair distribution function (mPDF) analysis in real space (**figure 1e**), a promising method for handling ill-ordered magnetic materials.

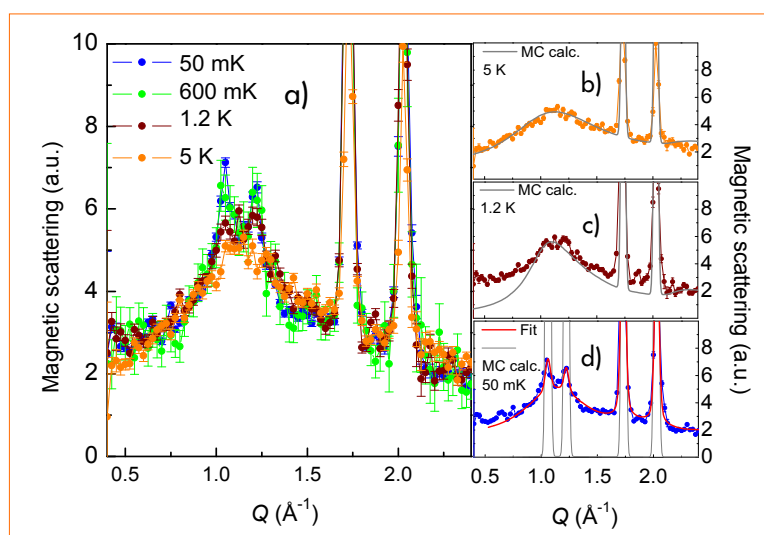
Finally, we have been able to model and interpret this peculiar magnetic ground state as well as the associated excitations probed by an inelastic neutron scattering experiment on IN6-SHARP. The key ingredients responsible for the resulting complex antiferromagnetic pattern (**figure 1d**) are tiny anisotropic terms. The effect of these usually neglected contributions in Gd compounds is actually exacerbated by magnetic frustration in this new member of the pyrochlore family, eventually giving rise to a magnetic moment decoupling mechanism.

Figure 2

a–d) Magnetic scattering of $Gd_2Ir_2O_7$ from D7 polarised neutron measurements at various temperatures.

b–d) Grey lines: Monte Carlo simulations of equal-time scattering functions using the instrumental Q resolution. The model takes into account the local field of the Ir, antiferromagnetic interactions between the Gd magnetic moments and tiny magnetic anisotropy terms.

d) Red line: FULLPROF refinement of the diffraction pattern, including an all-in/all-out component of the magnetic moments and Palmer–Chalker correlations of the perpendicular component.





Blair W. Lebert. Canadian and French University of Toronto, Canada
'I am post-doctoral researcher working on quantum spin liquids, thermoelectric materials and high-temperature superconductors using X-ray and neutron scattering. I received my PhD from Sorbonne Université, where I studied the magnetism of Fe and FeSe under pressure using neutron diffraction at the ILL.'

Epsilon iron as a spin-smectic state

High-intensity two-axis diffractometer with variable resolution D20

Our comprehensive experimental and theoretical approach delivers new insight into the controversial magnetic state of the high-pressure polymorph of iron. Neutron diffraction measurements on D20 played a key role. Using record-setting high-pressure/low-temperature conditions, we found no long-range magnetic order despite previous predictions. A novel 'spin-smectic' magnetic state, which corresponds with current experimental observations, is proposed.

AUTHORS

B.W. Lebert (University of Toronto, Canada)
 T. Gorni (Université Paris Sciences et Lettres, Paris, France)
 M. d'Astuto (UGA, Grenoble Université, France)
 M. Casula and S. Klotz (CNRS and Sorbonne Université, Paris, France)
 Th. C. Hansen (ILL)

ARTICLE FROM

Proc. Natl. Acad. Sci. USA (2019)—doi: 10.1073/pnas.1904575116t

REFERENCES

- [1] G. Steinle-Neumann, L. Stixrude and R.E. Cohen, Proc. Natl. Acad. Sci. USA 101 (2004) 33
- [2] S. Klotz, Th. Strässle, B. Lebert, M. d'Astuto and Th. Hansen, High Pressure Res. 36:1 (2016) 73
- [3] A. Papandrew *et al.*, Phys. Rev. Lett. 97 (2006) 087202

Iron is the prototypical ferromagnet and has long fascinated humankind. In the last few decades, it has been extensively studied under pressure, since it is the primary element of the Earth's core. The high-pressure polymorph of iron, the so-called epsilon iron phase, is formed above 1.5 GPa (1.50 000 times atmospheric pressure). Above this pressure, iron transforms from its ambient, body-centred cubic (bcc) crystal structure to a hexagonal close-packed (hcp) crystal structure (**figure 1**). This structural transition is accompanied by a loss of ferromagnetism; however, the magnetism of epsilon iron is unknown and controversial due to seemingly paradoxical results from theory and experiment. Here, we propose a novel, 'spin-smectic', state that is compatible with previous studies as well as with our current X-ray and neutron scattering studies.

First, we used an X-ray scattering technique called X-ray emission spectroscopy, which can measure local magnetic moments, *i.e.* the magnetism of individual atoms. We confirmed the existence of magnetic moments in epsilon iron and measured their pressure and temperature

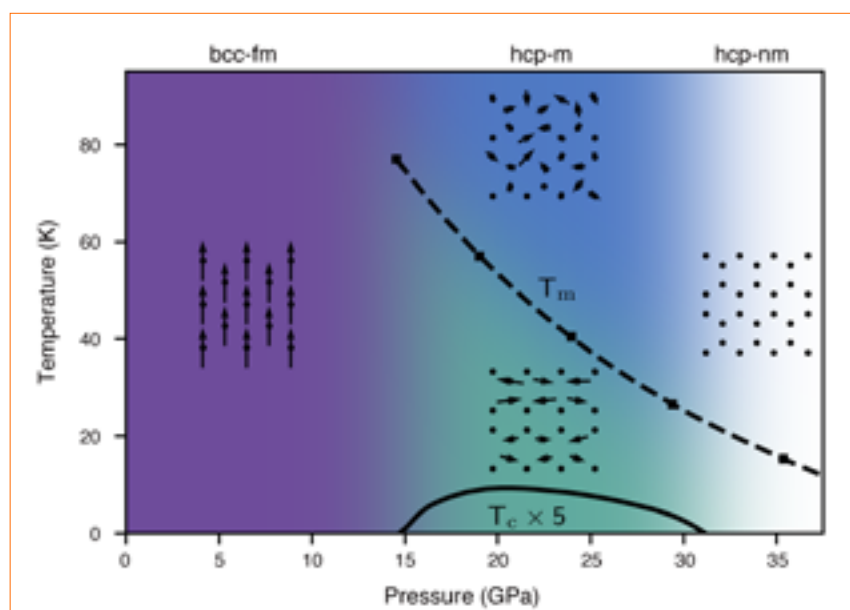
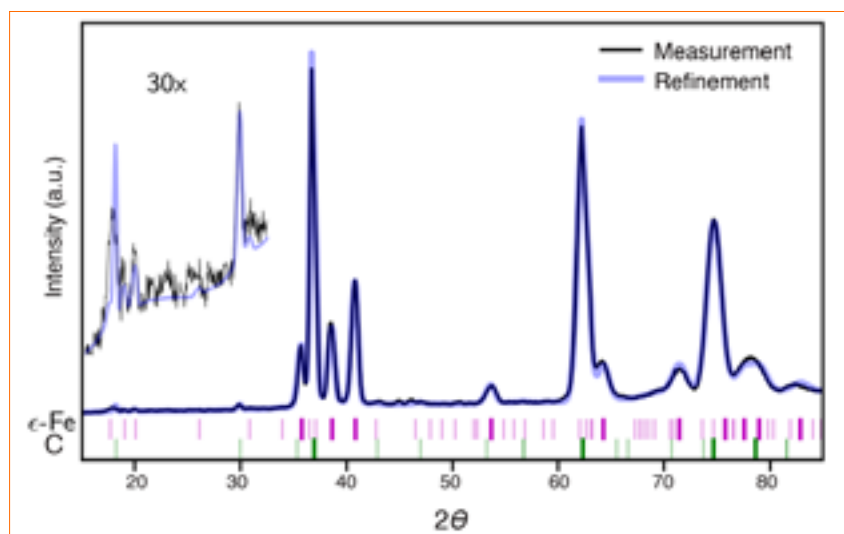


Figure 1

Schematic phase diagram of iron. The ambient, ferromagnetic, body-centred cubic phase (bcc-fm) is shown in purple. The high-pressure polymorph epsilon iron, which forms a hexagonal close-packed (hcp) structure, is shown in blue/green for magnetic phases (hcp-m) and white for non-magnetic phases (hcp-nm). We measured the crossover from hcp-m to hcp-nm using X-ray emission spectroscopy. Our calculations predict that the disordered moments (blue) form a spin-smectic state (green) below a critical temperature T_m , which may be related to ϵ -iron's superconductivity (T_c dome shown).

**Figure 2**

Neutron powder diffraction pattern of epsilon iron at 20.2 GPa/1.8 K performed with $\lambda = 1.3\text{\AA}$ neutrons. The diffraction measurement (black line) is shown with its Rietveld refinement (blue line). The peaks due to epsilon iron and diamond are shown as magenta and green ticks respectively, where the lighter peaks are due to secondary reflections from $\lambda/2$ contamination. A 30x zoom of the low-scattering angle region is shown to emphasise the lack of diffraction peaks due to long-range magnetic order.

dependence. These magnetic moments have no temperature trend; however, as we increase the pressure their magnitude decreases and approaches zero at around 30–40 GPa (**figure 1**).

X-ray emission spectroscopy is a powerful technique for detecting local magnetic moments. However, it provides no information on how these individual magnetic moments globally order, *i.e.* whether they have long-range magnetic order. Therefore, to detect the global magnetic order in epsilon iron we turned to neutron diffraction.

Previous theoretical studies of epsilon iron predict an antiferromagnetic magnetic structure where the magnetic moments alternate in direction between neighbouring atoms [1]. Antiferromagnetic magnetic structures have a larger unit cell than that of the crystal structure. Therefore, magnetic reflections are expected to occur at smaller scattering angles (2θ) that are separate from the nuclear diffraction peaks.

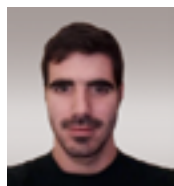
We performed high-pressure low-temperature diffraction on the D20 diffractometer using a Paris–Edinburgh cell at truly extreme P/T conditions. The iron sample was pressurised past the structural bcc–hcp transition and then cooled down while collecting diffraction data. The diffraction pattern shown in **figure 2** was measured at 20.2 GPa and 1.8 K, which is a record-setting high-pressure/low-temperature measurement [2]. Low temperature is critical in this study since long-range magnetic order can only occur well below room temperature.

Although the data contain strong diffraction peaks from the diamond anvils used in the Paris–Edinburgh cell, we were able to accurately refine the data as shown by the blue line in **figure 2**. There are no reflections evident at scattering angles below 30 degrees; therefore, a 30x zoom of this region is also shown in **figure 2**. It is important to note that all the diffraction peaks shown in the refinement in this region are due to the small (0.2 %) harmonic contamination from the monochromator in the

high-flux configuration of D20. In this zoom, we can see that the refinement corresponds well with our data and that there are no reflections due to long-range magnetic order. Through simulations, we placed an upper limit on the magnitude of the magnetic moment that was five times smaller than theoretical estimation [1]. Furthermore, the diffraction patterns showed no change from 1.8 K to 260 K. Theory estimates a critical temperature of around 75 K [3]. Therefore, if long-range magnetic order exists in epsilon iron we should have detected a change.

We detected local magnetic moments without global magnetic order. To reconcile these observations, as well as those of previous studies, we propose a new, spin-smectic, magnetic structure. We discovered this unique structure through extensive density functional theory and classical Monte Carlo simulations. As shown in **figure 1**, we predict that epsilon iron is paramagnetic but that if it is cooled below T_m it forms this spin-smectic state. The spin-smectic state is characterised by alternating magnetic and non-magnetic bilayers. The interaction between the magnetic bilayers is extremely weak, leading to very small interlayer correlations. Therefore, we predict an orientationally disordered state with no long-range magnetic order which would be undetectable by neutron diffraction, while the local magnetic moments are still detectable by X-ray emission spectroscopy.

Our measurements find local magnetic moments in epsilon iron at around 30–40 GPa without long-range order, which we suggest is because they form a spin-smectic state. Epsilon iron is known to superconduct at low temperatures from 15 to 32 GPa (T_c in **figure 1**). This pressure region coincides with where we observed a local magnetic moment. Therefore, we predict that magnetic fluctuations of the spin-smectic state play an important role in the superconductivity of epsilon iron. Future experiments to confirm the existence of the spin-smectic state in epsilon iron are planned.



Xabier Martínez de Irujo Labalde. Spanish

Department of Inorganic Chemistry,
Faculty of Chemistry, Complutense University
of Madrid, Spain

'I was awarded my PhD from the University
Complutense in Madrid, in 2019. My research
interests are the magnetic, electric and ultimately

magneto-electric properties in perovskite-related transition metal
oxides. Neutron diffraction is an ideal tool for establishing the
nuclear and magnetic structures of these complex systems.'

Multiferroism induced by spontaneous structural ordering in antiferromagnetic iron-perovskites

High-intensity two-axis diffractometer
with variable resolution D20

Perovskite-based compounds of type $\text{RE}_{1.2}\text{Ba}_{1.2}\text{Ca}_{0.6}\text{Fe}_3\text{O}_8$ adopt a layered arrangement of Re, Ba and Ca atoms, which induces FeO_4 -tetrahedra (T) and FeO_6 -octahedra (O) ordering in a polar crystal structure and antiferromagnetic ordering of Fe^{3+} up to 850 K. The combination of magnetic and polar properties results in a multiferroic oxide at room temperature. The nuclear structure of these oxides has been revealed by transmission electron microscopy techniques with atomic resolution [1], while the magnetic structure has been determined by neutron diffraction experiments.

AUTHORS

X. Martínez de Irujo-Labalde and S. Garcia-Martin (Universidad Complutense, Madrid, Spain)

U. Amador (Universidad San Pablo-CEU, Madrid, Spain)

C. Ritter (ILL)

ARTICLE FROM

Chem. Mater. (2019)—doi: <https://doi.org/10.1021/acs.chemmater.9b02716>

REFERENCES

- [1] X. Martínez de Irujo-Labalde, M. Goto, E. Urones-Garrote, U. Amador, C. Ritter, M.E. Amano Patino, A. Koedruad, Z. Tan, Y. Shimakawa and S. Garcia-Martin, Chem. Mater. 31 (2019)

The magnetic and nuclear structure of the oxide $\text{Tb}_{0.8}\text{Ba}_{0.8}\text{Ca}_{0.4}\text{Fe}_2\text{O}_8$, as a non-absorbing representative, was determined using the high-intensity powder diffractometer D20 and the high-resolution diffractometer D2B. A sample was placed inside a quartz tube open to the air to avoid oxygen loss on heating in a furnace at between room temperature and 1 000 K. **Figure 1a** shows part of the high-resolution data taken at 300 K and 1 000 K, with the background of the quartz tube removed.

The $\text{Tb}_{1.2}\text{Ba}_{1.2}\text{Ca}_{0.6}\text{Fe}_3\text{O}_8$ oxide presents a layered-type perovskite structure with a $\sqrt{2}a_p \times \sqrt{2}b_p \times 3c_p$ unit cell (Pb2₁m space group) related to the layered-ordering of A-cations in a Tb/Ca-Tb/Ca-Ba-Tb/Ca sequence with a combined T-O-O-T ordering sequence of the Fe-O polyhedra. The polar space group Pb2₁m of the oxide allows the existence of a net polarisation from uncompensated shifts of the ions within the structure, giving a polar moment of 23.2 $\mu\text{C}/\text{cm}^2$ along the b-axis. **Figure 2a** shows the unit cell of the crystal structure indicating polarisation associated with the atom displacements in the b direction.

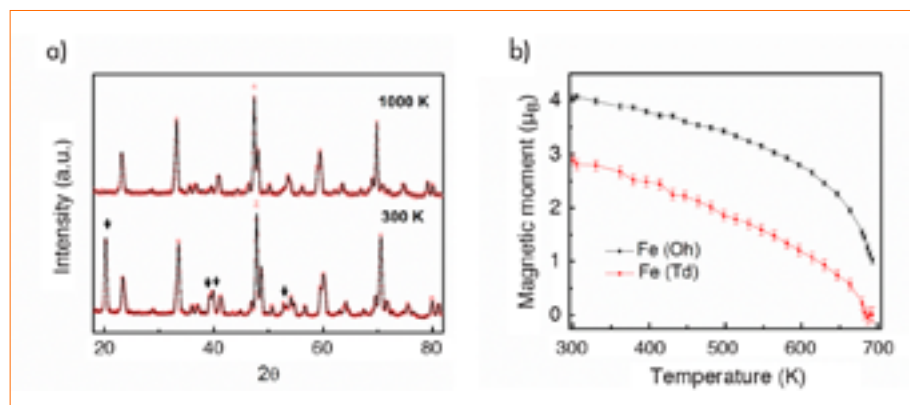
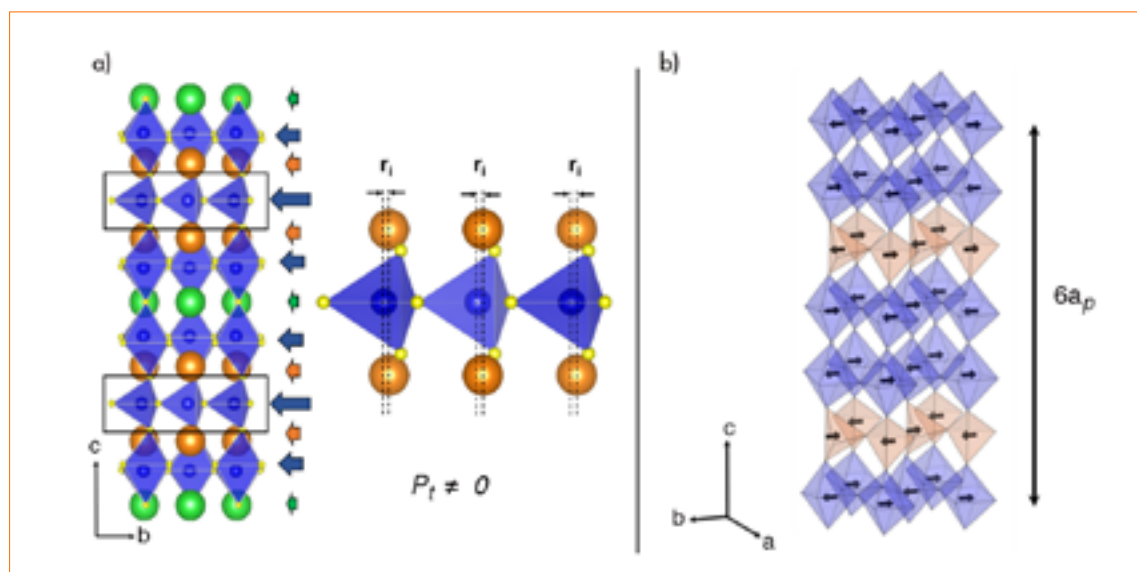


Figure 1

a) PND patterns of $\text{Tb}_{1.2}\text{Ba}_{1.2}\text{Ca}_{0.6}\text{Fe}_3\text{O}_8$ taken at below (300 K) and above (1 000 K) the magnetic transition. The arrows indicate the magnetic reflections.

b) Temperature dependence of the magnetic moment of Fe in the octahedral (black) and tetrahedral (red) sites of $\text{Tb}_{1.2}\text{Ba}_{1.2}\text{Ca}_{0.6}\text{Fe}_3\text{O}_8$.

**Figure 2**

a) Graphic representation of the polar unit cell of $\text{Gd}_{1.2}\text{Ba}_{1.2}\text{Ca}_{0.6}\text{Fe}_3\text{O}_8$. Arrows indicate the polarisation in the different layers (Ba-O layers in green, Gd/Ca-O in orange, Fe-O in octahedral layers and Fe-O in tetrahedral layers), including the anionic and cationic contributions along the b -axis. r_1 is the shift-distance of the Fe atoms with respect to the A cations along the b -axis. Room temperature multiferroism in polycrystalline antiferromagnetic $\text{Tb}_{1.2}\text{Ba}_{1.2}\text{Ca}_{0.6}\text{Fe}_3\text{O}_8$ is reported for the first time.

b) The magnetic unit cell of $\text{Tb}_{1.2}\text{Ba}_{1.2}\text{Ca}_{0.6}\text{Fe}_3\text{O}_8$. Arrows indicate the spin direction.

Reflections corresponding to long-range magnetic order are visible in the diffraction patterns (**Figure 1a**), while the D20 data are used to determine T_N to 690 K (see **Figure 1b**)—one of the highest transition temperatures reported in Fe-perovskites [1]. These magnetic reflections can be indexed by a propagation vector $[0\ 0\ \frac{1}{2}]$, producing a magnetic unit cell $\sqrt{2}a_p \times \sqrt{2}b_p \times 6c_p$. The magnetic structure adopted is depicted in **Figure 2b**. It consists of a three-dimensional, G-type, antiferromagnetically ordered arrangement of the Fe spins with the spin directions lying along the b -axis. This magnetic transition is associated with an electric transition of electron transport at the same temperature.

In summary, the combination of magnetic behaviour and polar structure makes this oxide, to the best of our knowledge, the first reported multiferroic polycrystalline material with an antiferromagnetic structure. In turn, the layered arrangement of the oxygen polyhedra around the Fe-atoms in a particular sequence, assisted by the A-cation ordering in this oxide, represents a novel approach to the design of multiferroic materials.



Anthony Higgins. British Swansea University, UK

'My research in the field of soft condensed matter investigates the physics of polymers near interfaces and in thin films. Understanding fundamental behaviour in such systems underpins many areas of life science, physical science and engineering. My current focus is on understanding the thermodynamics of polymer-based, thin-film systems for organic electronics applications.'

Equilibrium behaviour in polymer/small-molecule mixtures of organic solar cell materials

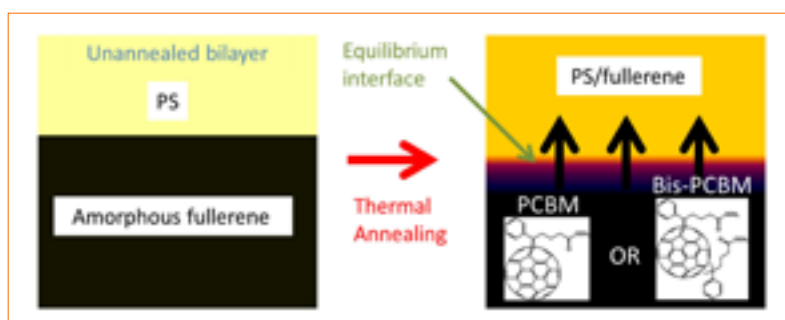
Horizontal reflectometer FIGARO and vertical reflectometer DI7

Horizontal reflectometer INTER (ISIS)

Organic photovoltaics (OPVs) are approaching the point where their use for building-integrated power generation is commercially viable [1]. However, challenges remain in terms of cost, efficiency and lifetime. The active layer of an OPV consists of interconnected domains of electron-donating and electron-accepting materials. The interfaces between domains within these 'bulk heterojunctions' are key locations at which photo-generated, bound electron-hole pairs (excitons) are separated into individual charges that can then be transported to the device electrodes. Our work investigates the applicability of equilibrium thermodynamic theories for describing the domain compositions and interfacial mixing within model binary mixtures containing OPV materials.

Figure 1

A schematic diagram illustrating the rapid diffusion of fullerene molecules into the top (polystyrene (PS)) layer. Two different PS/fullerene systems were investigated: PS/PCBM and PS/bis-PCBM.



AUTHORS

E.L. Hynes, D. Môn and A.M. Higgins (Swansea University, UK)
J.T. Cabral (Imperial College London, UK)
A.J. Parnell and A. Dunbar (Sheffield University, UK)
P. Gutfreund (ILL)
R. Welbourn (ISIS, UK)

ARTICLE FROM

Commun. Phys. (2019)—doi: 10.1038/s42005-019-0211-z

REFERENCES

- [1] S. Strohm, F. Machui, S. Langner, P. Kubis, N. Gasparini, M. Salvador, I. McCulloch, H.J. Egelhaaf and C.J. Brabec, *Energy Environ. Sci.* 11:8 (2018) 2225
- [2] L. Ye, H. Hu, M. Ghasemi, T. Wang, B.A. Collins, J.H. Kim, K. Jiang, J.H. Carpenter, H. Li, Z. Li, T. McAfee, J. Zhao, X. Chen, J.L.Y. Lai, T. Ma, J.L. Bredas, H. Yan and H. Ade, *Nat. Mater.* 17:3 (2018) 253
- [3] J.A. Bartelt, Z.M. Beiley, E.T. Hoke, W.R. Mateker, J.D. Douglas, B.A. Collins, J.R. Tumbleston, K.R. Graham, A. Amassian, H. Ade, J.M.J. Fréchet, M.F. Toney and M.D. McGehee, *Adv. Energy Mater.* 3:3 (2013) 364
- [4] D. Môn, A.M. Higgins, D. James, M. Hampton, J.E. Macdonald, M.B. Ward, P. Gutfreund, S. Lilliu and J. Rawle, *Phys. Chem. Chem. Phys.* 17:3 (2015) 2216

Bulk heterojunctions are most commonly made from a binary mixture of a semiconducting polymer and a small molecule that de-mix into separate (typically non-pure) phases during device fabrication. Recent work has uncovered a strong correlation between OPV performance and equilibrium parameters in polymer/small-molecule systems using bilayer mixing measurements [2]; equilibrium theory was used here to interpret domain compositions and quantitatively link the Flory–Huggins interaction parameter, χ (characterising the miscibility), to a key measure of the efficiency of a solar cell (the fill-factor), for an amorphous-polymer/fullerene and a range of polymer/small-molecule devices. Of key significance here, for a wide range of amorphous and semi-crystalline polymers, is the existence of mixed amorphous polymer/small-molecule phases, whose composition plays an important role in charge transport and charge recombination within devices [3].

Understanding equilibrium behaviour in these systems is important, as i) one needs to be sure that the system is properly equilibrated to extract χ correctly, and ii) the domain compositions can evolve towards their equilibrium compositions given sufficient mobility during operation (e.g. as provided by the elevated temperatures that are encountered under solar illumination). Domain composition evolution can lead to significant degradation of performance during operation if the as-fabricated domain compositions are optimised but not equilibrated.

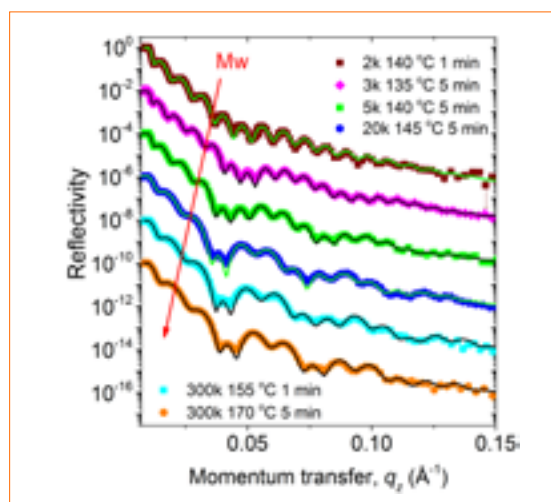
Figure 2

A selection of neutron reflectivity curves and fits (bilayer fits with Gaussian roughness at all interfaces) for a range of different molecular weight (Mw) PS/PCBM bilayer samples. Curves are offset vertically for clarity. This figure is reproduced from Hynes *et al.* *Commun. Phys.* 2:112 (2019) under a CC BY 4.0 license.

In this study we tested the hypothesis that model amorphous OPV blends can rapidly form a liquid/liquid equilibrium, by performing an in-depth investigation in which bilayer samples consisting initially of pure polymer and fullerene layers are thermally annealed (**figure 1**). The key parameter in our investigations was the molecular weight of the polymer, which theory predicts can have a strong influence on the thermodynamics in the bulk and at interfaces. We chose polystyrene as a model polymer because its low polydispersity (in contrast to typical semiconducting polymers) allowed us to conduct a high-resolution study. We investigated two closely related fullerenes, phenyl-C60-butyric acid methyl ester (PCBM) and bis-adduct phenyl-C60-butyric acid methyl ester (bis-PCBM), which differ in the number of sidechains on the C₆₀ cage (and consequently have different miscibility with polystyrene).

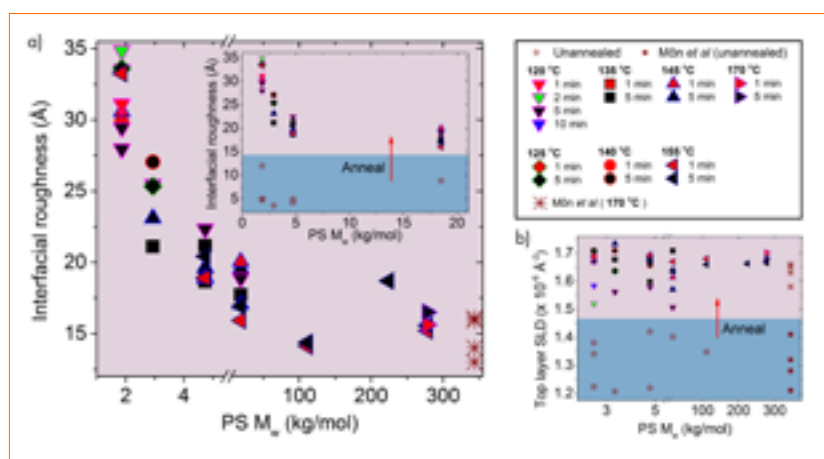
Neutron reflectometry measurements were performed on D17 and FIGARO (and also on Inter at ISIS). **Figure 2** shows a selection of reflectivity curves and fits for annealed PCBM/polystyrene bilayers that were investigated across an extensive set of measurement conditions, in which the annealing time, annealing temperature, layer thickness and molecular weight were varied. On annealing there is diffusion of PCBM into the polystyrene layer to form a polymer-rich layer, but no transfer of polystyrene into the PCBM layer (for all measurements conditions). This asymmetry is consistent with the expected equilibrium behaviour of a polymer/small-molecule system.

Figure 3 shows the key findings from the fits for polystyrene/PCBM: there is a systematic dependence of the interfacial width (roughness) between the polymer-rich phase and the fullerene phase in this system on the polymer molecular weight, but no



systematic differences in the polymer-rich layer composition (scattering length density) as a function of molecular weight. For comparison with theory, we extracted a χ parameter from layer composition measurements in the high molecular weight limit, and then predicted the behaviour at lower molecular weights in terms of both layer compositions and interfacial width. The findings in **figure 3** are consistent with the predictions of equilibrium theory: broader interfaces are obtained at lower molecular weight because of the increased entropy of mixing. For bis-PCBM/polystyrene bilayers (in which a lower value of χ is determined from high molecular weight measurements, indicating higher miscibility with polystyrene), both interfacial broadening and significant layer composition differences occur as the molecular weight is decreased (data not shown), which is again in agreement with theoretical predictions.

We conclude that the composition profiles that are rapidly established in these thin-film systems on annealing are well described as two co-existing phases in liquid-liquid equilibrium. We anticipate that this understanding will complement material synthesis and device optimisation work, and contribute to rational design of stable, high-performance OPVs.

**Figure 3**

Bilayer fit parameters for PS/PCBM bilayers annealed at various temperatures for various times, as a function of the weight-average molecular weight (Mw) of the PS

a) The (Gaussian) roughness of the buried PS/PCBM interfaces in annealed samples. Inset) The same data, but showing the lower Mw samples only, in conjunction with measurements on unannealed samples.

b) The scattering length density (SLD) of the top (initially PS) layer in the samples before and after annealing, showing no systematic Mw-dependent behaviour. The data points at 344 kg mol⁻¹ in a) and b) are from Mön *et al.* [4] (in each plot, three of these annealed data points are from samples that were heated for 10 minutes, the others for 60 minutes). The legend applies to the data points in both a) and b). This figure is reproduced from Hynes *et al.* *Commun. Phys.* 2:112 (2019) under a CC BY 4.0 license.



Max Wolff. German/Swedish
Department of Physics and Astronomy,
Uppsala University, Sweden
*'I am a lecturer in neutron scattering at
Uppsala University, Sweden, I am interested
in functional materials, with an emphasis on
energy materials, magnetic liquids and
polymers. Neutron scattering techniques provide unique and
decisive information in all these areas.'*

Nuclear spin-incoherent neutron scattering from quantum well resonators

*Reflectometer for the analysis of materials
SuperADAM*

The high penetration of neutrons allows for the study of buried interfaces, while the energy of cold neutrons makes them an excellent probe of dynamics. However, the limited brilliance of neutron sources makes the combination of reflectometry and spectroscopy challenging. This is especially true for thin films containing hydrogen, which scatters mainly nuclear spin-incoherent. On the one hand this scattering allows probing tracer diffusion but is, on the other hand, often seen as background signal in studies at low momentum transfer Q . We have quantified the nuclear spin incoherent scattering from a 100 nm thick metal hydride film, paving the way towards studies of surface dynamics using neutrons.

AUTHORS

M. Wolff (Uppsala University, Sweden)
A. Devishvili (ILL)
B.P. Toperverg (Petersburg Nuclear Physics Institute, Russia)

ARTICLE FROM

Phys. Rev. Lett. (2019)—doi: 10.1103/PhysRevLett.123.016101

REFERENCES

- [1] M. Wolff, EPJ Web of Conferences 188 (2018) 04002
- [2] W.A. Hamilton, G.A. Klein, G.I. Opat and P.A. Timmins, Phys. Rev. Lett. 58 (1987) 2770
- [3] F. Pfeiffer, V. Leiner, P. Høghøj and I. Anderson, Phys. Rev. Lett. 88 (2004) 055507
- [4] S.A. Holt, A.P. Le Brun, C.F. Majkrzak, D.J. McGillivray, F. Heinrich, M. Lösche and J.H. Lakey, Soft Matter 13 (2009) 2576
- [5] M. Wolff, A. Devishvili, J.A. Dura, F.A. Adlmann, B. Kitchen, G.K. Palsson H. Palonen, B.B. Maranville, Ch.F. Majkrzak and B.P. Toperverg, Phys. Rev. Lett. 123 (2019) 016101

Together with grazing-incidence neutron and X-ray scattering, surface science has advanced enormously. Nevertheless, many scientific questions remain unresolved. These include spin-wave dispersions, as well as dynamics of glass formers and self-assembled monolayers. An important aspect in biology is the dynamics of water close to membranes, while understanding the dynamics of lithium and protons in thin films is crucial for developing energy storage and conversion materials.

With neutrons, the density profile across an interface is extracted from specular reflectivity. Fewer studies probe in-plane structures [1] and almost none dynamics [2], since the brilliance of neutron beams is limited. One way to enhance surface signals is by using quantum resonators [3]. We combine this method with magnetic contrast variation [4] to gain additional control of the neutron wave field.

Figure 1 shows the scattering length density (SLD) profile of neutrons impinging under grazing incidence onto a 100 nm-thick vanadium hydride resonator sandwiched between iron layers. The film is grown epitaxially on MgO and covered by palladium and aluminium oxide to prevent oxidation. For

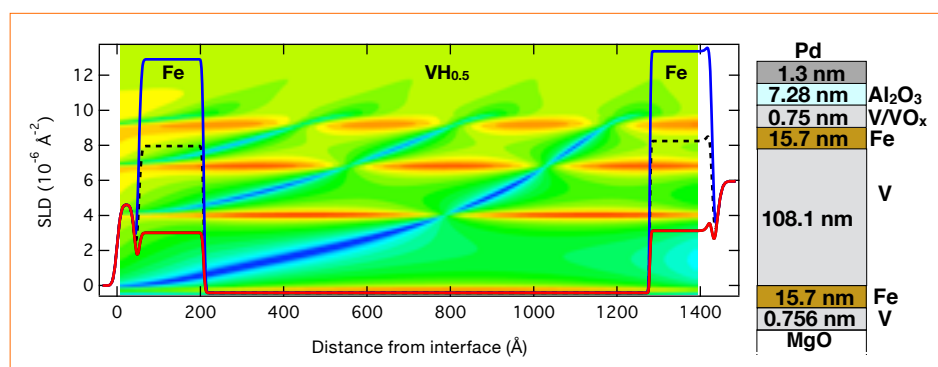


Figure 1

The SLD profile of a vanadium hydride resonator. The colour map represents the wave field for different incident wave numbers of the neutron. The panel to the right is a sketch of the sample structure.

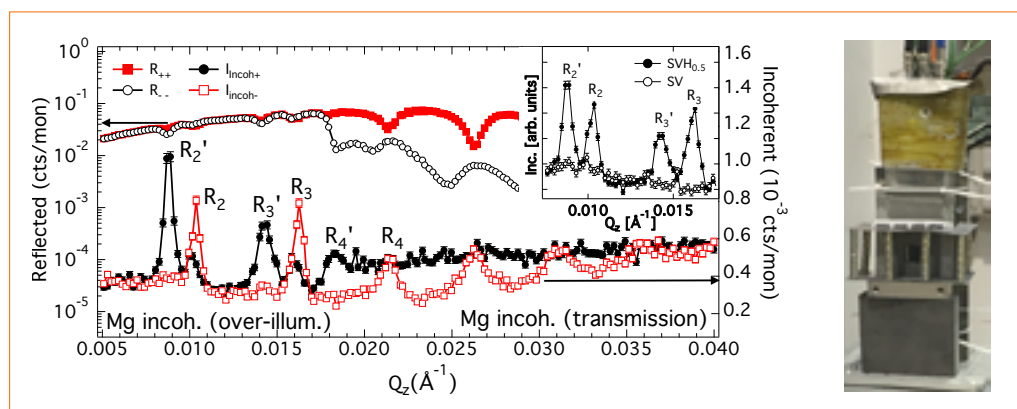


Figure 2

Intensity reflected from the sample surface (left axis) for + and - polarised neutrons plotted together, with the signal collected at a detector mounted directly behind the sample (photograph on the right-hand side) to measure the incoherent scattering. The insert to the upper right shows a comparison of a sample loaded with hydrogen and an empty one.

specific incident wave numbers, the neutron wave field (shown by the colour map) is enhanced (red colour), resulting in an increased scattering probability from nuclei inside the resonator.

Tracer diffusion is measured by neutrons via nuclear incoherent scattering. Since neutrons scatter from the nucleus, which is much smaller than the wavelength, this scattering is isotropic. To capture as much of it as possible we glued the sample onto a well-shielded neutron detector, leaving only a small window towards the sample open (see **Figure 2** photo on the right-hand side).

Figure 2 depicts the reflected neutron intensity from the sample, plotted together with the signal registered by the detector directly behind the sample. The region of total external reflection is visible for Q_z values below 0.018 \AA^{-1} . The dips in the signal are at the positions where the evanescent wave enters the resonator. At exactly these positions, the detector catching the incoherent scattering registers neutrons. To prove that the detected signal is indeed originating from the resonator, we magnetised the iron layers and used spin-polarised neutrons in the experiment to change the height of the resonator walls and shift the position of the resonances for the different polarisations of the incident neutron beam. As a second proof we compared the signal of a film loaded with hydrogen with an empty vanadium layer (**Figure 2**, panel top right). Clearly, only for the hydrogenated film significant nuclear spin-incoherent scattering is detected. Note the nuclear spin-incoherent cross section of vanadium is much smaller than that of hydrogen and the overall incoherent background results from the incoherent cross section of magnesium, which is of much larger volume.

Our measurements demonstrate that the incoherent signal from a thin film of 100 nm can be measured [5], paving the way towards experiments probing tracer diffusion and dynamics in thin films and at interfaces.



Pierric Lemoine. French
 Institut des Sciences Chimiques de Rennes
 (ISCR), France
'I received a PhD in Materials Chemistry in 2011 from the University of Nancy, France. After post-doctoral positions at the University of Manitoba, Winnipeg and the CRISMAT laboratory, Caen, I obtained a position as a CNRS researcher in 2014. My research focuses on crystal structure determination of thermoelectric sulphides, magnetic intermetallics and cluster compounds.'

Designing high power factor thermoelectric colusites by functionalisation of the conductive 'Cu-S' network

High-flux and high-resolution powder diffractometer D2B

Copper-rich sulphides with a complex crystal structure are very promising materials for thermoelectric applications in the mid-temperature range (300–700 K), due to their low thermal conductivities [1]. However, their power factors remain modest and significantly lower than those of state-of-the-art intermetallic thermoelectric compounds [2]. In this study, we report on the design of p-type ionic-covalent sulphides exhibiting the highest power factors to date by introducing hexavalent cations ($T = \text{Cr, Mo, W}$) in colusites $\text{Cu}_{26}\text{T}_2\text{Ge}_6\text{S}_{32}$ (figure 1).

Figure 1

Current state-of-the-art power factor (in $\text{mW m}^{-1} \text{K}^{-2}$) values at 300 K and 700 K in copper-based sulphides (n-type in orange, p-type in red, and present study in green).

AUTHORS

V. Pavan Kumar, O.I. Lebedev, B. Raveau and E. Guilmeau (CRISMAT Laboratory, Caen, France)
 A.R. Supka, R. Al Rahal Al Orabi and M. Fornari (Central Michigan University, Mt Pleasant, USA)
 P. Lemoine (Institut des Sciences Chimiques de Rennes, France)
 K. Suekuni (Kyushu University, Fukuoka, Japan)
 V. Nassif (Grenoble University UGA and CNRS – NEEL Institute, Grenoble, France)

ARTICLE FROM

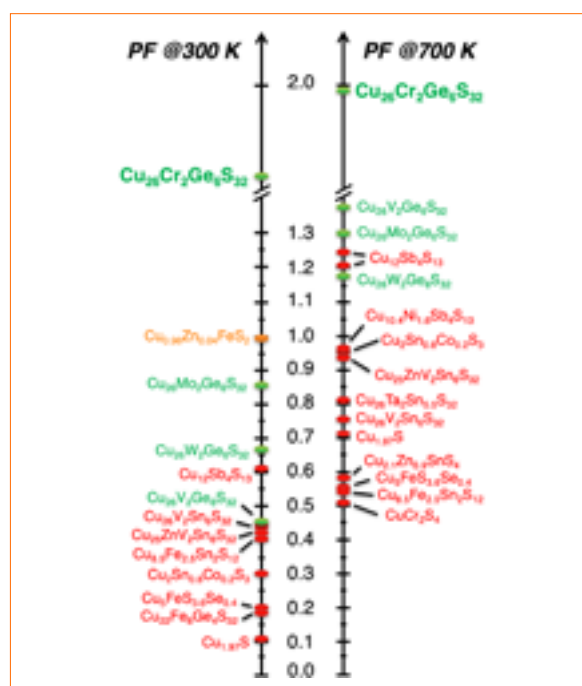
Adv. Energy Mater. (2019)—doi: 10.1002/aenm.201803249

REFERENCES

- [1] A.V. Powell, J. Appl. Phys. 126 (2019) 100901
- [2] G. Tan, L.D. Zhao and M.G. Kanatzidis, Chem. Rev. 116 (2016) 12123
- [3] C. Bourges, Y. Bouyrie, A.R. Supka, R. Al Rahal Al Orabi, P. Lemoine, O.I. Lebedev, M. Ohta, K. Suekuni, V. Nassif, V. Hardy, R. Daou, Y. Miyazaki, M. Fornari and E. Guilmeau, J. Am. Chem. Soc. 140 (2018) 2186 (and ILL Annual Report 2018, page 60–61)
- [4] V. Pavan Kumar, G. Guélou, P. Lemoine, B. Raveau, A.R. Supka, R. Al Rahal Al Orabi, M. Fornari, K. Suekuni and E. Guilmeau, Angew. Chem. Int. Ed. 58 (2019) 15455

Increasing need for renewable energy sources has made thermoelectric materials the object of extensive investigations over the past fifteen years [1, 2]. The conversion efficiency of thermoelectric materials is represented by the figure of merit $ZT = S^2T/\rho\kappa$ (T being the absolute temperature, S the Seebeck coefficient, ρ the electrical resistivity and κ the thermal conductivity). In terms of performance, ideal thermoelectrics must exhibit a high power factor $PF = S^2/\rho$ and a simultaneously low thermal conductivity. In addition, they must be easy to prepare and made of non-toxic and abundant precursors.

These cost and environmental constraints make copper-rich sulphides very promising thermoelectric materials [1, 2]. Within this family of compounds, synthetic colusite $\text{Cu}_{26}\text{V}_2\text{Sn}_6\text{S}_{32}$ appears to be one of the most promising p-type representatives in relation to its ability to accommodate structural disorder [3]. These structural features favour phonon scattering, and consequently are



responsible for the sharp reduction in the lattice thermal conductivity of this material. This leads to a material with the ZT value reaching unity. However, the power factor of colusite remains modest (**figure 1**) and significantly lower than those of state-of-the-art, intermetallic thermoelectric compounds [2]. The objective of our study was to optimise the power factor by substituting the pentavalent V^{5+} cations with hexavalent ones (*i.e.* Cr^{6+} , Mo^{6+} and W^{6+}) and to understand the impact of the crystal structure on the thermoelectric properties of colusite.

In this context, high-purity polycrystalline $Cu_{26}T_2Ge_6S_{32}$ ($T = V, Cr, Mo, W$) samples were synthesised by combining mechanical alloying and spark plasma sintering. The crystal structures of these synthetic colusites ($P\bar{4}3n$ space group) were studied using combined Rietveld refinements of X-ray powder diffraction and high-resolution neutron powder diffraction data recorded on D2B with a wavelength of 1.594 Å (**figure 2**). From these results we have shown that the ordered ‘ $Cu_{26}Ge_6S_{32}$ ’ sphalerite-derivative framework of colusite, constructed of corner-sharing GeS_4 and CuS_4 tetrahedra (**figure 3a**), can accommodate hexavalent d^0 cations at ‘interstitial’ T position, leading to TS_4 ($T = Cr, Mo, W$) tetrahedra sharing edges with CuS_4 tetrahedra (**Figure 3b**), a structural feature rarely observed in sulphides.

Moreover, we have demonstrated that the nature of the ‘interstitial’ cation can drastically modify the electronic properties to reach high power factors (**figure 1**). The maximum value of $1.94 \text{ mW m}^{-1} \text{ K}^{-2}$ at 700 K for $Cu_{26}Cr_2Ge_6S_{32}$ is comparable with those of the best state-of-the-art thermoelectric materials [2]. Thanks to combined structural analyses and electronic structure and transport calculations, we have shown that the electronic transport properties of the conductive ‘ $Cu_{26}S_{32}$ ’ framework (**figure 3c**) are governed by the presence of mixed tetrahedral–octahedral $[TS_4]Cu_6$ complexes in the colusite structure (**figure 3d**). In such complexes, the T cations are underbonded to sulphur and form metal–metal interactions with copper. In the case of Cr-colusite, the smaller size and lower electronegativity of hexavalent chromium cations introduces T -Cu interactions that limit the distortion of the

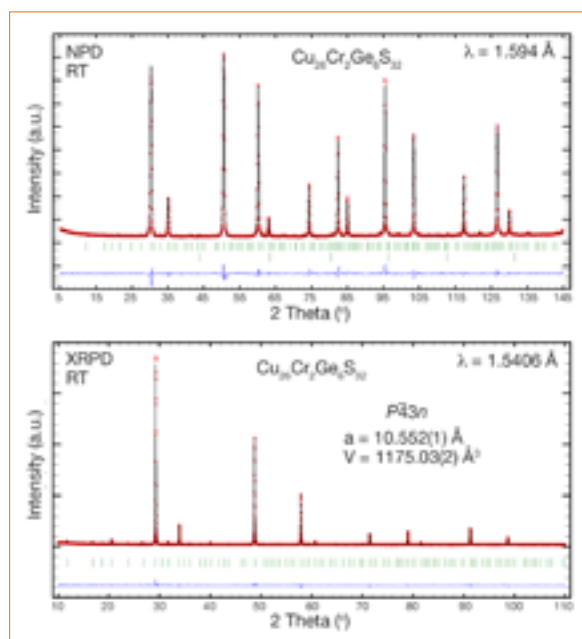


Figure 2

Combined Rietveld refinement of the high-resolution NPD (**top**) and XRPD (**bottom**) patterns of the $Cu_{26}Cr_2Ge_6S_{32}$ sample recorded at room temperature. Second sets of diffraction peaks on the NPD pattern are related to the vanadium sample-holder contribution.

conductive ‘ $Cu_{26}S_{32}$ ’ network and the perturbation of the electronic properties. The key role of the chemical bonds at the core of the mixed tetrahedral–octahedral complex over the transport properties was recently confirmed in $Cu_{26}Cr_{2-x}Mo_xGe_6S_{32}$ and $Cu_{26}Cr_{2-x}W_xGe_6S_{32}$ solid solutions [4].

Finally, the nature of the ‘interstitial’ cation does not influence the thermal conductivity of these synthetic colusites. It leads to a dimensionless figure of merit ZT up to 0.86 at 700 K for un-optimised pristine $Cu_{26}Cr_2Ge_6S_{32}$, and an average ZT near 0.5 over the full temperature range. The latter is, to the best of our knowledge, the highest average ZT for pristine sulphide materials without specific optimisation.

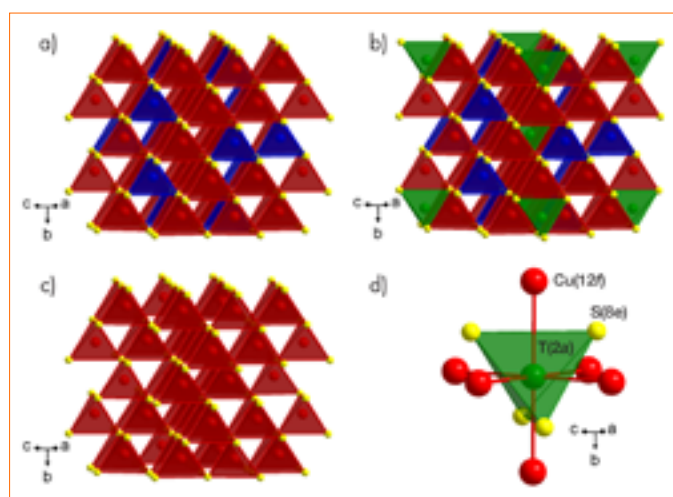


Figure 3

Representation of the **a)** ordered sphalerite framework ‘ $Cu_{26}Ge_6S_{32}$ ’ resulting from the omission of the $T(2a)$ atoms; **b)** $Cu_{26}T_2Ge_6S_{32}$ colusite structure; **c)** conductive ‘ $Cu_{26}S_{32}$ ’ framework (*i.e.* ordered sphalerite framework by simply omitting the Ge atoms); and **d)** mixed tetrahedral–octahedral complex $[TS_4]Cu_6$ —the Cu, T, Ge, and S atoms are depicted in red, green, blue and yellow, respectively.



Inés Puente Orench. Spanish Aragón Materials Science Institute, CSIC, Spain
 ‘Since 2007 I have been co-responsible for CRG-D1B, the powder neutron diffractometer at the ILL. Our research focus is the synthesis and characterisation of multi-metallic organic frameworks and their derived products. Powder neutron diffraction in combination with single crystal X-rays provides unique information about preferred co-ordination environments.’

Encoding metal cation arrangements in metal–organic frameworks for programming the composition of electrocatalytically active multi-metal oxides

High-intensity powder diffractometer DIB

Fuel cells are probably one of the best alternative energy sources to fossil fuel. However, the high cost and/or scarcity of some of their components have hindered their commercialisation. In particular, to obtain high oxygen reduction reaction (ORR) activity, a significant amount of platinum is used in cathodes. Spinel-type oxides have recently appeared as alternative electrocatalysts for this reaction. The activity of these solids strongly depends on their composition, and fine adjustment of the metal component and their ratios could lead to improvement in their performance. However, up until now the incorporation of three or four metal cations at precise atomic ratios in the same solid remains challenging with current synthetic routes.

AUTHORS

C. Castillo-Blas, N. López-Salas, M.C. Gutiérrez, E. Gutiérrez-Puebla, M. Ángeles Monge, Á. Monge and F. Gándara (CSIC, Madrid, Spain)
 I. Puente Orench (ILL and CSIC, Madrid, Spain)

ARTICLE FROM

J. Am. Chem. Soc. (2019)—doi: 10.1021/jacs.8b12860

Our study is based on the use of metal–organic frameworks (MOFs) that comprise multiple metal elements as platform materials for incorporating, in a controllable way, desired arrangements of selected metal cations. Post-synthetic transformation of these materials allows multi-metal spinel oxides with compositions that are programmable from the complex MOF precursors to be obtained. Some of these solids exhibit catalytic activity comparable with commercial platinum-based catalysts, in terms of current density and number of transferred electrons.

Metal–organic frameworks (MOF) are crystalline material, formed by the combination of metal clusters with organic linkers to produce extended, periodic structures. We have shown that through a careful combination of inorganic secondary building units (SBUs), network topology and initial molar ratios it is possible to obtain isoreticular MOFs incorporating up to four different metal cations distributed at specific locations. In particular, starting from an MOF formed by zinc and the organic linker 4,4′-(hexafluoroisopropylidene) bis(benzoic acid) ($H_2hfipbb$), we have successfully incorporated cobalt, manganese and calcium in the same SBU. By taking advantage of differences in the preferential co-ordination environment of selected metal elements, and with judicious adjustment of their initial molar ratios, it is possible to direct the location of these metal cations at specific positions, resulting in the formation of different binary, ternary and quaternary atomic sequences (**figure 1**).

Figure 1

The multi-metal MOF is formed by the combination of various cations (Zn^{2+} , Co^{2+} , Mn^{2+} and Ca^{2+}) forming a helical, inorganic SBU, and the organic linker $H_2hfipbb$ (left). The helical-shaped inorganic SBUs are formed by alternating tetrahedral and octahedral co-ordination polyhedra. The SBUs contain 2, 3 or 4 different metal elements (right).

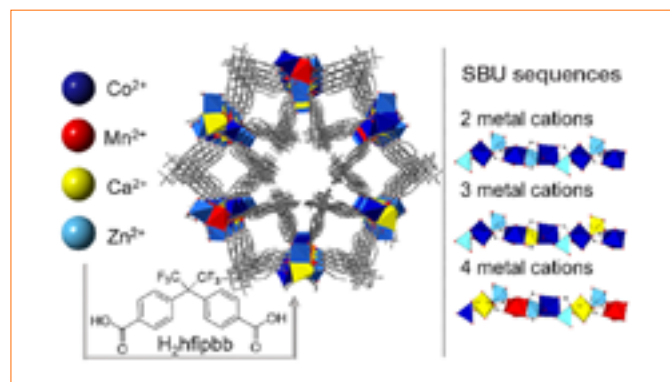
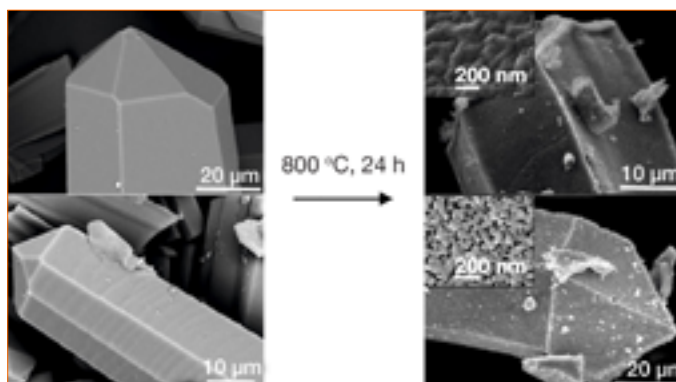
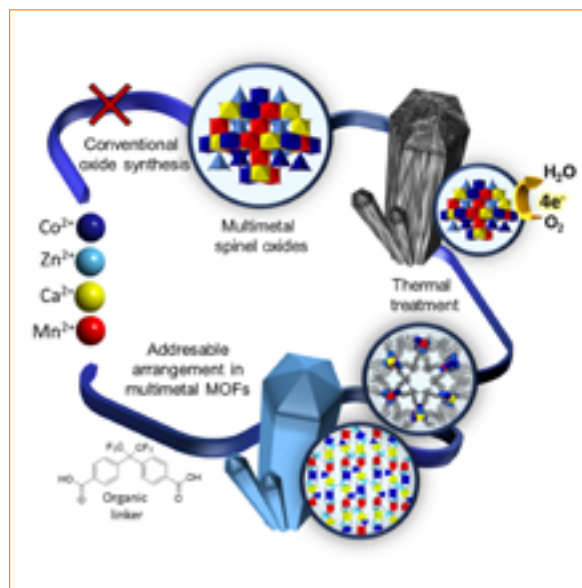


Figure 2

Thermal decomposition of multi-metal MOFs allow multi-cation oxides with compositions unattainable via conventional oxide synthetic routes to be obtained. The metal ratios in the resulting oxides are transferred from their corresponding parent MOFs.

Furthermore, we have since demonstrated that these complex compositions can be translated to other types of materials. Indeed, through a standard calcination process we have obtained multi-metal oxides that maintain the starting metal ratios of the parent MOFs. Notably, some of these metal oxides have compositions that are not attainable by other synthetic routes (**figures 2** and **3**). By combining single crystal and powder, Xrays and neutron diffraction, as well as electron microscopy techniques, we have completed the structural description of the starting MOF materials and fully characterised their metal oxides counterpart.

A strong correlation between the MOF initial metal arrangement and the type of oxide obtained is evidenced in this study. Thus, binary MOF systems tend to result in a mixture of crystalline phases, while for ternary ones the relative amount of cobalt in the MOF governs whether a mixture of phase or pure spinel oxides is obtained. For quaternary systems, a complex interplay between all four elements is observed, making it possible to obtain a large number of pure-phase spinel oxides with a variety of compositions. Through this methodology we have been able to produce up to seventeen multi-metal spinel-type oxides with compositions that are translated from the MOF precursor and which can be used as electrocatalysts for ORR. Although the relation between composition and ORR activity is yet to be understood, we have identified up to five solids that exhibit current density values that rival those of commercial platinum catalysts while showing excellent recyclability and stability in respect of poisoning with methanol.

**Figure 3**

SEM images of MOFs (**left**), and the corresponding calcination products (**right**), which are composed of the metal-oxides' nanoparticles.



Anne A.Y. Guilbert, French
Department of Physics, Imperial College
London, UK

Twitter: @AGuilbert9

*'I'm working on studying and exploring
structure and dynamics of semiconducting
organic materials for photovoltaic and*

*photocatalytic applications using synergistically various multi-scale
neutron scattering and multi-approach simulation techniques.'*

Neutron scattering sheds light on the structural dynamics of semiconducting organic materials for energy applications

*Three axis spectrometer IN1-Lagrange,
time-of-flight spectrometer IN6-SHARP,
spin-echo spectrometer IN11,
backscattering spectrometer IN16B,
and diffractometer D16*

Conjugated polymers are semiconducting organic macromolecules. They combine the optical and electronic properties of classical semiconductors such as silicon, with the ease of processing, light weight and flexibility of polymers. They are potential candidates for many applications (figure 1), such as light-emitting diodes, solar cells, transistors, water splitting and bioelectronics. Organic photovoltaics have a carbon footprint lower than all other solar technologies and as such have the potential to truly revolutionise the energy market [1].

Figure 1

Schematic illustration of one of our presently studied conjugated polymers, featured on the cover of Chemistry of Materials in December 2019.

AUTHORS

A.A.Y. Guilbert, J. Nelson and M.V.C Jenart (Imperial College London, UK)
P.A. Finn and C.B. Nielsen (Queen Mary University of London, UK)
M. Zbiri, P. Fouquet, V. Cristiglio and B. Frick (ILL)

ARTICLE FROM

Chem. Mater. (2019)—doi: 10.1021/acs.chemmater.9b02904

REFERENCES

- [1] <https://www.heliatek.com/blog/heliateks-truly-green-and-organic-solar-films/>
- [2] A.A.Y. Guilbert, M. Zbiri, P.A. Finn, M. Jenart, P. Fouquet, V. Cristiglio, B. Frick, J. Nelson, and C.B. Nielsen, Chem. Mater. 31, 23 (2019) 9635

The most appealing feature of conjugated polymers is their tunability through chemical design. If some design rules have been drawn from studying the relationship between chemical structure and properties, newly designed conjugated polymers often break those rules as structural dynamics also affects optical and electronic properties. Structural dynamics dictates how a material will interact, deform or rearrange under both external stimuli such as optical (presence of excitons) or electrical (presence of charges) stimuli or temperature, and the stress or strain that occurs when used on flexible substrates. The prompt relaxation of excited states involves mainly high-frequency skeletal motions. The delocalisation of excited states and charges are affected by the planarity of the polymer chains and molecular packing, thus involving low-frequency lattice vibrations. The conformational dynamics of the polymer chains is slow (relaxation), evolving on a longer time scale (up to the ns) and affecting the vibrational degrees of freedom, hence affecting fundamental optical and electrical transitions in these materials.

In this study [2] we showed that neutron spectroscopy is a powerful master tool for probing both vibrations and relaxation features of conjugated polymers. First, neutrons do not interact with the delocalised electronic system of the conjugated polymers. Thus, neutron spectroscopy enables us to probe the phononic landscape and structural dynamics of the polymer directly. In this respect it provides valuable complementary information to that provided by Raman and IR spectroscopy, both of which have been used extensively in the field. Second, by using deuteration we can highlight coherent or incoherent



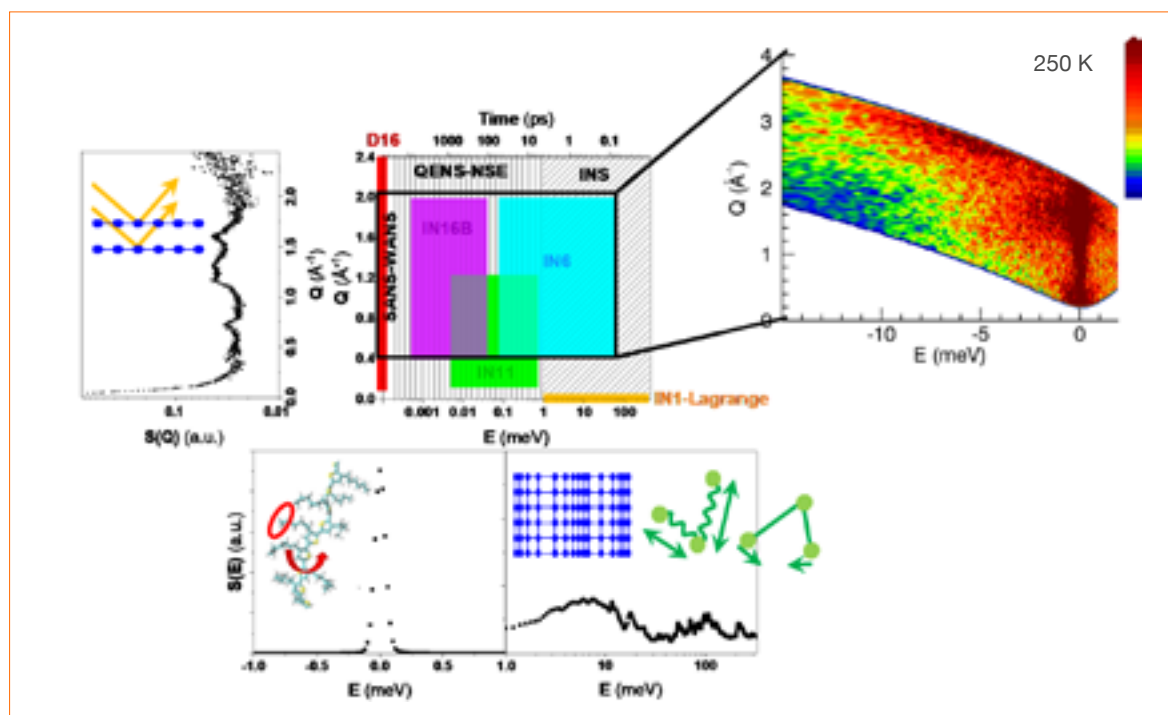


Figure 2

Schematic illustration of the probed length and time ranges, *i.e.* the momentum-energy (Q-E) space of the five different instruments used in this study.

Inset) The dynamical structure function map, $S(Q,E)$ of deuterated RR-P3HT (d-RR-P3HT) measured at 250 K on the IN6 spectrometer. The elastic signal, $S(Q)$, of d-RR-P3HT measured at 296 K using the D16 diffractometer is shown on the left-hand side. The Q -averaged QENS signal, $S(E)$, of d-RR-P3HT from IN6 is depicted on the bottom left-hand side, and the inelastic (INS) signal, $S(E)$, of d-RR-P3HT measured at 10 K on the IN1-Lagrange spectrometer, is depicted on the bottom right-hand side.

processes and tune the probe using contrast variation. This not only provides information about co-operative motions and self-motions but also enables us to hide or highlight part of the molecules. Third, neutron spectroscopy is one of the few techniques that allows the probing of both structure (Q-range or space) and dynamics (energy or time range) on the femtosecond to nanosecond time scale. Most exciton/charge transfer processes in conjugated polymers occur on the femtosecond to picosecond time scale. Charge transport, despite occurring by means of a hopping process and being characterised by a longer time scale of hundreds of picoseconds to tens of nanoseconds, results from charge transfer involving local energy sites. Thus, neutron spectroscopy allows us to cover the time scale relevant to optical and electronic processes.

We used a combination of five instruments at the ILL in synergy—the diffractometer D16, the cold-neutron time-of-flight spectrometer IN6, the backscattering spectrometer IN1B, the spin-echo spectrometer IN11 and the hot-neutron spectrometer IN1-Lagrange—to obtain a full map of the structural dynamics of a conjugated polymer model system poly(3-hexylthiophene) (**figure 2**):

- (i) We used neutron diffraction to primarily probe the crystalline/ordered structure of the polymer. Local and

vibrational dynamics were probed using synergistically different neutron spectroscopic techniques.

- (ii) Time-of-flight, backscattering and spin-echo measurements were performed to probe local and relaxation dynamics by covering both the picosecond and nanosecond time scales. These techniques allowed us to probe the structure (Q-range) and the dynamics (energy range) simultaneously and thus to gain deeper insight into the relationship between the two. Further insight into the dynamics was gained through deuteration and molecular dynamics (MD) simulations. MD enabled us to calculate both coherent and incoherent intermediate scattering functions.
- (iii) Hot-neutron vibrational spectroscopy was carried out to map out the full vibrational spectrum, including both the lattice (external) modes and the molecular (internal) degrees of freedom. Vibrational spectroscopy is not only sensitive to ordered phase but also to disordered phase. Thus, by combining neutron vibrational spectroscopy with MD, molecular and periodic density functional theory calculations, we bridged the gap between the molecular level and the solid-state scale.

This study [2] allowed us to put specific emphasis on the impact of disorder, degrees of freedom and packing, and on investigating the adequacy of the theory needed to describe and capture the essential structural and dynamical features of the conjugated polymers studied. Different length scales and time scales were appropriately covered, allowing us to describe the various phases and energy landscapes of the studied materials adequately. This is of the utmost importance, since tailoring materials for efficient energy applications depends on a better understanding of the underlying microstructural phases and the associated dynamical behaviours.



Adrien Perrichon. French Chalmers University of Technology, Sweden
 ‘My research focuses on the investigation of “energy materials” using several neutron scattering techniques (INS, QENS, NCS and ND) and first-principles calculations, specifically on complex non-stoichiometric oxides with proton or oxide-ion conducting properties.’

Local structure and vibrational dynamics of proton-conducting $\text{Ba}_2\text{In}_2\text{O}_5(\text{H}_2\text{O})_x$

Three-axis spectrometer IN1-Lagrange

Proton-conducting oxides are materials of huge interest for a variety of applications, such as electrolytes in membrane reactors or in proton-conducting fuel cells operating in the intermediate temperature $T = 200\text{--}500\text{ }^\circ\text{C}$. Inelastic neutron scattering (INS) and *ab initio* molecular dynamics (AIMD) simulations provide a powerful means of investigating the vibrational dynamics and local co-ordination of protons in these materials. This is essential for gaining insight into the microscopic mechanisms of proton diffusion, which allows for the rational design of materials with higher proton conductivity: a crucial requirement for the development of new technologies.

AUTHORS

A. Perrichon, L. Mazzei, S.M.H. Rahman and M. Karlsson (Chalmers, Göteborg, Sweden)
 M. Jiménez-Ruiz (ILL)

ARTICLE FROM

J. Mater. Chem. A (2019)—doi: 10.1039/c9ta04056k

REFERENCES

- [1] A. Jayaraman, A. Magrez, M. Caldes, O. Joubert, M. Ganne, Y. Piffard and L. Brohan, *Solid State Ionics* 170 (2004) 17
- [2] J.-R. Martinez, C.E. Mohn, S. Stølen and N.L. Allan, *J. Solid State Chem.* 180 (2007) 3388
- [3] R. Dervişoğlu, D.S. Middlemiss, F. Blanc, Y.-L. Lee, D. Morgan and C.P. Grey, *Chem. Mater.* 27 (2015) 3861
- [4] L. Mazzei, A. Perrichon, A. Mancini, G. Vahnström, L. Malavasi, S.F. Parker, L. Börjesson and M. Karlsson, *J. Mater. Chem. A* 7 (2019) 7360

Structurally related to the acceptor-doped perovskites, the hydrated $\text{Ba}_2\text{In}_2\text{O}_5(\text{H}_2\text{O})_x$ phases differ through the presence of extended static distortions. These distortions lead to the stabilisation of at least two distinct protons sites, H(1) and H(2) [1, 2], in a structure referred to as ‘pseudo-cubic’ (**figure 1**). Upon dehydration, oxygen vacancies tend to segregate to ultimately form the $\text{Ba}_2\text{In}_2\text{O}_5$ brownmillerite phase.

We performed INS measurements on the IN1-Lagrange spectrometer on fully and partially hydrated $\text{Ba}_2\text{In}_2\text{O}_5(\text{H}_2\text{O})_x$ phases. We also performed extensive AIMD simulations from which we calculated the vibrational densities of states, $G(\hbar\omega)$, and the neutron scattering cross section, $S(Q, \hbar\omega)$. By comparing the experimental and calculated $S(Q, \hbar\omega)$, and the infrared (IR) spectra, we proposed an assignment of the spectra of the fully hydrated phase (**figure 2a**). The bands (B), (D) and (G) are associated with the H(1) proton and correspond to the fundamental, degenerated $\delta(\text{O-H}(1))$ wag modes, their overtones and the $\nu(\text{O-H}(1))$ stretch mode, respectively. For the H(2) protons, the ‘in-plane’ (C_1) and ‘out-of-plane’ (C_2) $\delta(\text{O-H}(2))$ modes are clearly separated, with overtones (E_1 and E_2), while the band (F) corresponds to $\nu(\text{O-H}(2))$. In particular, we showed that the (β) bands at 250 and 300 meV in the

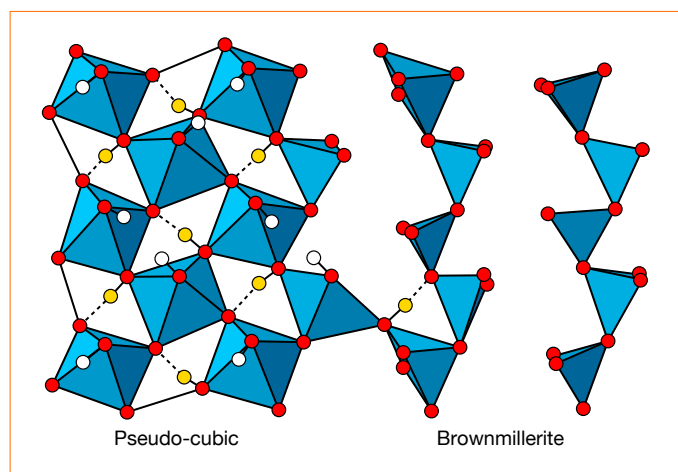


Figure 1

Schematic representation of the distorted layer of the brownmillerite-based $\text{Ba}_2\text{In}_2\text{O}_5(\text{H}_2\text{O})_x$, exhibiting hydrated ‘pseudo-cubic’ domains (**left**) and brownmillerite structured domains (**right**), respectively. InO_x polyhedra in blue, oxygen atoms in red, H(1) protons in white, H(2) protons in yellow.

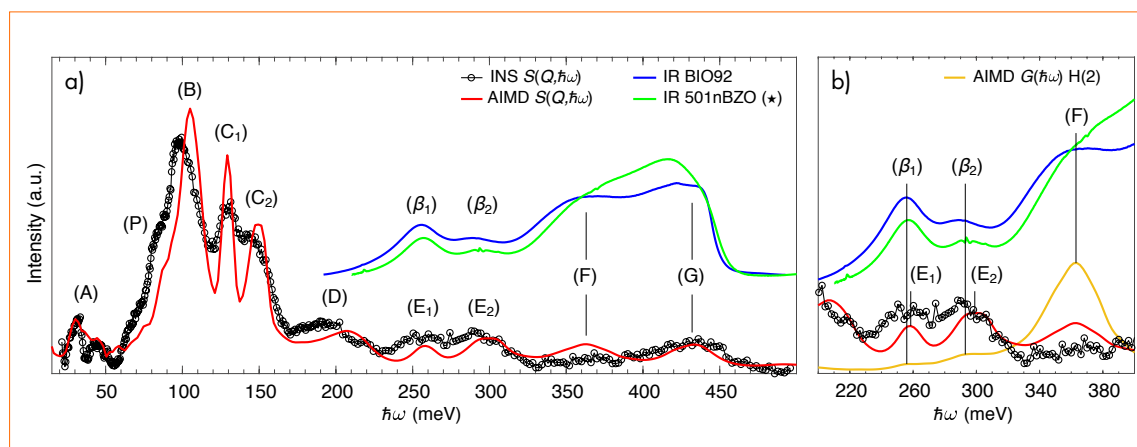


Figure 2

a) INS (black line and circles) and IR (blue line) spectra of $\text{Ba}_2\text{In}_2\text{O}_5(\text{H}_2\text{O})_{0.92}$, and calculated scattering function of the fully hydrated model (red line).

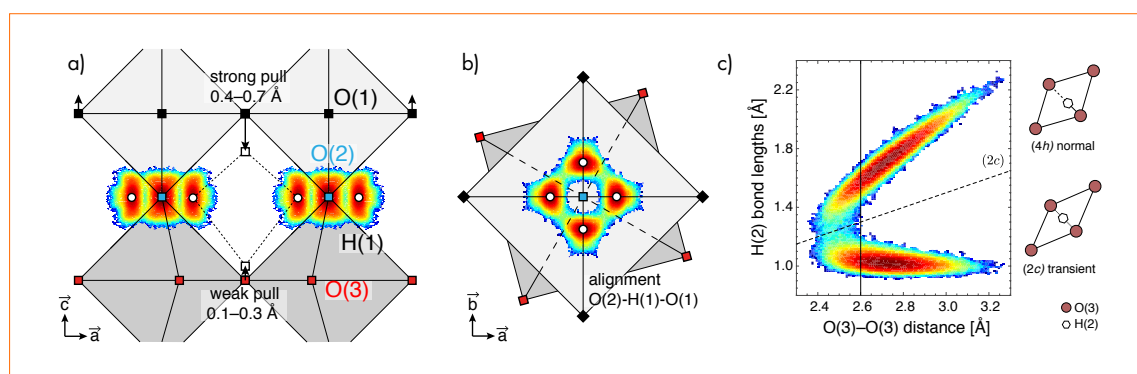
b) Close-up of the energy region of the (E) and (β) bands. The IR spectrum of 50In/BZO (green line), reproduced and adapted with permission from [4], is also represented.

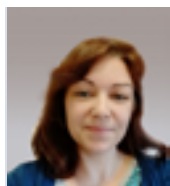
IR spectra are signatures, not of $\delta(\text{O-H}(2))$ overtones but of fundamental $\nu(\text{O-H}(2))$ modes associated with protons in a particularly strong hydrogen-bonding configuration (**figure 2b**). This feature is also present in related In-doped BaZrO_3 materials at high In-doping levels [4]. From the AIMD simulations, we correlated this specific H(2) population to configurations where the O(3)–O(3) distance of the O(3)–H(2)–O(3) pattern is $< 2.6 \text{ \AA}$, close to the transient state of H(2) proton transfer along its hydrogen bond (**figure 3c**). We also established that two local environments for H(1) coexist on the H(1) site, in accordance with recent studies [3], due to a difference in the amplitude of displacement of the acceptor oxygen atom [O(1), O(3)] to which the H(1) proton is hydrogen-bonded (**figure 3a**). The difference in the amplitude of displacement is notably due to the alignment of the covalent bond on the edge of the O(1)₄O(2)₂ octahedra (**figure 3b**).

For the partially hydrated phases, similar spectra are obtained, which suggests that hydrogen and oxygen atoms segregate and form hydrogen-rich, oxygen-rich domains that maintain the pseudo-cubic structure.

Figure 3

Schematic drawing of the pseudo-cubic phase showing the amplitude of displacement of O(1) and O(3) under the pull of the hydrogen bonds of H(1) protons (**a**), and the alignment of the O(2)–H(1) covalent bond with the edges of the O(1)₄O(2)₂ octahedra (**b**). Correlation between the bond lengths of the O(3)–H(2) covalent bond (below dashed line), the H(2)–O(3) hydrogen bond (above dashed line) and the O(3)–O(3) distance (**c**).





Laura Cañadillas-Delgado. Spanish The ILL

'I work on the synthesis and characterisation of multifunctional metal-organic materials, trying to ascertain structure-properties relationships in order to find clues on how to design new materials with desired assets.'

The determination of complete structural models including H atoms is necessary to identify relationships among the different properties. Neutron diffraction provides us with crucial information in this context.'

Incommensurate structures of the $[\text{CH}_3\text{NH}_3][\text{Co}(\text{COOH})_3]$ compound

Single-crystal diffractometers D19 and Laue single-crystal diffractometer CYCLOPS

The development and characterisation of new materials are key challenges in condensed matter, chemistry and physics. The ability of metal-organic frameworks to combine different physical properties within the same framework has attracted huge interest in recent years. We have focused our efforts on finding new multiferroic materials in which electric and magnetic order coexist. The $[\text{CH}_3\text{NH}_3][\text{Co}(\text{COOH})_3]$ (1) compound is a multiferroic of type I material that presents several structural phase transitions that affect its electrical behaviour. Neutron measurements have been crucial in studying the crystal structure of this compound in the different phases.

AUTHORS

L. Cañadillas-Delgado, L. Mazzuca, O. Fabelo, J.A. Rodríguez-Velamazán and J. Rodríguez-Carvajal (ILL)

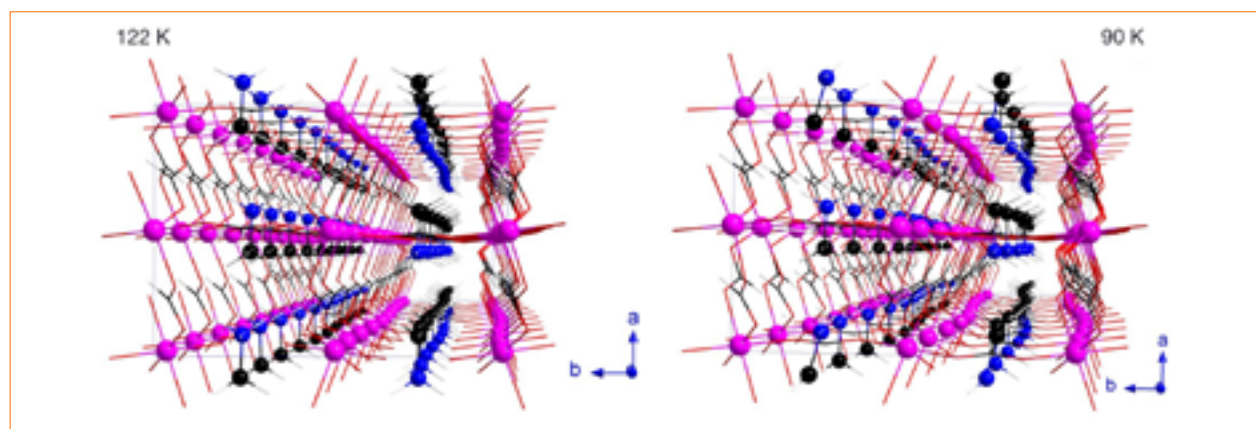
ARTICLE FROM

IUCr. (2019)—doi: 10.1107/S2052252518015026

Electric permittivity measurements on compound 1 showed a smooth change in its electric behaviour. However, measurement of the specific heat yielded no evidence about the phase transition temperatures. Single-crystal Laue diffraction is a good tool to survey structural changes, and in order to be sensitive to changes in the position of the hydrogen atoms we decided to use neutron diffraction. We used the ILL's CYCLOPS, a single-crystal, Laue neutron diffractometer with high flux and covering wavelengths from 0.8 to 3.2 Å, permitting a huge part of reciprocal space to be explored in only one image. We identified three phase transitions involving incommensurate structures. The model of each incommensurate structure needs the refinement of not only the positions and thermal ellipsoids of the main structure but also the amplitudes of the modulation of each atom. The refinement of these amplitudes is dependent on the intensity of the satellites; thus, a large number of observations, including high-Q satellite reflections, are needed. The capture of full scans at several temperatures above and below each phase transition on the monochromatic single-crystal neutron diffractometer D19 allowed us to obtain enough data even at high-Q, thanks to neutron scattering.

Figure 1

View along the wave-vector direction of the model. The graphical representations have been depicted considering a super-cell (10 times the average structure along the c-axis), in order to include at least one complete period.



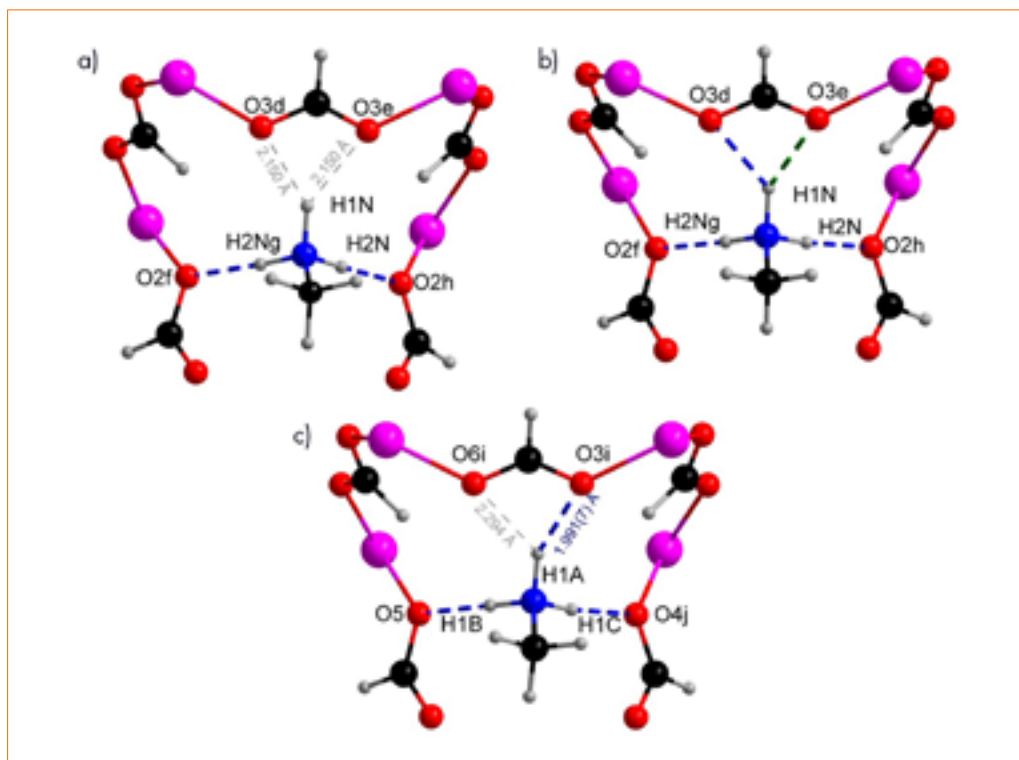


Figure 2

View of the possible hydrogen bonds, denoted by blue and green dashed lines, in the orthorhombic commensurate phase **(a)**, incommensurate phases **(b)** and commensurate monoclinic phase **(c)**. The distances denoted in grey are large in order to be considered as hydrogen bonds.

Upon cooling, at ~ 128 K compound **1** suffers a phase transition from the commensurate orthorhombic phase in $Pnma$ (I) to the orthorhombic incommensurate phase (II), crystallised in the $Pnma(00\gamma)0s0$ space group with $q = 0.143(1) \cdot c^*$. Below 96 K, a second orthorhombic incommensurate phase is observed involving an elongation of the modulation length ($q = 0.1247(10) \cdot c^*$) (**figure 1**). Analysis of the intensity of the satellites suggests a complex scenario with 'sluggish' or 'partly first-order' transition, which could also explain the lack of signal in specific heat measurements.

Below 78 K, the orthorhombic incommensurate phase becomes a monoclinic phase resulting in a twinned crystal. The twin domains are related by a rotation of 180° along the one that becomes incommensurate between 128 and 78 K.

In the incommensurate structures, two of the three H-atoms of the NH_3 group of the counter-ion are always establishing H-bonds, while the third fluctuates between two oxygen atoms from the same formate ligand (**figure 2**), giving rise to *flip-flop* behaviour. The variation in the H-bond lengths, due to the modulation, suggests that the competition between these interactions is responsible for the different phase transitions.



Joel Bertinshaw. Australian
Max Planck Institute for Solid State Research,
Stuttgart, Germany

'My research is focused upon the study of physics that underlie exotic ground states in complex oxides, using neutron and resonant X-ray scattering techniques. We collaborate

to combine detailed experimental studies with advanced theoretical approaches. Crystal and magnetic structural determination is a vital component of our research, making neutron diffraction an indispensable tool.'

A distinct crystallographic structure identified in a non-equilibrium state

Single-crystal diffractometer D9 with in situ applied DC voltage

The exploration of non-equilibrium phenomena in correlated-electron systems is a major frontier in condensed matter research. Recently, it was shown that the Mott insulator Ca_2RuO_4 expresses a rare example of a non-equilibrium state stabilised by electric current, involving the transition to an electrically conducting phase with strong diamagnetism. Combining neutron diffraction with dynamical mean field theory, we establish that this phase assumes a distinct crystal structure, which leads to a semi-metallic state with a partially gapped Fermi surface. This study provides a new basis for theoretical work on the origin of the anomalous diamagnetism and represents a new approach to tuning complex oxides.

Figure 1

a) Single-crystal neutron diffraction rocking scan around the (006) reflection at $T = 130$ K in the equilibrium state, shown as a map plotting the scattering angle versus the horizontal detector axis.

b) The same measurement under current flow reveals two separate peaks in the non-equilibrium state.

c) The fitted Q position of the reflections was used to calculate the temperature trend of the c-axis lattice parameters. The non-equilibrium S* and L*-phases display a behaviour distinct from the equilibrium S phase, shown in grey. The inset plots the *in situ* resistance of the two states.

AUTHORS

J. Bertinshaw and B. Keimer (MPI-FKF, Stuttgart, Germany)
B.J. Kim (Postech, Pohang, South Korea)
P. Hansmann (MPI-CPFS, Dresden, Germany)
O. Fabelo (ILL)

ARTICLE FROM

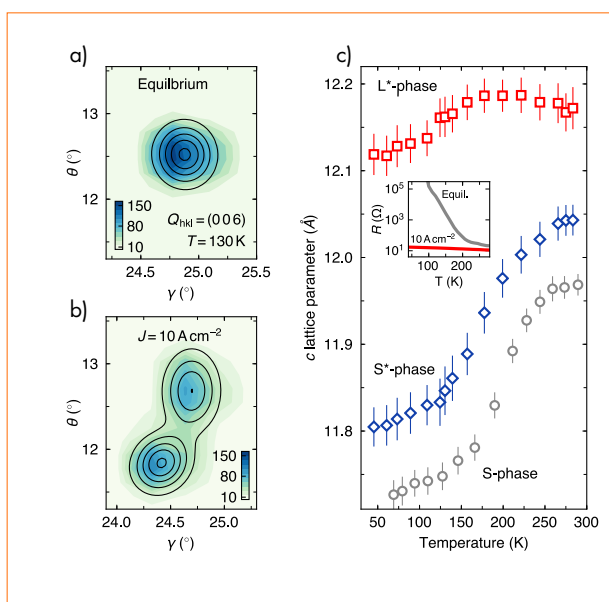
Phys. Rev. Lett. (2019)—doi: 10.1103/PhysRevLett.123.137204

REFERENCES

- [1] Jain *et al.*, Nat. Phys. (2017) (10.1038/nphys4077)
- [2] Sow *et al.*, Science (2017) (10.1126/science.aah4297)
- [3] Friedt *et al.*, Phys. Rev. B (2001) (10.1103/PhysRevB.63.174432)

The $4d$ -electron transition metal oxide Ca_2RuO_4 represents a convergence of spin-orbit coupling and strongly correlated electron-interaction energies that leads to exciting quantum phenomena [1]. Recently, it was established that under current flow the insulating ground state transforms into a semi-metallic phase with high diamagnetic susceptibility [2]. An important next step in our understanding of this non-equilibrium state is an accurate knowledge of the atomic positions, which would allow *ab initio* calculations of the electronic structure to be performed. Such information is difficult to obtain in pump-probe experiments; however, here the non-equilibrium phase is maintained by the applied current, offering a rare opportunity to apply neutron diffraction, which is also a direct probe of magnetic structures.

Neutron diffraction measurements were conducted with a high-quality Ca_2RuO_4 crystal, prepared using a floating-zone mirror furnace. The crystal was mounted in such a way that the *in situ* DC voltage was applied along the c -axis in a two-probe circuit. At $T = 280$ K, the applied voltage was systematically increased through the transition to the metallic regime before maintaining the current density at $J = 10 \text{ A}\cdot\text{cm}^{-2}$ for the experiment.



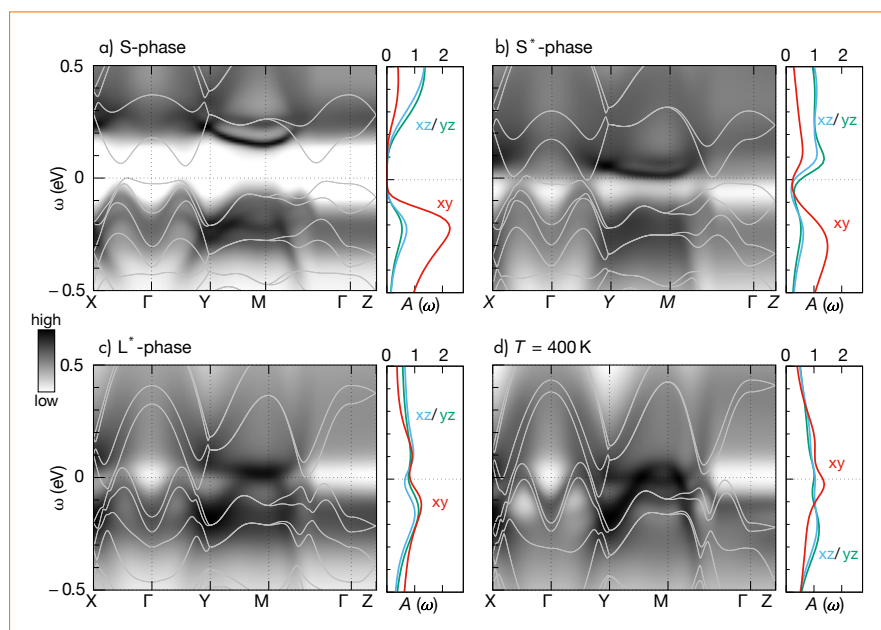


Figure 2

DMFT-calculated intensity maps for electron spectral function as a function of energy and momentum along high-symmetry directions in the Brillouin zone. The orbitally resolved local density of states is shown on the right of each panel. The light grey lines overlay equivalent Density Functional Theory (DFT) calculations. The *S*-phase is insulating (**a**), while in the *S**-phase the insulating gap is closed and small electron and hole pockets form at the Fermi surface, indicating semi-metallic behaviour (**b**). The overlap increases significantly in the *L**-phase (**c**), showing similarity with the $T = 400$ K equilibrium state (**d**).

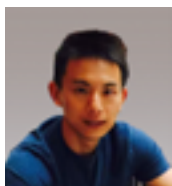
Rocking scans of the out-of-plane (006) reflection were performed at ~ 10 K intervals from 280 K through the magnetic transition $T_N = 110$ K. The process was then repeated without applied current for comparison with the equilibrium state. D9 uses an area detector; **figure 1a** and **b** plots scans conducted at $T = 130$ K as colour maps that sums the vertical detector range (perpendicular to the scattering plane). The single reflection in equilibrium splits into two reflections under current flow, indicating the presence of two phases. Using a 2D Gaussian least-squares fitting process (depicted as contour lines), the temperature evolution of the *c*-axis lattice parameter was calculated (**figure 1c**). It is apparent that the phases in non-equilibrium are distinct from the equilibrium state (known as the *S*-phase) and are assigned the shorter *c*-axis *S**-phase and the elongated *L**-phase. The *S**-phase expresses constant expansion over the equilibrium state that persists to the lowest measured temperatures, while the *L**-phase follows a trend similar to the equilibrium *L*-phase that arises at high temperatures ($T = 400$ K) [3].

A precise determination of the atomic positions of the *S** and *L** phases was achieved using an extensive range of reflections collected at $T = 45$ K and 130 K and $J = 10$ A·cm⁻². Compared with equilibrium, the *S**-phase atomic positions reveal distinct structural distortions, including a marked decrease in orthorhombicity combined with a relatively small reduction in tetragonal compression;

while the *L**-phase continues to share behaviour with the equilibrium *L*-phase. At the same time, we observed no sign of superstructure reflections, indicating that the equilibrium antiferromagnetic state is fully suppressed under current flow.

To study the sensitivity of the electronic state to these crystallographic distortions, band structure calculations were performed using dynamical mean field theory (DMFT), taking into account spin-orbit coupling and electronic correlations. **Figure 2** shows the calculated spectral function and the local density of states near the Fermi level for the *S*, *S** and *L**-phases along with the high-temperature *L*-phase from the literature [3]. The equilibrium *S*-phase is Mott-insulating, with a clear gap between the lower and upper Hubbard bands. In the *S**-phase, these bands broaden and overlap, releasing hole and electron charge carriers. The overlap is very small, suggesting a semi-metallic state with hole and electron pockets at the Fermi surface. On the other hand, the electronic states in the *L**-phase resemble those of the fully metallic, high-temperature *L*-phase.

These results reveal that the electronic band structure is extremely sensitive to current density through the RuO₆ distortions. Furthermore, the conspicuous deviation of the *S**-phase from the usual trend of other metallic phases in equilibrium indicates a unique mechanism for the current-induced state that underlies the strong anomalous diamagnetism.



Xianwen Mao. Chinese

Department of Chemistry and Chemical Biology, Cornell University, USA

Twitter: @XianwenMao

'I obtained my PhD in Chemical Engineering at MIT (USA) with a research focus on polymer and interface science. I am currently a

postdoctoral associate at Cornell University (USA), working on single-molecule techniques. Recently, I discovered that the self-assembled nanostructures in ionic liquids facilitate charge storage at electrified interfaces, as a result of a collaboration with the ILL D33 facility.'

Self-assembled nanostructures in ionic liquids facilitate charge storage at electrified interfaces

Small-angle instrument D33

High-temperature, small-angle neutron scattering (SANS) experiments have helped to elucidate the nanostructuring of new amphiphilic surface-active ionic liquids (SAILs) based on common surfactants. At an electrified surface, this structuring leads to enhanced charge storage performance by suppressing undesired over-screening effects found in normal, electrical double layers. As a result, this class of ILs may be used as high-energy-density electrolytes suitable for many emerging electrochemical technologies.

AUTHORS

X. Mao, P. Brown, Y. Ren, A. A. H. Padua, M. F. Costa Gomes and T. A. Hatton (Massachusetts Institute of Technology, USA)
C. Červinka (Ecole Normale Supérieure de Lyon, France)
G. Hazell and J. Eastoe (University of Bristol, UK)
H. Li and R. Atkin (The University of Western Australia, Australia)
D. Chen (Stanford University, USA)
I. Grillo (ILL)

ARTICLE FROM

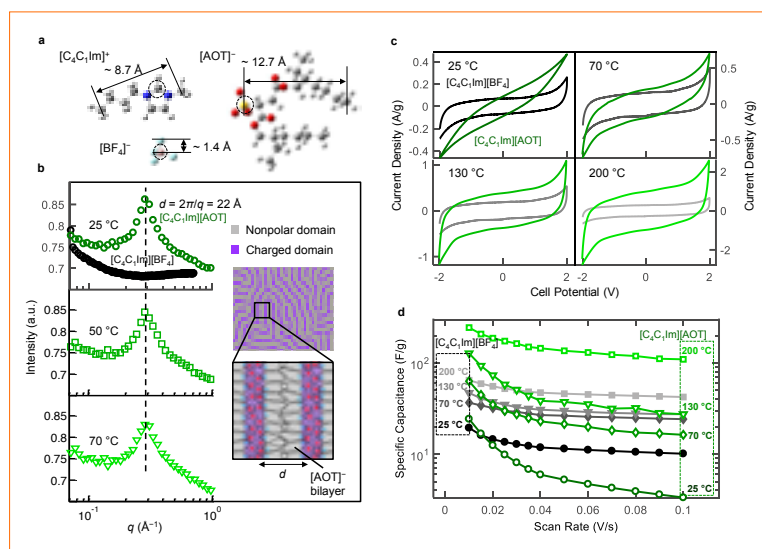
Nat. Mater. (2019)—doi: 10.1038/s41563-019-0449-6

Currently, aqueous and organic electrolytes are used in supercapacitors. More recently, however, ionic liquids (ILs) have been used as performance boosters, as they often have large electrochemical windows and are non-volatile. Although ILs are salts, at room temperature they are liquids and not crystalline solids. In a recent *Nature Materials* paper, new, highly efficient, detergent-like liquid electrolytes have been studied, leading to both a better understanding of electrolyte design and structuring and the generation of more efficient devices for storing electrical energy.

This study required the input of scientists with diverse skill sets ranging from chemical synthesis and electrical techniques to computational methods and neutron scattering. We discovered that SAILs exhibit significant and competing van der Waals interactions owing to the non-polar surfactant tails, resulting in unusual interfacial ion distributions. This sets them apart from conventional non-amphiphilic ILs, whose ion distribution is dominated by Coulombic interactions. Neutron scattering experiments performed on D33 at the ILL revealed the bulk structures of these SAILs, complementing results from atomic force microscopy (AFM) which have revealed the associated interfacial structures. Importantly, the sandwich-like bilayer structures generated by the SAILs can suppress undesired over-screening effects and thus impart much higher capacitances at elevated temperatures than those previously seen with traditional electrolytes.

This new class of electrolyte materials may be suitable for challenging operations, such as oil drilling and space exploration, but may also pave the way to improved supercapacitors in hybrid cars. These devices are essential components in modern hybrid cars and can outperform batteries in terms of higher power and offer better efficiency. This is particularly the case during regenerative braking; here, rather than being lost, mechanical work is turned into electrical energy that can be stored quickly, ready to be released, in supercapacitors. This reduces energy consumption and is much more environmentally friendly. Importantly, by using these new electrolytes future supercapacitors may even be able to store more energy than batteries can, potentially replacing batteries in applications such as electrical vehicles, personal electronics and grid-level energy storage facilities.

The design principles of these new electrolytes will continue to be improved using neutron scattering and reflectivity, as the ability to selectively contrast match individual ions is the principal advantage of neutron beams. Thus, only neutron techniques can provide molecular level insight into the packing and structures of the electrolytes at charged surfaces and in the bulk medium.

**Figure 1**

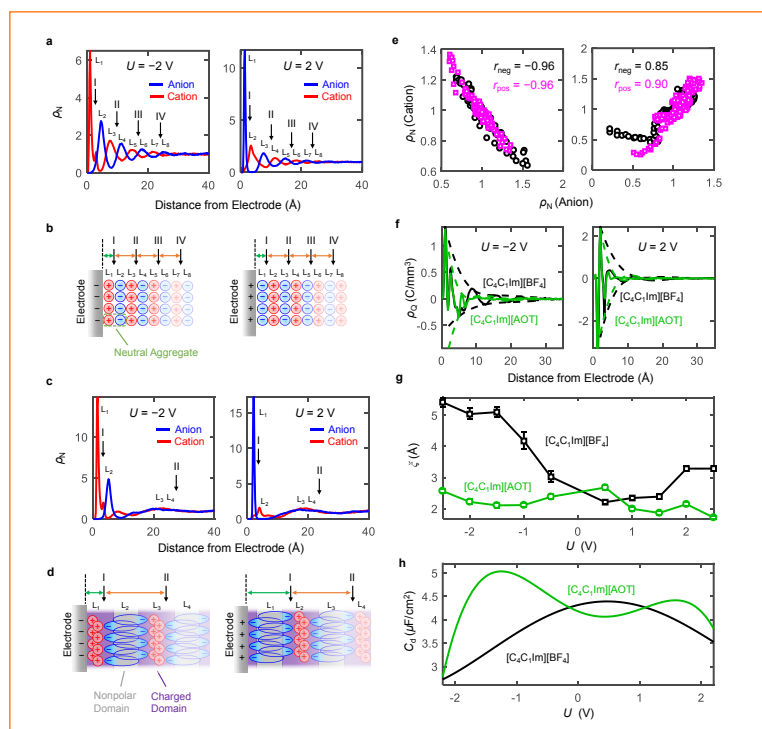
Bulk-phase structural and electrochemical characterisation of $[C_4C_1Im][AOT]$.

a) Molecular structures of $[C_4C_1Im]^+$, $[BF_4]^-$ and $[AOT]^-$ (H = white, C = gray, N = blue, S = yellow, O = red, B = pink, F = cyan). Typical distances in the molecular ions are indicated.

b) SANS profiles of a regular non-amphiphilic ionic liquid $[C_4C_1Im][BF_4]$ (25 °C) and the SAIL $[C_4C_1Im][AOT]$ (25, 50, 70 °C). **Inset)** Illustration of self-assembly of $[C_4C_1Im][AOT]$ leading to a repeating nanostructure comprising $[AOT]^-$ bilayers (cation = red, anion = blue).

c-d) Cyclic voltammetry profiles (scan rate = 20 mV/s)

(c) and specific capacitance versus scan rate **(d)** for $[C_4C_1Im][BF_4]$ or $[C_4C_1Im][AOT]$ at 25, 70, 130 and 200 °C.

**Figure 2**

Molecular dynamics simulations reveal unusual electric double layer structures of $[C_4C_1Im][AOT]$.

a-d) Ion number density (ρ_N) profile obtained from molecular dynamics simulations and schematic illustration of hypothesised ion arrangement for $[C_4C_1Im][BF_4]$ (**a, b**) and $[C_4C_1Im][AOT]$ (**c, d**) at negatively (left panel) and positively (right panel) charged interfaces with applied potentials (U) of ± 2 V. Black arrows with I, II, III and IV indicate possible positions corresponding to the AFM push-through locations.

e) Correlations between the cationic and anionic ρ_N obtained at positively (magenta, $U = 2$ V) and negatively (black, $U = -2$ V) charged interfaces for $[C_4C_1Im][BF_4]$ (left panel) and $[C_4C_1Im][AOT]$ (right panel) for the distance range of 10 to 40 Å away from the interface. r_{neg} and r_{pos} are the Pearson correlation coefficients for negatively and positively charged interfaces, respectively.

(f) Net charge density (ρ_Q) profiles (solid line) and corresponding envelope functions (dashed line) of $[C_4C_1Im][BF_4]$ and $[C_4C_1Im][AOT]$ at negatively (left panel, $U = -2$ V) and positively (right panel, $U = 2$ V) charged interfaces.

(g-h) Decay length (ξ) of the surface-induced ion layering (**g**) and differential capacitance (C_d) (**f**) as a function of U for $[C_4C_1Im][BF_4]$ and $[C_4C_1Im][AOT]$.

IN MEMORY of ISABELLE GRILLO

Isabelle Grillo passed away suddenly in her sleep at the beginning of August. She was just 46 years old.

Isabelle was a brilliant scientist. She joined the ILL at the tender age of just 25. In the space of two decades, she published some 225 articles, which have since been cited over 5 000 times.

Isabelle was truly committed to serving the ILL and its scientific community as a whole. This double page is dedicated to her.



Nico Carl. German

The ILL and the University of Paderborn, Germany
 'My work focuses on the self-assembly of polymers in aqueous solutions. Neutrons are a unique tool with which to study such structures, as they permit us to highlight certain parts of the self-assemblies by deuteration and contrast variation.'

Micellization of block copolymers with two anionic blocks

*Small-angle scattering instrument D11
 SAXS beamline ID02, ESRF*

Polyelectrolytes are macromolecules that carry an ionic group in the monomer unit. They are water soluble and highly relevant for industrial applications such as wastewater treatment or as rheology modifiers for concrete. We developed a block copolymer composed of two negatively charged polyelectrolytes, forming a new type of block copolymer micelles in the presence of Ca^{2+} . Micelle formation arises from selective complexation of Ca^{2+} with one of the blocks, as elucidated using small-angle neutron scattering (SANS).

AUTHORS

N. Carl and Klaus Huber (ILL & University of Paderborn, Germany)
 R. Schweins and Sylvain Prévost (ILL)

ARTICLE FROM

Soft Matter (2019)—doi: 10.1039/c9sm01138b

REFERENCES

- [1] R. Schweins, P. Lindner and K. Huber, *Macromolecules* 36 (2003) 9564
- [2] M. Hansch, H.P. Kaub, S. Deck, N. Carl and K. Huber, *J. Chem. Phys.* 148 (2018) 114906
- [3] H.B. Stuhmann, *J. Appl. Crystallogr.* 7 (1974) 173
- [4] C.G. Sinn, R. Dimova and M. Antonietti, *Macromolecules* 37 (2004) 3444

Sodium polyacrylate (PA) and sodium polystyrene sulfonate (PSS) are two negatively charged polyelectrolytes. Ca^{2+} cations bind to the anionic moieties of PA, which results in an aggregation and eventually precipitation of the polymer above a critical concentration [1]. This is commonly referred to as specific interaction. In contrast, Ca^{2+} does not bind to PSS and therefore no precipitation is observed [2]. Our study employed these considerably different interaction patterns by synthesizing a block copolymer of PA and PSS (**figure 1a**). In order to differentiate between the two polymer blocks in a neutron scattering experiment, the PA block was deuterated. This allows a contrast-variation SANS experiment to be performed [3] where the ratio of light H_2O and heavy water D_2O is systematically varied.

Figure 2 shows the SANS profiles of one of the polymers in the presence of Ca^{2+} at varying ratios of $\text{H}_2\text{O}/\text{D}_2\text{O}$. The contrast variation technique allows the scattering length of the solvent to be adjusted to that of the core and the corona, as well as to the average value of the polymer. The scattering curves from these measurements show that PA is complexed by Ca^{2+} and forms the core of the micelles. In contrast, PSS is located in the corona of the self-assemblies and stabilises them electrostatically. The

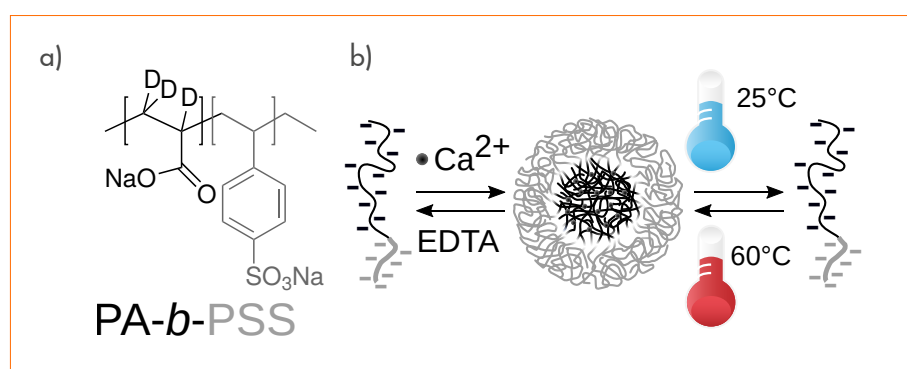
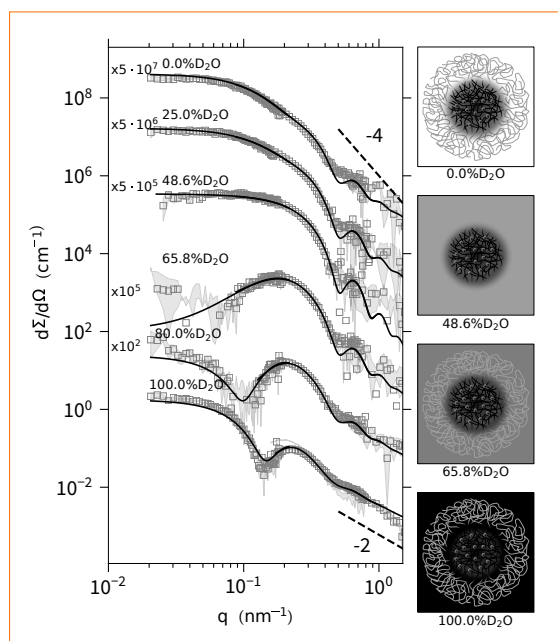


Figure 1

a) Chemical structure of the PA-*b*-PSS block copolymer.

b) Schematic representation of the micelle formation and its reversibility.

**Figure 2**

Contrast variation SANS experiment of PA-*b*-PSS block copolymer micelles. Solid lines indicate a fit to the model of a spherical, block copolymer micelle.

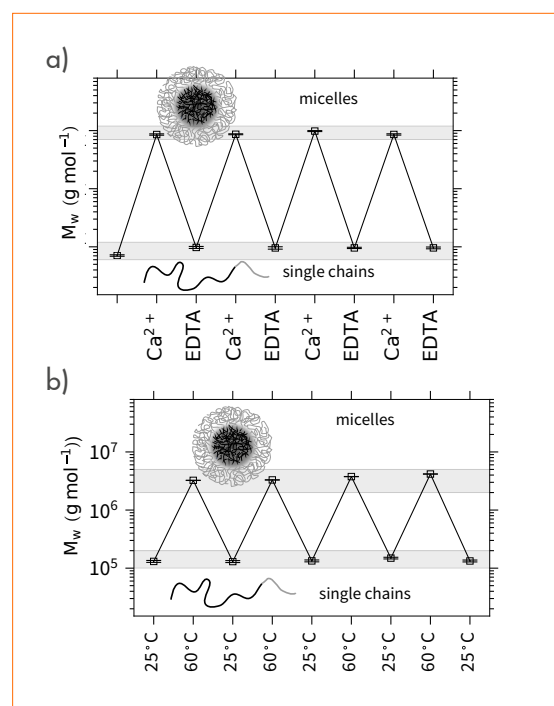
SANS instrument D11 at the ILL allows us to perform SANS experiments at very small momentum transfers with a high flux. This is crucial for the present study as the micelles are relatively large and the contrast variation technique results in a decrease of the scattering intensity, compared with classical experiments in full-contrast conditions.

In this study we also show that micelle formation is triggered by alternately adding Ca^{2+} cations and EDTA to a polymer solution. EDTA has a very high tendency to bind to Ca^{2+} cations and therefore reverses the micellization process (**figure 3a**). More strikingly, small temperature changes can also be employed to reversibly form ($\Delta T > 0$) and dissolve ($\Delta T < 0$) micelles (**figure 3b**). This feature arises from the entropically driven binding of Ca^{2+} to the PA block [4]. The binding is accompanied by the release of two sodium counter-ions and several water molecules from the hydrated shell, which is favourable in terms of entropy. The temperature increase therefore results in the stronger binding of Ca^{2+} to the PA block.

The micelle formation is entirely reversible and opens up a new route for the uptake and release of cargo. New contrast agents produced by using Gd^{3+} or Eu^{3+} and new strategies for ion separation are just a few of the possible applications of this block copolymer system.

Figure 3

Molecular weight after alternating additions of Ca^{2+} and EDTA (**a**) and temperatures cycles between 25 and 65 °C (**b**) indicating the reversibility of the micelle formation.





Andrea Lassenberger. Austrian
The ILL

'Multidisciplinarity is the key to understanding and progress in modern research. This approach is reflected in my research, which is driven by curiosity and an interest in how molecules and atoms assemble on the nanoscale. My main

interests are the synthesis, growth mechanisms and characterisation of metal oxide and organic nanoparticles, and the combination of these with biomaterials'.

Yeast-derived glycolipids make superparamagnetic iron oxide nanoparticles behave in biological systems

Vertical reflectometer D17 and small-angle scattering instrument D33 DUBBLE beamline at ESRF

Superparamagnetic iron oxide nanoparticles (SPIONs) smaller than ~20 nm in diameter are used in applications such as drug delivery, MRI and hyperthermia. The iron oxide cores must be coated with a defined hydrophilic shell in order to render them colloiddally stable and biocompatible. We synthesised monodisperse SPIONs with a single layer of irreversibly linked sophorolipids, a natural glycolipid produced in large amounts by the yeast *S. bombicola*. The core-shell structure of these nanoparticles can be resolved using a combination of SAXS and SANS: while X-rays are sensitive to the metal core of the nanoparticles, neutrons probe the highly hydrated polymer shell. This study demonstrates how the two complementary techniques are indispensable in nanomaterials research.

AUTHORS

A. Lassenberger, V. Cristiglio, I. Grillo and K. Batchu (ILL)
E. Reimhult and A. Scheberl (University of Natural Resources and Life Sciences, Vienna, Austria)
N. Baccile (Sorbonne Université, Paris, France)
D. Hermida-Merino (ESRF)

ARTICLE FROM

ACS Appl. Bio Mater. (2019)—doi: 10.1021/acsabm.9b00427

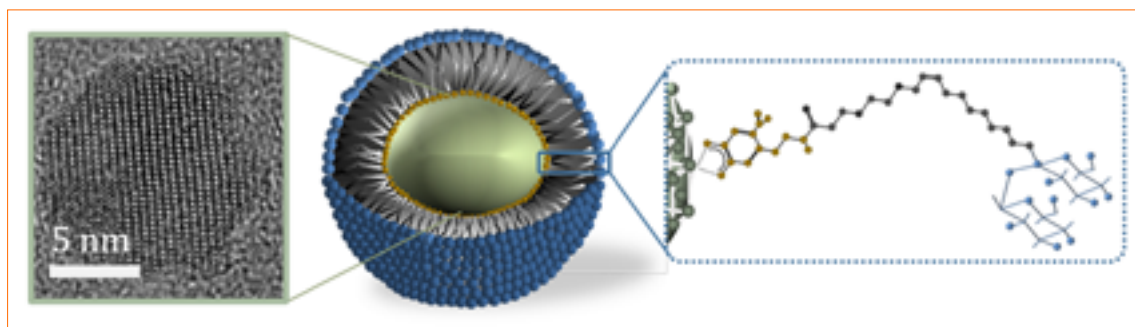
REFERENCES

- [1] N. Lee, D. Yoo, D. Ling, M.H. Cho, T. Hyeon and J. Cheon, *J. Chem. Rev.* 115:19 (2015) 10637
- [2] E. Amstad, T. Gillich, I. Bilecka, M. Textor and E. Reimhult, *Nano Lett.* 9:12 (2009) 4042
- [3] S. Singh, P. Patel, S. Jaiswal, A. Prabhune, C.V. Ramana and B.L.V. Prasad, *New J. Chem.* 33:3 (2009) 646
- [4] N. Baccile, R. Noiville, L. Stievano and I. Van Bogaert, *Phys. Chem. Chem. Phys.* 15:5 (2013) 1606

Magnetic nanoparticles, in particular, superparamagnetic iron oxide nanoparticles (NPs), have received increasing attention for biomedical applications due to their responsiveness to magnetic fields and negligible toxicity. While these properties are governed by their inorganic core, their surface properties play a crucial role in interfacing with biological systems such as cells and proteins [1]. This becomes particularly important for applications that require the targeting of tissue, for which NPs must be invisible to cells of the reticuloendothelial system while interacting with the cells of the target tissue. Thus, the surface of these NPs must be designed in a way that a) provides colloidal stability to the system, b) renders the NPs biocompatible and non-toxic and c) defines the specific interaction of the NPs with the target [2].

Sophorolipids (SL) are non-toxic, bio-based glycolipids produced by the yeast *S. bombicola* that can fulfill the functions required of a surface coating for nanoparticles. They are characterised by a bolaform structure, where one side is composed of a bulky sophorose headgroup and the other by a free carboxylic acid, separated by an oleyl C18:1 fatty chain. These molecules have been reported to have natural targeting abilities as well as anti-cancer and anti-bacterial properties. Because of these attractive properties, they have already been explored as dispersants for SPIONs [3, 4]. However, in this demonstration the SL was not engineered to bind irreversibly as a monolayer shell that ensures control over size and long-term structure in a biomedical application. Therefore, with the goal of stabilising biocompatible, core-shell, monodisperse SPION glyconanoparticles (**figure 1**) using a single, grafted sophorolipid layer, we modified the COOH endgroup of SL with nitrodopamine (NDA). NDA binds strongly to iron oxide and has been used to graft irreversibly bound dispersant shells to SPIONs [2].

We demonstrated the grafting of an SL monolayer onto the monodisperse SPION surface using a combination of synchrotron SAXS and SANS. Colloidal stability, biocompatibility and the absence of toxicity resulting from such a defined core-shell architecture were shown using a combination of cryo-TEM, dynamic light scattering (DLS) and thermal gravimetric analyses (TGA), as well as by cellular uptake and toxicity tests.

**Figure 1**

Schematic of sophorolipid-coated iron oxide nanoparticles. The COOH group of sophorolipids is modified by nitrodopamine, which binds to the SPION surface.

Neutrons are ideal for probing light elements like carbon, and especially hydrogen and deuterium, while X-rays are sensitive to heavy atoms such as iron. **Figure 2** presents SAXS and SANS scattering curves of the same sophorolipid-coated SPION sample, whose SPION diameter estimated by HR-TEM was $d = 4.6 \pm 0.3$ nm. Both SAXS and SANS data display the typical profile of a spherical object. The scattering data were fitted using a core-shell sphere model (red lines). The best fit for SAXS was obtained using a core diameter of 4.6 nm and a null value for the shell. The SANS pattern, in contrast, can be modelled using an imposed (from SAXS data) core diameter of 4.6 nm and a shell thickness of $t = 2.6 \pm 0.2$ nm. This simple model assumes a uniform scattering length density throughout the shell. This is obviously a simplification if one considers the difference in composition between the sophorose and oleic acid moieties of sophorolipids, as well as the space-filling of the high-curvature shell by NDA-SL. Nonetheless, this model is reliable enough to estimate the shell thickness by fitting the shift of the first minimum of the form factor observed in the SANS compared with the SAXS scattering curves. The calculated length of SL, given the 120° angle due to the mono-unsaturation of SL, can be estimated at 2.6 nm, where 1.6 nm is attributed to the fatty acid and 1 nm to the sophorose. The size of NDA is estimated to be about 1 nm. Under these conditions, the maximum expected size of SL NDA is about 3.6 nm. The modelled thickness of $t = 2.6 \pm 0.2$ nm is smaller than the maximum monolayer thickness. This demonstrates that the shell of monodisperse SL-IONP is composed of a single layer of SL-NDA of less than maximum density.

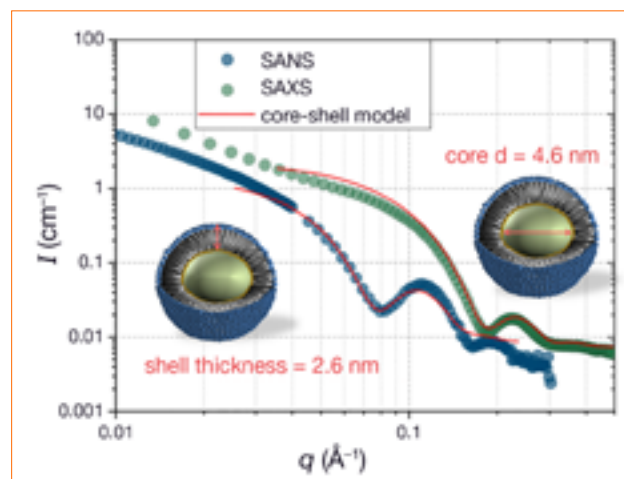
The solvent-core and solvent-shell scattering length density contrasts fitted from the SANS data were $\rho_{\text{solv}} - \rho_{\text{c}} = -0.57 \times 10^{-6} \text{ \AA}^{-2}$, while $\rho_{\text{solv}} - \rho_{\text{s}}$ was in the order of $3.0 \times 10^{-6} \text{ \AA}^{-2}$. This demonstrates that the contrast of the shell is higher than that of the iron oxide core and therefore dominates the scattering signal of the core-shell particle. We stress that the use of SANS was essential in determining the thickness of the shell in solution: the thin organic shell is invisible to X-rays, is overestimated by dynamic light scattering and requires staining prone to artifacts to be resolved by transmission electron microscopy.

SANS was also used to study the colloidal stability of the sophorolipid-coated SPIONs at high ionic strength (1 M NaCl), showing that the scattering profile is superimposable on that measured in pure water and thus demonstrating that the stabilisation is not of electrostatic nature. Additional stability experiments were performed using DLS in 10 % fetal calf serum heated from 20°C to 70°C . Sophorolipid-coated SPIONs showed excellent colloidal stability in such challenging biofluids. Nor did they affect the viability of human monocytes (U937) in cell culture.

In summary, this work illustrates how natural lipids, initially developed as biodegradable alternatives to petrochemical detergents, can be employed in a completely different field and in particular as stabilising agents for biomedical nanoparticles. The bulky sugar headgroups of these lipids, which orient in the outer part of the shell, are probably key to the excellent performance. As the SL-grafted SPIONs are non-toxic and biodegradable, we propose that they are an attractive alternative to synthetic dispersants with unique properties in the biomedical field. The use of a combination of SANS and SAXS was crucial to verify the design of the core-shell nanoparticles, also providing us with a quantitative measure of monolayer SL coating.

Figure 2

SANS (blue) and SAXS (green) profiles for 4.6 nm SL-IONP in D_2O . The red lines show the fit obtained from a core-shell sphere model. The best fit for SAXS was obtained using a core diameter of 4.8 nm and a null value for the shell.





Yuri Gerelli. Italian

The ILL

'I am the co-ordinator of the Partnership for Soft Condensed Matter at the ILL. My research focuses on the study of the structural dynamics in thin films.'

Phase transitions in a single supported phospholipid bilayer: real-time determination by neutron reflectometry

Vertical reflectometer D17 and PSCM

A lack of information on the phase transition behaviour of systems with low dimensionality, such as supported lipid bilayers (SLBs), still exists. Using D17, we identified the presence of an isothermal phase transition characterised by a symmetrical rearrangement of lipid molecules in both bilayer leaflets, followed by the main thermotropic phase transition characterised by an independent melting of the two leaflets. These results are highly relevant for the further understanding of co-operative structural dynamics in SLBs and for the investigation of thermally activated processes.

AUTHORS

Y. Gerelli (ILL)

ARTICLE FROM

Phys. Rev. Lett. (2019)—doi: 10.1103/PhysRevLett.122.248101

REFERENCES

- [1] B.R. Olden, C.R. Perez, A.L. Wilson, I.I. Cardle, Y.-S. Lin, B. Kaehr, J.A. Gustafson, M.C. Jensen and S.H. Pun, *Adv. Healthc. Mater.* (2018) 1801188
- [2] E.T. Castellana and P.S. Cremer, *Surf. Sci. Rep.* 61 (2006) 429
- [3] H.-L. Wu, Y. Tong, Q. Peng, N. Li and S. Ye, *Phys. Chem. Chem. Phys.* 18 (2016) 1411

Solid-supported lipid bilayers (SLBs) are widely used tools in biological and technological studies for investigating interactions and molecular processes involved in cell function and disease and for sensing applications [1, 2]. Moreover, SLBs are one of the prototypes of natural self-assembling systems.

Phase transitions in lipid bilayers have been widely studied in solution aggregates such as vesicles, and in solid-supported stacks of hundreds of bilayers in controlled humidity environments. However, in the case of SLBs, effects of supporting interfaces, finite size and planarity may have a large impact and modify the phase behaviour of these self-assembled systems. It is accepted that the main phase transition (known as *order-disorder* or *gel-fluid* transition) of bi-dimensional bilayers is characterised by a substantial broadening with respect to that observed in free-standing bilayers in solution. In addition, atomic force microscopy (AFM) experiments [3] have reported that the main phase transition in SLBs is mediated by the formation and growth of nanosized *fluid-in-gel* domains as the temperature is increased; such coexistence was detected up until the growing domains entirely replaced the starting phase. Moreover, these experiments indicated a decoupling between the thermodynamic behaviour of the lipid molecules 'strongly' interacting with the solid substrate (forming the proximal leaflet) and those facing the water reservoir (forming the distal leaflet). In particular, they hypothesised that the melting of the proximal leaflet is preceded by the complete melting of the distal one.

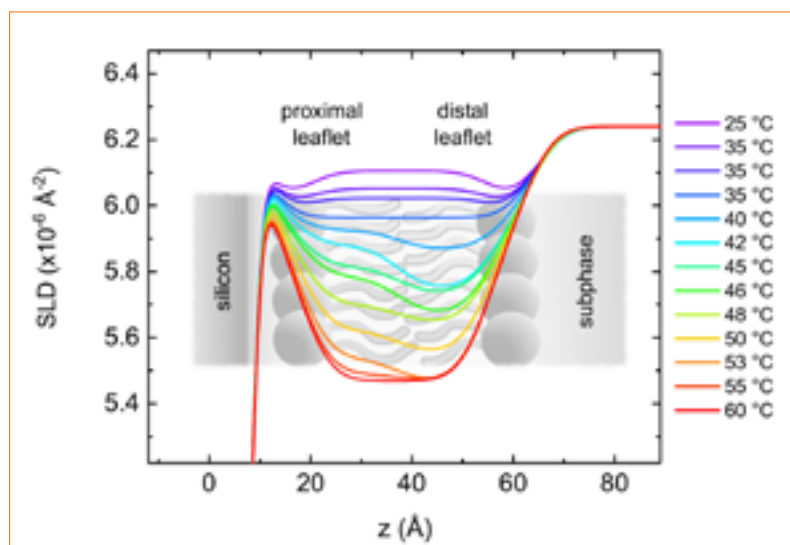


Figure 1

Selected SLD profiles (view zoomed in on the bilayer region) describing the structural changes in a d_{75} DPPC bilayer at different moments of the phase transition. The decrease in the SLD of the hydrophobic region (centred at $z \sim 40$ Å) at constant temperature is visible by comparing the profiles obtained at 35 °C. At higher temperatures, the early melting of the distal leaflet is clearly visible.

Time- and temperature-resolved neutron reflectometry performed on the high-flux, time-of-flight reflectometer D17 allowed us to provide a real-time, direct characterisation of the internal structural changes taking place in SLBs across their phase transitions. In particular, we demonstrated how this method can be used to obtain direct information on the melting behaviour of the proximal and distal leaflets in SLBs and thus to quantify their degree of coupling. By interpreting the scattering length density profiles obtained by data modelling, we have demonstrated that during the main phase transition (broader than the one observed in free-standing bilayers, in accordance with the literature) the bilayer structure was characterised by a minor, but not negligible, degree of asymmetry induced by the presence of a solid substrate (**figure 1**). However, the energy required for their melting did not vary between proximal and distal leaflets, indicating the absence of the strong thermodynamic decoupling suggested by earlier studies. These results are essential to a better understanding of the structural behaviour in systems at low dimensionality, and to tackling new, challenging problems related to their structural dynamics.



Tommy Nylander. Swedish
Department of Chemistry, Lund University, Sweden
'I work with various types of biomolecules, such as lipids, proteins and carbohydrates. I use neutron scattering and reflectometry because I want to know the relation between their function and structure at bulk and interfaces.'

Interfacial properties of lipid, sponge-like nanoparticles and the role of a stabiliser on particle structure and surface interactions

*Reflectometer for the analysis of materials
SuperADAM*

The formulation of drugs, e.g. for cancer treatment, genetherapy, metabolic disorders, opioid dependence, is a question not only of solubilising the therapeutic compound but also of making sure that it stays dispersed for a long time. Non-lamellar lipid liquid crystalline nanoparticles (LCNPs) are now widely considered in many applications as they have good solubilising capability and tuneable properties and can be prepared from natural lipids. Our study is directed at understanding their structure and properties so that in the future we can produce long-lasting, stable formulations. We use neutron surface and bulk scattering as well as reflectometry techniques for this purpose, as we want the formulation to be deposited at a targeted interface and not get to stuck at the walls of a container or delivery system.

AUTHORS

M. Valldeperas and T. Nylander (NanoLund and Lund University, Sweden)
G.K. Pålsson and A. Vorobiev (ILL and Uppsala University, Sweden)
A. Dabkowska (IMED Biotech Unit, AstraZeneca, Gothenburg, Sweden)
and J. Barauskas (Camurus AB, Lund, Sweden)

ARTICLE FROM

Soft Matter (2019)—doi: 10.1039/c8sm02634c

REFERENCES

- [1] K. Larsson, *J. Phys. Chem.* 93 (1989) 7304
- [2] K. Larsson, *Curr. Opin. Colloid Interface Sci.* 5 (2000) 64
- [3] L. Sagalowicz and M.E. Leser, *Curr. Opin. Colloid Interface Sci.* 15 (2010) 61
- [4] J. Barauskas and T. Nylander, in *Delivery and Controlled Release of Bioactives in Foods and Nutraceuticals*, Woodhead Publishing Limited, Abington, England (2008) 107
- [5] C.E. Conn and C.J. Drummond, *Soft Matter* 9 (2013) 3449
- [6] V. Razumas, J. Kanapienienė, T. Nylander, S. Engström and K. Larsson, *Anal. Chim. Acta* 289 (1994) 155
- [7] J. Gilbert, M. Valldeperas, S.K. Dhayal, J. Barauskas, C. Dicko and T. Nylander, *Nanoscale* 11 (2019) 21291
- [8] B. Angelov, A. Angelova, R. Mutafchieva, S. Lesieur, U. Vainio, V.M. Garamus, G.V. Jensen and J.S. Pedersen, *Phys. Chem. Chem. Phys.* 13 (2011) 3073
- [9] D.P. Chang, J. Barauskas, A.P. Dabkowska, M. Wadsäter, F. Tiberg and T. Nylander, *Adv. Colloid Interface Sci.* 222 (2015) 135
- [10] P. Vandoolaeghe, R.A. Campbell, A.R. Rennie and T. Nylander, *J. Phys. Chem. C* 113 (2009) 4483
- [11] A. Vorobiev, A. Devishvili, G. Pålsson, H. Rundlöf, N. Johansson, A. Olsson, A. Dennison, M. Wollf, B. Giroud, O. Aguetaz and B. Hjörvarsson, *Neutron News* 26 (2015) 25

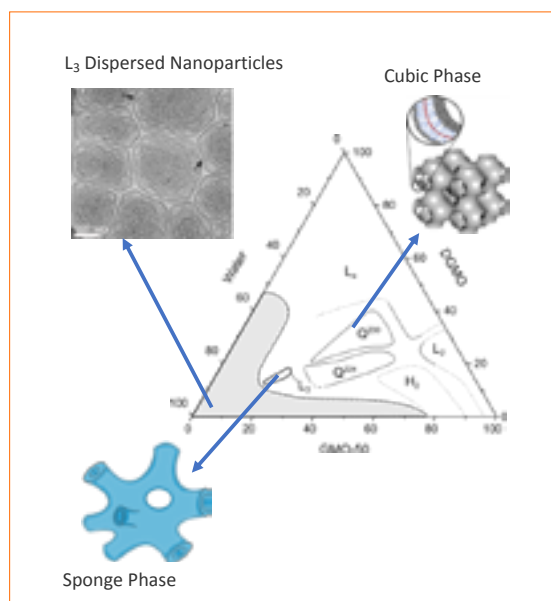
It is by now well-established that lipid-forming liquid crystalline phases can be dispersed into nanoparticles, where the lipid composition can be used to tune the internal structure to an inverse cubic, sponge-phase or hexagonal structure (cubosomes, spongosomes and hexosomes, respectively) [1–3]. They have a larger surface area per volume ratio and a larger capability to solubilise both hydrophilic and hydrophobic molecules compared with their lamellar analogues (vesicles) [2–3]. Due to their well-defined internal structure, colloidal stability and tuneable internal structure, they have found applications in drug delivery and in protein encapsulation or crystallisation [2–6].

This study focuses on the lipid sponge phase (L_3), which is more flexible, has a greater capacity to form larger aqueous pores compared with the structurally similar bicontinuous cubic phase and is therefore capable of encapsulating larger bioactive molecules such as enzymes [7–8]. We have previously examined the interfacial properties of cubosomes and hexosomes in order to understand the nature of the interactions between these LCNPs and various interfaces that mimic storage or administration vessels, such as glass vials, catheters and syringes [9–10].

The current study also provided the means to determine the colloidal stability of these particles and give insight into their surface properties. Colloidally stable LCNPs with a narrow size distribution are ensured by using a stabiliser that reduces the LCNP aqueous phase interfacial tension. Common stabilisers are Pluronic F127 and Polysorbate 80; they are not only stabilisers but have also been found to affect the internal particle structure [10].

Figure 1

The phase diagram of the system studied. We used a mixture of diglycerol monoolein (DGMO), which promotes lamellar phase, L_{α} , Capmul® GMO-50 (main component monoolein) and which in turn promotes a reverse phase, and the dispersant polysorbate 80 (P80), which promotes swelling of the cubic phase into a sponge phase and facilitates dispersions into particles. By varying the ratio of DGMO and GMO-50 we could also vary the type of structure formed. Here, reverse bicontinuous cubic (Q of spacegroup 224 (Q²²⁴) and 230 (Q²³⁰)), reverse hexagonal (H_2), lamellar (L_{α}) and sponge (L_3) phases are indicated. Illustrations of the cubic and sponge phases are inserted, as is a Cryo-TEM image of the dispersed sponge nanoparticles (L_3 -NP).



The role of P80 in the formation of sponge-like nanoparticles was revealed in this study using a combination of SANS (SANS2D at the ISIS Neutron and Muon source of the STFC Rutherford Appleton Laboratory, Didcot, UK) and neutron reflectometry (the reflectometer SuperADAM [11], the Swedish CRG instrument at the ILL). The L_3 -NPs structure features local phase separation, as the more swollen bilayer type of structure on the particle surface is rich in P80 at the expense of a more DGMO/GMO-50-rich core. The sponge phase inner structure of the core was found to be retained. Our study clearly demonstrated that Polysorbate 80 both contributes to the formation of highly swollen inverse bicontinuous phases and acts as a stabiliser of the formed particles.

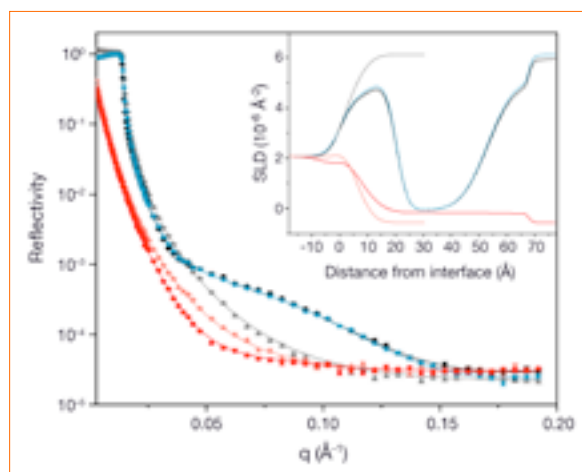
So how does this swollen, yet structured, core shell particle interact with an interface? To reveal the formed interfacial layer when the particles attach to a surface we used neutron reflectometry, benefitting from the high resolution of SuperADAM. **Figure 2** shows the significant adsorption of L_3 -particles, characterised by the appearance of a fringe in the reflectometry curve. Such a fringe does not show up for the bare silica in a D_2O buffer. The reflectivity curves recorded in the H_2O solvent contrast are also significantly different. The interfacial lipid film structure was not altered by rinsing, as the curves recorded before and after rinsing in the D_2O contrast were found to be almost identical.

The results of fitting a four-layer model to the data are presented as the SLD profile inserted in **Figure 2**. The four-layer model consisted of the following: 1. SiO_2 ; 2. Lipid headgroups; 3. Lipid hydrocarbon tails; and, 4. Lipid headgroups, where the inner and outer headgroups were considered equivalent in terms of thickness and SLD. The total thickness of the lipid layers formed by adsorption from an L_3 -dispersion on hydrophilic silica was found to be 63 Å.

Figure 2

Neutron reflectivity curves, illustrating the effect of L_3 -NP adsorption on a (hydrophilic) silicon surface, are shown as a function of momentum transfer (q). The curves were recorded before addition of L_3 -NPs (grey for D_2O and light red for H_2O), after adsorption of L_3 -NPs in the deuterated buffer (black) and after rinsing with deuterated (blue) and protonated water (red). Experimental and fitted data are depicted as symbols and a solid line, respectively. The embedded plot shows the scattering length density (SLD) values as a function of distance from the interface obtained from the fitting.

This is an order of magnitude thinner than the diameter of the particles, which shows that the particles spread to form a thin film, corresponding to lipid bilayer, on hydrophilic silica, confirming the flexibility of the particles. It is noteworthy that the headgroup region is highly hydrated ($\approx 80\%$) and also thinner than the headgroup layer in P80 micellar dispersions as observed by SANS, which was found to be 23 Å. Taking into account the fact that the thickness values are averaged over the whole surface, *i.e.* that the headgroups of DGMO and GMO-50 are smaller, the results show that the reduced thickness observed reflects the fact that the adsorbed layer is a mixture of lipids and stabiliser. In the 33 Å thick hydrocarbon region—there is almost no solvent—as expected because of its hydrophobicity. This value is slightly larger than those found for the L_3 dispersion studied by SANS. This suggests that the lipids in interfacial bilayer might be more ordered than those in the bilayers of the L_3 dispersions. The tail layer thickness on the adsorbed layer is less than twice the P80 tail size in the micelles and the tails may be interdigitated or tilted when confined at an interface.





Alessio De Francesco. Italian Consiglio nazionale delle Ricerche (CNR, IT) c/o OGG, Grenoble.

'In recent years, my work has been devoted to the search for data analysis methods that are able to provide solid and statistically based support for the results of analyses thanks to a Bayesian approach.'

A Bayesian approach to the study of time correlation functions in a soft complex system

Spin-echo spectrometers IN11 and IN15

If we could repeat a measurement many times, the average of the results would provide a robust estimate of our observations. However, a measurement is usually a single-time event from which some general law needs to be deduced. In this situation, the help of Bayesian inference [1], here implemented within a Markov Chain Monte Carlo (MCMC) numerical recipe integrated with a Reversible Jump algorithm [2], becomes invaluable. Furthermore, the use of a multi-exponential expansion of the Neutron Spin Echo (NSE) signal, in principle extendable to any time correlation function [3], enabled us to capture the 'fine-structure' of relaxation processes in polymer-coated, gold nano particles (PEG-AuNP) (**figure 1**, left) and to compare them with the dynamics of the free polymer chain solution. Disentanglement of the internal dynamics of polymer chains from other contributions, whenever achievable, would not be possible with a commonly used description of the time correlation function decay in terms of stretched exponentials.

Figure 1

Left panel) Sketch of a functionalised PEG AuNP.

Right panel) Representative series of NSE curves representing $I(Q, t)/I(Q, 0)$ of the PEG2000 AuNPs dispersed in D_2O at neutron wavelength $\lambda = 10 \text{ \AA}$ and a temperature of $T = 280 \text{ K}$ (symbols). The Q values increase from top to bottom. The lines represent the best fits to the data.

AUTHORS

A. De Francesco (CNR IOM c/o ILL, Grenoble, France)
L. Scaccia (Università di Macerata, Italy)
E. Guarini (Università di Firenze, Italy)
U. Bafile (CNR IFAC, Firenze, Italy)
P. Falus (ILL)
M. Maccarini (Université Grenoble Alpes, Grenoble, France)
A. Cunsolo (NSLS-II, BNL, Upton, USA)

ARTICLE FROM

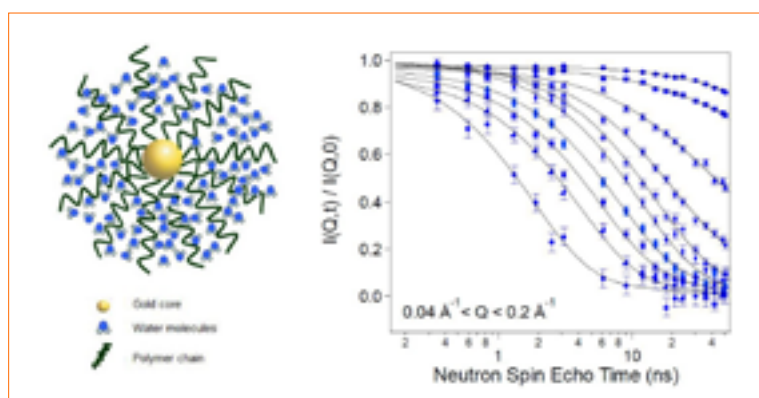
Phys. Rev. E (2019)—doi: 10.1103/PhysRevE.99.052504

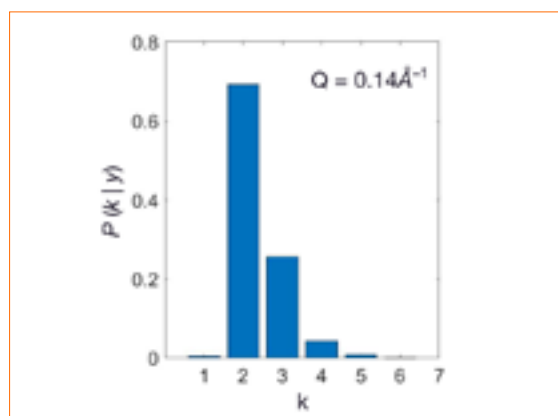
REFERENCES

- [1] T. Bayes and R. Price, *Philos. Trans. R. Soc.* 53 (1763) 370
- [2] P.J. Green, *Biometrika* 82 (1995) 711
- [3] F. Barocchi, U. Bafile and M. Sampoli, *Phys. Rev. E* 85 (2012) 022102 and F. Barocchi, E. Guarini and U. Bafile, *Phys. Rev. E* 90 (2014) 032106
- [4] A. De Francesco, L. Scaccia, R.B. Lennox, E. Guarini, U. Bafile, P. Falus and M. Maccarini, *Phys. Rev. E* 99 (2019) 052504

In recent decades, the steady improvement of instrument performance in research, in the field of spectroscopy in particular, has made an enormous amount of new data available on a variety of physical systems. While in the early years a merely phenomenological observation of new spectral features was considered a result *per se* warranting scientific attention, increased accuracy in data acquisition has shifted the objective towards a more quantitative and physically insightful scrutiny of the line shape. Rather than minimising uncertainties, the improved quality of measurements has often paradoxically encouraged bold speculations, ultimately challenging scientific rigour and accuracy. To overthrow this course of events, new data analysis protocols capable of quantifying the reliability of a given model are needed, in order to avoid over-parameterisation, minimise subjectivity in the choice of model and, ultimately, warn researchers off hazardous speculations.

To advance along this difficult route we applied a Bayesian approach, previously used on (energy-resolved) Brillouin neutron and X-ray spectra, to model the time decay of the intermediate scattering functions (ISFs) measured by spin-echo spectroscopy (NSE) of aqueous solutions of polymer-functionalised gold nanoparticles (**figure 1**, right) [4].

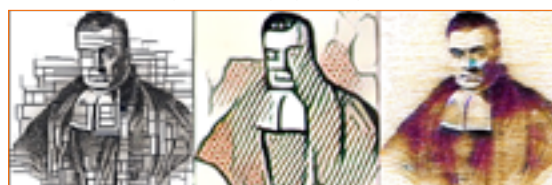


**Figure 2**

An example of a posterior distribution for the number k of possible relaxation channel decays of PEG2000 polymer solution in D_2O , as derived by measurements on IN11 and IN15. The maximum at $k = 2$ of the $P(k|y)$ immediately suggests a two-exponentials model for the decays of the relative ISFs.

Figure 3

The three faces of Bayes (© Slackprop, Wordpress).

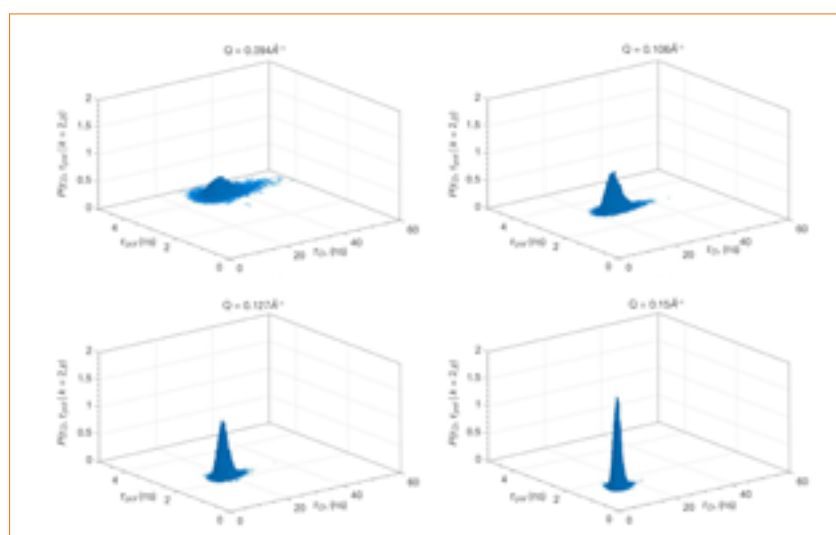


This approach directly addresses an issue as fundamental as the choice of the most grounded model for the time-dependence of ISFs, based on a probabilistic inference of the number and form of individual decay processes contributing to it.

The analysis presented does not resort to a preselected interpretative framework and can thus be considered model-free. In fact, the reversible jump technique allows, by switching between different dimensions in the model hyperparameter space, one to choose from a large class of models—*i.e.* any model that might be considered a particular case of a sum of stretched or simple exponentials or a combination of them, here including the Rouse and Zimm models—and to treat the number k of decay channels as a parameter itself to be estimated conditionally on the available data. As a result, comparison of the ISFs of either PEG-coated or PEG2000 nanoparticle suspensions enabled us to disentangle the translational diffusion of the nanoparticles from the internal dynamics of the polymer grafted to them.

Our findings also indicate that the relaxation of the polymeric corona takes the form of a simple exponential decay—as it should once this particular dynamics is singled out—and is still perfectly consistent with a

Rouse description of a tethered polymer brush. Most importantly, this inferential method clearly favours a multi-exponential profile over more involved ansätze based on the Kohlrausch–Williams–Watts distribution of relaxation times. The latter modelling, often argued to be the most appropriate for complex materials, can at best provide an approximated phenomenological description of ISFs, even when supported by theoretical predictions. Its use, besides being often poorly justified by experimental evidence, leads to relevant physical insight derived from ISFs being overlooked while delivering confusing and fuzzy portrayals of relaxation dynamics. Conversely, implementing a multi-exponential model into the Bayesian inference approach gives a better account of the dynamical complexity of the system under scrutiny by unveiling the fine structure of ISFs without the risk of over-parameterisation, since the Bayes theorem naturally integrates an elegant and effective implementation of the Occam's razor principle. This Bayesian approach not only provides a quantitative evaluation of the statistically most supported model (**figure 2**), it also draws an entire distribution for each model parameter (**figure 3**). Instead of delivering apodictic or conclusive statements on the physics under study, Bayesian methods assist investigators in the search of an evidence-based, probabilistic interpretation of experimental data.

**Figure 3**

Joint posterior distribution at four selected momentum transfer Q values, and marginalised with respect to the other model parameters, for the two relaxation times in the decay model recognised as the most statistically supported by the experimental data for a PEG2000 AuNP water solution at $T = 318$ K and $\lambda = 10$ Å. From the shape of such a joint distribution the absence of correlation between the two parameters and how the precision in the determination of the parameters changes with Q can be observed.



Svetlana Antonyuk, British Department of Biochemistry, University of Liverpool, UK.
 'We've been using neutrons since 2008, in addition to our synchrotron and XFEL experiments. Neutrons have allowed us to look at our enzyme from a different perspective.'

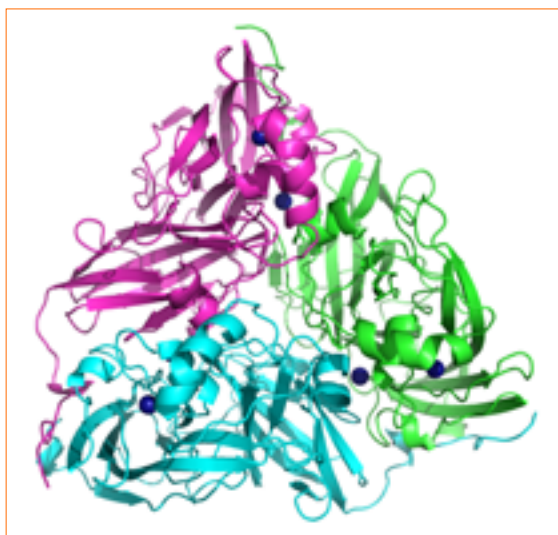
Neutron structure of a denitrifying enzyme provides new insights into the catalytic mechanism

Quasi-Laue diffractometer LADI-III

Copper nitrite reductases are a family of metalloenzymes that convert nitrite to nitric oxide in the denitrification pathway. As such, they are of central importance in nitrogen-based energy metabolism. To gain further insight into the enzyme mechanism we used neutron crystallography. This revealed unexpected protonation states for key residues and important details concerning hydration.

Figure 1

Ribbon diagram of the AcNiR trimer. The copper ions are shown as dark blue spheres.



AUTHORS

S.V. Antonyuk (University of Liverpool, UK)
 M.P. Blakeley, M. Moulin and M. Haertlein (ILL)

ARTICLE FROM

IUCr. (2019)—doi: 10.1107/S2052252519008285

REFERENCES

- [1] S.V. Antonyuk et al., Proc. Natl. Acad. Sci. USA 102 (2005) 12041
- [2] M.P. Blakeley, S.V. Antonyuk and S.S. Hasnain, IUCr. 2 (2015) 464

Denitrification is the process by which some micro-organisms couple respiratory ATP synthesis with the reduction of nitrite (NO_2^-) to dinitrogen (N_2) via the gaseous product nitric oxide (NO). Denitrification forms an important step in the global nitrogen cycle. It has agronomic, environmental and medical impacts. The individual reactions of denitrification are catalysed by distinct reductases that can contain a variety of metal or heme centres.

Copper-containing nitrite reductases (CuNiRs) are involved in the first step of the denitrification pathway, catalysing the reduction of nitrite to nitric oxide in a one-electron two-protons reaction. The biological assembly is a trimer, with each monomer containing two distinct types of copper (Cu) centre (**figure 1**). The type 1 Cu ion (T1Cu) site is responsible for transferring an electron to the type 2 Cu (T2Cu) site, where catalysis occurs. The T2Cu is co-ordinated by three histidine (His) residues, plus a ligated water that is displaced when nitrite binds to the oxidized T2Cu. Two additional residues located close to the T2Cu site are known to be essential for enzymatic activity: an aspartic acid (Asp^{cat}) and another histidine (His^{cat}). Asp^{cat} is hydrogen-bonded to the T2Cu ligated water and also to His^{cat} via a bridging water.

A number of atomic resolution structures of CuNiRs from the soil bacterium *Achromobacter cycloclastes* (AcNiR) were determined using X-rays, including oxidized and reduced forms as well as nitrite-bound complexes [1, 2]. However, despite a large proportion of hydrogen (H) atoms being visible, many of the key H atoms of the catalytic T2Cu site were not. Moreover, like all metalloenzymes, AcNiR is very susceptible to radiation damage from X-rays, imposing a serious limitation on unravelling details of the resting state of AcNiR at the atomic level. For this reason, in parallel to our synchrotron and XFEL studies we chose to use neutrons, since they offer a way to determine damage-free structures of enzymes at room temperature and can provide details of protonation and hydration, necessary for determining catalytic pathways.

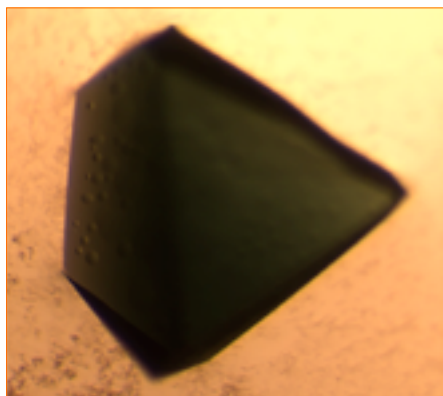


Figure 2

The AcNiR crystal used for neutron data collection.

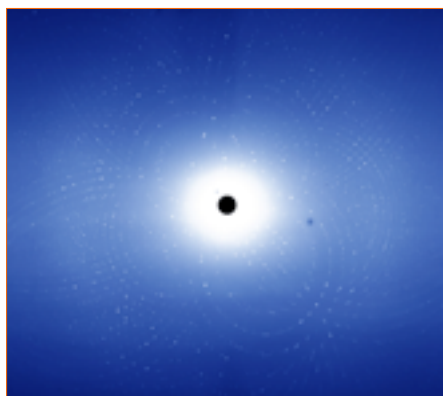


Figure 3

A neutron diffraction pattern (exposure time of 18h) from the AcNiR crystal.

While the benefits of neutrons are clear, they bring their own specific challenges. These include deuteration and the need to grow large crystals (0.1 to 1 mm³). For the production of perdeuterated AcNiR, we benefitted from the excellent assistance and facilities of the Deuteration Laboratory platform. Large crystals of perdeuterated AcNiR were then grown in Liverpool, using hanging-drop vapour diffusion methods in combination with seeding/feeding (**figure 2**). Neutron diffraction data were collected at room temperature using LADHII to a resolution of 1.8 Å (**figure 3**) from a 0.36 mm³ crystal.

The resulting structure revealed that in the resting state of AcNiR, at pH values close to the optimum for activity, Asp^{cat} is observed in a charged state (*i.e.* deprotonated) as expected, while His^{cat} is unexpectedly seen in a neutral state (*i.e.* singly protonated). In addition, the catalytic T2Cu-ligated water (D1 in **figure 4**) is observed as a neutral D₂O molecule—as opposed to D₃O⁺ or OD⁻, which have previously been proposed as possible alternatives—while the bridging water (D2 in **figure 4**) is also observed as a neutral D₂O molecule, positioned with one deuteron directed towards Asp^{cat} O^{δ1} and one towards His^{cat} N^{ε2}. These details have allowed us to revisit the catalytic mechanism. We suggest that upon the binding of nitrite, a proton is transferred from the bridging water (D2) to the O^{δ2} atom of Asp^{cat}, prompting electron transfer from T1Cu to T2Cu and reducing the catalytic redox centre. This triggers the transfer of a proton from Asp^{cat} to the bound nitrite, enabling the reaction to proceed.

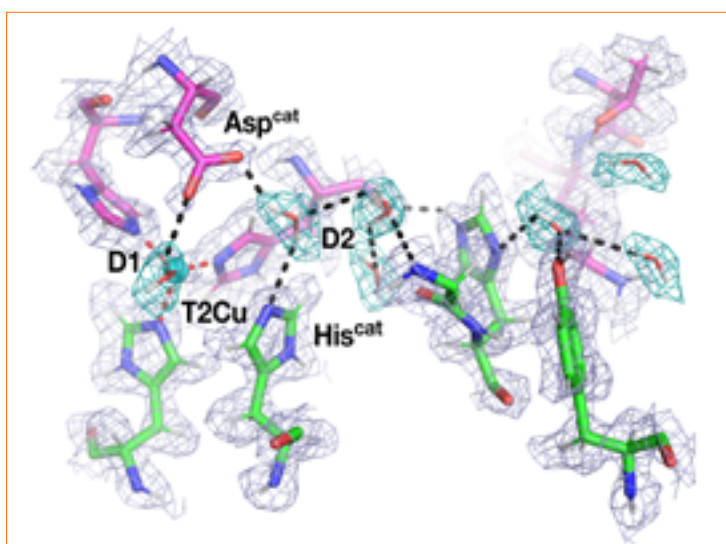


Figure 4

Nuclear scattering density at the T2Cu site and its surroundings. The protonation states of key residues, including Asp^{cat} and His^{cat}, are shown in grey; the positions and orientations of bound water molecules, including the T2Cu-ligated water (D1) and the bridging water (D2), are shown in turquoise.

During this project, M. Grimaldo, H. Lopez (TU Dublin) and F. Roosen-Runge (Malmö University) have been postdoctoral/visiting fellows at the ILL, and C. Beck a PhD student, jointly funded by the ILL and the University of Tübingen. This research was supported by the grant 'ImmunoglobulinCrowding' jointly funded by the DFG and ANR.

The effect of polydispersity on protein diffusion in naturally crowded cellular environments

Backscattering spectrometer IN16B, small-angle scattering instrument D11, theory and D-Lab

The interior of living cells is marked by the presence of various macromolecules at high concentrations. Combining high-resolution neutron spectroscopy with computer simulations, the effect of the polydispersity within such a naturally crowded environment can be quantitatively understood on nanosecond time and nanometre length scales. In a pioneering study, this approach has been established employing immunoglobulins as tracer proteins. The resulting knowledge will contribute to our understanding of intracellular transport and assembly.

AUTHORS

M. Grimaldo and T. Seydel (ILL)
 H. Lopez (ILL and UGA Grenoble University, France)
 C. Beck (ILL and Tübingen University, Germany)
 F. Roosen-Runge (Malmö University, Sweden)
 F. Schreiber (Tübingen University, Germany)

ARTICLE FROM

J. Phys. Chem. Lett. (2019)—doi: 10.1021/acs.jpcclett.9b00345

REFERENCES

- [1] M. Grimaldo, H. Lopez, C. Beck, F. Roosen-Runge, M. Moulin, J. Devos, V. Laux, M. Härtleln, S. Da Vela, R. Schweins, A. Mariani, F. Zhang, J.L. Barrat, M. Oettel, V.T. Forsyth, T. Seydel and F. Schreiber, J. Phys. Chem. Lett. 10 (2019) 1709

In pursuit of predicting biological dynamics at the molecular level, physical concepts can greatly advance quantitative modelling. Notably, concepts from colloid physics can help us to understand the diffusion of biological macromolecules on the nanometre length scale commensurate with molecular dimensions. Neutrons provide an ideal probe, being able to access the short-time tracer diffusion without causing any damage to the fragile biological samples and allowing selective information via the scattering contrast without the need for any labels on the proteins.

We combined high-resolution neutron spectroscopy experiments with computer simulations on samples closely mimicking the natural, crowded macromolecular environment but allowing for systematic control of the system parameters, such as the tracer protein and crowder concentrations (**figure 1**) [1]. Complementary small-angle X-ray and neutron scattering experiments helped to further characterise the samples, confirming the presence of macromolecules and assemblies with a very broad range of shapes and length scales.

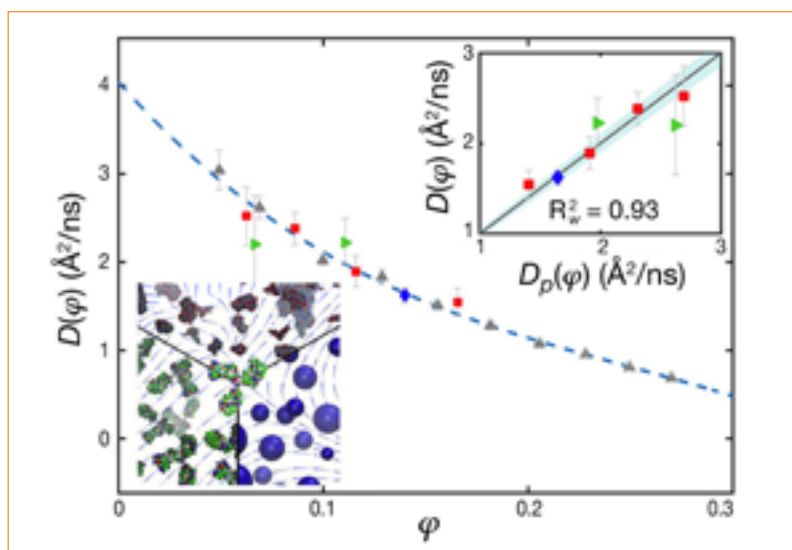


Figure 1

Experimental agreement of immunoglobulin diffusion under polydisperse and monodisperse crowding.

Main figure: experimental apparent diffusion coefficient $D(\phi)$ versus the total volume fraction ϕ of Ig and lysate combined; grey symbols = Ig without lysate; coloured symbols = Ig-lysate mixtures. Dashed line = polynomial fit $D_p(\phi)$ of the diffusion of Ig in pure D_2O .

Top inset: $D(\phi)$ versus $D_p(\phi)$ for the samples with lysate (R^2_w : weighted coefficient of determination). The shaded area depicts a $\pm 5\%$ deviation of $D(\phi)$ from $D_p(\phi)$.

Bottom inset: artistic view of the two experimental systems (Ig- D_2O , bottom left, and Ig-lysate mixture, top) and of the simulations of hard-sphere suspensions (bottom right), all demonstrating the importance of hydrodynamic interactions.

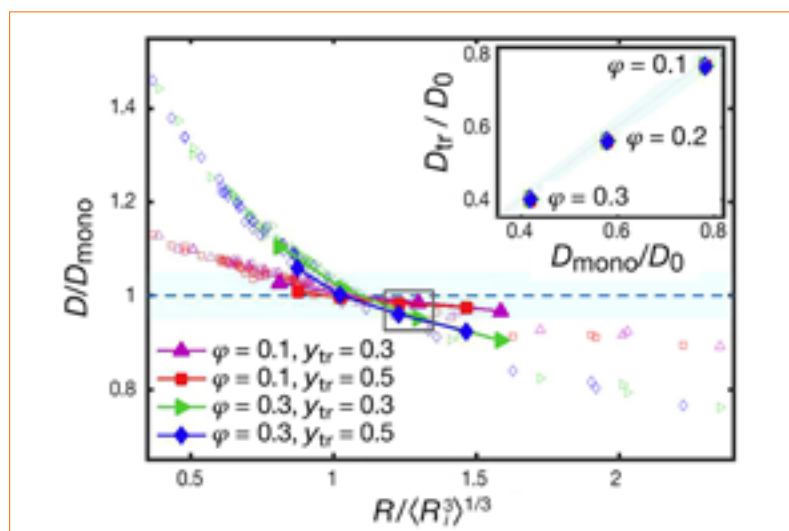


Figure 2

Simulated difference (agreement for $R \approx R_{\text{eff}}$) in particle diffusion between polydisperse and monodisperse crowding.

Main figure: normalised translational diffusion coefficient D/D_{mono} of spheres with radius R versus the rescaled radius R/R_{eff} . D_{mono} is the diffusion coefficient in a monodisperse solution of spheres with radius R at similar volume fraction φ . The effective radius $R_{\text{eff}} = \langle R_i^3 \rangle^{1/3}$ characterises the crowding in a mixture of spheres with radii R_i . The filled symbols depict the diffusion coefficients of the *tracers* at the ratios $y_{\text{tr}} = \varphi_{\text{tr}}/\varphi$, with the tracer volume fraction φ_{tr} . In particular, the filled symbols in the grey rectangle refer to the experimental radius of Ig. In this case, the deviations of the diffusion in the polydisperse environment from that in a monodisperse system are less than 5%. The empty symbols denote the diffusion of the *crowders*, plotted for $R_{\text{tr}} = R_{\text{lg}}$.

Inset: reduced tracer diffusion D_{tr}/D_0 with the dilute limit coefficient D_0 , for an Ig-sized tracer ($R = R_{\text{lg}} = 5.5$ nm) versus the reduced diffusion coefficient D_{mono}/D_0 in the monodisperse suspension. The shaded areas (main figure and inset) depict a $\pm 5\%$ deviation of D_{tr} from D_{mono} .

For the experiments, fully deuterated cellular lysate from *Escherichia Coli* cells was produced and mixed with natural, *i.e.* protonated polyclonal Immunoglobulin (Ig), tracer proteins and deuterated water (D_2O). The difference in the neutron scattering cross sections from the deuterated and protonated components of the samples allowed us to focus on the scattering signal from the Ig. Surprisingly, we found that the diffusion of Ig in both lysate and pure Ig solutions depends on the total volume fraction of Ig and lysate only, *i.e.* no effect of polydispersity was observed in the experiments.

Subsequently, the experimental results were analysed using theoretical concepts from colloid physics, in particular Stokesian dynamics computer simulations (**figure 2**). In this way, the protein diffusion was accessed on nanosecond time scales where hydrodynamic interactions dominate over negligible protein collisions. Combined with these coarse-grained simulations, the experimental results for the complex, flexible molecules can be understood consistently using colloid theory. The simulations show that tracer proteins in polydisperse solutions close to an effective particle radius diffuse approximately, as in a monodisperse suspension. Furthermore, macromolecules of sizes that are different from the effective radius are slowed differently even on nanosecond time scales. This result is highly relevant for a quantitative understanding of cellular processes.



Fabrizia Foglia, Italian University College London (Chemistry Department), UK
 'My research is focused on understanding how membrane morphology controls transport and therefore how best to tailor and design nanostructures to optimise performance, and membrane technology generally. I primarily use neutron techniques to advance our basic understanding of, and therefore to resolve, molecular-level assembly mechanisms and pathways from a structural and dynamical point of view.'

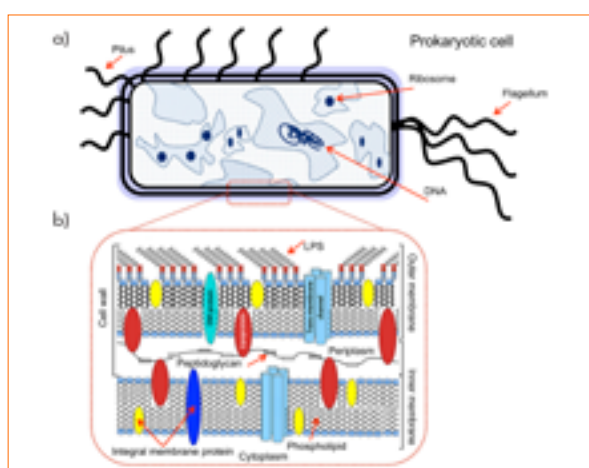
In vivo water dynamics in *Shewanella oneidensis* bacteria at high pressure

Time-of-flight spectrometer IN6-SHARP

IRIS spectrometer (ISIS, UK)

TOF-TOF spectrometer (FRM-II, DE)

Studying how bacteria function under high-pressure conditions is necessary for understanding both how extremophile organisms survive in the Earth's deep biosphere and how they respond to hyperbaric treatments for sterilising foodstuffs, pharmaceuticals and agricultural products. A core aspect of cellular activity involves the mobility of water inside the cell, as well as its transport across the cell envelope. Here we present a study on *Shewanella oneidensis* MR-1 before and after high-pressure treatment.



AUTHORS

F. Foglia and P.F. McMillan (University College London, UK)
 R. Hazael (Cranfield University at the Defence Academy, UK)
 F. Meersman (University of Antwerp, Belgium)

ARTICLE FROM

Sci. Rep. (2019)—doi: 10.1038/s41598-019-44704-3

REFERENCES

- [1] V.A. Shepherd, *Curr. Topics Developmental Biol.* 75 (2006) 171
- [2] J. Spitzer and B. Poolman, *FEBS Lett.* 587 (2013) 2094
- [3] L.E. Bove *et al.*, *Phys. Rev. Lett.* 111 (2013) 185901
- [4] F. Foglia *et al.*, *Sci. Rep.* 6 (2016) 18862

It has long been assumed that the internal structure of bacterial cells consists of unencapsulated nucleic acid material suspended in a homogeneous gel-like mixture of proteins and other macromolecules along with aqueous electrolyte solutions that form the cytosol. In the context of this model, primary questions concerning water mobility arose around the 'crowded' nature of the macromolecular environment and how the presence of dissolved ions, metabolites and macromolecular species affect the aqueous relaxation and transport dynamics. An emerging approach to understanding the internal structure of prokaryotic cells now suggests a more structured environment with a dynamically evolving but co-operatively organised 'superclustered' arrangement of proteins and macromolecular complexes, separated by channels containing the aqueous electrolyte solution [1, 2].

Our experiments using quasi-elastic neutron scattering (QENS) shed new light on how water transport inside bacterial cells is affected by high-pressure conditions. **Figures 1a** and **1b** illustrate the process.

QENS provides information on diffusive and rotational relaxation dynamics in water and aqueous solutions on picosecond (ps) to nanosecond (ns) time scales over real space correlation lengths of between ~ 3 to 60 \AA [3], which are relevant to internal bacterial dimensions. In a previous study we applied high-P QENS combined with a wide range of H/D isotopic substitution contrasts to study water dynamics in wild type (WT) *Shewanella oneidensis* at ambient and $P = 200 \text{ MPa}$ (*i.e.* 2 000 atm) [4]. Our initial data showed that H_2O mobility across the cell envelope was not affected by pressure, presumably due to the location of transmembrane Aquaporin water transport channels located within relatively well-ordered and hence incompressible regions of the membrane structures. Studying the internal dynamics suggested that water mobility inside the cells was reduced, but the data overlapped with the range of diffusivity results observed for aqueous solutions or water confined in nanoscale environments (**figure 2**).

Using a combination of the facilities at the ILL and ISIS (UK), we have since extended the pressure range of our investigations of intracellular water dynamics up to 500 MPa (**figure 3**). (We have also studied pressure-resistant (PR) strains produced by sequential compression and recovery experiments carried out in stages up to a maximum pressure of 750 MPa [4].) As the pressure was increased to 200 and then to 500 MPa , the intracellular self-diffusion coefficient (D_{T}) values became

Figure 1

a) Schematic drawing showing a prokaryotic cell; the cytoplasm is represented according to the model presented by Spitzer & Poolman [2].

b) Schematic drawing showing IM, OM and periplasmic space for β -bacteria.

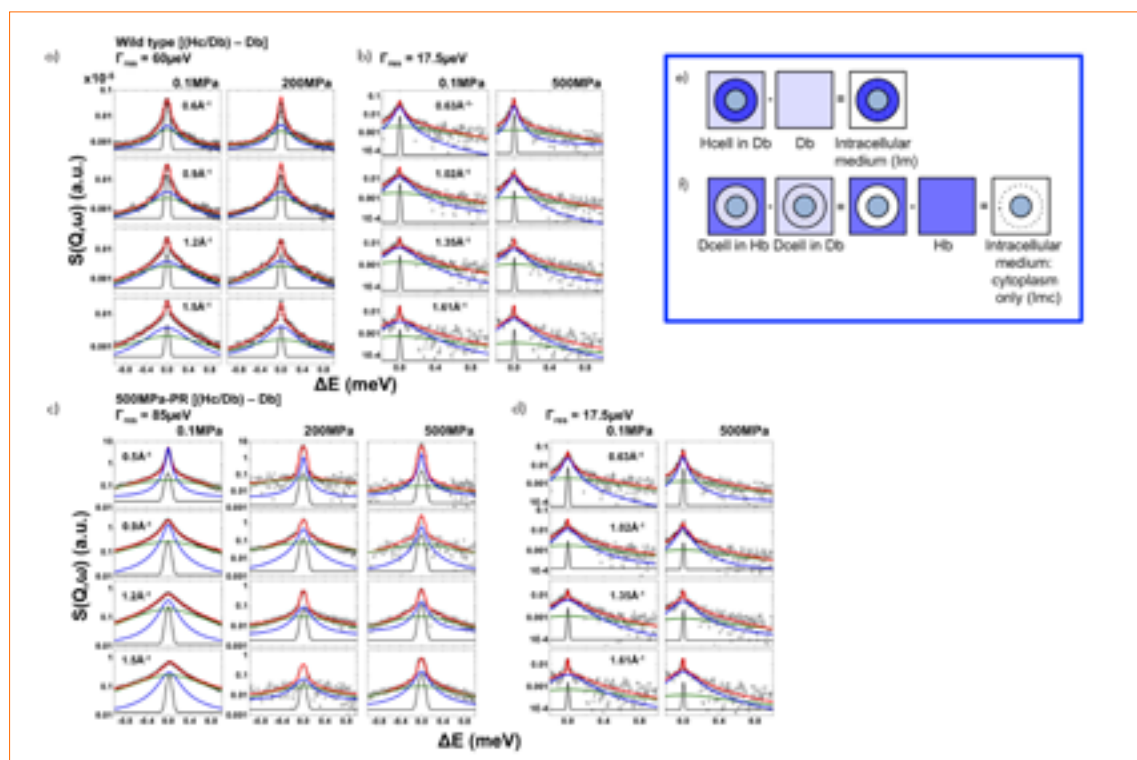


Figure 2

Analysis of the neutron dynamic scattering function $S(Q, \omega)$ for the dynamics of the intracellular medium for *Shewanella oneidensis* Wild type (WT) and cultured under 500 MPa pressure (500 MPa-PR) recorded at room temperature between 0.1 and 500 MPa.

Panels **a–b**) data for WT obtained from TOF-TOF (FRMII, Germany) and IRIS (ISIS, UK).

Panels **c–d**) data for 500 MPa-PR obtained from IN6 spectrometer (ILL, France) and IRIS (ISIS, UK). The central line (grey) represents a delta function convoluted with the instrumental resolution function. For aqueous solutions, both translational (blue) and translational-rotational (olive) Lorentzian components were used. The global fit (red continuous curve) is overlaid on the data points (black).

Panels **e–f**) Cartoon depicting isotopic QENS dataset subtractions applied to highlight intracellular water dynamics in different spatial regions: **e**) Intracellular medium (*Im*) dynamics—this dataset subtraction provides information on the dynamics of all species contained within the cell envelope; **f**) Intracellular medium cytoplasm-only (*Imc*) dynamics—this isotopic subtraction gives information on the cytoplasm dynamics only.

increasingly lower relative to bulk aqueous solutions while the rotational relaxation time scales increased, demonstrating that water dynamics inside the cells exhibit significantly greater slowdown compared with bulk water or aqueous electrolyte solutions.

We have proposed that the enhanced D_T slowdown is associated with closing down diffusional bottlenecks along with increased interactions with macromolecules lining the walls of the nanoscale intracellular channels. Our QENS results for live bacteria under high-pressure conditions are consistent not with the expected evolution of water dynamics under compression in a homogeneous, gel-like medium, but rather with channel closure occurring in emerging models of a dynamically structured ‘supercluster’ arrangement of macromolecular components in the cytoplasm, affording channels for water diffusion to transport ions and hydrophilic molecules within the cell. Our findings thus support this new model of intracellular organisation in prokaryotic organisms and can lead to new insights regarding the biological functioning of organisms under ambient- and high-pressure conditions.

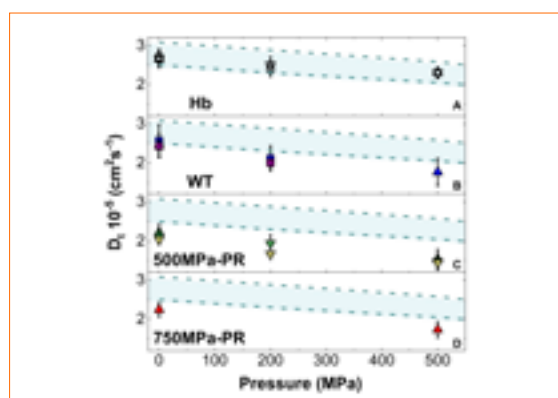


Figure 3

Compilation of translational self-diffusion coefficients (D_T) extracted from QENS data obtained from the three spectrometers and neutron scattering facilities. Data from TOF-TOF are shown as square symbols, from IRIS as upward-pointing triangles and from IN6 as downward-pointing triangles. Panel **a**) D_T values for the H-buffer (Hb).

Panels **b–d**) D_T values for the intracellular [$Hc/Db - Db$; blue symbols] and the cytoplasm [$[Dc/Hb] - [Dc/Db] - Hb$; purple] medium for *Shewanella oneidensis* WT cells (**b**); 500 MPa-PR cells (**c**) and 750 MPa-PR cells (**d**). The dashed lines enclosing the light blue shaded area correspond to the range of literature values reported for bulk water and aqueous solutions between 298–308 K.



Carlos Guerrero. Spanish
Universidad de Sevilla, Seville, Spain
Centro Nacional de Aceleradores (CNA),
Seville, Spain

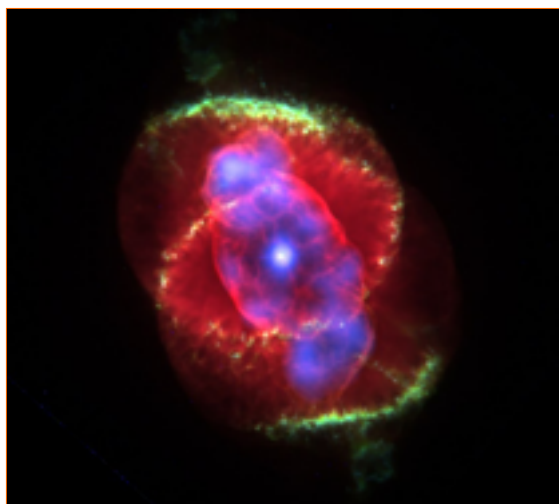
*'I am a Ramón y Cajal researcher currently
working at the CNA (Spain) after a six-year
period working at the n_TOF facility at CERN*

*(Switzerland). In the field of experimental nuclear physics I perform cross
section measurements, in most cases induced by neutrons, that are of
interest to astrophysics, nuclear technology and medical physics.'*

From the ILL reactor core to the LiLiT neutron beam: a nuclear astrophysics experiment to better understand the nucleosynthesis of elements in the universe

*V4 beam tube at the ILL, the PSI
radiochemistry laboratory and the
SARAF accelerator facility*

Among the nuclear reactions occurring in the stars, neutron capture is the driving force behind the production of more than half of the isotopes in our universe. The study of this reaction is key to a better understanding of stellar nucleosynthesis; and it is particularly interesting in the case of reactions in unstable nuclei that act as branching points along the so-called slow (or s-) process.



AUTHORS

C. Guerrero, J. Lerendegui-Marco and J. M. Quesada (Universidad de Sevilla & Centro Nacional de Aceleradores CNA, Spain)
M. Tessler, M. Paul, S. Halfon, T. Palchan-Hazan and L. Weissman (Hebrew University & SNRC, Israel)
S. Heinitz, E. A. Mauger, R. Dressler, N. Kivel and D. Schumann (Paul Scherrer Institut PSI, Switzerland)
C. Domingo-Pardo (Instituto de Física Corpuscular IFIC-CSIC, Spain)
U. Köster (Institut Laue-Langevin ILL, France)

ARTICLE FROM

Phys. Rev. B (2019)—doi: <https://doi.org/10.1016/j.physletb.2019.134809>

REFERENCES

- [1] J.A. Johnson, Science 363 (2019) 474
- [2] F. Käppeler, R. Gallino, S. Bisterzo and W. Aoki, Rev. Mod. Phys. 83 (2011) 157
- [3] W. Ratynski and F. Käppeler, Phys. Rev. C 37 (1988) 595
- [4] D. Studer, S. Heinitz, R. Heinke, P. Naubereit, R. Dressler, C. Guerrero, U. Köster, D. Schumann and K. Wendt, Phys. Rev. A 99 (2019) 062513

The chemical elements of our universe are created through nuclear reactions occurring in the stars. The vast majority of elements heavier than iron are made through various forms of neutron capture, a process in which a neutron is absorbed and retained by a nucleus thereby increasing its mass number by one unit. This process occurs sequentially until the newly formed nucleus becomes unstable; when this happens, a branching point is reached and competition arises between additional neutron capture and the beta-decay of the nucleus. The latter means the production of a different chemical element. The sequence of neutron captures and beta-decays taking place mostly in AGB (Asymptotic Giant Branch) stars is known as the s-process and is responsible for the production of about half of the elements in our universe.

In this context, the study of neutron capture reactions in the laboratory provides a key quantity for nucleosynthesis network calculations: the Maxwellian-Averaged Cross Section (MACS). This quantity is related to the probability of a neutron capture reaction occurring for a neutron with the equivalent kinetic energy of those in the stellar sites where the s-process takes place. Experiments to determine this quantity, the MACS, produce neutron beams of the appropriate energy distribution that are used to irradiate a target made up of the isotope of interest. Then, the number of reactions that have taken place is determined by looking at the decay of newly formed nuclei.

Figure 1

A planetary nebula like the Cat's Eye one shown here is created when an AGB star blasts part of its content via strong stellar winds into the environment. Thus, the elements formed in the s-process contribute to the normal chemical composition of the universe. [Picture from NASA (public)]

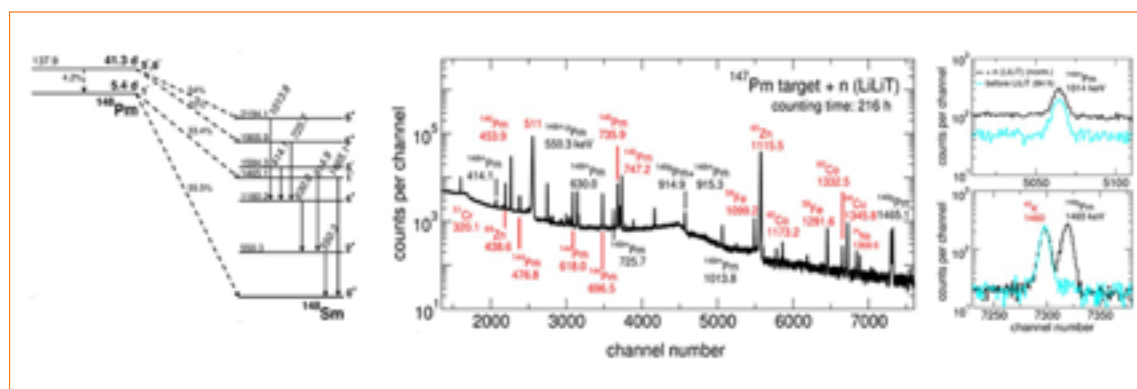


Figure 2

^{148g}Pm and ^{148m}Pm produced by neutron activation of the ^{147}Pm target are identified by their characteristic gamma rays. The decay scheme (**left**) with the relevant transitions (energies in units of keV) and the measured gamma-ray spectrum of the ^{147}Pm target after activation recorded by a HPGe detector (**right**), show the above-mentioned gamma rays plus additional ones from activated contaminants (marked in red).

While these neutron ‘activation’ experiments have been carried out for most of the stable isotopes on the chart of nuclides and can be performed at medium-size accelerator facilities, it is particularly challenging to perform them for the most interesting cases: the above-mentioned branching points in which the target nucleus is radioactive. To do so, one must first artificially produce the atoms of the isotope of interest, which will necessarily be a small amount. Next, one must make a suitable (high purity) target and then perform the neutron irradiation with an epithermal neutron beam of high intensity to make up for the limited number of atoms available.

In the study reported here, close to the core of the ILL reactor (at the V4 position) we inserted 98.2 mg of Nd, in the form of a $^{146}\text{Nd}_2\text{O}_3$ enriched to 98.8 %, over a period of 54 days. Following each neutron capture a nucleus of ^{147}Nd was formed, which decayed with a half-life of 11 days to ^{147}Pm —the isotope of astrophysics interest. The irradiated material was then shipped to the PSI in Switzerland, where it was dissolved and chemically purified to make a high-purity and high-quality ^{147}Pm target suitable for an activation experiment. Even though the target contained just 56 μg , it represents the highest mass of ^{147}Pm put together to date for this purpose. In order to then produce enough activity from neutron capture, the irradiation of the target was performed at the LiLiT facility in Israel, featuring the highest intensity beam of epithermal neutrons in the world. At the LiLiT, a radio-frequency, superconducting linear accelerator delivers a proton beam of 1.93 MeV with a current of about 1.5 mA that hits a liquid lithium target, producing neutrons with an energy distribution equivalent to that of the s-process that occurs in

the ^{147}Pm target. The activity induced by neutron capture was then assessed by studying the characteristic γ -ray emission of ^{148}Pm from its ground and metastable states, with quite different half-lives of 5.4 days and 41 days, respectively. The data analysis produced a MACS value of 826(57) mb at 30 keV, as the sum of the partial cross section values 469(50) and 357(27) mb, respectively.

The success of the experiment described briefly above could only be achieved thanks to the close collaboration of three major players in the nuclear physics community: the ILL reactor, the PSI radiochemistry lab and the SARAF accelerator facility hosting LiLiT, co-ordinated by the Universidad de Sevilla and aided by the Hebrew University in Jerusalem. The result of this work is now in the hands of the astrophysics community studying the nucleosynthesis of elements. However, more interesting results are on their way as a result of this collaboration established for this study. The ^{147}Pm target has also been used to identify individual epithermal neutron resonances in an experiment performed at the CERN n_TOF facility, while part of the repurified ^{147}Pm enabled high-resolution laser spectroscopy studies to be performed at Mainz University. This resulted in the first experimental determination of the ionisation potential of the chemical element promethium (which does not possess any stable isotope), filling the last remaining gap in the periodic table for this fundamental property—a timely occurrence for the 150th anniversary of the periodic table of the elements. Moreover, radioactive targets of ^{171}Tm and ^{204}Tl have already been produced at the ILL and used for irradiations at the LiLiT and the CERN n_TOF facility; new targets of ^{163}Ho and ^{79}Se are planned in the coming years.

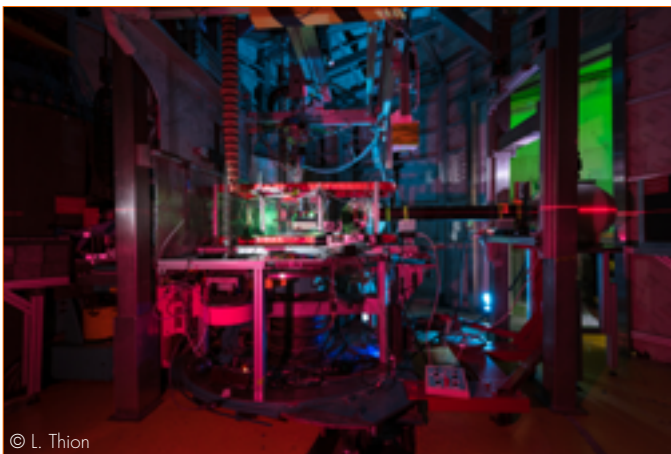


Armin Danner, Austrian
Atominstytut, TU Wien
'We perform neutron interferometer experiments to give new insights and interpretations on quantum mechanics. Coming to Grenoble for this purpose is always exciting—it gives and takes a lot at each visit.'

Inertia of intrinsic spin observed in neutron interferometry

Interferometer S18

Inertia is a key property in both general relativity and quantum theory. While inertia is usually associated with mass, intrinsic spin can exhibit similar behaviour in the form of spin-rotation coupling. This coupling is a quantum mechanical extension of the Sagnac effect and manifests itself as an additional phase in the neutron wave function. Such experiments were proposed as far back as thirty years ago. With the instrument S18, we were finally able to conduct a high-precision experiment using the technique of neutron interferometry to confirm the effect.



© L. Thion

AUTHORS

A. Danner, B. Demirel, W. Kersten, R. Wagner and S. Spöner (TU Wien, Austria)
H. Lemmel (ILL and TU Wien, Austria)
Y. Hasegawa (TU Wien, Austria and Hokkaido University, Japan)

ARTICLE FROM

npj Quantum Information 6, 23 (2020) - doi:10.1038/s41534-020-0254-8

REFERENCES

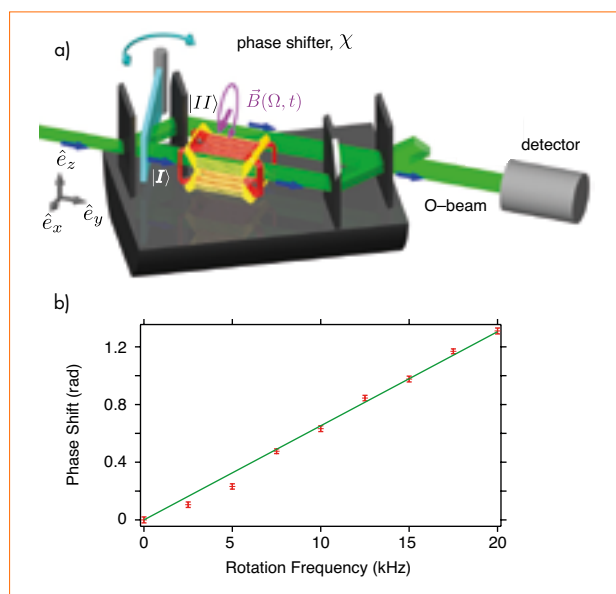
- [1] G. Sagnac, *Comptes Rendus Acad. Sci.* 157 (1913) 1410
- [2] H. Rauch and S.A. Werner, Oxford University Press (2000)
- [3] B. Mashhoon, *Phys. Rev. Lett.* 61 (1988) 2639
- [4] B. Mashhoon and H. Kaiser, *Physica B* 385–386 (2006) 1381

When Georges Sagnac conducted his famous interferometer experiment with light [1], he was convinced that he had found proof of the ether. In his rotatable set-up, a light wave is split in an interferometer where both partial waves propagate through a ring interferometer in opposite directions. The relative phase shift at recombination is linearly dependent on the rotation frequency. Although we strongly favour the framework of special relativity to describe his results today, the experiment itself is still an interesting one: without external reference, observers in a rotating frame are able to measure the rotation of their system. This was also demonstrated in the rotating frame of the Earth in the Michelson–Gale experiment with light and by Werner *et al.* with neutrons [2].

In the rotating system, we can express the phase shift in the Sagnac interferometer as a coupling $\sim \vec{\Omega} \cdot \vec{A}$, where $\vec{\Omega}$ is the rotation vector and \vec{A} the oriented area of the interferometer. Alternatively, one can write this as $\sim \vec{\Omega} \cdot \vec{L}$, with the orbital angular momentum \vec{L} . For an observer in the rotating frame, accelerations of particles require different forces depending on the direction of their orbital angular momentum and linear to their mass. When extending the orbital angular momentum to the total angular momentum, an additional spin contribution $\sim \vec{\Omega} \cdot \vec{S}$ naturally appears, called spin-rotation coupling. To confirm this effect, various neutron interferometer experiments have been suggested [2, 3]. The coupling has been used in NMR to describe the rotation of the polarisation vector in rotating magnetic fields for a long time. However, semi-classical Bloch equations suffice to describe those experimental results where only the orientation of the polarisation vector is observed.

Figure 1

The neutron interferometry station S18.

**Figure 2**

a) Schematic of *set-up*: monochromatised neutrons, with polarisation vector parallel to the direction of propagation (+y), enter the interferometer. Inside the interferometer, a rotating magnetic field $\vec{B}(\Omega, t)$ is generated in path I, rotating on a plane perpendicular to the neutron beam. After recombination at the final interferometer plate, the neutrons in the forward direction (O-beam) are detected in a ^3He counter tube. Spin directions are indicated with blue arrows, the magnetic field in violet. The phase shifter plate consists of a slab of sapphire and is rotated to record interferograms by inducing additional relative phase shifts χ between the paths.

b) Final results: linearly fitted phase of the interferograms relative to the static case dependent on the rotation frequency of the magnetic field.

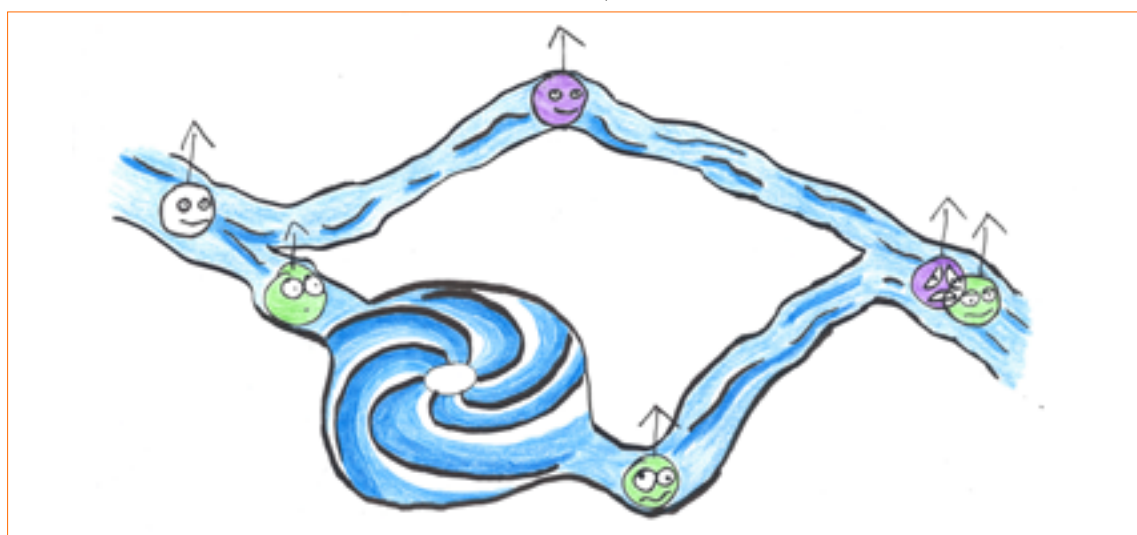
The goal of our present experiment was to reveal the purely quantum mechanical aspect of spin-rotation coupling as an extension of the Sagnac effect in a neutron interferometer experiment [4], as suggested by [3], using the instrument S18 (**figure 1**). Our *set-up* is shown in **figure 2a**. The first interferometer plate coherently splits a beam of polarised neutrons. In path I, the neutron spin interacts with a magnetic field of variable rotation frequency. The field amplitude is tuned according to the frequency to produce cyclic spin evolution paths. Initial and final spin states differ only in their phase. The last interferometer plate acts as a projector, comparing the additional phase with that of the reference beam in path II. In our experiment, only the outgoing O-beam (**figure 2a**) is of importance. Our final results are presented in **figure 2b**. Since the results are in the form of a phase shift the Bloch-equations are insufficient to describe them, so we must rely on the Schrödinger equation.

As predicted by theory, the phase shift is found to be linearly dependent on the rotation frequency of the magnetic field. The observed phase shift can also be described by a combination of dynamical and geometric phases in the inertial frame. However, our present *set-up* focuses on a specific configuration where the quantum mechanical extension of the Sagnac effect is revealed.

This means that we can give an alternative explanation for the results in terms of the Mashhoon effect of spin-rotation coupling in the rotating frame. A rotating observer has to apply different forces on a particle depending on its spin state in order to accelerate it. This is why ref. [3] interprets this effect as the ‘inertia of intrinsic spin’. Spin-rotation coupling can likewise be used to determine the rotation of a system.

Figure 3

Cartoonistic impression of the neutron interferometer experiment by Armin Danner.





Costel Petrache. Italian
CNRS/IN2P3, University Paris-Sud,
Orsay, France

'I am a professor at the University Paris-Sud and my research activity is performed at the Centre de Sciences Nucléaires et Sciences de la Matière, CNRS/IN2P3, Orsay, France.'

My field of interest is nuclear spectroscopy. I study medium-heavy nuclei using fusion-evaporation and $(n\alpha, \gamma)$ reactions, with a particular focus on collective excitations such as chiral and wobbling bands in triaxial nuclei and intruder bands in mid-shell Sn nuclei.'

Shape coexistence in Sn isotopes: evidence for collective structures in ^{116}Sn based on 2 particle-2 hole proton configuration

Fission Product Prompt gamma-ray Spectrometer FIPPS

The fast timing technique was used to measure the lifetime of the second excited 4^+ state in ^{116}Sn , providing the first evidence obtained in $(n\alpha, \gamma)$ experiments for a band based on an intruder configuration and shape coexistence in the semi-magic ^{116}Sn nucleus. The Fission Product Prompt gamma-ray Spectrometer (FIPPS) array, equipped with 16 LaBr_3 fast scintillators, was used for to detect the gamma rays emitted following ^{115}Sn $(n\alpha, \gamma)$ reactions.

AUTHORS

C.M. Petrache (Centre de Sciences Nucléaires et Sciences de la Matière, France)
J.-M. Régis (Köln University, Germany)
C. Andreoiu (Simon Fraser University, Canada)
C. Michelagnoli (ILL)

ARTICLE FROM

Phys. Rev. C 99 (2019)—doi: 10.1103/PhysRevC.99.024303

REFERENCES

- [1] J.-M. Régis, M. Dannhoff and J. Jolie, Nucl. Instrum. Methods Phys. Res. A 897 (2018) 38
- [2] J.L. Pore *et al.*, Eur. Phys. J. A 53 (2017) 27
- [3] D.S. Cross *et al.*, Eur. Phys. J. A 53 (2017) 216

Sn isotopes play a pivotal role in the development of our understanding of nuclear structure, particularly because they are some of the best examples of seniority structures in nuclei. Indeed, the near constancy of the $2^+_{1\gamma}$ energies from $N = 52$ (^{102}Sn) to $N = 80$ (^{130}Sn) is remarkable (**figure 1**). Another well-documented phenomenon in Sn isotopes is shape coexistence. The lifetimes of the $0^+_{2,3}$ and $4^+_{2\gamma}$ states assigned to intruder bands built on 2 particle-2 hole proton configurations are poorly known or only have lower/higher limits determined, preventing clear conclusions being drawn on the collectivity of the bands and their band-heads. The band-head of the intruder band of the neutron mid-shell nucleus ^{116}Sn was recently assigned the $0^+_{3\gamma}$ state, which is more strongly populated from the $2^+_{2\gamma}$ state of the intruder band than is the $0^+_{2\gamma}$ state.

The present study was concerned with measuring the lifetimes of the low-spin, highly excited, normal and intruder states, in particular of the $4^+_{2\gamma}$ state of the intruder band. We determined the lifetime of the $4^+_{2\gamma}$ 2 529 keV state of ^{116}Sn using the FIPPS array in conjunction with LaBr_3 ancillary detectors (**figure 2**). Moreover, we demonstrated the utility of $(n\alpha, \gamma)$ reactions for probing low-spin, highly-excited states and measuring their lifetimes, which are often in the range of 1–200 ps.

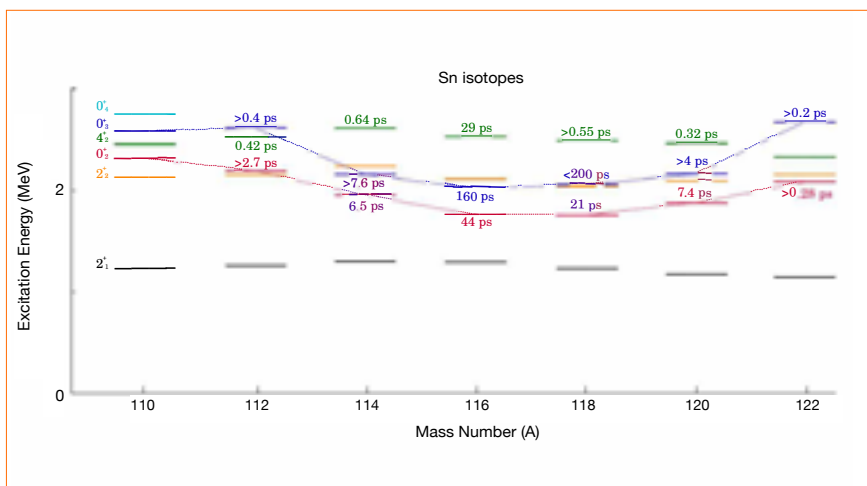


Figure 1

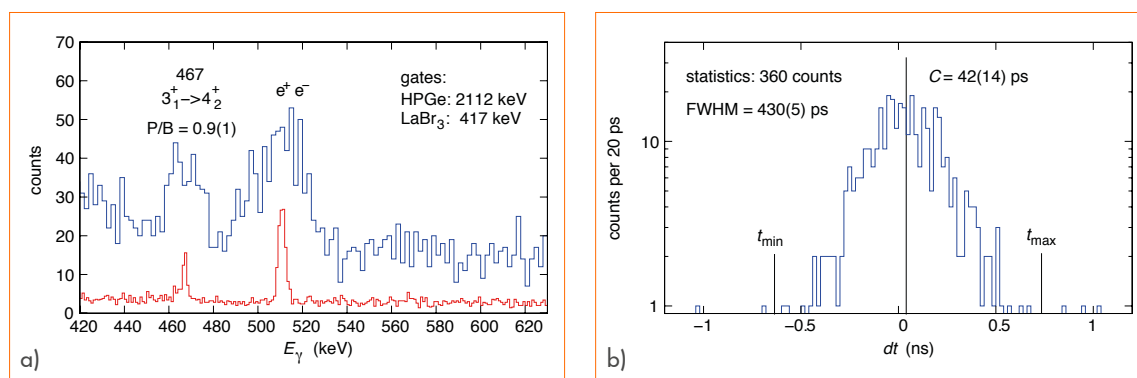
Systematics of the Sn isotopes showing the half-lives or the half-life limits of the $0^+_{2\gamma}$ (red), $0^+_{3\gamma}$ (blue) and $4^+_{2\gamma}$ (green) states.

**Figure 2**

FIPPS set-up. **Left)** FIPPS+LaBr₃ set-up. **Right)** 16 LaBr₃ detectors (IKP Cologne and IFIN HH Bucharest) installed at an angle of 45° relative to the beam axis were coupled to the 8 FIPPS HPGe clovers placed in a central ring perpendicular to the beam axis for one reactor cycle in 2018.

We used the $^{115}\text{Sn}(n_{th},\gamma)^{116}\text{Sn}$ reaction at the collimated neutron guide of the FIPPS set-up, with a neutron flux of 10^8 n/(cm²s) and a 1 cm diameter beam spot at the target position. The γ -ray detection set-up around the target consisted of eight HPGe clovers, each made of 4 Ge crystals, and 16 LaBr₃ scintillator detectors. The excellent energy resolution of the HPGe detectors permits precise selection of a γ -ray from a specific triple- $\gamma\gamma\gamma$ cascade and produces clean LaBr₃ coincidence spectra, as illustrated in **figure 3a** for the 4_2^+ state of ^{116}Sn using the 2 112 keV $2_2^+ \rightarrow 0_1^+$ transition. The lifetime of a nuclear excited state is deduced from LaBr₃-LaBr₃ time-difference measurements between the γ -rays feeding and de-

exciting an excited state, as described in reference [1]. After corrections (shifts) for the energy-dependent mean zero-time response of the whole set-up and the time contributions of the Compton background, the centre of gravity of the time distribution directly corresponded to the lifetime of the 4_2^+ state of ^{116}Sn of 42(14) ps, corresponding to a half-life $T_{1/2} = 29(10)$ ps [2, 3]. Comparison of the experimental data with the results of the Interacting Boson Model (IBM-2) calculations with mixing shows that the intruder states in ^{116}Sn have dominant contributions of the 2 particle-2 hole configuration but are strongly mixed with normal configurations.

**Figure 3**

Doubly-gated coincidence γ -ray spectra generated to investigate the quality of the 467 keV peak and the Ge (2 112 keV)-triggered time-difference distribution between the 467 keV and 417 keV transitions feeding and de-exciting the 4_2^+ state of ^{116}Sn .



Bruno Tomasello, Italian

The ILL (Oct. 2016–Sep. 2019)

'I am interested in the physics of quantum many-body systems. As a junior theorist I specialise in rare-earth compounds and frustrated magnetism. I am also engaged in fostering co-operation amongst communities

and am committed to contributing to the unique know-how of large-scale scientific facilities.'

How monopoles determine dynamic correlations in spin ice

Spin ice materials are archetypical examples of frustrated magnets. This study highlights an intriguing and hitherto poorly understood correlation in the dynamics of spin ices, whereby a monopole locally alters the spin background and the latter predetermines whether and how fast the former can hop. We discover a bimodal distribution of temperature-independent spin-tunnelling time scales dictated solely by the crystalline, dipolar and exchange interactions. The picture of spin ice that emerges is one in which classical and quantum physics interact in a seductive way: the monopole is a classical quasi-particle, but quantum tunnelling of individual spins is responsible for its stochastic diffusion.

AUTHORS

B. Tomasello (ILL)

C. Castelnovo (University of Cambridge, UK)

R. Moessner (Max Plank Institute for the Physics of Complex Systems, Germany)

J. Quintanilla (University of Kent, UK)

ARTICLE FROM

Phys. Rev. Lett. (2019)—doi: 10.1103/PhysRevLett.123.067204

REFERENCES

- [1] S.T. Bramwell and M.J.P. Gingras, *Science* 294 (2001) 1495
- [2] C. Castelnovo, R. Moessner and S.L. Sondhi, *Nature* 451 (2008) 42
- [3] I.D.C. Jaubert and P.C.W. Holdsworth, *J. Phys. Condens. Matter* 23 (2011) 164222
- [4] K. Matsuhira, C. Paulsen, E. Lhotel, C. Sekine, Z. Hiroi and S. Takagi, *J. Phys. Soc. Jpn.* 80 (2011) 123711

The magnetism of rare-earth crystals can vary substantially depending on the chemical elements and the geometry of the lattice. A prominent characteristic of rare-earth ions is their sizeable *spin-orbit* coupling; and in magnetic *pyrochlore* oxides, despite similarities in structure this leads to a wide variety of phenomena—spin glass, spin ice and spin liquid are just a few examples of so-called exotic phases. These arise because the natural tendency to develop long-range order is frustrated by the geometrical constraints of the crystal [1].

A system is said to be frustrated if competing interactions lead to conflicting classical minima in energy. In spin ice, the magnetic moments of the rare-earth ions, which sit at the vertices of a lattice of corner-sharing tetrahedra, are forced by the crystal fields to point along the axis joining adjacent tetrahedral centres. At temperatures of a few kelvin, *i.e.* the order of spin-spin interactions, frustration and crystal field anisotropy favour correlated configurations with a degree of degeneracy that maps to the proton arrangement in water ice. Such spin configurations are summarised by the 'ice rules', which consist of two spins per tetrahedron pointing toward its centre and another two pointing outward. These imply a ground state whose degeneracy scales with the size of the lattice. An illustrative example is presented in **figure 1**, which shows just 1 of the total 13 122 equivalent configurations for the 2-in/2-out ground state of a unit cell of order 10 Å. Excitations above the ground state correspond to local violations of the ice rules: they consist of tetrahedra hosting

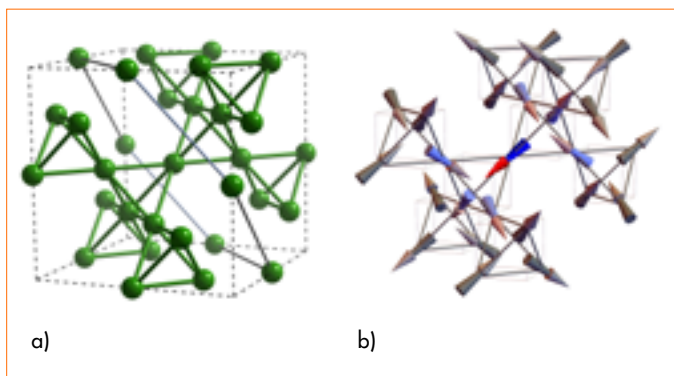
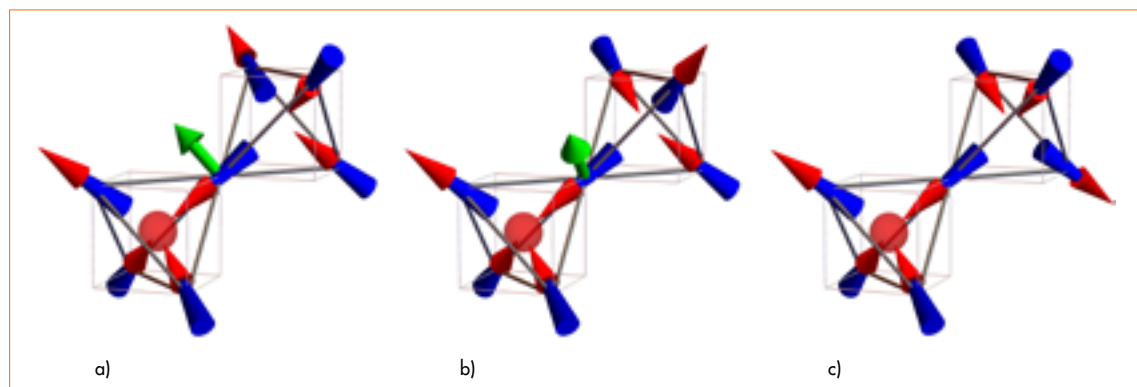


Figure 1

a) Unit cell of a magnetic pyrochlore oxide. Green spheres represent rare-earth ions.

b) Example of spin-ice anisotropies for the pyrochlore lattice contained in **(a)**. Notice that **(b)** is an example of a ground-state configuration (2-in/2-out per tetrahedron).

**Figure 2**

The three inequivalent, low-energy configurations of a 2-tetrahedron system hosting only one monopole (red sphere). Effective fields on the central spin due to its nearest neighbours spins are purely transverse (green arrows) to the central axis of anisotropy in **(a)** and **(b)**, and identically null in **(c)**.

3-in/1-out or 3-out/1-in spin configurations (a few 3-in/1-out examples are shown in **figure 2**). These defects are called magnetic monopoles, because they act as sources and sinks of magnetisation fluxes in the otherwise ‘vacuum’ of the 2-in/2-out spin background [2].

The success of this formulation aside, magneto-dynamics are nevertheless poorly understood [3]. A comprehensive understanding of experimental relaxation time scales is still lacking and the detection of a temperature-independent regime is the only common denominator among all probes [4]. As this is ascribed to quantum spin-tunnelling due to monopole hopping, we based our theory on spin fluctuations originating from localised, isolated monopoles. Our model is material-dependent, with the crystal-field Hamiltonian being the ‘foundation’ for setting up the Hilbert space, and with the dipolar and exchange energy-terms as the ‘building blocks’ of interactions for creating dynamics and *realistic* estimation of timescales thereof.

Our principal finding is that there is a fundamental correlation between spin dynamics, monopole excitations and their local environment. Indeed, in the case of low densities of monopoles, whereas the vast majority of spins in the sample experience net longitudinal fields, those adjacent to a monopole have such longitudinal components suppressed. Moreover, as illustrated in **figure 2**, the same monopole induces, statistically, a *bimodal* distribution of *transverse* fields: specifically, with two-thirds probability the central spin experiences a finite transverse field of strength ~ 0.35 teslas (**figures 2a** and **2b**), while with one-third probability the field vanishes (**figure 2c**).

As transverse fields induce spin-tunnelling, these results imply that for a ‘flippable’ spin next to a monopole two very distinct rates, τ^{fast} and τ^{slow} , appear with a 2:1 ratio. The spin dynamics is therefore remarkably correlated with the local environment and the propagation of monopoles is intrinsically stochastic. Contrary to conventional modelling, which assumes a uniform distribution of hopping amplitudes, this opens up the study of monopole dynamics accounting for correlated statistics as well as percolation effects which may also play a prominent role in understanding the so-called quantum spin ices.

The time scales obtained for monopole motion are found to be slower than expected decoherence times. This reconciles the view of spin-ice monopoles as classically diffusing quasi-particles with the fact that their motion requires quantum fluctuations. We propose a model based on the quantum Zeno effect, where the hopping is effected by decoherence.

The *quantitative* benefit of this theory is intimately related to neutron scattering in condensed matter. The best determinations of the crystal field Hamiltonian are obtained thanks to the inelastic interaction of the spin- $1/2$ magnetic moment of the neutron with the magnetic moments of a given compound. Our approach demonstrates how theoretical analyses can tailor the quantitative prediction of neutron studies well beyond conventional expectations.



Nicolás A. García. Argentinian
The ILL

'I was awarded a PhD degree in Physics from the Universidad Nacional del Sur in 2015. My research interests include polymer physics and colloidal systems. Nowadays, I am a postdoctoral researcher at the ILL, my investigation

focus being the fundamental properties of heterogeneous polymers such as block copolymers, nanocomposites and polymer rings.

Always working in close collaboration with experimentalists, I try to reveal the secrets of these fascinating systems.'

Confinement disentangles polymer chains in thin films

Polymer thin films are ubiquitous in our daily life, encompassing applications ranging from packaging and food wrapping to adhesives, lubricants and protective coatings for furniture and glasses. They are also widely used in microelectronics and nanotechnology. On a day-to-day basis, the thickness of the films decreases to dimensions comparable with the size of a single polymer chain. Hence, an important question arises as to whether such small dimensions under confinement changes the fundamental properties of polymers. In this paper, we shed light on this intriguing issue.

AUTHORS

N.A. García (ILL)
J.-L. Barrat (UGA, Grenoble University, France)

ARTICLE FROM

Macromolecules (2018)—doi: 10.1021/acs.macromol.8b01884

REFERENCES

- [1] M. Doi and S.F. Edwards, Oxford University Press: Oxford (1986)
- [2] A. Korolkovas, P. Guffreund and J.-L. Barrat, J. Chem. Phys. 145 (2016) 124113
- [3] M. Kröger, Comput. Phys. Commun. 168:3 (2005) 209
- [4] Y.H. Lin, Macromolecules 20 (1987) 3080

The mechanical and viscoelastic response of polymers in melts and concentrated solutions depends fundamentally on the molecular weight of the chains. Indeed, when their molecular weight increases the chains' mobility with respect to each other is constrained by the simple fact that they cannot cross each other. In this way, so-called entanglements occur naturally [1]. Nowadays, we know that these topological constraints dictate the fundamental properties of polymers. Thus, a logical approach to answering our question is to investigate the network of entanglements and how it is affected by confinement. As entanglements are not directly observable via experiments, numerical simulations are essential for exploring their nature.

We performed numerical simulation using a recently proposed coarse-graining method [2], which models the chains as pseudo-continuous bodies interacting through ultrasoft potentials to speed up the simulation. The motion is then resolved using Brownian dynamics with large time-steps.

The topological analysis was performed using the Z1 algorithm [3], a method that detects entanglement through geometrical minimisation. Furthermore, the algorithm provides the position of entanglements within the film.

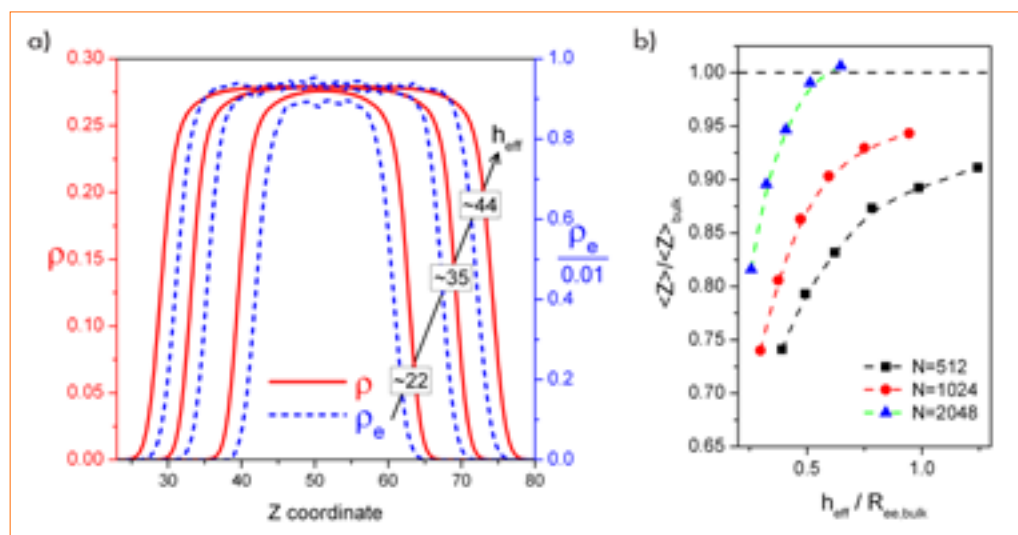
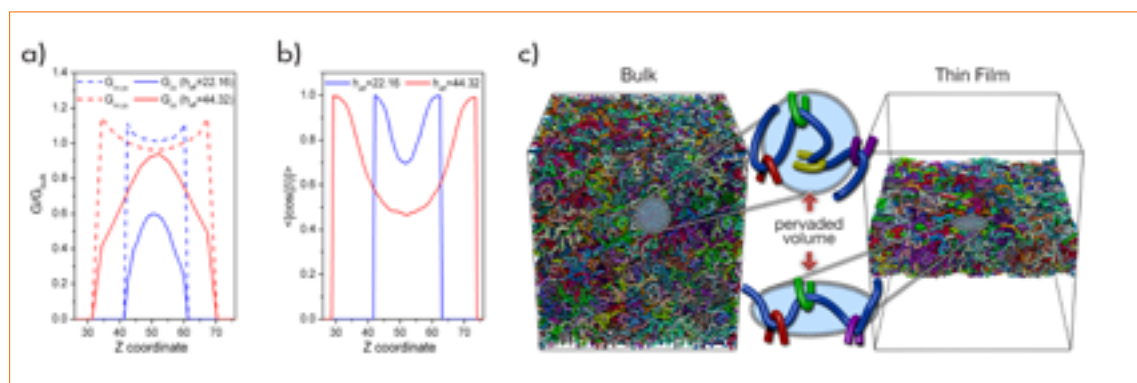


Figure 1

a) Comparing monomer and entanglement density profiles for three different films constructed with chains of length $N = 1\,024$. Two different scales (left, blue and right, red axes) are used to plot these quantities in the same figure to aid comparison. The labels on the curves indicate the film thickness.

b) Normalised reduction of entanglements per chain as a function of confinement for all free-standing films' thicknesses studied here for chain lengths $N = 512, 1\,024, \text{ and } 2\,048$.

**Figure 2**

Profiles evaluated using the location of the centre of mass of the chains within the film of:

a) Bulk normalised and temporal-averaged components of the radii of gyration G_{xx} , G_{yy} and G_{zz} ; and

b) The cosine director of the most important direction in which the chain is elongated with respect to the surface of confinement. These observables were evaluated for two film thicknesses: $h_{eff} = 22.16$ (in blue) and $h_{eff} = 44.32$ (in red).

c) Snapshot of the polymer melts simulated here in bulk (left) and thin films (right). In the centre, a sketch illustrates the idea of how the volume pervaded is compressed by the confinement in thin films while remaining isotropic in bulk.

A spatially resolved profile of the entanglement density across the film for three different films are compared with their associated monomer density profile in **figure 1a**. Note that the entanglements do not sample all the volume available in the film, as is evident in **figure 1a** where the two density profiles do not match exactly.

The integrated contribution of this surface effect is summarised in **figure 1b**, which shows the total number of entanglements per chain compared with its bulk value, for thin films of various thicknesses. The film thickness is normalised here using the average end-to-end distance in bulk conditions for the same chain length. Overall, we find that confinement leads to a decrease in the average number of entanglements per chain. Qualitatively, these results are in good agreement with those observed in experiments using thin films and nanocomposites. It is interesting to note that this trend of ‘confinement disentangles the chains’ is valid for all the cases studied here; however, the decrease is not dramatic, being 30 % at most for a strong confinement strength.

In order to understand the fundamental reasons for this outcome we performed several statistical analyses, one of which provided us with a clear picture. This arose from studying how confinement alters the overall shape of the chains. To do this, we used the gyration tensor (G), whose three diagonal components, G_{xx} , G_{yy} and G_{zz} , account well for the spatial conformations of the chains.

Figure 2a shows the averaged value of these components normalised with the corresponding bulk value as a function of the chain position within the film.

The figure shows that for both thicknesses (continuous lines) the component G_{zz} , associated with the direction of confinement, tends to induce a noticeable shrinking of the chains in that direction, *i.e.* the chains break their spatial isotropy and tend to adopt a flat shape near the free surface. Conversely, the components G_{xx} and G_{yy} experience a slight change in their values in terms of increasing by as much as 10 % with respect to the bulk state (dashed lines in **figure 2a**).

By diagonalising the G tensor and studying the cosine director of the eigenvector associated with the minimum eigenvalue (which represents the most important direction in which the chain is elongated), it was possible to determine the main direction of the flatness. **Figure 2b** illustrates how the average orientation of this vector is dictated by the position of the chains within the film. Independently of the molecular weight, all chains are flat at the edges of the film; this effect then decreases monotonically as the chains enter the film.

This anisotropic compression seems not to be wholly compensated for in the other directions, leading to an effective decrease in the volume pervaded by the chain. This decrease reduces the number of neighbour chains inside the shared space, lowering the potential inter-chains contacts and resulting chiefly in the effective reduction of entanglements. This idea is illustrated in **figure 2c**. The assumption that the number of entanglements is proportional to the volume pervaded by the chain is supported by the chain packing model [4], which unequivocally links both quantities.

MODERNISATION PROGRAMMES AND TECHNICAL DEVELOPMENTS

74 MODERNISATION PROGRAMME AND INSTRUMENT UPGRADES

82 TECHNICAL DEVELOPMENTS

60M€



ENDURANCE

8 YEARS (2016–2023)

WASP

RECEIVED ITS FIRST NEUTRONS IN **2019**



- INCREASED FLUX
- REDUCED BACKGROUND
- LARGER DETECTORS
- IMPROVED RESOLUTION
- ENHANCED CAPABILITIES
- RELIABILITY & PERFORMANCE



KEEP UP-TO-DATE:

 facebook.com/ILLGrenoble

 twitter.com/ILLGrenoble

 linkedin.com/company/institut-laue-langevin

Endurance: from design to implementation and science, and more...

Because of complications in the manufacturing of the replacement H1-H2 beam tube, as well as the ILL's commitment to minimising disruption to the provision of neutrons for science, the long H1-H2 shutdown is now planned for mid-2021 to mid-2022. This means that the installation work for the Endurance H24 and H15 package of guides and instruments will also now begin at this time. The positive side to this delay is that it has given the Projects and Techniques Division (DPT) time to strengthen the feasibility and design phase of the complex H15 guide renewal project. The project has now been simplified, with particular emphasis on the 'trumpet' section in which the main guide fans out into separate sub-guides. Neutronic simulations and detailed engineering studies of the future guide, its instruments and associated infrastructure have been performed. The engineering plans for this high-performance guide, covering factors such as instrument location, neutronic performance, have now been validated and a thorough assessment of the radioprotection, background and shielding requirements has been completed. The use of simulation tools in this way is an enormous aid in optimising the performance of new instruments while reducing the potential radioprotection and background issues on new and existing instrumentation.

The executive phases of these instrument and infrastructure renewal programmes, however, remain a significant challenge for the ILL and in particular for the Projects and Techniques Division. The success of the H24 and H15 projects depends on our ability to manage significant civil engineering works, followed by the alignment of approximately 500 metres of new neutron guides and instrument installation, and all in parallel with replacement of the H1-H2 beam tube and other important maintenance work on the reactor.

The new timeframe has given us the opportunity to review the ILL's project management framework and introduce 'resource-loading' and centralised co-ordination for all projects. The resources required are identified by project managers and interconnections between different projects identified at an earlier stage. This is a key aspect of our strategy for maintaining and modernising our highly efficient infrastructure. The DPT contributes its expertise in the state-of-the-art technology required for detectors, neutron guides, neutron optic components, sample environment equipment and innovative data acquisition and analysis, strongly supported by input from the Science Division.



The year 2019 saw good progress on the ILL's instrument upgrade programmes. This includes, for example, the start of commissioning of the new thermal time-of-flight spectrometer PANTHER and headway on the complex cryogenic work on SuperSUN, the ILL's future ultra-cold neutron source which should be ready for commissioning in 2020. A great many other projects continue in parallel, such as the construction of new detectors and innovative data acquisition and storage techniques. This work is crucial if the ILL's instruments are to continue to be of the highest standards. One of the Division's objectives is to develop technologies that are sufficiently flexible to adapt to a range of instrumentation. The prototype detector for XtremeD, for example, has now been adapted for the detector replacement projects on D16 and D20.

The Projects and Techniques Division also has an important part to play in the day-to-day running of our research facility. This covers everything from maintaining and upgrading the ILL's non-scientific software applications to the renovation and improvement of our buildings, roads and parkland. In 2019 the ILL launched its new Reinforcement of Physical Protection project, of which the DPT oversees the civil engineering component.

As new projects bring new expertise to the Division's already considerable store of experience, we have become a reference point in the field of neutron infrastructure. We feel it is important to share our experience with other centres, whether through European projects or through other initiatives such as LENS, for example, the new League of advanced European Neutron Sources.

Jérôme Estrade
Associate Director
Head of the Projects and Techniques Division

Endurance: Instrument Upgrade Programme

The pace of Endurance continues with the delivery and roll-out of new and upgraded instrumentation, capabilities and infrastructure. The scope of the programme has increased dramatically since 2016. In 2017 a grant from French national and regional funds allowed us to integrate additional projects as an extension to Endurance 1. With the tentative scope of a second phase of Endurance independently reviewed, endorsed by the Scientific Council and costed, the ILL associates began partial funding of Endurance 2 in 2019 and funding is now secured for the full programme up to 2023. The number of projects completed, in-progress and yet to be launched is considerable. A summary plus a brief description and the expected scientific gains of all Endurance projects is given in Table 1, while a roundup of some of the highlights during 2019 is given below. As depicted by the opening line of Charles Dickens' novel *A Tale of Two Cities*: 'It was the best of times, it was the worst of times'. In other words, all has not been straightforward in the roll-out of Endurance.

AUTHORS

C. Dewhurst and J. Estrade (ILL)

H1-H2: The two major guide infrastructure and instrument projects, **H24** and **H15**, both rely on critical changes to the reactor in-pile neutron guides as part of the **H1-H2** project. The original plan for a long H1-H2 shutdown between winter 2020 and autumn 2021 could not be maintained, principally due to fabrication difficulties and delays in the manufacturing of the H1-H2 beam tube. These problems have now been resolved, thanks to a two-pronged approach and risk mitigation strategy, but with the knock-on effect of a delayed H1-H2 shutdown now scheduled for summer 2021 to summer 2022. A new plan for key reactor works and the roll-out of Endurance has been established, reinforcing and respecting the ILL's priorities for delivering the highest quality science while securing the future of our neutron source. With this goal, and by incorporating critical parts of the Endurance 2 **H15** guide renewal project into the **H1-H2** shutdown, the new plan aims to have completed **H24** and associated instruments by summer 2022 and the roll-out of all major guide infrastructure and instrument projects by the end of 2023. This is a challenge for the ILL, but we are in the process of identifying and planning the critical resources required to achieve this target and the timely delivery of Endurance.

Endurance 1: The backbone of Endurance 1 is the 'Chartreuse' project, involving the renewal of the **H24** thermal neutron guide and the upgrade of the **D10+** single-crystal diffractometer and **IN13+** (CRG) backscattering spectrometer, as well as a new extreme-conditions powder and single-crystal diffractometer, **XtremeD** (CRG). All major instrument and guide components for the project are ready and awaiting installation during the **H1-H2** shutdown.

The new thermal TOF spectrometer, **PANTHER**, is close to completion. It will be ready for commissioning during the first cycle of 2020, following a six-month delay in obtaining authorisation for its installation from the nuclear safety authorities. The potential fire risk from the vast quantities (30 tonnes) of high-density polyethylene used in background-shielding the instrument has been mitigated, while a full evaluation and reduction of the total calorific load (combustible materials) within the reactor building has been made. **SuperSUN**, the new, intense source of ultra-cold neutrons, has still to begin commissioning but is close to completion. From a cryogenic point of view, **SuperSUN** is an extremely complicated assembly of cryogenic equipment containing a ^3He refrigerator, a converter cryostat and a UCN extraction system with state-of-the-art heat exchangers and super-leak





components. Supplying the considerable manpower required in the design, construction, mounting and commissioning of **SuperSUN** has fallen, for the most part, on the ILL's sample environment service members, who at the same time are responsible for providing sample environments for the user programme. The (second) most rapid (after **FIPPS**) project to be completed under Endurance 1 is the renewal of **H16** and its focusing guide for the **IN5** cold TOF spectrometer. Compared with the old instrument, the new 'high-*m*' and elliptically focusing guide delivers three times the neutron flux at the sample position at 2 Å. Importantly, it also extends the useful wavelength/energy range to much shorter wavelengths and higher energies, providing excellent complementarity with the capabilities of **PANTHER**. **D3** remains out of action because of a delay in receiving the replacement H4 beam tube. H4's replacement, scheduled for summer 2020, will allow the re-installation of the **D3** instrument and the commissioning of new area detector and polarisation components optimised for the study of hydrogenated liquid samples on **D3-Liquids**. **IN20** will also be upgraded during 2020, with the installation of a new double-focusing graphite monochromator, analyser and velocity selector. The upgraded **IN20** will offer a more intense and better focused monochromatic (energetic) beam with efficient, higher order wavelength suppression.

Endurance 2: A first selection of independent instrument projects was launched in 2019, in a first wave of Endurance 2 projects. **DALI**, a second Laue protein crystallography station, will provide additional capacity and capabilities compared with the existing LADI instrument, using a velocity selector for variable- and broad-band monochromatisation. Installation of **DALI** in the previous **IN11** position begins in spring 2020. The small- and wide-angle scattering instruments, **D11**, **D22** and **D16** all have new detectors in advanced stages of preparation. The additional new detector on **D22++** will offer an extremely wide dynamic *q*-range in a single measurement. This will save time in terms of instrument reconfiguration and allow access to the highest *q*'s, important for problems in biological and soft matter systems. The **D22++** detector

is due for installation and commissioning at the end of 2020. **D11** will also receive a new detector; the current smaller, limited count-rate and ageing detector will be replaced by a modern, multitube design maximising the area coverage within the detector tank. Users can expect a much improved dynamic *q*-range and considerably enhanced performance from the instrument by the end of 2021 (depending on instrument availability within the **H15** project). The cold neutron **D16** will receive its wide-angle (85 °) detector at the end of 2021. The new **D16** detector is based on the novel, trench multi-wire-proportional-counter technology developed for **XtremeD**. Again, the larger angular coverage and improved efficiency and performance promise exciting gains in instrument performance and capability in the future.

The 'Vercors' project will see the renewal of the cold neutron guide **H15** and the associated suite of upgraded instruments, **D7+**, **D11**, **T3** and **SHARP+** (CRG) as well as an additional CRG instrument **SAM** (SANS). Each instrument will receive its own high-performance and dedicated end-of-guide beam position. A re-scoping and simplification of this vast and complex project during 2019 was necessary to mitigate the risks associated with the complexity of the engineering, radioprotection concerns and to advance the project timeline for installation beginning during the **H1-H2** shutdown. During 2019 the **H15** guide project moved into the detailed design phase, with the first expanding 'trumpet' section of the guide having been ordered. All **H15** guide branches are expected to be ordered within the first half of 2020 while momentum on the instrument projects is ramped up.

As Dickens said, 'This is the epoch of belief'. With positive reinforcement words like 'Endurance', 'well-advanced' and 'momentum', the reader is encouraged to focus on the fantastic progress and capabilities being achieved by the Endurance programme. But Endurance requires stamina: it is a challenging programme and subject to a mixed bag of constraints, circumstances and fortunes, as described here. That said, we believe that the ILL is well-placed to deliver Endurance by 2023, enabling our users to deliver world-leading science into the 2030s.

MODERNISATION PROGRAMME AND INSTRUMENT UPGRADES

Table 1

Matrix of performance and capability gains by Endurance project

Instrument/ Project	Flux ϕ	Background Reduction	Detector $\Delta\Omega$	Measurement Range (q, E)	Reliability, Longevity	Capabilities, Features, Options	Status
Endurance 1 + CPER extension (2016–2018)							
PANTHER	x2	x10	x3	✓ (q,E)	✓	Multi- λ mode. Double-focusing monochromator. 2D Position sensitive detector. Unique, high-energy TOF spectroscopy.	Commissioning 2020
FIPPS 1 FIPPS 2.1	-	x1.5 (anti- Compton shields)	-	✓ (γ)		New instrument, new capability – prompt γ fission.	User operation since 2016
SuperSUN	x100	-	-	-		A source of ultra-cold neutrons with UCN density ~ x100 the previous record. PANEDM collaborative experiment to install on SuperSUN source for world-record measurements of the neutron electric dipole moment.	Commissioning (phase 1) 2020
Rainbows	x10	-	-	-	✓	Re-scoped from the original Endurance proposal. Renewed focusing guide to maximise ‘coherent summing’ method for specular reflectivity measurements.	User operation since 2019
H24	x4	✓	-	-	✓	Crucial infrastructure renewal of ageing (1972) thermal neutron guide. High-performance, modern, multiple-branch neutron guide. x4 capacity for end-of-guide, optimised, thermal-neutron instrumentation.	Awaiting H1-H2 installation
D10+	x5	-	x2	-	✓	Modernisation of this ageing workhorse instrument. x5 flux on the sample due to the new H24 guide and larger, modernised monochromators. x2 gain in detector efficiency with the new detector.	Awaiting H1-H2 installation
IN13+	x4	-	-	-	✓	Modernisation and re-siting of IN13 on to the new H24 guide. A new thermal gradient monochromator and deflector to allow IN13 to capitalise on the increased flux of the new H24 guide.	Awaiting H1-H2 installation
XtremeD	-	-	-	-		Spanish CRG powder and single-crystal diffractometer. Optimised for diffraction measurements under extreme conditions. Expected performance comparable with that of D20.	Awaiting H1-H2 installation
NESSÉ	-	-	-	-	✓	Stimulus and new capabilities in sample environment for neutron scattering measurements across all instruments and scientific domains. Improved reliability, faster sample environment, quicker turnaround, reduced beamtime losses.	Continuous delivery to 2020
BASTILLE	-	-	-	-	✓	Stimulus, new capabilities and maintenance of scientific software for data treatment and analysis. The ILL joins the international Mantid data treatment project.	Continuous delivery to 2019
IN5+ / H16	x3	✓	-	✓ (q,E)	✓	H16 guide & instrument focusing guide renewal. Access to shorter λ , higher E. Flagship instrument pushing the boundaries further.	User operation since 2019
D3-Liquids	-	-	x10	✓		Wide-angle detector for liquids studies. Polarisation and analysis for studies of hydrogenated liquids. A novel and important extension to D3’s capabilities.	Commissioning 2020
IN20- Upgrade 1	x2	✓	x10 (multiplex analyser)	✓ (q,E)		Higher order and background suppression. Improved flux and polarisation. Unrivalled thermal TAS spectroscopy.	Commissioning 2020–2021
Endurance 2.1 (2019)							
D11 Detector	-	-	x2	✓ ($\Delta q \times 1.5$)	✓	Large, modern, high count-rate detector. Workhorse instrument, necessary upgrade.	Delivery 2021
D22++ Detector	-	-	x10	✓ ($\Delta q \times 10$)	-	Second large, modern, high count-rate detector for extended q-range. Flagship instrument with cutting-edge science pushing the limits of SANS.	Delivery 2020

Instrument/ Project	Flux ϕ	Background Reduction	Detector $\Delta\Omega$	Measurement Range (q, E)	Reliability, Longevity	Capabilities, Features, Options	Status
Endurance 2.1 (2019) continued							
D16 Detector	-	-	x4.5	✓ (Δq x4.5)	✓	Modern, larger, high count-rate detector. Larger solid angle and dynamic q-range. Unique cold-neutron diffractometer.	Delivery 2021
DALI	-	-	-	-	-	x2 protein crystallography capacity. Higher resolution mode. Best in the world instrument. High-impact science.	Commissioning 2020
NeXT	✓	✓	✓	✓	✓	New capability and public neutron imaging instrument. State-of-the-art capabilities and ILL neutron flux for imaging promises a world leading instrument.	Delivery / Commissioning 2020–2022
Endurance 2.2 H15 (2020–2023)							
H15	x4	-			✓	Crucial infrastructure renewal of ageing (1972), low-performance, cold-neutron guide. High-performance, modern, multiple-branch neutron guide. x5 capacity for end-of-guide, optimised, cold-neutron instrumentation.	Requires H1-H2 renewal Delivery / Commissioning 2023
D11 collimation	x1.4	✓			✓	Flux gain due to new H15 guide. Replace unreliable, difficult to maintain, optically poor collimation. Remove parasitic scattering and reflections.	Requires H1-H2 renewal Delivery / Commissioning 2023
D7+	x20	✓			✓	Dedicated H15 end-of-guide position. Full renewal of primary spectrometer: monochromator optics, polarisation components. Massive improvement to D7, realising its full potential and making TOF spectroscopic studies realistic. Unique instrument with yet-to-be-unleashed capabilities.	Requires H1-H2 renewal Delivery / Commissioning 2023
SHARP+ (c.f. IN6)	x5	✓	x2	✓ (q,E)	✓	Renewal path IN6 \rightarrow Sharp (CRG) \rightarrow Sharp+ (CRG). High-performance, cold-neutron TOF spectrometer, comparable with IN5. Massive gains over existing IN6 with increased detector area, dedicated H15 end-of-guide position.	Requires H1-H2 renewal Delivery / Commissioning 2023
SAM (c.f. Paaxy LLB)	x5					New CRG SANS instrument. Additional capacity. MEIZE capability option. An LLB instrument with ILL flux.	Requires H1-H2 renewal Delivery / Commissioning 2023
Endurance 2.2 Independent Projects (2020–2023)							
FIPPS 2.2		x2 (definition of fission fragments)	✓	✓ (fission product mass)		New capability. Gas-Filled-Magnet (GFM) fission product mass spectrometer. Combine with existing γ spectrometer for precise fission fragment identification. Unique instrumentation.	Pre-project evaluation
D20c Detector					✓	Critical replacement of ageing detector. Workhorse, high-demand, impact instrument.	Pre-project evaluation
MARMOT (ThALES)			x25 (multiplex analyser)	✓ (q,E)		An optimised, multiplexed analyser detector for ThALES. Simultaneous multi-channel energy analysis over a wide angular range.	Pre-project evaluation
NESSÉ2					✓	Continued stimulus and new capabilities in sample environment for neutron scattering measurements across all instruments and scientific domains. Improved reliability, faster sample environment, quicker turnaround, reduced beamtime losses.	Sub-projects under evaluation
BASTILLE2					✓	Continued stimulus, new capabilities and maintenance of scientific software for data treatment and analysis	Launched Continuous delivery to 2023



Jacques Ollivier. French
The ILL

'As the person responsible for IN5, I have led several projects aimed at improving the performance of the instrument. My present scientific interests are frustrated magnetism, molecular magnetism, quantum liquids and solids, and water clathrates.'

The Endurance project IN5+: enhancing the potential of the IN5 spectrometer

Two important projects have been completed over the past 12 months around the IN5 instrument. On the one hand, as part of the Endurance upgrade programme the guide delivering neutrons to the instrument has been almost entirely refurbished, increasing the flux at the sample by an average factor of three. On the other, a 10-Tesla vertical field magnet has been commissioned and is now in use for regular experiments.

Figure 1

Roland Gandelli and Julien Bonnevaux installing and aligning the last guide pieces between the choppers and the sample chamber.



AUTHORS

J. Ollivier, B. Giroud and M.M. Koza (ILL)

REFERENCES

- [1] J. Ollivier, M. Plazanet, H. Schober and J.C. Cook, *Physica B* 350 (2004) 173
- [2] J. Ollivier and H. Mutka, *J. Phys. Soc. Jpn.* 80 (2011) SB003
- [3] J. Ollivier, B. Giroud, M. Kreuz, E. Farhi, J. Beaucour and C. Dewhurst, *J. Neutr. Res.* 20 (2018) 123

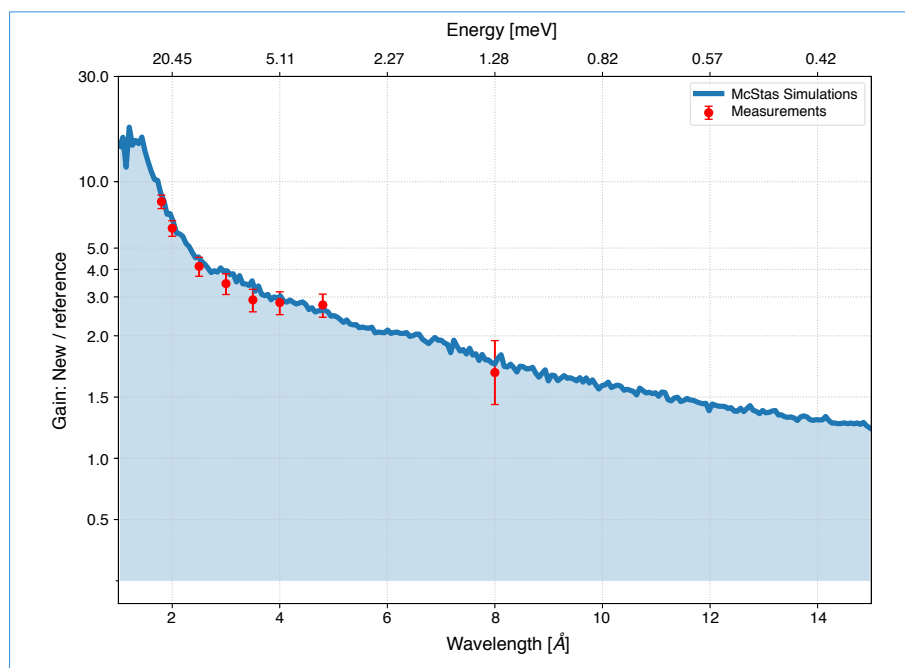
The IN5 instrument has undergone regular improvements over the years, approximately once every ten years. However, the neutron guide that transports neutrons to the instrument has never been completely renewed in any of these upgrades. The focus of the various projects has always been downstream, on the instrument itself: sample environment, choppers and instrument focusing guide, detectors and flight chamber [1, 2].

Amongst these projects, a refurbishment of the last straight 15 m guide was undertaken in 2000-2002, within the framework of the Upgrade of Five Instruments projects, together with the introduction of a new chopper system for monochromatising the beam. It was decided at that time to benefit from the full upstream (width x height) 30 x 200 mm² guide cross section and focus on a 15 x 50 mm² area at the sample position, using a tapered, supermirror-coated guide with coatings ranging from $M = 1$ to $M = 3$ in the high-focus section. At the time they were installed, the guide and its coatings were at the cutting-edge of technology. Since then, however, only the first section of the guide—close to the reactor core and in the light water pool—has been upgraded, with an $M = 2$ coating, performed during the ten-yearly beam tube refurbishment operation in 2006. The resulting gain in neutron transport was annihilated, however, because the curved guide section situated between the new section and the instrument guide was left unchanged.

New guide

More recently it was decided, within the framework of the Endurance programme, to take the opportunity presented by the next ten-year refurbishment of the H1 beam tube to replace this heterogeneous, state-of-the-art, ballistic guide. The challenge was to renew the guide while retaining most of the components of the existing IN5 instrument, particularly the chopper system, and without moving the time-of-flight chamber. The aim, apart from limiting costs, was to get the guide installed early in the life of the Endurance programme and minimise downtime for the in-high-demand IN5 (**figure 1**).

Despite the constraints, refurbishment of the guide has brought a substantial although finite gain in neutron flux; in particular, it now favours warmer neutrons, which were previously disadvantaged by the natural nickel, curved guide (**figure 2**). Computed optimisation resulted in an $M = 2$ to $M = 6$ supermirror-coated elliptic guide with reduced height (150 mm) in the straight section following the curved guide section [3]. As the aim was to focus on sample heights of below 30 mm, such a highly focusing guide

**Figure 2**

Flux gains: simulations (blue), measurements (red dots).

cannot benefit from the original 200 mm height as losses are significant in the vertical direction. The expected wavelength-dependent gain (an average gain factor of around three) has been confirmed by measurements (**figure 2**). A more surprising consequence of the perfectly aligned new guide is the transport of high-energy neutrons in the beam. These were scarcely present before, and extra shielding has had to be installed to reduce their impact on the spectrum background.

Sample environment

It quickly became clear, after the first experiments on single crystals on IN5, that a high-field magnet would boost the study of magnetic materials. This was not new; such equipment exists on time-of-flight instruments at other neutrons centres. A design by Cryogenics Inc. (London, UK) was chosen, featuring a large, horizontal, angular opening (almost 100 degrees horizontally and 30 degrees vertically) and a high maximum field (10 T). The magnet was ordered in 2015 but only became ready for use on the instrument at the beginning of 2019. Work was performed in the meantime to remove any magnetisable elements close to the sample area, such as the choppers' steel base plates. Commissioning of the magnet with choppers in rotation (**figure 3**) revealed the need to reinforce the magnetic shielding against stray fields incompatible with the rotating aluminium disks. The shielding, made of Telar-57 soft iron, was calculated, designed and installed in-house.

The magnet was commissioned just before the first reactor cycle in 2019 and first used for regular experiments up to the maximum field of 10 T in July 2019. More experiments have now been scheduled for the next reactor cycles.

Neither of these projects would have been possible without the commitment of many inside and outside the ILL. They deserve to be warmly thanked for their contributions.

**Figure 3**

Magnet during commissioning in May 2019: **upper left**) the magnet in place on IN5; **upper right**) logbook and choppers monitoring; **lower right**) Cryogenics power supply showing the achieved field (9.995 T~ 10 T).



Christian Tötze. German
Institute for Environmental Science and
Geography, University of Potsdam
*'Fast neutron tomography is a unique tool for
analysing the dynamic transfer of liquids in
porous material systems, time-resolved and in
three dimensions.'*

Record-fast neutron tomography tracks water pathways into plants

Neutron tomography is ideally suited to visualising plant root systems and the 3D water distribution in the surrounding soil. However, until now the major limitation for 3D imaging of dynamic water transfer in root-soil systems has been insufficient acquisition speeds. We used the high neutron flux available at the tomography station NeXT to dramatically speed up the acquisition time for fast neutron tomography. We succeeded in acquiring full tomographies (155 projections over 180 °) with a physical spatial resolution of 200 µm within 1.5 s. This is about 6.7 times faster than the current record for high-speed acquisition. We used the technique to investigate water infiltration in soil using a living lupine root system. The fast-imaging set-up will be part of the future instrument NeXT at the ILL in Grenoble and will offer a vast array of possible future applications.

AUTHORS

Ch. Tötze (University of Potsdam, Germany)
A. Tengattini (ILL)

REFERENCES

- [1] A.G. Bengough, *Vadose Zone J.* 11 (2012)
- [2] N. Kardjilov, I. Manke, R. Woracek, A. Hilger and J. Banhart, *Mater. Today* (2018)
- [3] C. Tötze, N. Kardjilov, I. Manke and S.E. Oswald, *Sci. Rep.* 7 (2017) 6192
- [4] C. Tötze *et al.*, *Opt. Express* 27 (2019) 28640

How plants take up water and nutrients from soil depends largely on the transport properties of the soil next to the roots, an area known as the rhizosphere. Intense root-soil interactions modify the structural and biochemical properties of the soil in this area, which in turn affects the transfer of water and nutrients into the roots [1]. Neutron imaging is an ideal approach for studying hydraulic transfer in soil because it provides an excellent contrast between the water and soil matrices. Neutrons can also distinguish hydrogen isotopes and their compounds. For example, while normal water, H₂O, and heavy water, ²H₂O, are physically and chemically very similar, there is an order of magnitude difference in attenuation between them, making heavy water an ideal contrast agent to normal water [2]. However, the normally relatively slow acquisition speed of neutron imaging made it challenging to use for time-resolved 3D studies of fast processes such as water infiltration of soil and root water uptake. Recent technological improvements to neutron imaging stations have opened up new avenues for the 3D imaging of fast processes at high spatiotemporal resolution [3]. Since NeXT has the most intense cold neutron flux for imaging purposes in the world, it offers extraordinary conditions for high-speed neutron tomography. We used this approach to analyse the imbibition of water in root-soil systems after the injection of deuterated water.

Figure 1 illustrates the principle of the set-up used for the water infiltration experiment. The lupine plant placed in front of the scintillator rotated at a constant speed of 0.33 rps while the sCMOS camera recorded radiographic projection images at high speed.

Figure 2 shows a time series of tomograms after the injection of 4 ml of deuterated water at the bottom of the plant container. As the D₂O invades the soil pores it displaces the light water (H₂O) present, which consequently forms a water front that moves upwards in the soil column. At 90 s after injection the front comes to a halt, stopped by a hydraulic barrier, *i.e.* a layer of coarse sand installed halfway up the soil column.

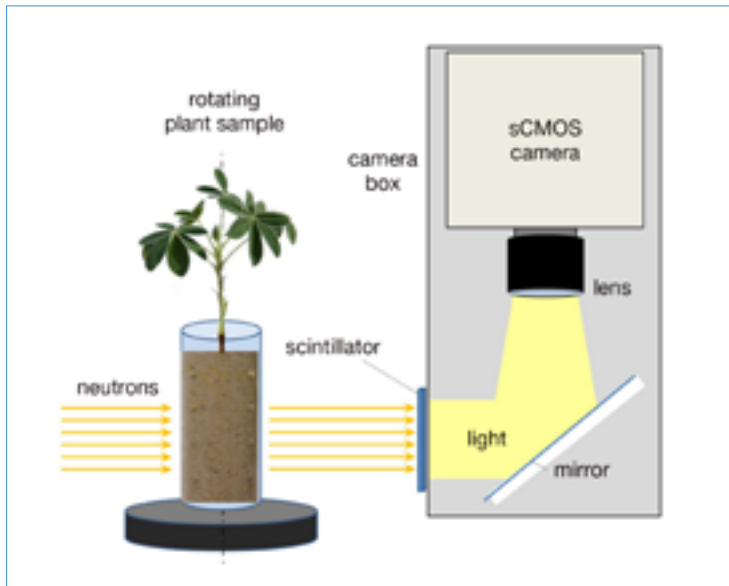


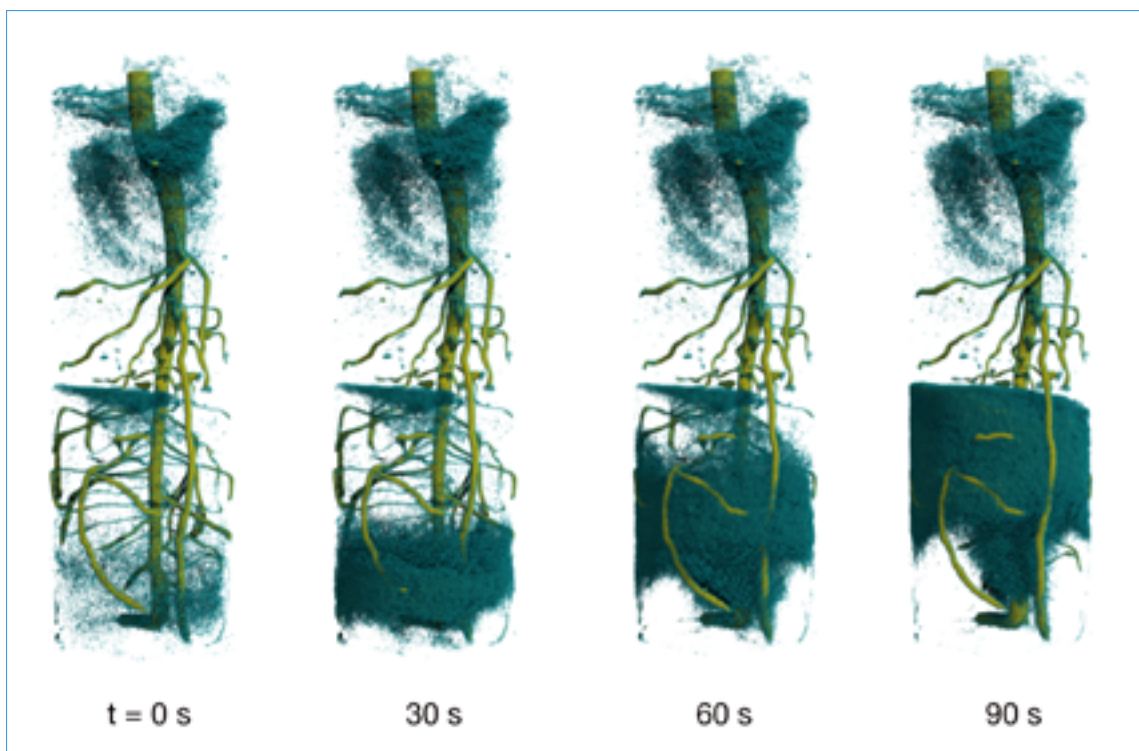
Figure 1

Scheme of the experimental setup. The potted lupine plant mounted on the sample manipulation stage rotates in front of the neutron detector at a constant speed of 0.33 rps. Adapted from [4].

In our pilot study, we demonstrated the feasibility of studying dynamic water transfer in root-soil systems by high-speed neutron tomography. With a 1.5 s acquisition time per tomogram, we have set a new benchmark for time-resolved neutron tomography. This record demonstrates most impressively the potential of the instrument NeXT, pointing to many further applications in the fields of soil, materials and geosciences.

Figure 2

Time series of neutron tomograms, showing the rise of water in a soil column with a living lupine root system after injection of deuterated water through the bottom. Time resolution is 3 s per tomogram. Adapted from [4].



H16 guide renewal: a successful project to boost performance levels on IN5

Thanks to the ILL's efficient project management system, the project to overhaul the guide H16, which delivers neutrons to IN5, has been completed ahead of time and under budget, and has successfully achieved the targeted average gain of a factor of three on the flux.

Figure 1

H16 casemate and its guide during the replacement work.



AUTHORS

J. Beaucour, J. Bonnevaux, P. Cogo, E. Courraud, L. Didier, C. Dewhurst, R. Gandelli, Y. Gibert, B. Giroud, J. Halbwachs, B. Jary, P. Lachaume, C. Monon, M. Kreuz, J. Ollivier and F. Rencurel (ILL)

REFERENCES

- [1] Project team: J. Beaucour, J. Bonnevaux, P. Cogo, E. Courraud, L. Didier, Ch. Dewhurst, R. Gandelli, Y. Gibert, B. Giroud, J. Halbwachs, B. Jary, P. Lachaume, C. Monon, M. Kreuz, J. Ollivier, F. Rencurel
- [2] 'The Endurance project IN5+: enhancing the potential of the IN5 spectrometer', ILL Annual Report (2019) p. 78

IN5 is installed in the guide hall ILL7 at the end of the 45-metre long, curved cold guide H16. The guide's main section (21 m long) was an obsolete $M = 1$ borkron guide installed in 1972. It was decided, in September 2017, to launch the execution phase of the 'H16 guide renewal' project ahead of the upcoming replacement of the H16 in-pile section, as part of the H1-H2 renewal project.

A dedicated project team was appointed, headed by B. Giroud as Technical Project Leader and with scientific support from J. Ollivier as Initiator Project Leader, in compliance with the ILL's project management guidelines [1]. The design phase started in parallel with work to optimise neutron transport, with the aim of achieving a flux gain of a factor of three. The guide was optimised [2] in order to obtain the highest flux at the maximum divergence measurable by the geometry of IN5's detection system and for a reduced sample size (30 x 15 mm²). Only 75 % of the upstream guide section (200 mm x 30 mm) was necessary for this maximum useable flux on IN5, leaving 25 % of the guide section available for a possible upgrade.

The design phase was carried out between May and October 2017. The decision to issue the call for tenders as early as June proved to be good forward planning, since it allowed us to order the guide in December and receive all the parts and most of the guide components by July 2018. This in turn made it possible to prepare installation of the guide during the winter shutdown. Unfortunately, on certain guide components the supermirror coating proved to be unstable, requiring the manufacturer to replace the most deteriorated parts between July and November 2018 in order to be ready for the installation phase. The manufacturer has undertaken to replace the final deteriorated parts in time for the long H1-H2 shutdown.

The guide installation and alignment phase started in early November 2018 during the winter shutdown and was successfully completed within the 10 weeks scheduled, thanks to the very efficient co-operation of all the teams involved. A four-week break in the installation work was necessary, however, to deal with the delamination issue with the manufacturer. Nevertheless, by the end of February 2019 the installation work was completed, ready for the restart of IN5 during the first reactor cycle of 2019.

The overall project lasted 16 months, from the start of the execution phase to commissioning, making it probably one of the fastest guide projects ever carried out at the ILL. On the budgetary side, it is worth noting that the final cost of the project for procurement and studies (820 k€) came in below the allocated budget as estimated at the end of the feasibility phase (900 k€).

During commissioning a background of high-energy neutrons was detected, transmitted, it transpired, by garland reflexion due to the high quality of the guide alignment. This could be corrected without affecting the flux gains by adding a 1 mm borated mask to the external lateral side of the guide. In the end, the anticipated average gain factor of three was achieved, along with an even higher gain for 1.5 Å neutrons not transported by the old $M = 1$ guide.

FIND US ON:   **Péter Falus**, Hungarian
The ILL

'I am an instrument scientist at the ILL. My main area of interest is improving spectroscopy instruments for soft matter studies. I have worked at the X-ray Photon Correlation Spectroscopy beamline at the

Advanced Photon Source and I participated in the upgrade of the IN15 neutron Spin-Echo Spectrometer. I have been the scientific project leader of the WASP instrument since 2013.'

WASP takes off

The first neutron spin-echo instrument, IN11, was built at the ILL and was in operation for 40 years. After all those years of exciting science, the moment has come to turn the page and welcome the newest spin-echo instrument: WASP. The new instrument has just begun commissioning but already surpasses IN11 in both intensity and the highest available resolution. In 2020, WASP will take over from IN11 and will complement the high-resolution spin-echo instrument IN15 for wide-angle measurements.

Neutron Spin-Echo (NSE) reveals atomic motions by encoding the neutron energy into the number of rotations of the neutron spin. Since the number of spin rotations depends on the strength of the magnetic field, the secret to a good NSE instrument is creating symmetric magnetic fields (so-called 'precession fields') before and after the sample.

All functioning, non-resonant NSE spectrometers use the basic IN11A design, where the precession field is generated by long solenoids along the neutron beam. This construction—while it gives high resolution—limits the angular coverage and count rate of the instruments.

About 20 years ago, the IN11 set-up was upgraded to make a wide-angle coverage, neutron spin-echo instrument, IN11C [1], equipped with a flattened solenoid. It has a 30 degree-wide angular coverage but limited range in spin-echo time. This instrument was practically trading intensity for resolution, but was a very successful compromise at the time. The SPAN instrument [2] at HZB extended the angular coverage even further. A pair of coils in the anti-Helmholtz configuration created an azimuthally symmetric magnetic field, which in theory could allow almost 360-degree detector coverage.

The newly commissioned WASP uses an improved SPAN construction [3]. It aims to have a detected intensity 500 times higher than that of IN11A while the resolution remains the same. Compared with IN11C, WASP aims to have 25 times the intensity and six times the resolution.

AUTHORS

O. Czakkel, P. Falus, B. Faragó and P. Fouquet (ILL)

REFERENCES

- [1] B. Farago, *Physica B* 241–243 (1998) 113
- [2] C. Pappas *et al.*, *Physica B* 267–268 (1999) 285
- [3] P. Fouquet *et al.*, *J. Neutron Res.* 15 (2007) 39

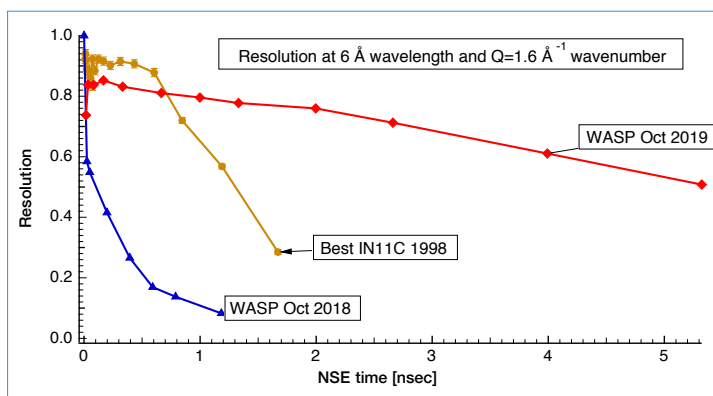


Figure 1

Resolution functions versus spin-echo time. The longer the function time, the higher the instrument resolution. The red WASP curve clearly surpasses the yellow best resolution of IN11C.

Construction of the instrument was completed in October 2018, and during 2019 the commissioning and alignment continued to achieve echo signals in all three 30-degree-wide detector banks. The three banks are motorised, covering the -60 to +135 degree scattering angle range. At a 6 Å wavelength on the same sample a single WASP detector bank has eight times the IN11C count rate, while 25 times higher intensity can be achieved using all three banks. In the future, more banks will cover the whole angular range without having to move the detectors. In the medium term, a chopper system will run the instrument with pulsed neutrons simulating capabilities at ESS or SNS. The paramagnetic echo option has just been installed and the range of wavelengths and sample environments available will gradually be expanded.

Before any NSE measurement, a resolution function is measured on a non-moving reference. Ideally, this resolution has a constant value of unity as a function of time. Imperfections in the instrument will make this resolution function drop for higher spin-echo times. The higher the spin-echo times that we can reach without the resolution dropping to zero, the better the instrument's energy resolution. **Figure 1** plots the resolutions of IN11C and WASP before and after tuning at a 6 Å wavelength, respectively, showing WASP to surpass IN11C in both intensity and resolution.

In conclusion, the new instrument WASP bridges the gap between high-resolution spin-echo and backscattering instruments. It offers a similar wave number range to that achieved through backscattering, and slightly higher resolution. It also complements backscattering by measuring $S(Q,t)$ in the time space, not $S(Q,w)$ in the energy space. At the other end of the spectrum, WASP and IN15 will complement each other too. The lowest WASP Q-values will slightly overlap with the highest IN15 Q-values, and the WASP NSE times at the longest wavelengths will be just about the same as the IN15 NSE times at the shortest wavelengths.

WASP is ready to welcome all users who need better resolution than backscattering can achieve, or wider q-range than classical spin-echo can achieve.



Judith Peters. German
Université Grenoble Alpes, LiPhy, and the ILL
'I hold a professorship in Physics at the Université Grenoble Alpes and am co-responsible for the IN13 backscattering spectrometer at the ILL. My research interests include dynamical studies of bio-systems under high-pressure conditions and, in particular, the adaptation mechanisms of lipids, proteins and cells to such harsh environments.'

High-pressure cells and sticks for investigating systems in solution and membrane layers

The number of publications listed in the Web of Science about experiments under high hydrostatic pressure has increased by 50 % over the last ten years, as has the number of pressure experiments performed at the ILL. This shows the scientific community's increasing interest in this area and the need for suitable equipment. The new high-pressure cells and sticks available for interested users on many of the ILL's instruments have been developed in collaboration with the ILL's Service for Advanced Neutron Environments (SANE).

AUTHORS

J. Peters (UGA, Grenoble, France)
E. Lelièvre-Berna (ILL)

ARTICLE FROM

J. Neutron Res. 19 (2017) —doi: DOI 10.3233/JNR-170044
and J. Neutron Res. 20 (2018)—doi: DOI 10.3233/JNR-180055

REFERENCES

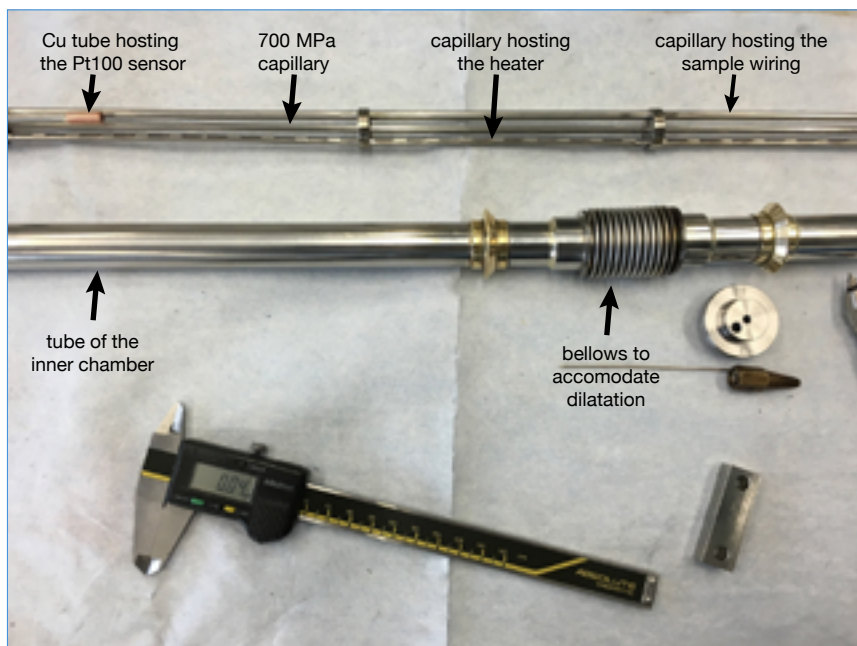
- [1] F. Meersman *et al.*, *Rev. Mineral. Geochem.* 75 (2013) 607
- [2] R.E. Collins, G. Rocap and J.W. Deming, *Env. Microbiol.* 12 (2010) 1828
- [3] K. Takai *et al.*, *Proc. Nat. Acad. Sc.* 105 (2008) 10949
- [4] A.A. Yayanos, *Proc. Nat. Acad. Sc.* 83 (1986) 9542

The pressures required for investigating biological systems in solution or membranes are relatively low compared with those required in other scientific domains, as biomolecules are very sensitive to pressure and can undergo unfolding in the range of 400 MPa to 1 GPa (100 MPa = 1 kbar) [1]. However, the range of physico-chemical conditions under which microbial life has been observed is expanding, including metabolic activity at $-40\text{ }^{\circ}\text{C}$ [2], cell proliferation at $122\text{ }^{\circ}\text{C}$ [3] and bacteria surviving at 130 MPa [4]. Deep sea hydrothermal vents present one of the most fascinating biotopes on the planet and have been suggested as places where life could have originated. They correspond to extreme conditions in more than one respect: strong temperature gradients prevail, combined with high pressures and salinity. In order to shed more light on how life developed, there is a need to reproduce such conditions in laboratories. It was in this context that new high-pressure equipment has been developed recently at the ILL.

High-pressure sample sticks have to fulfil specific functions, such as protecting the fluids that transmit the hydrostatic pressure to the sample in the cell from freezing. As the sticks are often used in a cryostat or cryofurnace, a cold point can develop close to the central high-pressure capillary. We have designed a stick with a capillary that is thermally isolated from the cryogen bath and heated to a desired temperature (**figure 1**). The maximum pressure able to be applied remotely to the sample through this stick is 700 MPa, while the sample temperature can be controlled from 1.8 to 550 K. Moreover, the ILL has recently purchased two high-pressure regulators that automatically control and adjust the pressure levels and continuously record the pressure in NOMAD data files. The equipment has been successfully tested on a number of different instruments with the adequate infrastructure (IN13, IN6, IN5, IN16B and D16). These sample sticks are available with 50 mm and 70 mm diameters and can be booked for experiments.

Figure 1

Photo taken during the assembly of a sample stick. The bellows are welded to the inner tube and the capillaries are assembled together before insertion.



The high-pressure cells used for neutron experiments have to withstand huge forces without absorbing too many neutrons. We have therefore also designed and produced several high-pressure cells using different materials. These include the titanium null-matrix alloy (Ti) and zirconium (Zr), which provide a total coherent scattering length equal to zero; and the fully hardened CuBe2 alloy, which can be employed at temperatures of up to 300 °C for pressures lower than 700 MPa (**figure 2**). These cells can be combined with Al inserts equipped with rectangular slits. These in turn can host lipid membrane layers deposited on silicon wafers to model biological membranes, for instance. The wafers are surrounded by water and thus protected from breakage, permitting *in situ* studies of membrane layers under high pressure and high temperature conditions.

Acknowledgments

We gratefully acknowledge the CNRS – Défi Instrumentation aux limites 2014 – for financing the development of the high-pressure cell.

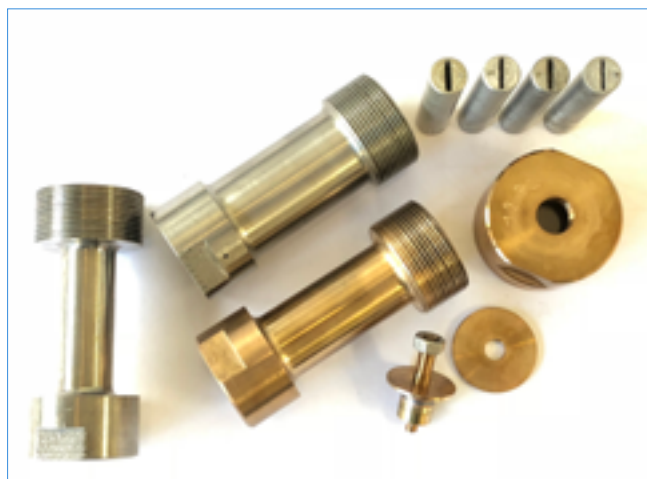


Figure 2

Photo of the 250 and 600 MPa TiZr cells, the 700 MPa CuBe2 cell, Al inserts and sealing components.



Bruno Démé. French and German
Institut Laue Langevin, Grenoble, France
 'I am a scientist in the Large Scale Structures (LSS) group and I'm responsible for the D16 instrument. I'm interested in model and biological membranes, with a focus on membrane interactions in oriented lipid multilayers.'

Ultimate humidity chambers for neutron diffraction

High-resolution diffractometer with variable vertical focusing D16 instrument

The characteristics and behaviours of biological or soft-matter samples investigated in neutron scattering experiments are strongly coupled to the temperature and relative humidity of the surroundings. Accurate observation and control of these parameters is crucial to the success of such experiments, as is control of thermodynamical parameters such as the osmotic pressure of samples in equilibrium with humid air. We, along with colleagues from Helmholtz-Zentrum Berlin (HZB), have therefore designed a precision humidity chamber for neutron diffraction that allows a 20 mm x 60 mm² sample to be maintained at temperatures ranging from ambient to 80 °C in a relative humidity of between 20 % to 100 %.

AUTHORS

B. Demé, O. Aguetaz, S. Baudoin, N. Belkhier, E. Bourgeat-Lami, J. Gonthier and E. Lelièvre-Berna (ILL)

ARTICLE FROM

J. Neutron Res. (2019)—doi: 10.3233/JNR-190109

REFERENCES

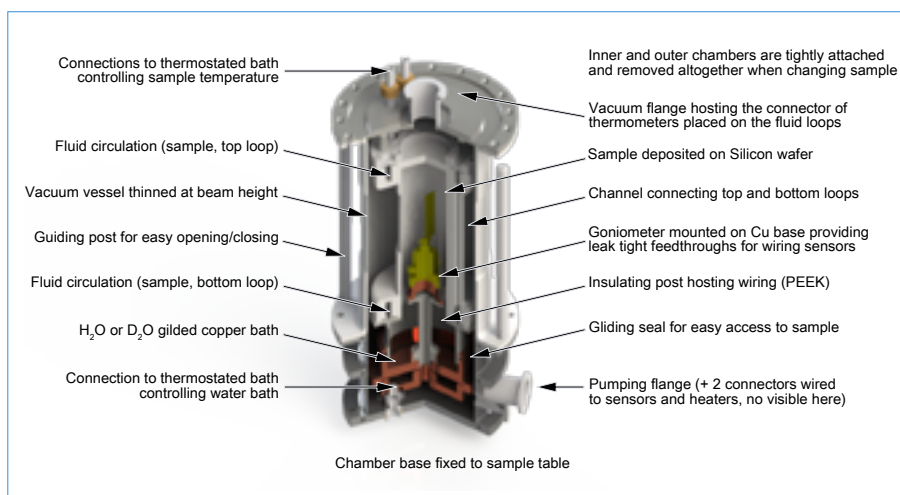
- [1] A. Carotenuto and M. Dell'Isola, *Int. J. Thermophys.* 17 (1996) 1423
- [2] M. Kanduc *et al.*, *Nat. Commun.* 8 (2017) 1
- [3] N. Kucerka *et al.*, *Biophys. J.* 88 (2005) 2626
- [4] G.S. Smith *et al.*, *Phys. Rev. Lett.* 60 (1988) 813

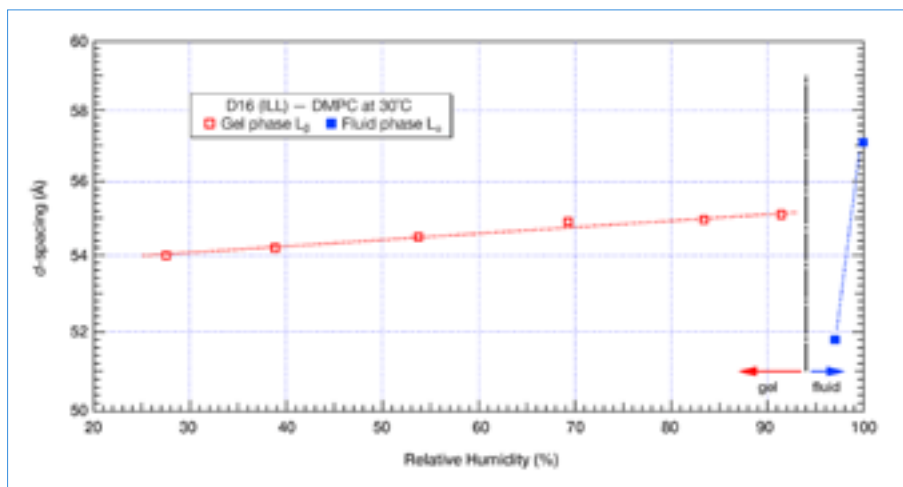
Biological systems are generally warm and moist, if not directly in contact with liquid water. We can get insights into their behaviour *in situ* only by creating experimental conditions that closely match their natural conditions. In recent years, efforts have been made to produce humidity chambers using techniques such as saturated salt solutions [1], saturated/dry gas flow and partial vapour pressure through temperature regulation of a water reservoir [2]. However, because of the unreliability of humidity sensors and the presence of thermal gradients resulting in undesired condensation, these systems have been restrictive or finicky. In particular, it has been difficult to achieve relative humidities above 95 %, this near-saturation regime being of special interest to the field of biological sciences.

We therefore decided to create relative humidity using a water reservoir (H₂O, D₂O, or a mix of both) regulated at a temperature deduced from Antoine's equation. The sample space and the water reservoir are decoupled from the experimental environment by a double-wall geometry allowing the sample space to be vacuum-insulated. The dimensions were optimised in an iterative process to determine the geometry, resulting in the most stable, thermal gradient-free design. Each step in this iterative design process was scrutinised using finite element simulations of thermal equilibrium and convection.

Figure 1

CAD design of the humidity chamber. The temperature of the water bath is controlled by a thermostated bath connected to the base of the chamber. The sample, mounted on a goniometer insulated from the water bath, is thermalised with a second thermostated bath connected to the top of the chamber.



**Figure 2**

The d -spacings of DMPC measured by neutron diffraction at 30 °C from 27.5 % to 99.9 % relative humidity. The open markers correspond to the gel phase L_{β} , the filled ones to the fluid phase L_{α} .

The final design, shown in **figure 1**, allows the control of relative humidity of up to 99.9 % with an accuracy of ± 0.05 % RH. The lower part of the humidity chamber, which is fixed to the D16 sample table, contains the water bath and several access ports for evacuating the chamber, reading sensors and heating the base of the goniometer. The water is poured in a gold-plated copper bath decoupled thermally from the sample space. The upper part controls the sample temperature and is removable to provide quick access to the sample.

In order to quantify the absolute precision of the humidity chamber, we measured the d -spacing of a lipid standard DMPC (1,2-dimyristoyl-sn-glycero-3-phosphocholine) and DOPC (1,2-dioleoyl-sn-glycero-3-phosphocholine) on the neutron diffractometers D16 (ILL) and V1 (HZB), at various temperatures and relative humidities. The final test consisted of measuring the d -spacing at the highest possible relative humidity. We tuned the chamber to 100 % RH and stored the cell apart for one day until we remeasured the d -spacing on D16. We fitted a d -spacing

of 57.1 Å, which corresponds to a relative humidity of 99.9 % according to [3]. The d -spacings of DMPC measured from 27.5 % to 99.9 % RH are presented in **figure 2** and follow the phase diagram published in [4].

Three identical chambers are available at the ILL on D16 allowing samples to be measured after short or long off-line equilibration times, thereby saving precious neutron beamtime. Sample alignment can be performed off-line thanks to a dedicated optical bench equipped with a laser. The equilibration of samples can be started anytime during or before an experiment, with no need to access the instrument area or the neutron beam.

Acknowledgements

The authors thank the technical staff at Helmholtz-Zentrum Berlin, and the DFG for financial support. This project received funding from the European Union's 7th Framework Programme for research, technological development and demonstration under the NMI3-II Grant number 283883.

**Figure 3**

The D16 instrument.



Fabienne Duc. French

High Magnetic Field National Laboratory of Toulouse, France

'I am a CNRS scientist actively involved since 2006 in projects combining high-pulsed magnetic fields with X-ray and neutron scattering techniques. In particular, I am

responsible for the 30 T and 40 T pulsed-field generators used, respectively, for X-ray absorption spectroscopy measurements and neutron diffraction; and for assisting synchrotron and neutron users in their experiments. My research interests are magnetic field-induced phases in strongly correlated electron systems (magnetic quantum spin systems and heavy fermions).'

40 Tesla pulsed-field cryomagnet for single-crystal neutron diffraction

The CEA-Grenoble, the LNCMI-Toulouse and the ILL have together developed a 40 T pulsed-field cryomagnet for neutron diffraction, featuring an unprecedented duty cycle of 28 sec per day at 30 T and 16 sec per day at 40 T. The sample temperature can be regulated at between 2 and 300 K, independently of the generation of the pulsed fields. The magnet can be made available to users within the framework of a collaboration between the CEA-Grenoble (which runs the CRG triple-axis IN22 instrument at the ILL) and the LNCMI-Toulouse, which produced the coil and its 1.15 MJ mobile generator.

AUTHORS

F. Duc (High Magnetic Field National Laboratory of Toulouse, France)

F. Bourdarot (ILL and CEA Grenoble, France)

E. Lelièvre-Berna (ILL)

ARTICLE FROM

Rev. Sci. Instrum. (2018)—doi: <https://doi.org/10.1063/1.5028487>

REFERENCES

- [1] F. Duc, X. Fabrèges, T. Roth *et al.*, Rev. Sci. Instrum. 85 (2014) 053905
- [2] W. Knafo, F. Duc, F. Bourdarot *et al.*, Nat. Commun. 7 (2016) 13075

In order to perform experiments in static fields greatly exceeding 15 T (vertical field) or 17 T (horizontal field), the CEA-Grenoble, the LNCMI-Toulouse and the ILL have designed and constructed the first long-duration and high duty-cycle pulsed-field cryomagnet producing a maximum horizontal field of 40 T for neutron diffraction. Compared with preceding systems, this magnet offers a much increased pulse duration and higher angular access in the scattering plane, thanks to conical openings of $\pm 15^\circ$ and $\pm 30^\circ$ upstream and downstream of the sample.

The coil, designed and built by the LNCMI-Toulouse, possesses a rapid-cooling technique by which liquid nitrogen cooling channels are directly inserted into the winding. To ensure high mechanical strengths, CuAg wire reinforced with Zylon was wound onto a coil body of glass fibre-epoxy composite (G10), which was itself placed around a highly non-magnetic, 1 mm-thick, double-cone of AISI 304L stainless steel. Using the 1.15 MJ transportable power supply developed at the LNCMI-Toulouse [1], the coil produces a maximum pulsed field of 40 T, with a rise time of 23 ms and a total duration of more than 100 ms every 9 min. The time between pulses is reduced at lower fields: every 7 min and 5 min, at 36 T and 31 T, respectively.

The coil is installed horizontally inside a cryostat developed by the ILL. A large, centrally placed, liquid nitrogen bath surrounded by a liquid helium jacket ensures that the coil can easily be replaced and cooled (**figure 1**). The initial cool-down time is 2.5 hours. The main current leads are fixed on one side of the coil, the heat exchanger on the opposite side along the upper surface of the cone onto which the coil is wound (scattered beam side). To avoid eddy currents and minimise the neutron background, the heat exchanger is made of Tordon and sapphire (**figure 2**). The sample is glued onto a holder also made from single crystalline sapphire and introduced into the heat exchanger. The maximum sample volume available is $8 \times 6 \times 6 \text{ mm}^3$ and the cool-down time to 2 K does not exceed 30 min.

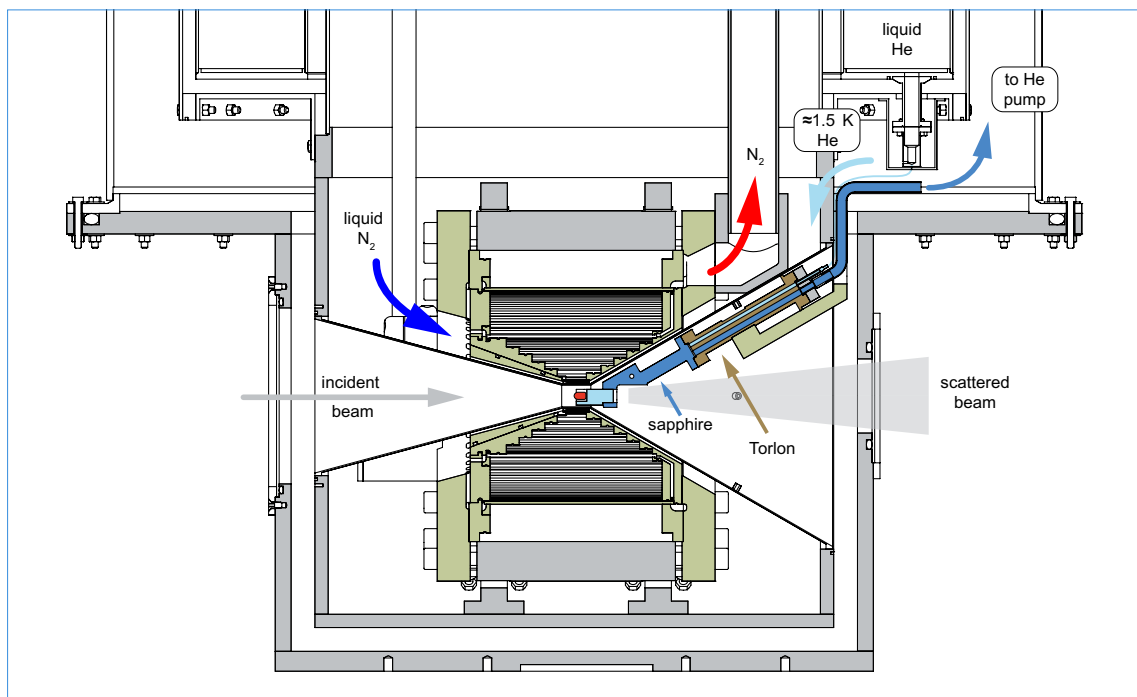


Figure 1

Overview of the tail of the 40 T cryomagnet. The coil is immersed in liquid nitrogen and the sample is fixed to the end of a cold finger made of sapphire.

The cryomagnet is used on the IN22 three-axis spectrometer in the elastic mode with no modification to the spectrometer required. The sample is usually oriented with a crystallographic axis parallel or slightly misaligned to the horizontal magnetic field, to reach the most interesting part of the reciprocal space. Neutron pulses are recorded with a digital data recorder measuring the generator voltage and current and the voltage on the pick-up coil. After correction for the neutron time of flight, the field dependence of the neutron intensities at each momentum transfer is extracted by summing the data accumulated over a few identical pulsed-field shots, with either constant time- or constant field-integration windows.

Several experiments have already been carried out successfully [2], and experience shows that about 40 pulses are sufficient to measure variation in the intensity of a Bragg peak with a field of up to 40 T, *i.e.* about 6 hours, providing that $V[\text{mm}^3] \times (m[\mu_B/\text{at}]/v_0[\text{\AA}^3])^2 > 3.2 \times 10^{-4}$, with V the sample volume and m and v_0 , respectively, the moment and volume of the unit cell.

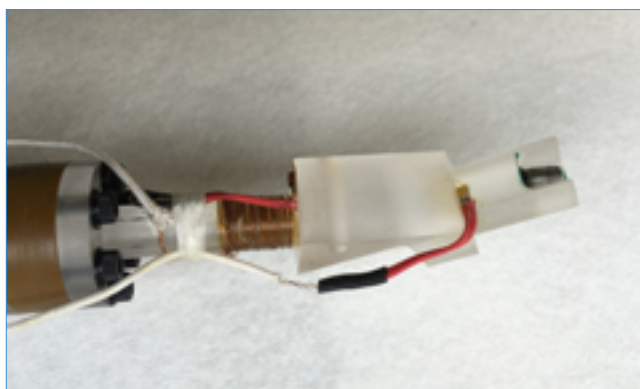


Figure 2

Photo of a sample glued onto the end of the sapphire holder. The thermal expansion of He is performed at the end of the brown Torlon tube in which helium circulates, against the flange of the sapphire sample-holder.

INDUSTRIAL ACTIVITIES

The ILL provides industrial users with access to state-of the art neutron instrumentation and the expertise of its scientific and technical staff. The Industry Liaison Unit (ILU) is the focal point of industrial activities at the ILL. The objective of the Unit is to bridge the gap between the ILL as a facility, which is to a large extent oriented towards academic research, and industry research that may benefit from neutron techniques.

Contact: industry@ill.eu

SINE 2020 Industry WP

37 ACCEPTED
PROPOSALS

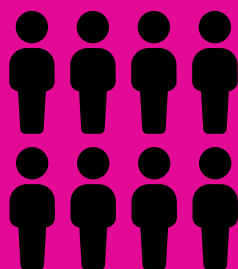
for a total of **55** days

6 returning companies

20 InnovaXN
PROJECTS SELECTED OUT
OF THE 60 RECEIVED FROM
EUROPEAN INDUSTRY AND THEIR PARTNERS

15

CUSTOMERS



KEEP UP-TO-DATE:

 facebook.com/ILLGrenoble

 twitter.com/ILLGrenoble

 [linkedin.com/company/
institut-laue-langevin](https://linkedin.com/company/institut-laue-langevin)

THE ILU's work has two main strands: the first entails significant outreach efforts, the need for this being significant since neutron scattering is not a lab-based technique; the second involves exploring different ways of working with industry, ranging from funded research projects to paid-for services. One important activity in 2019 was therefore the renewal of the industry web pages on the ILL site (<https://www.ill.eu/neutrons-for-society/industry>).

Most techniques of interest to industry are high throughput, like imaging, SANS, reflectometry and powder diffraction. Moreover, the costs for direct industry use of these techniques is reasonable, since one day of beamtime is often sufficient to collect data on several tens of samples. However, strain scanning is an exception to this rule. With the development of additive manufacturing (AM) and increasing understanding of ageing in critical metallic components, this technique is of growing interest to industry. Following the involvement of SALSA scientists in pre-standardisation activities for AM, an MoU will be signed early in 2020 with the Manufacturing Technology Centre (Coventry, UK) and the ESRF and the ILL together.

Energy materials, and battery research in particular, present an exciting opportunity for advanced analytical techniques, industry and innovation. ILU and ILL scientists have joined up with the ESRF and the CEA, under the banner of GIANT, to promote characterisation techniques for modern batteries. The ILL has also become an active member in a consortium of over 30 industrial and academic partners for the European Call LC-BAT-12-2020 for Battery 2030+. If successful, this exciting project will place neutron techniques and the ILL at the forefront of long-term, battery technology research in Europe.

Funded projects remain a key mechanism for opening up academically developed research techniques to industry R&D in order to drive innovation. The industry consultancy work package in the EU-funded SINE2020 (see p. 110) focused on outreach actions (including, e.g. a SANS animation movie) and feasibility studies for industrial R&D. The ILU also played a leading role in the obtention and first phases of the Horizon2020, MSCA COFUND PhD programme InnovaXN—Innovation with X-rays and Neutrons (see p. 110).



Anne Martel on D22.

The IRT-nanoelec (Research Institute for Technology for Nanoelectronics) is a French government-funded project that has led to the creation of the Platform for Advanced Characterisation in Grenoble (PAC-G). The Platform offers a range of advanced neutron (ILL), X-ray (ESRF) and other analytical techniques to the electronics industry. Funding for the programme, involving the ILL, ESRF, LPSC and CEA, has recently been extended to 2020. A second phase of the IRT is being prepared for the period 2021–2025.

The PAC-G team is now adapting to offering its services on the ILL's public instruments, as with other activities within the ILU unit, and developing dedicated services, in particular concerning the irradiation sensitivity of electronics.

D50 is an instrument that enables neutron imaging, a technique that will be of considerable interest and benefit to industry. It is to be implemented at the ILL, in collaboration with Grenoble-Alpes University—see <https://next-grenoble.fr/>. In 2019, D50 achieved excellent levels of performance, including 1-second tomography measurements, 4-micron spatial resolution and 85 % of experiments combining *in situ* neutron and X-ray capability. Benefitting from a major upgrade under the Endurance programme, D50 will be dedicated to neutron imaging from mid-2020 and will become a public imaging instrument in the Large-Scale Structures group.

EXPERIMENTAL AND USER PROGRAMME

- 93 ACADEMIC RESEARCH
- 93 INDUSTRY AND INDUSTRY-SPONSORED ACCESS
- 94 USER AND BEAMTIME STATISTICS
- 98 INSTRUMENT LIST

The **User Guide** contains all the practical information required to prepare a visit

<https://www.ill.eu/users/user-guide/>

Detailed information on the experimental programme can be found at <http://www.ill.eu/users>

625

EXPERIMENTS

including **14 DDT**,
99 EASY and
24 internal
research experiments



101 DAYS OF NEUTRONS
2 740 DAYS FOR SCIENCE



1 6 1 1
INDIVIDUAL
U S E R S

2 3 7 1
USER VISITS

U S E R
SATISFACTION
A B O V E

95 %

* feedback participation rate 61 %



KEEP UP-TO-DATE:

 facebook.com/ILLGrenoble

 twitter.com/ILLGrenoble

 [linkedin.com/company/
institut-laue-langevin](https://linkedin.com/company/institut-laue-langevin)

User programme

PROPOSAL SUBMISSION FOR ACADEMIC RESEARCH

Neutrons beams and instrument facilities are free of charge to academic users of accepted proposals. There are various ways of submitting a proposal to the ILL, as summarised in the following table.





Detailed information can be found at <https://www.ill.eu/users/applying-for-beamtime/>.

Table 1

Mechanisms for submitting a proposal to the ILL. All type of access (except DDT) are reserved for users from ILL member countries or for collaborations between non-member and member teams. The stopwatch symbol indicates quick access. Most types of proposals are submitted via the User Club interface <https://userclub.ill.eu/userclub/>.

INDUSTRY-SPONSORED ACADEMIC RESEARCH AND INDUSTRIAL USERS

Neutrons have significant, specific applications for industry. Beamtime can be sold directly for proprietary research, in which case the experimental data is not made publicly available. The Industry Liason Unit (ILU) is the single point of contact for industry looking to use the ILL's facilities (see p.90). However, around 25 % of industry's use of the ILL is done via academia. The data from these experiments is publicly available and the results may be published. The ILL is now measuring the number and nature of industry-via-academia experiments more accurately, with a view to promoting this use of neutrons and potentially enhancing it in the future. In 2019, **32 experiments were sponsored by industry.**

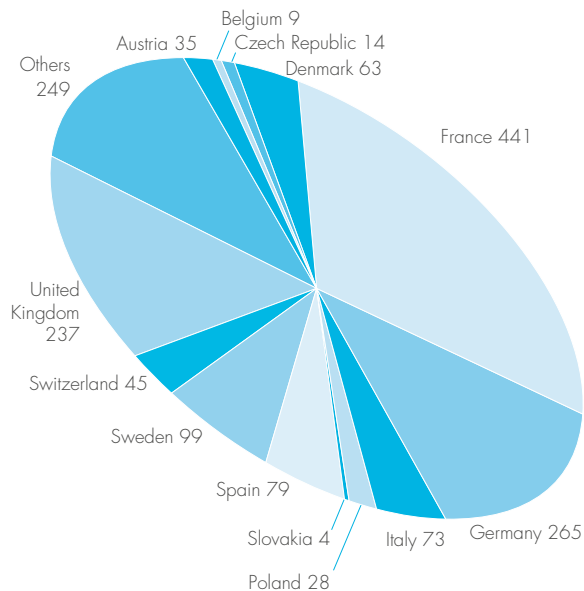
TYPE	APPLIES TO	WHEN	WHO FOR	RESPONSE TIME
External peer review				
Standard	All experiments, all instruments, all conditions	Deadlines twice a year, spring and autumn	All users from member countries (and non-members via 2/3 rule)	4 to 8 months after deadline
BAGs	College 8 proposals on D22	Deadlines twice a year, spring and autumn	All users from member countries (and non-members via 2/3 rule)	4 to 8 months after deadline
CRG	All experiments, CRG instruments, all conditions	Depends on CRG policy	All users from CRG collaboration	Depends on CRG policy
D-Lab	Access to the ILL sample deuteration lab	All year	All users from member countries	
Internal peer review				
DDT	Urgent experiments, hot topics, excellent science from non-member countries, all instruments, all conditions	All year	All users	ASAP 
EASY	A small amount of beamtime, not a full experiment (must be very simple measurements), all instruments, limited number of configurations	All year	All users from member countries	From one to a few weeks 
LTP	All instruments, for projects over several cycles if it can be demonstrated that they bring extra resources or capabilities that are of benefit to all users	Once a year, autumn round	All users from member countries	4 to 8 months after deadline
No peer review				
TEST	Test of sample, equipment, instrument configuration, all instruments	All year	All users from member countries	Usually on same day 
INDU	Proprietary beamtime	All year	Contact the Industrial Liaison Office	ASAP 

USER AND BEAMTIME STATISTICS

USER AND BEAMTIME STATISTICS

Figure 1

National affiliation of ILL users in 2019.



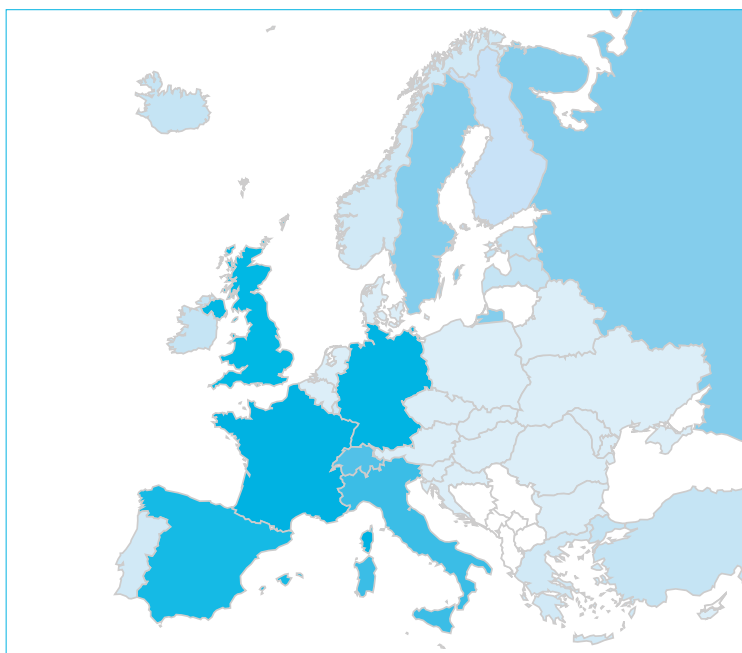
The ILL welcomed 1 611 users in 2019, including 441 from France, 265 from Germany and 237 from the UK. Many of our visitors were received more than once (giving a total of 2 371 user visits).

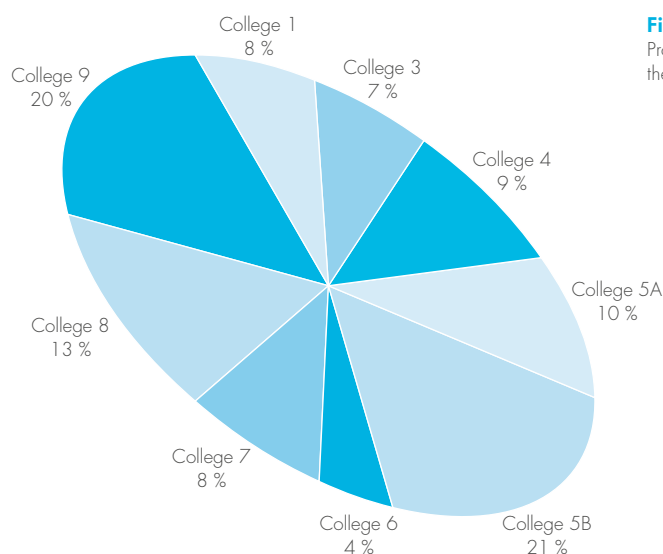
PUMA-BI is new ILL software, developed as part of the FILL2030 project. It brings together the ILL's proposals and publications databases and the Web of Science, in order to help us gain a comprehensive understanding of beamtime use based on a wide range of analyses. It should also allow us to identify laboratories and countries that might be interested in working with us in the future. Another feature of PUMA-BI is its ability to match proposals with publications, enabling the scientific process from idea to experiment to outcome to be tracked. This is a continuous, ongoing process that we will extend to ILL users in the next few months.

Overall, the panel meetings during the November 2018 and April 2018 rounds examined 1 140 proposals requesting 6 962 days in the originally scheduled three cycles in 2019. Of these, 688 proposals received beamtime, requiring the allocation of 3 158 days of beamtime on the various instruments and corresponding to 758 experiments. However, as the ILL was unable to operate the last scheduled cycle in 2019, we will operate an additional cycle in 2020 (three in total) and the backlog experiments will be scheduled in the first cycle of 2020.

Figure 2

Chart obtained with the PUMA-BI software, showing the European origins of authors of ILL publications (taken from the addresses of their associated institutes). Authors associated with the ILL have been removed from the data.



**Figure 3**

Proposals are divided amongst the various colleges. Figure 3 shows the distribution amongst the colleges of those that were accepted.

	Request days	Request %	Allocated days	Allocated %
AT	211.66	3.06	83.55	2.65
BE	21.98	0.32	14.21	0.45
CH	391.02	5.65	122.94	3.89
CZ	83.92	1.21	43.34	1.37
DE	1 580.85	22.84	771.65	24.44
DK	201.32	2.91	76.59	2.43
ES	398.02	5.75	208.19	6.59
FR	1 876.41	27.11	833.03	26.38
GB	1 168.84	16.89	703.75	22.29
IT	406.46	5.87	80.93	2.56
PL	147.33	2.13	57.88	1.83
SE	419.18	6.06	152.18	4.82
SK	15.32	0.22	9.26	0.29
Total	6 922.31	100.00	3 157.5	100.00

Table 1

Distribution amongst the ILL member countries of beamtime requested and allocated in the November 2018 and April 2018 panel meetings. Accepted proposals were scheduled in 2019. Proposals from purely non-member countries do not appear in this table; therefore, the total requests and allocations are different in Table 2.

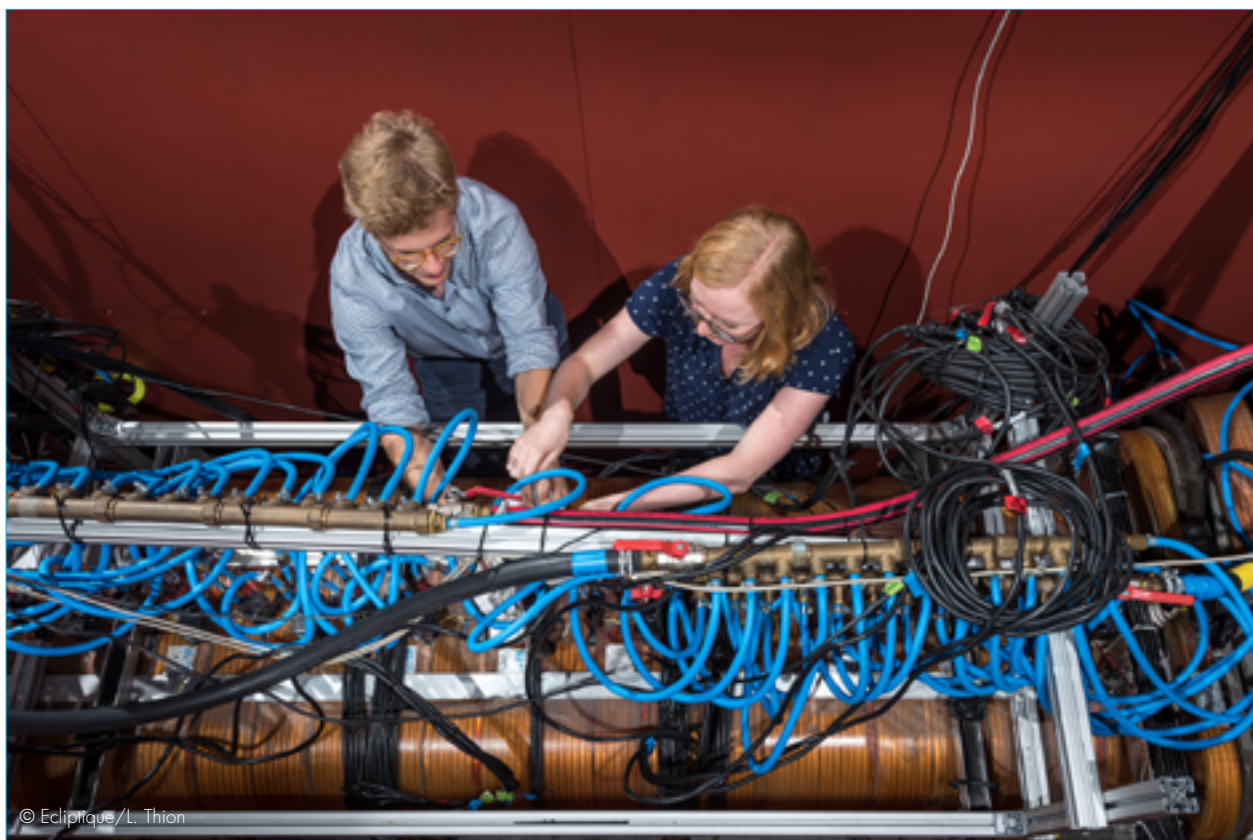
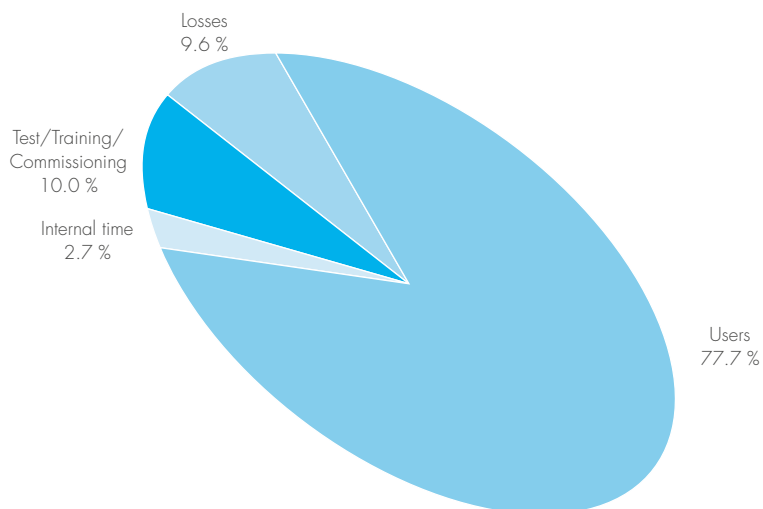
In calculating the statistics for **beamtime per country** shown in **Table 1**, the attribution is based on the location of the laboratory of the proposers, not their personal nationality. For a proposal involving laboratories from more than one member country, the total number of days is divided amongst the collaborating countries and weighted by the number of people from each. Local contacts are not counted as proposers. The beamtime requested by and allocated to scientists from the ILL is allocated to the member countries according to a weighting system based on the fractional membership of the country of the institute concerned. When a proposal involves collaboration with a non-member country, the allocated time is attributed entirely to the collaborating member countries. Proposals in which all proposers are from non-member countries, therefore, do not appear in this table.

USER AND BEAMTIME STATISTICS

Table 2 gives a summary of **instrument performance** for 2019. Approximately 2 649 days were made available to our users in 2019 on ILL and CRG instruments (either via standard request or via the EASY and DDT routes), which represents about 78 % of the beamtime available. A total of 91 days was used by ILL scientists to carry out their own scientific research. About 10 % of the total beamtime available on the ILL instruments was allowed for tests, calibrations, scheduling flexibility, recovery from minor breakdowns and student training. Finally, a total of 329 days were lost as a result of various malfunctions, which represents less than 10 % of the total beamtime available.

In 2019, the reactor operated for two of the originally planned three cycles. This represents 101 days of neutrons, during which **a total of 625 experiments were performed** (including 14 DDT, 99 EASY and 24 internal research experiments). **Beam days given to science (used for users and internal research) in 2019 totalled 2 740 (84 % of the total days available).**

Figure 4
Use of ILL beamtime



© Ecliptique/L. Thion

Table 2

Beamtime request/allocation (via standard subcommittees and Director Discretion Time —DDT—together) by instrument and instrument performance. CRG instruments are in blue.

* 'days allocated' refers only to those days reviewed by the subcommittees (i.e. excluding CRG days and DDT)

** 'days available' are the days available on each instrument

*** 'days used' refers to the total number of days given to users (i.e. including CRG days for CRGs and DDT)

PF2 consists of various set-ups where several experiments are running simultaneously. The values given are averages for these positions.

D4 and IN1 share the same beam port and cannot be run simultaneously.

D3 was not available in 2019 because the new H4 beam tube was not delivered on time for its anticipated installation in the summer.

Instrument	Days requested	Days allocated*	Number of accepted experiments	Available days**	Days used for users***	Days lost	Days for test/ commissioning /training	Days for internal research	Days for EASY/ DDT
D10	164	135	20	101	97	3	1	0	0
D11	220	110	61	101	80	3	12	0	6
D16	200	100	19	101	78	8	4	11	0
D17	189	104	32	101	75	3	17	3	3
D19	202	106	15	101	85	3	10	0	3
D1B	156	62	29	101	87	4	3	1	6
D20	183	102	49	101	86	5	5	2	3
D22	226	97	53	101	73	5	19	3	1
D23	152	42	8	101	86	2	10	3	0
D2B	168	105	51	101	80	2	5	5	9
D33	249	105	36	101	83	3	13	0	2
D3	209	31	5						
D4	110	47	12	53	40	2	9	0	2
D7	253	101	20	101	86	2	11	0	2
D9	207	109	13	101	95	3	3	0	0
FIGARO	203	118	39	97	69	13	6	3	6
FIPPS	156	110	7	101	74	22	4	1	0
IN11	233	91	13	101	37	52	1	4	7
IN12	189	35	7	82	67	2	5	7	1
IN13	89	55	8	101	76	13	12	0	0
IN15	208	87	18	101	83	5	10	2	1
IN16B	276	107	30	101	57	22	21	1	0
IN1	137	40	13	47	31	5	7	2	2
IN20	98	90	15	101	86	6	9	0	0
IN22	142	43	7	101	48	30	23	0	0
IN5	311	104	32	101	77	7	16	0	1
IN6-SHARP	177	65	22	101	95	5	1	0	0
IN8	161	97	19	101	81	3	17	0	0
LADI	286	98	11	101	54	2	45	0	0
PF1B	367	166	9	101	69	24	8	0	0
PF2 normalised	160.6	133.5	18	101	59	27	1	14	0
PN1	265	127	14	101	68	28	5	0	0
S18	135	18	2	101	94	5	2	0	0
SALSA	125	54	19	101	59	6	13	23	0
SUPERADAM	100	46	10	101	89	2	9	0	1
THALES	256	117	22	101	87	2	4	6	2
Total	6 962.6	3 157.5	758	3 410	2 591	329	341	91	58
Percentage					76.0 %	9.6 %	10.0 %	2.7 %	1.7 %
					Days for science	2740	84%		
						2591+91+58			

INSTRUMENT LIST

INSTRUMENT LIST – JANUARY 2020

ILL INSTRUMENTS		
D2B	powder diffractometer	operational
D3	single crystal diffractometer	operational
D4 (50 % with IN1-LAGRANGE)	liquids diffractometer	operational
D7	diffuse-scattering spectrometer	operational
D9	single crystal diffractometer	operational
D10	single crystal diffractometer	operational
D11	small-angle scattering diffractometer	operational
D16	small momentum-transfer diffractometer	operational
D17	reflectometer	operational
D19	single crystal diffractometer	operational
D20	powder diffractometer	operational
D22	small-angle scattering diffractometer	operational
D33	small-angle scattering diffractometer	operational
FIGARO	horizontal reflectometer	operational
FIPPS	fission product prompt gamma-ray spectrometer	operational
IN1-LAGRANGE (50 % with D4)	three-axis spectrometer	operational
IN5	time-of-flight spectrometer	operational
IN8	three-axis spectrometer	operational
IN11	spin-echo spectrometer	operational
IN16B	backscattering spectrometer	operational
IN20	three-axis spectrometer	operational
PANTHER	time-of-flight spectrometer	commissioning
PF1	neutron beam for fundamental physics	operational
PF2	ultra-cold neutron source for fundamental physics	operational
PN1	fission product mass-spectrometer	operational
PN3 – GAMS	gamma-ray spectrometer	operational
SALSA	strain analyser for engineering application	operational
ThALES	three-axis spectrometer	operational
WASP	wide-angle spin-echo spectrometer	operational

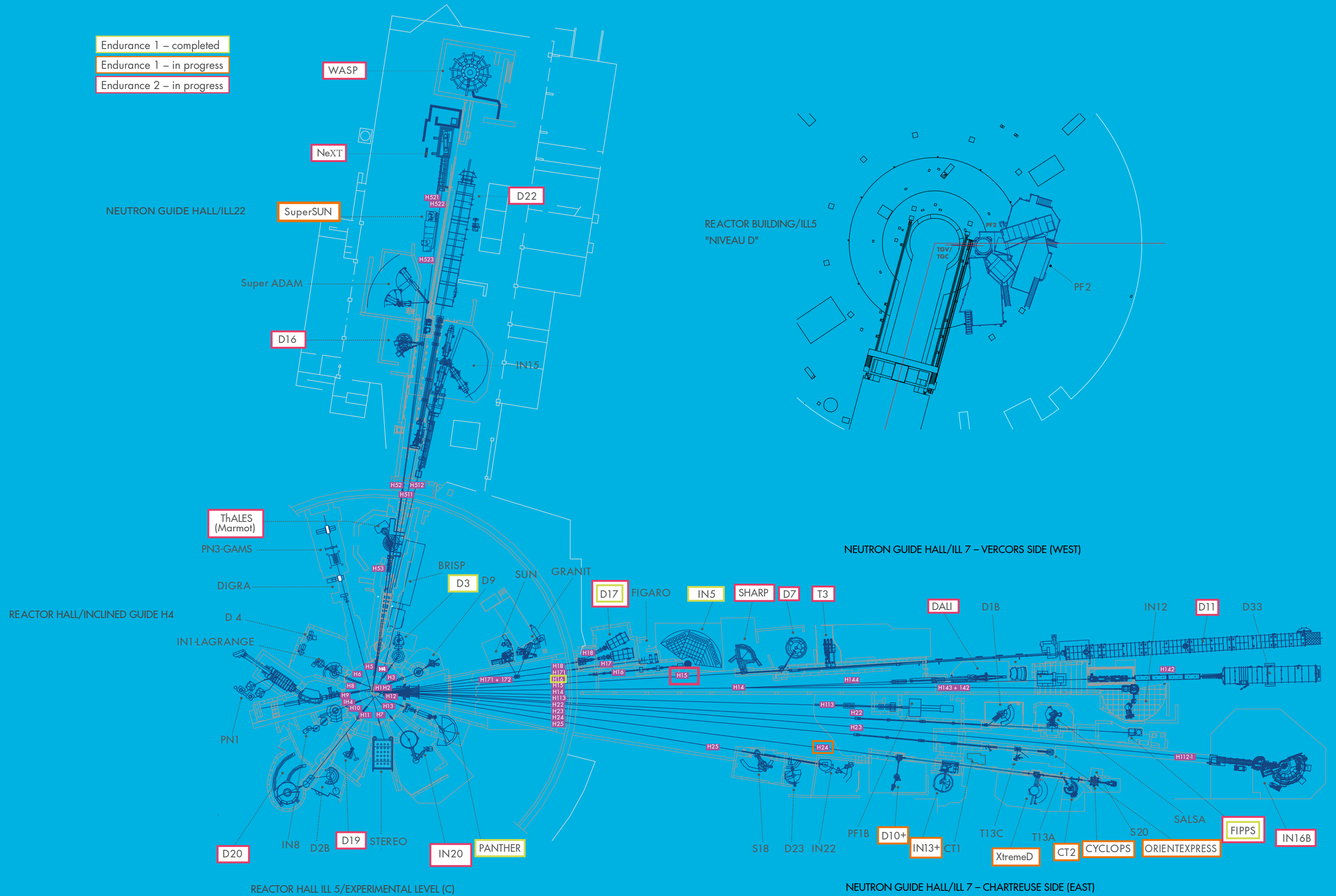
CRG INSTRUMENTS		
BRISP	Brillouin spectrometer	CRG-B on hold
D1B	powder diffractometer	CRG-A operational
D23	single crystal diffractometer	CRG-B operational
GRANIT	gravitation state measurement	CRG operational
IN6-SHARP	time-of-flight spectrometer	CRG-A operational
IN12	three-axis spectrometer	CRG-B operational
IN13	backscattering spectrometer	CRG-A operational
IN22	three-axis spectrometer	CRG-B operational
SuperADAM	reflectometer	CRG-B operational
S18	interferometer	CRG-B operational

JOINTLY FUNDED INSTRUMENTS		
LADI (50 %)	Laue diffractometer	operated with EMBL
IN15	spin-echo spectrometer	operated with FZ Jülich
NeXT (75%)	Imaging instrument	operated with UGA and HZB
GRANIT	gravitation state measurement	operated with LPSC (UJF, CNRS)
STEREO	search for sterile neutrino	operated with CEA Saclay, LAPP Annecy, LPSC Grenoble, MPIK Heidelberg

TEST AND CHARACTERISATION BEAMS	
CT1, CT2	detector test facilities
CYCLOPS	Laue diffractometer
TOMOGRAPHY	neutrography
OrientExpress	Laue diffractometer
T3	neutron optics test facility
T13A, C	monochromator test facility
T17	cold neutron test facility

Details of the instruments can be found at <http://www.ill.eu/users/instruments/>.

- Endurance 1 – completed
- Endurance 1 – in progress
- Endurance 2 – in progress



The instrument facilities at the ILL are listed in the table on the left, and shown in the plan on p. 99. Besides the 28 ILL instruments, there are 10 Collaborative Research Group (CRG) instruments.

CRGs can build and manage instruments at the ILL to carry out their own research programmes. These instruments are made available to the ILL's scientific user programme for 50 % (CRG-A) and 30 % (CRG-B) of available beamtime. The CRG-C external group has exclusive use of its beamtime. Details about the framework for the operation of CRGs can be found at <https://www.ill.eu/users/instruments/crgs/>.

All current CRGs are of either type A or type B—the only exception being GRANIT which, because it is a CRG-C instrument, is not available as a 'user' instrument; IN15 has special status since it is a joint venture of the ILL and FZ Jülich; and the instrument STEREO is jointly funded by the ILL and CEA Saclay, LAPP Annecy, LPSC Grenoble and MPIK Heidelberg.

INSTRUMENT LAYOUT

REACTOR OPERATION

102 REACTOR OPERATION IN 2019

TWO CYCLES AND

101

DAYS OF
OPERATION
IN 2019



A THERMAL
POWER OF
58.3 MW



KEEP **UP-TO-DATE**:

-  facebook.com/ILLGrenoble
-  twitter.com/ILLGrenoble
-  linkedin.com/company/institut-laue-langevin

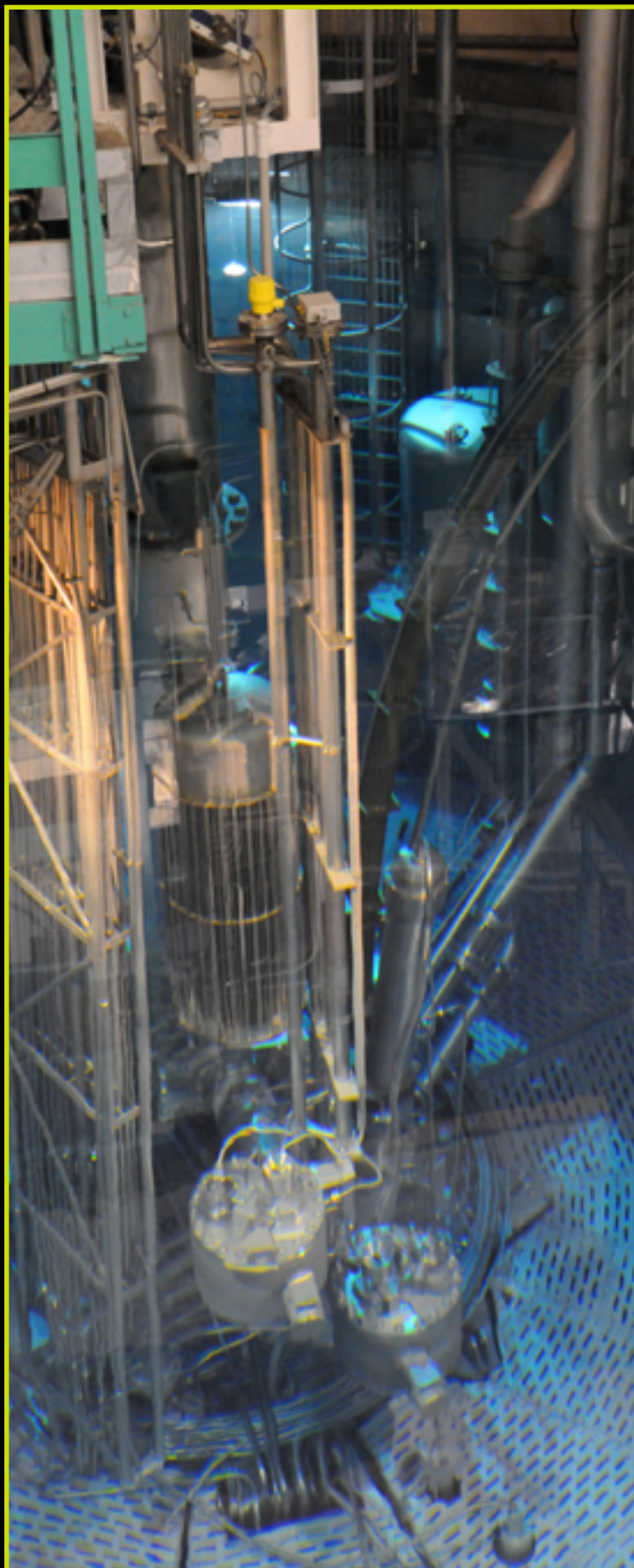
THE ILL'S High-Flux Reactor (HFR) produces the most intense neutron flux in the world: 1.5×10^{15} neutrons per second per cm^2 , with a thermal power of 58.3 MW. It normally operates four reactor cycles per year. At the end of each cycle there is a shutdown period, during which the fuel element is changed and a number of checks are carried out. Occasional longer shutdowns are scheduled to allow for equipment maintenance.

At maximum power, the reactor's fuel element can provide 46 days of operation per cycle. For almost the last ten years, our 'contract' with our scientific users has been to provide 200 days of operation per year (excluding maintenance and upgrade work). At nominal power this allows for 4.5 cycles per year.

For obvious practical reasons this number of annual cycles is not ideal; for the Reactor Division it involves the same amount of work as having five operating cycles, since the tests to be carried out and fuel loading operations are the same before every start-up irrespective of the length of the cycle. As the performance of the instruments has generally been increased over the years thanks to regular upgrade programmes, we have recently decided to provide the 200 days of operation over four 50-day cycles at slightly lower power.

Following the nuclear disaster at Fukushima in 2011, the French nuclear safety authority (ASN) ordered additional safety assessments to be carried out on all French basic nuclear installations (INBs), including the ILL. The Post-Fukushima programme has now ended. The safety of the reactor is guaranteed, even in the event of an extreme earthquake-and-flood combination following the rupture of the dams upstream, well beyond previous dimensioning standards.

The ASN has also asked the ILL to reorganise our working methods to make them better and more secure, by implementing an Integrated Management System (SMI) (INB Decree of 2012) and incorporating it into the ILL's operating procedures. The ASN decisions are extremely demanding and involve a lot of work. However, such work is essential and remains a top priority for the ILL.



REACTOR OPERATION 2019

Three reactor cycles were planned in 2019. As a result of the need to replace a pyrotechnic valve, the third cycle has since been postponed until the beginning of 2020. The two achieved cycles went perfectly, using two fuel elements and delivering a total of 101 days of scientific activity.

Cycle n°	Start of cycle	End of cycle	Number of days of operation	Number of days scheduled	Power in MW	Number of unscheduled shutdowns
185	13.06.19	04.08.19	52	53	51	0
186	28.08.19	15.10.19	48	48	55	0
Total			100	101	53	0

THE ILL INTEGRATED MANAGEMENT SYSTEM

The implementation of the Integrated Management System (INB Decree of 2012) and its incorporation into ILL's operating procedures, together with the *Groupe Permanent* safety review and the Reinforcement of Physical Protection (RPP) project, not only require the use of temporary staff but also put demands on our permanent staff.

The ILL's commitment to technical compliance is well recognised by the ASN. Regarding regulatory compliance, the Reactor Division and indeed the whole of the ILL have invested a great deal of time and effort in implementing the Integrated Management System, since mid-2017 in particular. It is extremely important to comply with the provisions of the INB decree and with all ASN decisions arising from this decree, of which there are many. We must also comply strictly with all the new IMS processes and their requirements. In this context, we have already made major changes to more than 1 000 existing procedures. The ASN decisions are extremely demanding and involve a lot of work, as we must not only demonstrate compliance but also verify compliance on a regular basis. However, such work is essential and remains our top priority until we restore the ASN's confidence in the ILL in this regard. The Head of the Reactor Division has devoted much of his time to managing and verifying the compliance of maintenance operations and modifications to equipment. These efforts led to the restart of the reactor on 13 June 2019.

The Reinforcement of Physical Protection (RPP)

project was launched in early 2017. The work on the ZAC perimeter fence started in September of this year. We must also provide updated security studies for subsequent stages of the project by the end of 2019. It is extremely important that we adhere to the timetable established for the RPP project. An HFDS (Haut Fonctionnaire de Défense et de Sécurité) technical visit took place on 30 September and was an opportunity for the ILL to demonstrate the progress already made.

The examination of the 10-year safety review

officially began on 11 February. It is due to be completed by the end of 2019, with the meeting of the *Groupe Permanent* to take place early in May 2020. The Institute for Radiological Protection and Nuclear Safety (IRSN) has already faxed us over 500 questions, 20 technical meetings have taken place and more than 200 internal ILL documents have been sent to the IRSN to meet its requirements. The questions have now covered around 95 % of the ILL safety assessment and we have had no difficulty answering them, even those received at a very late date. A three-day ASN inspection took place on 21, 22 and 23 October to deal with this topic. The results of this inspection were positive and there were few comments or questions. We are now waiting for the official inspection follow-up letter.

FIRE PROTECTION

In view of changes to regulations, the following operations must be completed by the end of 2021:

- Replacement of old fire detectors with ionisation smoke detectors (currently 70 % completed, although only 20 % have received final acceptance with respect to the APSAD regulation R7 on 'Automatic fire detection')
- Fire treatment of the 12 posts on reactor level C supporting the concrete floor slab of Level D.

The shutdowns were used for a host of important maintenance and other operations and for installing major processes:

- Fire treatment of the posts on reactor level C
- Hafnium safety rods qualification
- Replacement of beam tubes H4
- Removal of beam tube V4 and its replacement with a sealing plug
- Replacement of four pyrotechnic VPFN valves for prevention maintenance
- Anticipation video inspections of the reactor block
- Anticipation maintenance on the control rod mechanism.

THE KEY REACTOR COMPONENTS (KRC) PROGRAMME

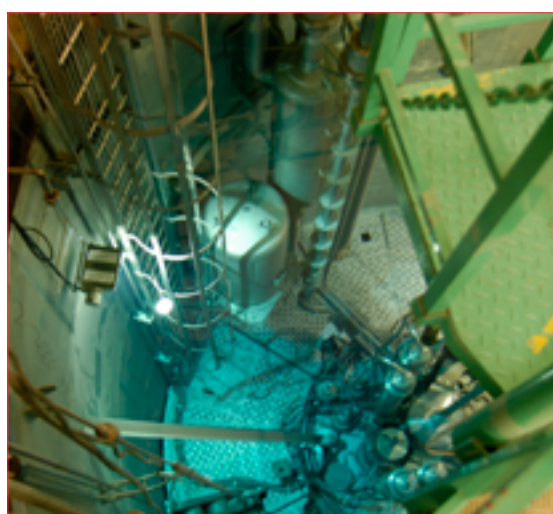
The aim of the KRC programme is to ensure the upgrade and maintenance of the reactor’s most important components, thus guaranteeing the reliability of reactor operations for the future. The main components concerned are the cold neutron sources, the fire protection equipment and the physical protection equipment.



RADIOACTIVE WASTE AND EFFLUENTS

The ILL’s activities in 2019 generated waste and effluents in respect of the regulatory limits applicable to our installation, as follows:

Evacuation of radioactive waste	Quantity
Decay bin (60 L)*	0
5 m ³ pre-concreted crate (low- and intermediate-level waste)	0
5 m ³ crate (low- and intermediate-level waste)	3
HDPE 200 L drums of ‘incinerable’ waste	0
HDPE 120 L drums of ‘incinerable’ waste	0
HDPE 120 L drums (laboratory waste)	8
30 L cylinders (liquid)	1
Radioactive liquid effluents from the reactor	30.7 m ³



*The decay bins contain very active waste. They will be transferred to ANDRA’s new storage centre CIGEO as soon as it becomes available, after an interim period in special storage.

Gaseous effluents	Released in 2019 (TBq)
Tritium	5.8
Rare gas	0.76
Carbon-14	0.066
Iodine	0.00000069
Aerosols	0.00000017



Liquid effluents	Released in 2019 (TBq)
Tritium	0.053
Carbon-14	0.00013
Iodine	0.00000023
Other activation products	0.000047

© C. Tresca

MORE THAN SIMPLY NEUTRONS

106 SCIENTIFIC SUPPORT LABORATORIES

108 TRAINING AND OUTREACH

110 EUROPEAN PROGRAMMES

ACCESS

TO **13 LABORATORIES**
HOSTING **25 MAJOR PIECES**
OF EQUIPMENT VIA THE **PSCM**



9 ... NO FEWER THAN
DIFFERENT EU PROJECTS



 **18 PARTICIPANTS**
@ the ILL-ESRF Summer School

HERCULES: 64 PARTICIPANTS AND
23 DIFFERENT NATIONALITIES
WORKING IN 16 DIFFERENT COUNTRIES



40

PHD STUDENTS

71

TRAINEES



KEEP UP-TO-DATE:

 facebook.com/ILLGrenoble

 twitter.com/ILLGrenoble

 [linkedin.com/company/
institut-laue-langevin](https://linkedin.com/company/institut-laue-langevin)

IN ORDER to maintain their ranking at an international level, European research institutes must optimise their resources and develop synergies at every level. The ILL is located in the so called 'EPN campus' which hosts other major European institutes—such as the ESRF and EMBL, as well as France's IBS—providing a genuine hub for international science in the Grenoble region.

The ILL is firmly committed not only to building high-performance instruments, but also to offering the best scientific environment for the user community. We have also established successful collaborations with neighbouring institutes over the years and launched successful scientific and support partnerships.

The history of the ILL is one of European collaboration, and today the Institute is involved in no fewer than nine different projects funded by the European Commission. The benefits are not merely financial; the ILL also benefits from associated networks and resources, which improve its integration with other facilities and the user community. The ILL is currently the co-ordinator and sole beneficiary of **FILL2030** (with a grant of 4 M€).

As the **SINE2020** project—of which we were also the co-ordinator—comes to an end, we are also close to the end of the Horizon 2020 framework programme. The funding schemes in the new Horizon Europe programme are still to be defined.

The EU provides not only financial support but also a framework for collaboration and synergy; several existing networks have benefitted so far, and this must continue if future neutron and muon communities in Europe are to thrive. Europe's neutron facilities are now building on recent experiences of collaboration (NMI3 and SINE2020) with the launch of LENS, the League of advanced European Neutron Sources. This initiative will nurture the environment required for sustainable collaboration.

Local collaboration is equally important. ILL has started together with the ESRF, InnovaXN—a doctoral training programme bringing together the expertise of large-scale research infrastructures with the R&D needs of European industry. This project will allow us to train young researchers in advanced synchrotron X-ray and neutron techniques in an international, innovative and multidisciplinary environment.

Last but not least, the ILL is committed to training and outreach, providing this in many different forms. Whilst the ILL Graduate School and PhD programme are now training future generations of neutron users, we also run neutron schools and other events for MSc and PhD students. In addition, our open days and annual contributions to the local science festival help attract young talent to science and improve the general public's understanding of the science we perform.



© C. Tesco

SCIENTIFIC SUPPORT LABORATORIES

PARTNERSHIP FOR SOFT CONDENSED MATTER

The Partnership for Soft Condensed Matter (PSCM) is a joint initiative established by the ILL and the ESRF on the EPN Campus.

The PSCM's main mission is to provide support services to ILL and ESRF scientists tackling contemporary challenges in soft matter research (nanomaterials, environmental and energy sciences, biotechnology and related fields). The PSCM provides users with access to 13 laboratories and 25 technical facilities, together with the necessary sample preparation equipment. This will include, as of January 2020, new equipment such as a micro-calorimeter and a spin-coater.

It is also the Partnership's mission to strengthen the soft matter research community by establishing long-term collaborations to develop specialised instrumentation and sample environment facilities. Six new partnership projects will start in 2020, competitively selected through a call for proposals.

The PSCM is located, along with the Soft Matter Science and Support group, on the 2nd floor of the EPN Campus Science Building. Neutron users wishing to use the PSCM laboratories and equipment in conjunction with their neutron measurements should indicate this when submitting their request for beamtime.

Further details can be found at

<http://www.epn-campus.eu/pscm/>.

PARTNERSHIP FOR STRUCTURAL BIOLOGY

The Partnership for Structural Biology (PSB) operates a powerful set of technology platforms provided and managed by the partner institutes (ILL, ESRF, EMBL, IBS). These provide advanced capabilities to complement the neutron-scattering facilities available to ILL users: synchrotron X-rays, electron microscopy, high-field nuclear magnetic resonance, high-throughput methods (e.g. soluble expression and crystallisation), and a range of biophysical techniques such as isothermal calorimetry and surface plasmon resonance. The PSB also includes the Deuteration Laboratory (see below), operated as a user platform within the ILL's Life Sciences Group, and the joint SANS/SAXS platform.

There are strong links and collaboration between the ILL and ESRF life sciences/structural biology and industry groups. The aim of the PSB is to enhance the interdisciplinary capabilities of each of the facilities located on the site and to widen the scientific scope of the external user communities. The Carl-Ivar Brändén building acts as home to the PSB and its partner organisations.

Check the website for more information:

<http://www.psb-grenoble.eu/>.

THE LIFE SCIENCES GROUP AND ITS DEUTERATION LABORATORY

The Deuteration Laboratory (D-Lab) is located and operated as a PSB platform within the ILL's Life Sciences Group. Its user programme uses *in vivo* recombinant expression approaches to provide deuterated analogues of proteins, nucleic acids and lipids for the study of structure (crystallography, SANS, fibre diffraction, reflection) and dynamics using neutron scattering. The D-Lab is therefore of central importance to all the ILL instrument groups involved



in biological research. Furthermore, every year the Group receives a small number of undergraduate placement students for training in the various techniques.

The Life Sciences Group is additionally involved in a wide variety of externally funded programmes exploiting the capabilities of the site's Partnership for Structural Biology, as well as promoting interdisciplinary structural biology. It also interacts strongly with industry. In addition, it is involved in the operation and development of the cryo-EM capabilities being set up with the installation of Titan Krios at the ESRF, in collaboration with the ESRF, IBS and EMBL.

As part of its partnership with Keele University (UK), the Life Sciences Group has just created a joint-appointment faculty position in cryo-EM and neutron scattering. This position has recently been filled by Dr Daouda Traore, positioning the ILL as an equal partner in this important new development on the site.

Access to the D-Lab is gained through a rapid peer-review proposal system (see <http://www.ill.eu/instruments-support/instruments-groups/groups/lsg/user-platforms>). The Lab is available to all the ILL member countries, regardless of where the neutron scattering study is carried out. It is also available to users from non-member countries, although these users are expected to cover the costs involved.

CHEMISTRY LABORATORIES

The Soft Matter Science and Support Group (SMSS) manages the ILL chemistry laboratories, together with the PSCM laboratories. Its main goal is to give ILL users the ability to prepare and characterise their samples during their neutron experiments; however, it also supports the in-house research conducted by instrument scientists and PhD students.

The laboratories are stocked with the basic equipment (glassware, consumables and chemicals) necessary for preparing samples for a variety of neutron experiments, as well as more specific facilities such as high-temperature furnaces, a glovebox and an enclosure for handling nano-powders. The PSCM laboratories provide various means of characterising samples, such as UV-Vis, FTIR and light scattering.

The main facilities are located in the Science Building. In addition, three sample preparation labs can be found in the guide halls ILL 7 and ILL 22.

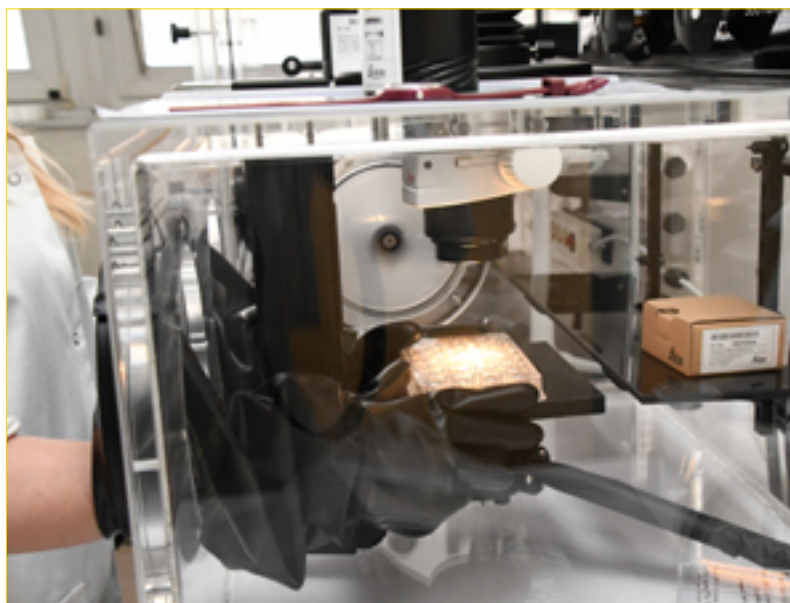
Further information on the Chemistry Laboratories can be found at

<https://www.ill.eu/users/support-labs-infrastructure/chemistry-laboratories/>.

MATERIALS SCIENCE SUPPORT LABORATORY

The joint ILL-ESRF Materials Science Support Laboratory group (MSSL) provides a range of support to our users, from advice on experiment proposals to assistance with preparing samples and performing the experiments. The Lab has equipment for tensile testing, hardness testing and microscopy, as well as equipment for producing specialised sample holders.

The Lab staff work with users to optimise their experimental methodology before the start of an experiment. This can involve standardised specimen mounting, digitisation of samples and defining measurement macros. It is recommended that users get in touch well in advance and arrive at the ILL a day or two before the start of an experiment, to enable these off-line preparations to be performed.



TRAINING AND OUTREACH

STUDENT TRAINING

The **ILL Graduate School** has grown in strength over recent years as the ILL PhD programme has evolved. It provides training and funding for the equivalent of 40 full-time, three-year PhD students from different European countries. It also takes in a number of PhD students with external funding. By October 2019, a total of 48 PhD project applications had been received in response to our call for PhD proposals; these were being assessed at the time of writing. Five to ten 'full-time-equivalent' projects will be selected, prior to the recruitment of PhD students in 2020.

The year 2019 also saw the start of the **InnovaXN PhD programme**, financed by the EU via the Marie-Curie training programme. InnovaXN projects differ from the ILL's other PhD projects in that they involve industrial partners; InnovaXN projects must have industrial applications. An important aspect of the programme is the few months during their PhD that these students spend on their industrial partner's site. The InnovaXN programme will run for five years. Recruitment will begin in early 2020 for PhD students to work at the ILL on the ten recently accepted projects; these students will start their PhD work in September. [see commentary below]

The International Summer School for undergraduate students, organised by the ILL and the ESRF, took place in September 2019. The school has been held every year since 2014 and allows undergraduate students from all our member countries to spend a month on the site. The students follow a series of lectures and seminars on the fundamentals of X-rays and neutrons and their use in science today. They also each work on a personal project, supervised by the ILL or ESRF scientists and PhD students. The ILL hosted nine such projects in 2019 (half of the 18 students). These were selected from approximately one hundred applications, from universities in Belgium, Denmark, Germany, Hungary, Italy, Poland, Russia, Spain and the UK.

The ILL welcomed a total of **71 trainees** in 2019 (including 8 from the ILL-ESRF Summer School), of 21 different nationalities (including 9 German, 20 French, 10 British and 19 from other ILL member countries).

HERCULES SCHOOL

The Hercules School has been held every year since 1991. It is a one-month course on neutron and synchrotron radiation for condensed matter studies for students and young scientists. It includes lectures, hands-on sessions and tutorials in small groups, a poster session, and visits to partner facilities.

The 2019 event was held from 18 March to 19 April and attracted over 140 applications. Sixty-four students attended, representing 23 different nationalities based in 16 different countries; most came from the European Union, but others came from Taiwan, India, Argentina, China and Russia. A special 'Practicals and Tutorials' session was organised, hosted by the different partner institutions in Grenoble and other European facilities.

More information is available at <http://hercules-school.eu/>.

Participants at the Hercules 2019 session.



GRENOBLE'S 2019 SCIENCE FESTIVAL

On Saturday 12 October the four institutes that make up the EPN Campus came together to run a stall at Grenoble's 'Fête de la Science', enthusiastically demonstrating the variety of research being performed on the campus. The year 2019 is the International Year of the Periodic Table, and an Escape Game on the theme was one of the activities on offer. It appeared to help the visitors understand how the elements are organised and the important role the table plays in our scientists' work. In any event, it was very popular! Over 1 600 students and 1 800 visitors spent time at the stall.



The wonders of smallness, through a microscope's eyes.

European collaborations

SINE2020 received 10.8 M€ from the European Commission under INFRADEV-01-2014 and a direct contribution of 1.2 M€ from the Swiss government to the Swiss participant. At its conclusion, the project had produced 112 deliverables and 10 milestones. During the period 2015–2019, approximately 120 experts from 18 different institutions—neutron and muon facilities, universities and other academic organisations—participated in the project’s networking activities and Joint Research Activities.

This collaboration has been marked by a high degree of commitment from all the participants, with high-quality work completed within the deadlines. Both the new and long-established networks have conferred demonstrable benefits on the European neutron and muon communities, most of the technical projects have shown feasibility and several of them are ready for production and application in the various centres should investment materialise. On the industrial R&D side of the project, one conclusion of the SINE2020 Industry Consultancy work has been that companies are very interested in collaborative research, which is an obvious strength of neutron facilities. This is certainly one pillar of a sustainable model for ‘working with Industry’ in the future (see **figure 1**).

FILL2030 is a mono-beneficiary project, dedicated to ensuring the long-term sustainability of the ILL business model. Part of the EU’s ‘Horizon 2020’ research and innovation programme, it has been granted 3.98 M€ to achieve its mission. The grant will finance the development of new service packages for academia and industry, innovative improvements to the ILL’s funding model, tools for identifying emerging user groups and showcases illustrating the socio-economic impact of ILL research.

FILL2030’s initial efforts have concentrated on the need to secure continuous income from its current Associate and Scientific Member countries. Relations have been strengthened in this respect, focusing on the needs and expectations of each partner country. The ILL is now actively communicating on the impact of

the neutron science it produces and the return on investment received by its funders, country by country. Most member country contracts have been successfully renewed.

At the same time, FILL2030’s outreach activities (roadshows, workshops, tours of the installations and media communications) have extended the pool of potential new partners, in Europe and beyond. Successful events and workshops have been organised in Finland, Hungary, Italy, Ireland, Lithuania, Portugal, Romania and Spain; others have been scheduled for 2020. Furthermore, to date over 30 open-access publications have been financed by the project (with even more to come).

ILL aims to identify new international partners, attract new scientific communities and ensure that users are fully exploiting the European potential. A set of bibliometric tools has been developed, capable of analysing the activity of European neutron scattering communities. These will help to unravel the complex, transnational networks of collaboration and identify potential areas for growth. Existing paradigms have been adapted and extended with the introduction of new mechanisms for access and funding that correspond more closely to the new community’s needs. Last but not least, as part of FILL2030’s ‘Transnational Access’ scheme, beamtime is granted to users from ILL non-member countries in Europe and beyond.

PaNOSC, the Photon and Neutron Open Science Cloud, is an EU-funded project that provides joint policies, strategies and solutions for enabling Open Science through the adoption of FAIR principles. Since the project’s start in December 2018, six strategic European photon and neutron (PaN) sources (the ESRF, CERIC-ERIC, ELI-DG, ESS, XFEL and ILL) and the e-infrastructures EGI and GÉANT have been collaborating to make FAIR data a reality at PaN facilities; this is being achieved through the development and provision of services for scientific data, and their subsequent connection to the European open science cloud (EOSC).

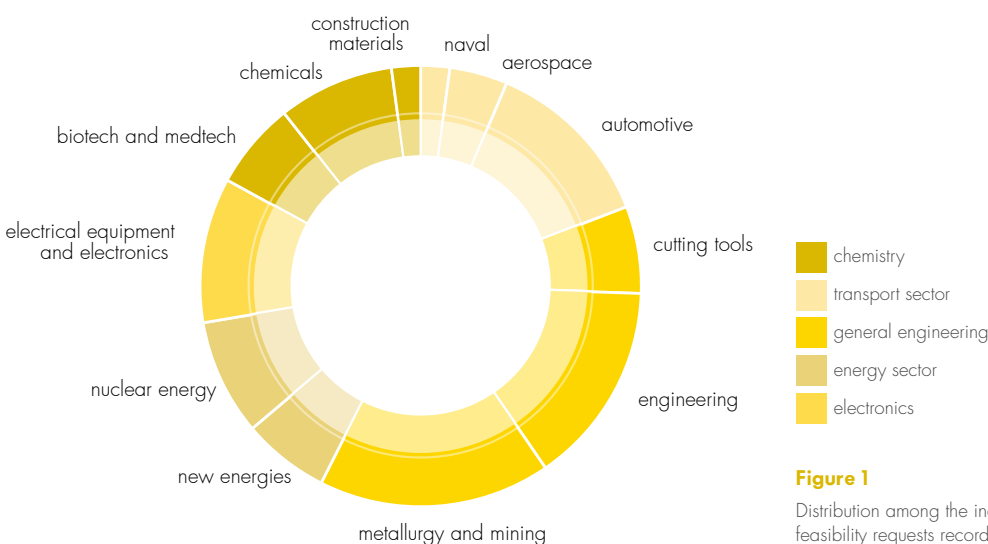
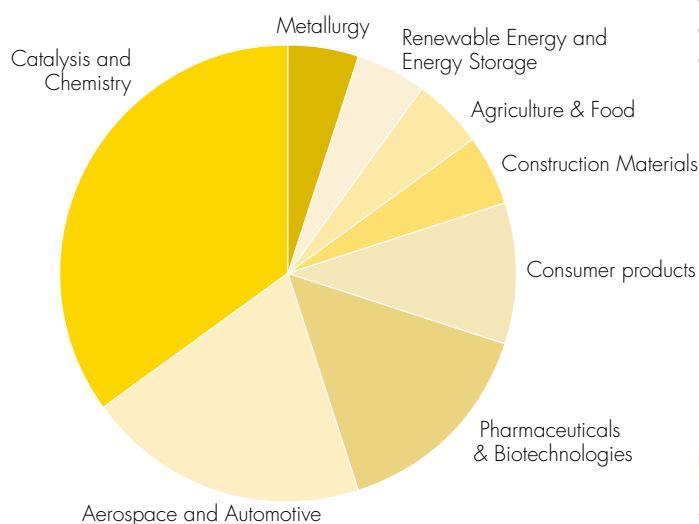


Figure 1
Distribution among the industrial sectors of the feasibility requests recorded during SINE2020

In 2019 PaNOSC's partners drafted a new data policy framework to make scientific data produced at Europe's major PaN sources fully compatible with FAIR principles. The framework will be finalised in 2020 and then submitted to the partners. In order to ensure the proper implementation of FAIR data, PaNOSC is working to establish a useful set of metadata and design an extensible query interface to enable searches with these terms. The six partners are committed to implementing FAIR principles in their data catalogues to allow searches across the catalogues of all the facilities involved. The existence of a federated data catalogue will give access to other services, as well as to software for data analysis and simulation which will be developed as part of the project. The ultimate aim is to provide a portal offering each facility access to remote data analysis services, allowing users to analyse experimental data through remote desktops and Jupyter notebooks.

InnovaXN is a five-year Doctoral Programme initiated in 2019 by the ESRF and the ILL. It brings to innovators with neutrons and synchrotron X-rays an exceptional training opportunity for 40 PhD students whose research will be driven by pre-competitive R&D, in close collaboration with an industrial partner. This will provide a unique cross academic-industry science setting, secondment opportunities and society-relevant research, and training the future key researchers able to tackle major research and societal challenges by exploiting the academic-industry interface.

In November 2019, the **InnovaXN** scientific review board selected 20 projects out of the 60 received from European industry and their partners. The approved projects cover a wide range of research fields such as chemistry, catalysis, aerospace, automotive and consumer products (see **figure 2**). Recruitment of students occurred in February 2020.



The League of advanced European Neutron Sources (LENS)

is a strategic consortium of European neutron sources that aims to act as guide and advocate for the European neutron user community. It will promote neutron science as a fundamental component of European scientific research and innovation.

LENS unites the European neutron sources under a single banner. Under its charter it aims to 'facilitate any form of discussion and decision-making process that has the potential to strengthen European neutron science via enhanced collaboration among the facilities'. Other facilities may join the League in the future; several neutron facilities are interested to join LENS as observers or members.

LENS was officially launched on 26 March 2019 at the General Assembly and Executive Board meetings in Liblice, Czech Republic. The Director of the ILL, Helmut Schober, was elected LENS Chair, with the Director of the UK's ISIS Neutron and Muon Source, Robert McGreevy, elected Vice-Chair. The signing ceremony was followed by a public celebration in the presence of some 80 government representatives as well as national representatives of the European Strategy Forum on Research Infrastructures (ESFRI), the European Commission and the wider scientific community.

LENS met again on 22–23 October 2019, at the ILL, for meetings of its five working groups and the LENS Executive Board; these were followed by the second General Assembly, chaired by Helmut Schober. At these meetings, the working groups and leaders of the different member facilities, in consultation with the European Neutron Scattering Association (ENSA), decided on the pilot activities to be performed. Work in progress was presented for the first time to the organisation as a whole.

The pilot activities proposed demonstrates the collaborative spirit of the organisation. It includes strategic contributions to health, climate and the environment, food and energy, and materials research with neutrons. Technical collaboration on neutron technologies is also planned, as is work on data management and analysis. Other issues will also be pursued, such as closer cooperation concerning the organisation of the LENS neutron centres, new forms of access for academia and industry, the exchange of best practice, training and management.

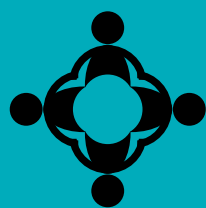
Figure 2

Distribution among Industrial sectors of the 20 accepted InnovaXN PhD projects

WORKSHOPS AND EVENTS

113 CHRONICLE

114 SCIENTIFIC EVENTS



15

47

GENERAL
SEMINARS

AND **8**

COLLOQUIA

SCIENTIFIC EVENTS
(WORKSHOPS, SCHOOLS
AND CONFERENCES)



KEEP **UP-TO-DATE:**

 facebook.com/ILLGrenoble

 twitter.com/ILLGrenoble

 [linkedin.com/company/
institut-laue-langevin](https://linkedin.com/company/institut-laue-langevin)

ILL Chronicle 2019

8 JANUARY

Visit by Jean-Eric Paquet, Director General Research & Innovation, European Commission

10 JANUARY

Visit by Edith Heard, Director General, EMBL

15 MARCH

Visit by Prof. Christine Jørgensen, Deputy Director General, Danish Agency for Science & Higher Education

9-12 APRIL

Subcommittee meetings and 100th meeting of the ILL Scientific Council

22 MAY

Meeting of the Subcommittee on Administrative Questions (SAQ)

17-18 JUNE

Visit by a delegation from Oak Ridge National Laboratory, USA

26 JUNE

Meeting of the ILL Steering Committee

27 JUNE

Meeting of the ILL's Scientific Members

15 JULY

Signing ceremony for the renewal of Switzerland's Scientific membership

5 SEPTEMBER

Visit by a delegation from the China Institute of Atomic Energy (CIAE)

3 OCTOBER

Signing of MoU with the Extreme Light Infrastructure – Nuclear Physics (ELI-NP), Romania

16-17 OCTOBER

Meeting of the Subcommittee on Administrative Questions (SAQ)

5-8 NOVEMBER

Subcommittee and ILL Scientific Council meetings

27-28 NOVEMBER

Meeting of the ILL Steering Committee, including the celebration of the 31st Anniversary of Spanish Scientific membership at the ILL

9 DECEMBER

Visit by Pascal Bornozy, new Consul General for Switzerland in Lyon

16 DECEMBER

Visit by a delegation from Beijing Research Centre for Science of Science, Republic of China



WORKSHOPS AND EVENTS

Scientific events

In 2019, the ILL organised (or co-organised) 15 scientific events (workshops, conferences and schools). A total of 47 general seminars and 8 colloquia were also organised.

10–14 FEBRUARY

New Excitations in Spintronics (in Ireland)

17–22 MARCH

ADD2019

18 MARCH–19 APRIL

HERCULES 2019—European School

3–6 APRIL

Membrane Biophysics of Exo-Endocytosis: from Model Systems to Cells (in Nice)

8–11 APRIL

Simulations of Small-Angle Scattering for Soft Matter and Life Sciences

18–19 MAY

Oxford–Grenoble Symposium: 30 years of co-operative research in condensed matter physics and structural biology

4–5 JULY

PSB Symposium, EPN Campus, Grenoble

1–28 SEPTEMBER

X-Ray and Neutron Science—International student summer programme at the ILL/ESRF

23–27 SEPTEMBER

EMBO practical course, Grenoble

21–25 OCTOBER

AFMBioMed School

25 OCTOBER

FULLPROF School

12–14 NOVEMBER

Artificial Intelligence Applied to Photon and Neutron Science

17–22 NOVEMBER

USTV school—How to assess the structure of glasses?

28–29 NOVEMBER

CARAC 2019

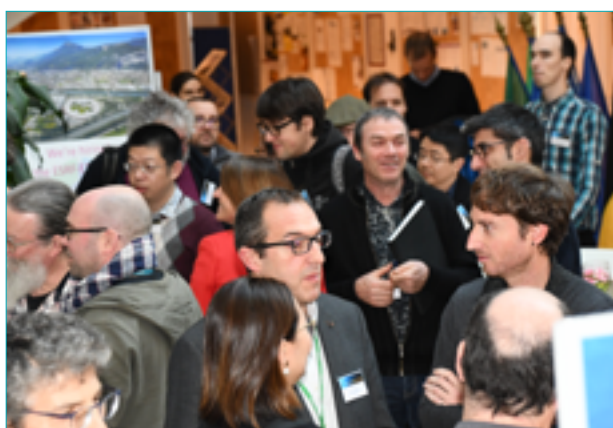
11–13 DECEMBER

Bilayers at the ILL



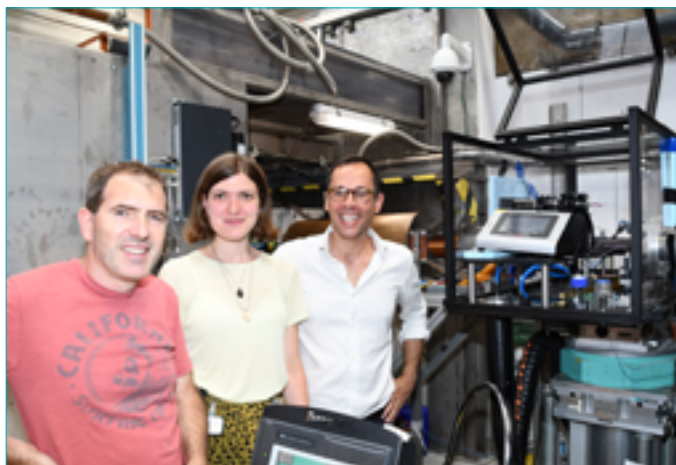
Top: Bilayers workshops, held at the ILL in December.

Bottom: Participant to the HERCULES European School.

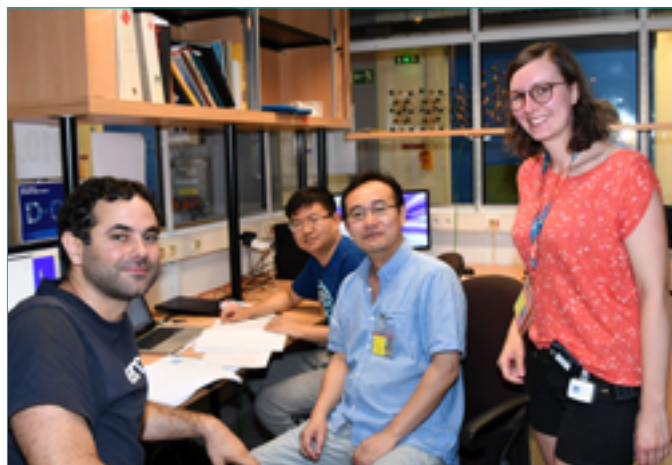


Over 150 attendees from around the world attended the workshop 'Artificial Intelligence Applied to Photon and Neutron Science', to discuss the potential of AI and machine learning in photon and neutron science. The workshop triggered global interest, and live video-streaming of the entire event was made available on the ILL website.

HAPPY USERS @ ILL



1.



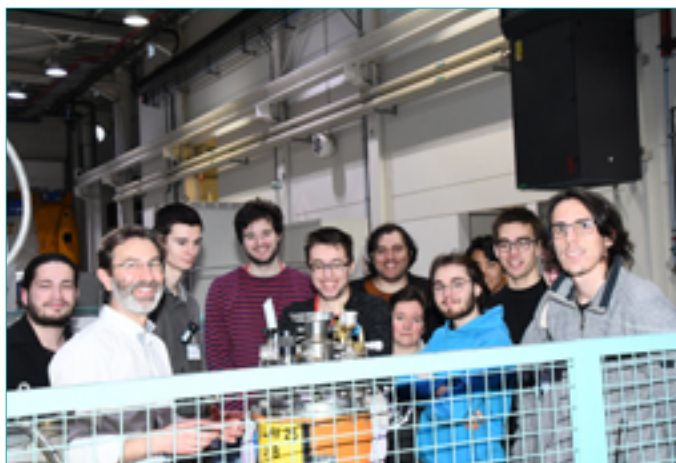
4.



2.



5.



3.



6.

1. From left to right: Lione Porcar (ILL), Liva Donina and João Cabral (Imperial College, London) during their microfluidic-SANS experiment on D22.

2. Arnaud Desmedt (ISM_Bordeaux, current president of the ILL's Scientific Council) studying with his team (Cyrielle Métails, centre, and Charlene Gimpier) the transport properties of gaseous species within artificial $\text{CO}_2\text{-N}_2$ hydrate bearings on IN5.

3. Andrea Orecchini (Perugia University, second from the left) and a group of students (UGA Grenoble) visiting the ILL to learn about neutron scattering and how it is used to answer important scientific questions.

4. From left: Navid Qureshi (ILL), Xiao Wang and Su YiXi Su (JCMS, Jülich) with Kitty Beauvois (ILL) during a diffraction study of the pressure-induced dimerised phases on $\alpha\text{-RuCl}_3$.

5. Nicole Husener and Marius Milatz (Hamburg University of Technology) studying partial saturation on granular media on D50.

6. Armando Maestro (ILL, centre) doing a test experiment with the new adsorption troughs suite on FIGARO with his PhD student Andreas Santamaria (left) and Antonio Rubio (master's student from Murcia University, Spain).

Let's tweet again



FACTS AND FIGURES

119 FACTS AND FIGURES

121 PUBLICATIONS

123 ORGANISATION CHART

549

PUBLICATIONS
RECORDED IN 2019



1611
INDIVIDUAL USERS
FROM **40 COUNTRIES** IN 2019

488

STANDARD
EXPERIMENTS
PERFORMED*



523
MEMBERS OF
STAFF



KEEP **UP-TO-DATE**:

 facebook.com/ILLGrenoble

 twitter.com/ILLGrenoble

 [linkedin.com/company/
institut-laue-langevin](https://linkedin.com/company/institut-laue-langevin)

* (as well as 14 DDT, 99 EASY and 24 internal experiments).

STAFF ON 31/12/2019

523 people, including 75 experimentalists in the scientific sector and 40 thesis students.

370 French; 37 German; 32 British; 52 scientific participating countries; and 32 others.

Nationality		%
French	370.0	70.75 %
German	37.0	7.07 %
British	32.0	6.12 %
Member countries	52.0	9.94 %
Others	32.0	6.12 %
Total	523.0	100 %

REVISED BUDGET 2019: 101 277 M€ (excluding taxes)

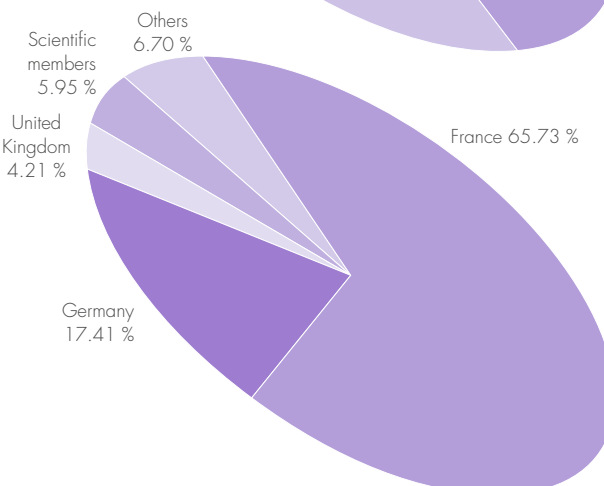
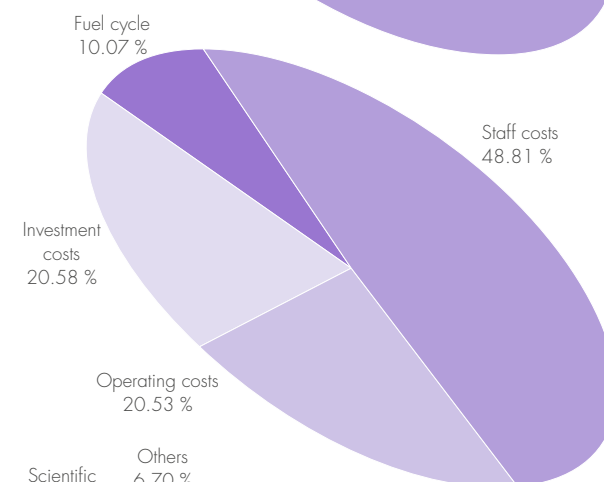
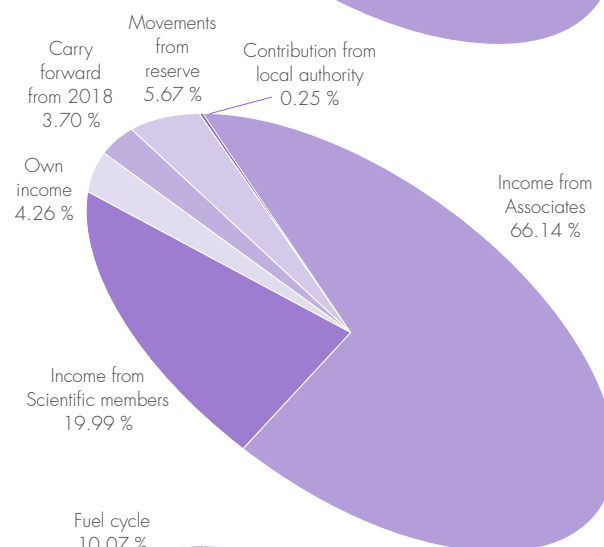
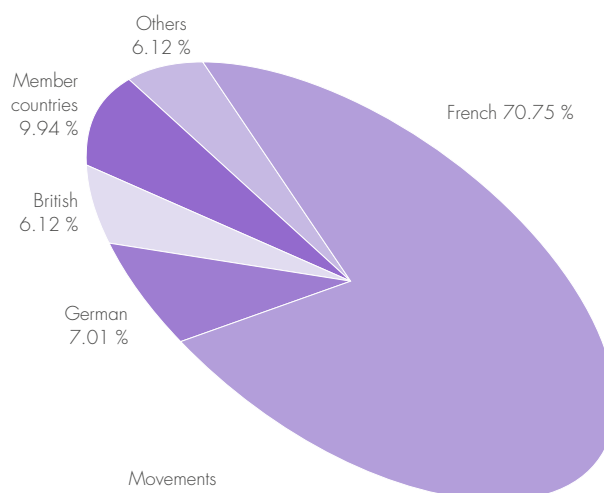
Income	M€	%
Income from Associates (incl. Fukushima & Millennium Programme & add. nuclear tax)	66.99	66.14 %
Income from Scientific members	20.24	19.99 %
Own income	4.31	4.26 %
Carry forward from 2018	3.74	3.70 %
Movements from reserve	5.74	5.67 %
Contribution from local authority	0.25	0.25 %
Total	101.28	100.00 %

Expenditure	M€	%
Staff costs	49.44	48.81 %
Operating costs	20.79	20.53 %
Investment costs	20.85	20.58 %
Fuel cycle	10.20	10.07 %
Total	101.28	100.00 %

PURCHASING STATISTICS 2019

	M€	%
France	26.90	65.73 %
Germany	7.12	17.41 %
United Kingdom	1.72	4.21 %
Scientific Members	2.44	5.95 %
Others	2.74	6.70 %
Total	40.92	100.00 %

France captive market	12.57	23.50 %
Total captive/non captive	53.49	0



FACTS AND FIGURES

NAME

Institut Max von Laue-Paul Langevin (ILL)

FOUNDED

19 January 1967

Intergovernmental Convention between France, Germany and United Kingdom (19/07/1974)

ASSOCIATES

France

Commissariat à l'Énergie Atomique et aux Energies Alternatives (CEA)

Centre National de la Recherche Scientifique (CNRS)

Germany

Forschungszentrum Jülich (FZJ)

United Kingdom

United Kingdom Research & Innovation (UKRI)

COUNTRIES WITH SCIENTIFIC MEMBERSHIP

Spain

MCIU Ministerio de Ciencia, Innovación y Universidades

Switzerland

Staatssekretariat für Bildung, Forschung und Innovation (SBFI)

Italy

Consiglio Nazionale delle Ricerche (CNR)

Belgium

Belgian Federal Science Policy Office (BELSPO)

Sweden

Swedish Research Council (VR)

Denmark

Danish Agency for Science and Higher Education

Poland

(NDPN) Consortium of Polish Scientific and Research Institutions

CENI (Central European Neutron Initiative)

Consortium composed of:

Austria: Österreichische Akademie der Wissenschaften

Czech Republic: Charles University, Prague

Slovakia: Comenius University, Bratislava

SUPERVISORY AND ADVISORY BODIES

Steering Committee, which meets twice a year

Subcommittee on Administrative Questions, which meets twice a year

Audit Commission, which meets once a year, and statutory auditor

Scientific Council with 9 Subcommittees, which meets twice a year

REACTOR

Operating 2 cycles in 2019

101 days in total, average power (p. 102)

EXPERIMENTAL PROGRAMME

488 experiments accepted by the Subcommittees on 28 ILL funded and 10 CRG instruments

1 611 visitors from 40 countries

Publications in 2019

In 2019, the ILL received notice of 549 publications by ILL staff and users.

They are listed on the ILL website:
<https://www.ill.eu/about-ill/documentation/scientific-publications/scientific-publication-list/>.

THE DISTRIBUTION BY SUBJECT IS AS FOLLOWS

Applied Physics, Instrumentation and Techniques	25
Biology	60
Crystallography and Chemistry	62
Liquids and Glasses	13
Magnetic Excitations	35
Magnetic Structures	96
Materials Science and Engineering	53
Medicine	8
Nuclear and Particle Physics	76
Soft Condensed Matter	79
Spectroscopy in Solid State Physics and Chemistry	22
Theory	18
Other	2

ILL PHD STUDENTSHIPS

Fulltime-equivalent ILL-funded PhD projects in 2019	40
PhD students working on ILL PhD projects in 2019*	55-60
Successfully defended ILL PhD theses in 2019	13

* includes PhD projects that are co-financed or completely externally financed.

REVIEW PANELS



Key

Chair/focus group Chair

ILL college secretary/focus group secretary

ILL specialist

REVIEW PANELS

APPLIED METALLURGY, INSTRUMENTATION AND TECHNIQUES

M. Strobl (PSI, Switzerland)

S. Cabeza

T. Pirling/A. Wildes/ L. Porcar

NUCLEAR AND PARTICLE PHYSICS

M. Van der Grinten (STFC, UK)

C. Michelagnoli

M. Jentschel

MAGNETIC EXCITATIONS

A. Boothroyd (Oxford University, UK)

L. Mangin-Thro

P. Steffens

CRYSTALLOGRAPHY

K. Edkins (Manchester University, UK)

O.R. Fabelo Rosa

C. Ritter

MAGNETIC STRUCTURES

O. Zaharko (PSI, Villigen, Switzerland)/

M. Laver (Birmingham University, UK)

J.A. Rodriguez-Velamazán/T. Saerbeck

N. Qureshi

STRUCTURE AND DYNAMICS OF LIQUIDS AND GLASSES

L. Bove (Pierre and Marie Curie University, Paris, France)

M.M. Koza

T. Seydel

SPECTROSCOPY IN SOLID STATE PHYSICS AND CHEMISTRY

M. de Boissieu (Simap, Grenoble, France)

T. Weber

P. Fouquet

STRUCTURE AND DYNAMICS OF BIOLOGICAL SYSTEMS

J. Lawrence (Manchester University, UK)

N. Coquelle

M. Blakeley/J. Peters

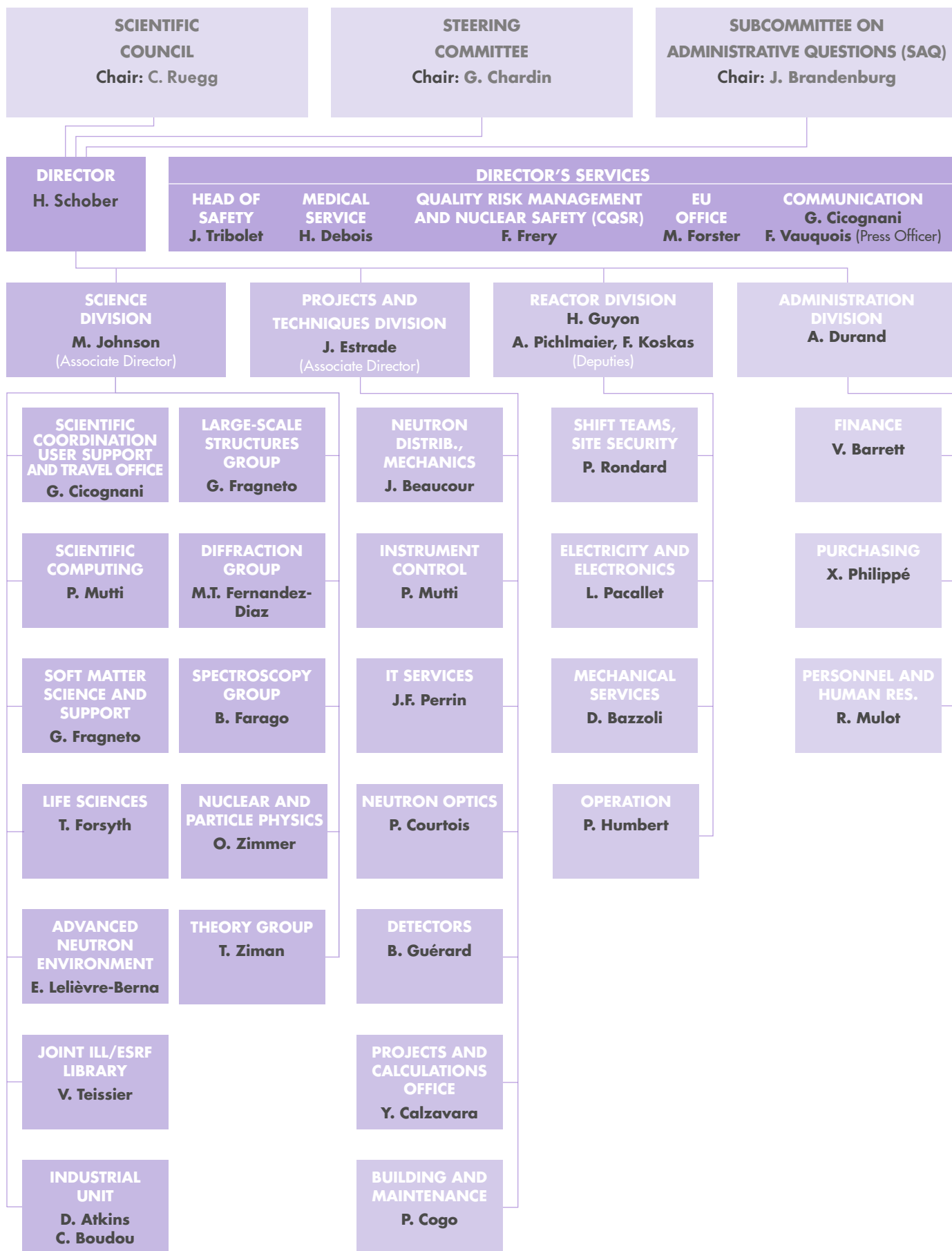
STRUCTURE AND DYNAMICS OF SOFT CONDENSED MATTER

R. Jacobs (Oxford University, UK)/

A. Zarbakhsh (University of London, UK)

S. Prevost/A. Maestro

O. Czakkel/Y. Gerelli



71, avenue des Martyrs
38000 Grenoble
France

www.ill.eu



This report has been printed using FSC certified paper www.fsc.org